Carlos Julio Cortés Rodríguez

Cutting edge preparation of precision cutting tools by applying micro-abrasive jet machining and brushing

kassel university press

Die vorliegende Arbeit wurde vom Fachbereich Maschinenbau der Universität Kassel als Dissertation zur Erlangung des akademischen Grades eines Doktors der Ingenieurwissenschaften (Dr.-Ing.) angenommen.

Erster Gutachter: Prof. Dr.-Ing. Franz Tikal
Zweiter Gutachter: Prof. Dr.-Ing. Jens Hesselbach

Tag der mündlichen Prüfung 17. April 2009

Bibliografische Information der Deutschen Nationalbibliothek
Die Deutsche Nationalbibliothek verzeichnet diese Publikation in der Deutschen Nationalbibliografie; detaillierte bibliografische Daten sind im Internet über http://dnb.d-nb.de abrufbar

Zugl.: Kassel, Univ., Diss. 2009
ISBN print: 978-3-89958-712-8
ISBN online: 978-3-89958-713-5
URN: urn:nbn:de:0002-7135

Druck und Verarbeitung: Unidruckerei der Universität Kassel
Printed in Germany

Vorwort

Die vorliegende Dissertation entstand während meiner Arbeit als Doktorand am Instituts für Produktionstechnik und Logistik der Universität Kassel im Fachgebiet Produktionstechnik und Werkzeugmaschinen.

Dem Fachgebietsleiter, Herrn Prof. Dr.-Ing. Franz Tikal, danke ich herzlich für seine Unterstützung und hilfreichen Anregungen, die diese Arbeit ermöglichten.

Herrn Prof. Dr.-Ing. Jens Hesselbach, danke ich für die Übernahme des Korreferates.

Den Herren Prof. Dr.-Ing. Eberhard Paucksch und Prof. Dr.-Ing. Wolfgang Klose danke ich für die Bereitschaft zur Teilnahme an der Prüfungskommission.

Mein Dank gilt darüber hinaus dem Kollegium des Fachgebiets, das durch die fruchtbaren Discussionen und Anregungen zum Gelingen dieser Arbeit beigetragen hat.

Der Universidad Nacional de Colombia danke ich für die Unterstützung und der Stiftung COLFUTURO für die finanzielle Hilfe. Der KAAD danke ich für die Gewährung eines Stipendiums über 22 Monate und dem ALBAN Programm danke ich für die Gewährung eines Stipendiums über 18 Monate.

Ein besonderer Dank gilt meinen Eltern Luis und Alicia, die meine Ausbildung ermöglicht haben und meiner Frau Patricia und meinen Kindern Sebastian und Juliana für die liebevolle Unterstützung und die mir ihre Geduld und Zeit geschenkt haben.

Kassel, im April 2009 Carlos Julio Cortés Rodríguez

Abstract

For the systemic development of precision cutting tools, it is indispensable to observe four related aspects; the cutting tool material, the coating technology, the macro geometry of the tool and the cutting edge preparation. The present work is focused on the last aspect. In accordance with the specified requirements of the machining process to achieve the quality characteristics of the workpiece, it is necessary to keep in mind the specifications of the cutting tool and particularly their cutting edge preparation. Therefore, to achieve a cutting edge preparation to satisfy the requirements, in terms of reproducibility, quality, cost and flexibility, the selection and planning of the preparation process has special importance. In this work, in first instance, a reproducible methodology of characterization of the cutting edge preparation was proposed, in terms of micro and meso geometry of the cutting tool, as well as the corresponding required measurement strategy by using a chromatic sensor. For the above-mentioned, concepts of differential geometry and fractal geometry were used, together with the existent international norms for surface measurement. Considering this characterization of the geometry of the cutting edge, three cutting edge preparation processes for cemented carbide tools were analyzed; micro-abrasive jet machining, brushing-polishing and brushing with abrasive filaments. By using design of experiments (DoE) and regression analysis, the influence of the process parameters on the quantity of removed material and on the characteristics of the surface of the cutting tool was observed. Aspects as radius of the cutting edge, notchedness (chipping) of the cutting edge, and microstructuring of the cutting tool surfaces were considered for each process. Additionally, machining experiments to observe the influence of the radius of the cutting edge and the preparation process on the cutting forces and the wear of the cutting tool were carried out. With the obtained information from DoE and regression analysis, as well as of the machining experiments, the considered preparation processes can be evaluated, compared, selected and planned.

A planning strategy for cutting edge preparation processes considering the nominal removed area as process time function, and an equation to express the development of the notchedness as function of process time, was proposed. The presented aspects of process planning can be applied to other preparation processes. By using DoE, the variability of the obtained cutting edge radius is analyzed, and experimental models that express the removed area as function of the process parameters for the considered preparation processes, were developed. Considering the results of orthogonal cutting tests, the preparation by means of rounding of the cutting edge has a positive effect, compared with sharp edges, in the decrease of the cutting forces and force ratio after that a critical point in the development of the test was reached. Additionally, the tools with rounded cutting edges showed a lower final flank wear than the sharp edges. Differences in flank wear for cutting edges with the same radii but obtained by different preparation processes can be explained by differences in notchedness and microstructuring. Likewise, the existence of an optimal radius that causes the lower final flank wear, is observed.

Kurzfassung

Für eine systematische Entwicklung von Präzisionszerspanungswerkzeugen, ist es notwendig vier zusammenhängende Aspekte zu beachten: den Schneidstoff, die Beschichtungstechnologie, die Makrogeometrie und die Schneidkantenpräparation. Die vorliegende Arbeit behandelt den letzten dieser vier Aspekte. Bestimmte Anforderungen an die Zerspanungsverfahren sind notwendig, um die geforderten Qualitätsmerkmale von Bauteilen zu garantieren. Es ist daher erforderlich die Spezifikationen der Zerspanungswerkzeuge zu kennen, insbesondere die Schneidkantenpräparation. Hierbei spielt die Auswahl und Planung der Schneidkantenpräparation eine wichtige Rolle um den Anforderungen in Hinblick auf Reproduzierbarkeit, Qualität, Kosten und Flexibilität zu genügen. In dieser Arbeit wird an erster Stelle eine Methode zur Charakterisierung der Schneidkantenpräparation in Hinblick auf Meso- und Mikrogeometrie vorgeschlagen, welche mit Hilfe entsprechender Messtechnik und basierend auf dem Einsatz eines chromatischen Sensors durchgeführt wird. Für diese Methode wurden Konzepte der differentiellen und fraktalen Geometrie, sowie internationale Normen zur Oberflächenmessung angewendet. Zur vorgeschlagenen Charakterisierung der Geometrie der Schneidkante, wurden drei Schneidkantenpräparationsverfahren von Hartmetallwerkzeugen analysiert: Mikrostrahlen, Bürsten-Polieren und Bürsten mit abrasiven Filamenten. Mittels statistischer Versuchsplanung (DoE) und der Regressionsanalyse wurde der Einfluss der Prozessparameter auf das Abtragsmaterial und auf die Merkmale der Werkzeugoberflächen bestimmt. Weitere Aspekte wie der Schneidkantenradius, Schartigkeit und die Mikrostrukturierung der Span- und Freifläche, wurden für jedes Schneidkantenpräparationsverfahren untersucht. Zusätzlich wurden Zerspanungsversuche durchgeführt, um den Einfluss des Schneidkantenradius und der Präparationsverfahren auf die Schnittkräfte und den Freiflächenverschleiß zu bestimmen. Mit den Ergebnissen der statistischen Versuchsplanung, der Regressionsanalyse sowie der Zerspanungsversuche können verschiedene Präparationsverfahren verglichen, ausgewertet, geplant und ausgewählt werden.

Eine Planungsstrategie zur Schneidkantenverrundung unter Berücksichtigung der Abtragsfläche, der Abtragsrate und eine Gleichung zum Verhalten der Schartigkeit als Funktion der Bearbeitungszeit werden vorgeschlagen. Durch DoE werden die Streuung des erzielten Kantenradius bestimmt und experimentelle Modelle vorgeschlagen, um die Abtragsfläche als einen Parameter bei der Präparationsverfahren mit einzubinden. In Anbetracht der Ergebnisse der Versuche mit Orthogonalprozessen und im Vergleich mit scharfen Kanten hat die Verrundung der Schneidkante einen positiven Effekt in Bezug auf die Verringerung der Schnittkräfte nach dem kritischen Punkt. Zusätzlich zeigten die Werkzeuge mit verrundeten Schneidkanten am ende der Versuche einen niedrigeren Freiflächenverschleiß als solche mit scharfen Kanten. Unterschiede des Freiflächenverschleißes bei Kanten mit gleichen Radien aber verschiedenen Präparationsverfahren können durch Unterschiede in der Schartigkeit und der Mikrostrukturierung erklärt werden. Ebenso wird beobachtet, dass ein optimaler Radius den Freiflächenverschleiß reduzieren kann.

Contents

Nomenclature

Symbol	Unit	Meaning
a_p	mm	depth of cut
A	-	abrasive/adhesive wear constant
A_m	m^2	area of machined surface
A_b	-	type of abrasive
A_r	μm^2	removed area
$A(t)$	mm^3/s	material removed as function of time
A_t	$\mu m^2/s$	area removal ratio
A_α	-	tool flank
A_γ	-	tool face
b_γ	μm	length of land
b_n	μm	length of chamfer
B	-	diffusive wear constant
B_t	-	brush type
d_a	μm	mean diameter of abrasive grains
d_b	mm	brush diameter
d_n	mm	nozzle diameter
C	%	coverage of the abrasive jet
C_1	%	coverage of the abrasive jet for a passung
D	-	fractal dimension
E	g/g	erosion rate
$E(A(t))$	-	material removed effectiveness
E_p	Pa	elastic modulus of the polishing pad
f	mm/rev	feed rate
F_{bn}	N	brushing normal force
F_{bs}	N	brushing shear force
F_c	N	cutting force
F_{cn}	N	normal cutting force
F_p	N	plowing or ploughing force
F_r	N	resultant force
F_γ	N	face friction force
$F_{\gamma n}$	N	face normal force

Symbol	Unit	Meaning
f_t	1/min	table oscillation frecuency
F_x, F_y, F_z	N	force system of dynamomether
G	mesh grade	grit of abrasive
h	μm	uncut chip thickness
h_c	μm	chip thickness
h_{min}	μm	minimum chip thickness
H_m	HV	hardness of material
H_p	HV	hardness of polishing pad
H_t	HV	hardness of cutting tool material
H_w	HV	hardness of workpiece
K	-	constant for polishing removal rate model
K_c	MPam$^{1/2}$	workpiece toughness
K_{IC}	MPam$^{1/2}$	material toughness
$\kappa 2[\phi]$	1/mm	curvature function
K_β	-	factor that depends on the wedge angle to calculate the removed area
L	mm	length of abrasive filament
L_a	N	applied load for abrasion
MRR	mm^3/s	material removal rate
m_{r1}	%	material portion level that separates the high peaks from the profile roughness
m_{r2}	%	material portion level that separates the deepest valleys from the profile roughness
n	-	nose tip of the edge contour
n_p	-	number of passings
n_v	-	velocity exponent for erosion
N	1/min	brush rotation speed
N_a	particles/s	effective number of abrasive particles impacting per unit time
N_g	-	geometry of nozzle
p	Pa	polishing pressure
P_a	bar	air jet pressure
$P(\omega)$	μm^2	Fourier power spectrum
r_c	μm	radius of the tungsten carbide grain
r_d	μm	nose radius of the cutting edge
r_n	μm	radius of the cutting edge
r_{1n}	μm	initial radius of the cutting edge
r_{2n}	μm	final radius of the cutting edge
R	μ	radius of abrasive particle
R_a	μm	arithmetical mean value of surface roughness

Symbol	Unit	Meaning
R_k	μm	core roughness depth of the profile
R_{max}	μm	maximum height of surface irregularities
R_{pk}	μm	reduced peak height of the profile
R_{sm}	μm	mean spacing between successive profile peaks
R_t	μm	maximum peak to valley height of the profile
R_{vk}	μm	average valley depth of the profile
R_z	μm	mean roughness depth
S	-	stagnation point
S_a	μm	arithmetical mean height of the surface (ISO 25178)
S_{A_r}	μm^2	standard deviation of removed area
S_d	mm	sliding distance
S_c	-	asymmetry of the edge contour
S_k	μm	core roughness depth of the surface
S_{ku}	μm	kurtosis of height distribution (ISO 25178)
S_{mr1}	%	material portion level that separates the high peaks from the surface roughness
S_{mr2}	%	material portion level that separates the deepest valleys from the surface roughness
S_p	μm	maximum peak height of the surface (ISO 25178)
S_{pk}	μm	reduced peak height of the surface
S_q	μm	root mean square height of the surface (ISO 25178)
S_{r_n}	μm	standard deviation of cutting edge radius
$S_{r_{1n}}$	μm	standard deviation of initial radius
$S_{r_{2n}}$	μm	standard deviation of final radius
S_{sk}	μm	skewness of height distribution (ISO 25178)
S_v	μm	maximum height of valleys (ISO 25178)
S_{vk}	μm	average valley depth of the surface
S_z	μm	maximum height of surface roughness (ISO 25178)
S_α	μm	length of rounding in the tool flank
S_γ	μm	length of rounding in the tool face
t_m	s	machining time
t_j	s	effective jet working time
t_b	s	brushing time
t_h	s	honing time
T_f	°C	cutting temperature in the tool flank zone

Symbol	Unit	Meaning
u_c	J/m^3	specific cutting energy
v_a	m/s	velocity of abrasive grains
v_c	m/min	cutting speed
v_d	m/min	sliding speed
v_f	m/min	feed speed
v_s	m/min	travel speed of the jet in horizontal direcction
v_t	m/s	tangential velocity of brushing
v_{wl}	m/s	relative velocity between workpiece and pad
V	cm^3	removed volume
VB	mm	flank wear land width
y	mm	jet distance
y_b	mm	brush penetration depth
y_h	mm	honing penetration depth
α	degrees	tool clearance
α_b	degrees	chamfer angle
α_e	degrees	effective clearance
β	degrees	wedge angle
Δ_r	μm	parameter to describe rounding of cutting edge
ΔS	μm	thickness of the primary shear zone
Φ	degrees	shear angle
ϕ	-	contour of the cutting edge
ϕ_e	-	effective contour
γ	degrees	nominal rake angle
γ_b	degrees	angle of chamfer
γ_e	degrees	effective rake
Λ	-	topothesy
μ	-	friction coefficient between tool and workpiece
ζ_{SB}	-	factor for tool-chip friction
ζ_{rake}	-	factor for friction on rake
θ	degrees	turning angle
θ_1	degrees	turning angle (flank)
θ_2	degrees	turning angle (face)
θ_s	degrees	stagnation angle
ϑ	°C	tool temperature
ρ_a	g/cm^3	density of abrasive
ρ	degrees	friction angle
σ_p	-	standard deviation of height of polishing pad
σ_{yw}	Pa	flow stress of the workpiece or target material

Symbol	Unit	Meaning
φ	degrees	angle of the highest point of the contour
φ_j	degrees	impingement angle
φ_b	degrees	brush position angle
φ_h	degrees	honing position angle
Ω	degrees	orientation angle of the filament
ω	$\mu\mathrm{m}^{-1}$	spatial frequency

Acronyms	Meaning
AFM	abrasive flow machining
BNAF	brushing with nylon abrasive filaments
BP	brushing-polishing
CBN	cubic boron nitride
CNC	computer numerical control
CCD	charged-coupled device
CVD	chemical vapor deposition
DoE	design of experiments
EDX	energy dispersive X-ray analysis
HSC	high speed cutting
HSS	high speed steel
PM-HSS	powder metallurgy- high speed steel
MAJM	micro-abrasive jet machining
MRR	material removal rate
NAF	nylon abrasive filaments
PCBN	polycrystalline cubic boron nitride
PCD	polycrystalline diamond
PVD	physical vapor deposition
SEM	scanning electron microscopy
WC	tungsten carbide

1 Introduction

The requirements in quality of the finished product, decrease of costs, flexibility, reduced times of production, productivity, capacity to process new materials and miniaturization, among others, have outlined developments in the modern machining process. The conception of new systems for machines tools as well as the development of new characteristics in precision cutting tools have been part of the solution to reach these demands. Particularly, the development of new concepts in the cutting tools has been focused in four aspects: new cutting tool materials (substrates), surface engineering and coating technology, optimization of the cutting tool geometry and new approaches for the cutting edge preparation.

The research and innovation has been carried out principally in the first three aspects. Regarding cutting edge preparation, the work has been centered in the industrial application of preparation processes based mainly on abrasion and erosion, and experimentation of cutting edge micro-geometries for different machining applications. The central goal of the cutting edge preparation process is to generate a specific geometry in the contour of the cutting edge (rounding or chamfer or combination of both), and to produce an improvement in the cutting edge microtopography (notchedness[1] or chipping) and to adapt the surface of the cutting edge and cutting surfaces for the subsequent coating process of the cutting tool or for the improvement of the contact behavior for an specified machining application.

In the last decade the research works on cutting edge preparation have increased due to its importance in micro-machining applications, and equally for the observed influence of the cutting edge preparation in different aspects of the machining process, mainly in wear development and tool life, cutting forces and moments, distribution of the temperature field, chip formation, chip flow and transportation, stress and strain field during the cutting process, surface integrity of the workpiece, precision and accuracy in the geometry of the workpiece and the coating quality of the cutting tool in terms of adhesion and uniformity.

Currently, in the precision cutting tool industry, the application of cutting edge preparation processes are based mainly on honing by means of abrasive filament brushing, micro-abrasive jet machining (microblasting), brushing-polishing (with diamond paste), drag-finishing (with granulate), water-jet machining, abrasive flow machining and

[1] The word *notchedness* corresponds to the word *Shartigkeit* in German language. From *notched: schartig*. Another word that corresponds to *Shartigkeit* is *chipping*

magnetic-finishing. Additionally there are other processes, in development, based on mechanical, thermal and chemical principles.

To select the appropriate process and to carry out its planning, the relationship between the variables of the cutting edge preparation process and its response is required. Additionally for quality control, the characterization of the cutting edge preparation and their corresponding measurement is required in order to carry out a systemic analysis of potentialities and disadvantages of the processes.

To reach the exposed requirements, in this work , were considered as central tasks: to define the characteristics of quality associated with the cutting edge preparation, to define the associated measurement technology, to analyze the relationship among the parameters of the process and its response and the process reproducibility, to outline a process planning methodology for a required preparation and to evaluate the preparation processes by means of machining tests to observe the influence of the preparation in the behavior of the precision cutting tool.

In chapter 2, a description of the problem is made, and the details of the definition of the research problem are presented. Likewise, the interrelation between the different variables and concepts and the specific objectives and the corresponding methodology are considered.

In chapter 3, fundamentals that are required for the understanding of the concepts used in the solution of the problem are presented. Emphasis is made in the importance and the influence of the cutting preparation in the behavior during the operation of a precision cutting tool. Likewise, the concepts related with the abrasion, erosion and wear of the cemented carbides are presented. In chapter 4, the current state of the art for cutting edge preparation as well as the corresponding characterization of the obtained preparation and the available measurement technology are considered . In chapter 5, the measurement technology and the proposed characterization in terms of micro- and meso-geometry of the cutting tool are presented. Aspects related to edge contour description by means of curvature function, definition of notchedness and characterization of the surfaces of the cutting tool by means of the international normalization and fractal geometry are considered.

In chapter 6, aspects related to process planning are presented. The concepts of nominal removed area, area removal ratio are proposed. Likewise, the sources of process variability and selection of process parameters are analyzed.

In chapters 7 to 9, the considered preparation processes; micro-abrasive jet machining, brushing-polishing and brushing with nylon abrasive filaments are studied. The description of the process and the effect of the involved variables on the response are analyzed by means of design of experiments an regression models.

In chapter 10, the evaluation and comparison of the cutting edge preparation processes are presented. The results of machining tests considering the different processes with different cutting edge radii are analyzed. The cutting forces and the wear of the cutting tool were observed.

2 Problem outline and objectives

2.1 Problem definition

For the manufacturing of products by using machining processes with defined cutting edges, it is necessary to achieve a set of product specifications and production requirements. Inside the product specifications are the geometry which considers the corresponding dimensional, shape and position tolerances, and the surface integrity, which considers apart from the surface finishing, other factors like residual stresses, tribological, metallurgical, visual and physical aspects. On the other hand, inside the production requirements, productivity, flexibility, costs, production time, quality insurance, and environmental and health aspects are considered.

To achieve the product specifications and the production requirements, it is required to consider the appropriate integration of the following aspects (see **Figure 2-1**): workpiece (material, shape and dimensions), machining process (kinematics, cutting conditions), machine tool (static and dynamic rigidity), surroundings (cutting fluid, thermal conditions) and cutting tool (substrate, coating, macro geometry and cutting edge preparation).

This work is focused on the cutting edge preparation. Follow several aspects of the cutting edge preparation process and its effects are presented. In **Figure 2-2** two states of a cutting edge are shown, in the left side a sharp edge and in the right side a prepared edge. Before the cutting edge preparation process, the sharp cutting edge presents typical edge defects (burrs, micro fractures, and irregularities), surface defects and low mechanical strength that cause chipping of the edge and instability of the cutting process obtaining low tool life, low tool reliability and negative influence on the workpiece quality.

The application of the edge preparation process seeks to solve this problem by means of the elimination of defects and irregularities and by the generation of a defined edge geometry and by modifying the micro-topography of the edge (notchedness) and the microstructuring of the face and flank of the tool (see right side of **Figure 2-2**). The consideration of these cutting preparation aspects influences the cutting process causing improvements in tool life, tool reliability and workpiece quality.

To use systematically this improvement of the cutting edge in the chain of production of precision cutting tools, the process should be planned, reproducible and controllable. Likewise, a reliable and reproducible measurement technology necessary for the quantification of the quality characteristics of the cutting edge preparation is required. In

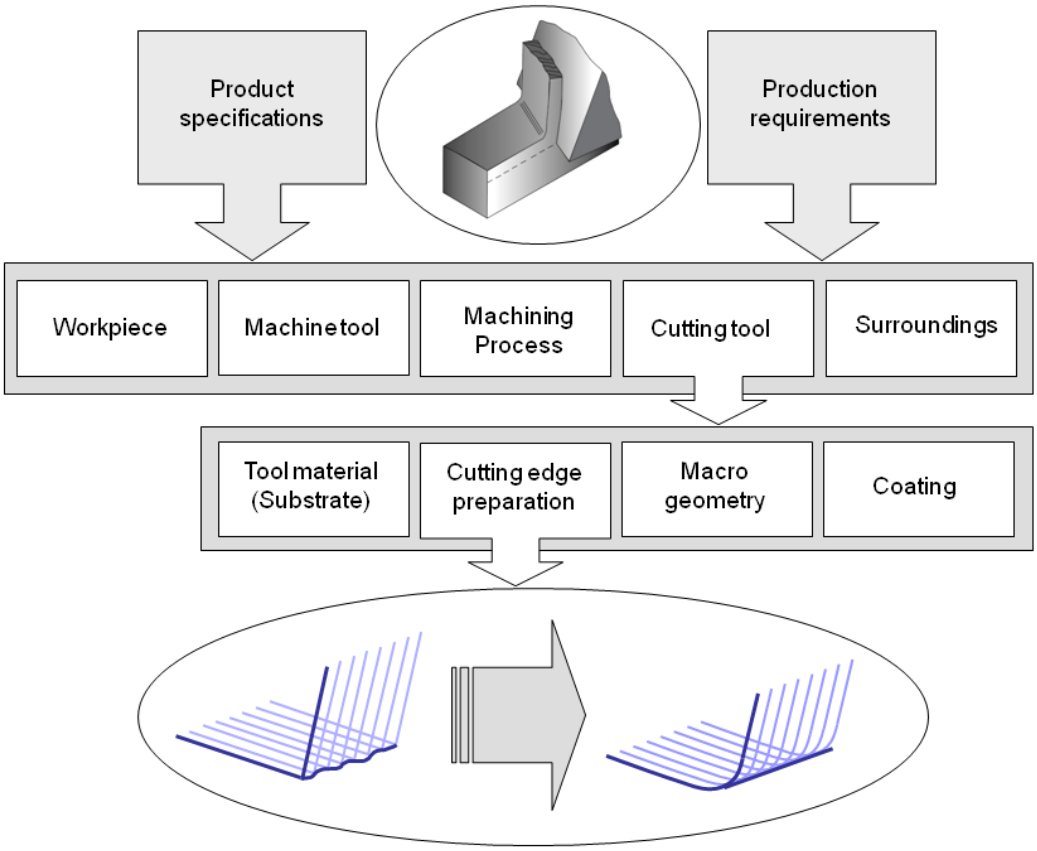

Figure 2-1: General aspects of the problem framework

addition, it is necessary to observe the grade of improvement of the performance of the cutting tool generate by the cutting edge preparation process.

The difficulties to measure, with reproducibility, geometric characteristics of the cutting edge, such as the edge contour which can have radii of the order of 5 μm, as well as slope changes and curvature variations that hinder their simple measurement by means of tactile and optic methods, added to the difficulty for the determination of the microtopography of the cutting edge, demand the proposal of a measurement methodology and the definition of the quality characteristics of the cutting edge.

In **Figure 2-3** the consequences of deficiencies of the cutting edge and the achievements of cutting edge preparation are related, likewise the requirements to carry out systemically the edge preparation process are considered.

In **Figure 2-4** a perspective to handle the problem is presented. From this perspective, in first instance the characterization of the cutting edge preparation, in terms of

geometry of the edge contour, notchedness and the microstructuring of the cutting surfaces are considered. Additionally, it is necessary to define the measurement technology of such characteristics. Equally, for planning and selecting the process, it is required to carry out an analysis to find a model of the relationship between the parameters of the process and the obtained quality characteristics. Also it is important to determine the variability of the process. Complementary, to observe the improvement of the cutting edge performance, it is required an evaluation of the prepared precision cutting tool by means of machining test in order observe cutting forces and tool wear.

To propose a methodology to handle the requirements presented previously, it is necessary to define the limits of the application frontier. In this work micro-abrasive jet machining (MAJM), brushing-polishing (BP) and brushing with nylon abrasive filaments (BNAF) were considered as preparation processes. As cutting tool material, uncoated cemented carbide (hard metal)was selected and the cutting edge preparation is focused on the rounding of the cutting edge.

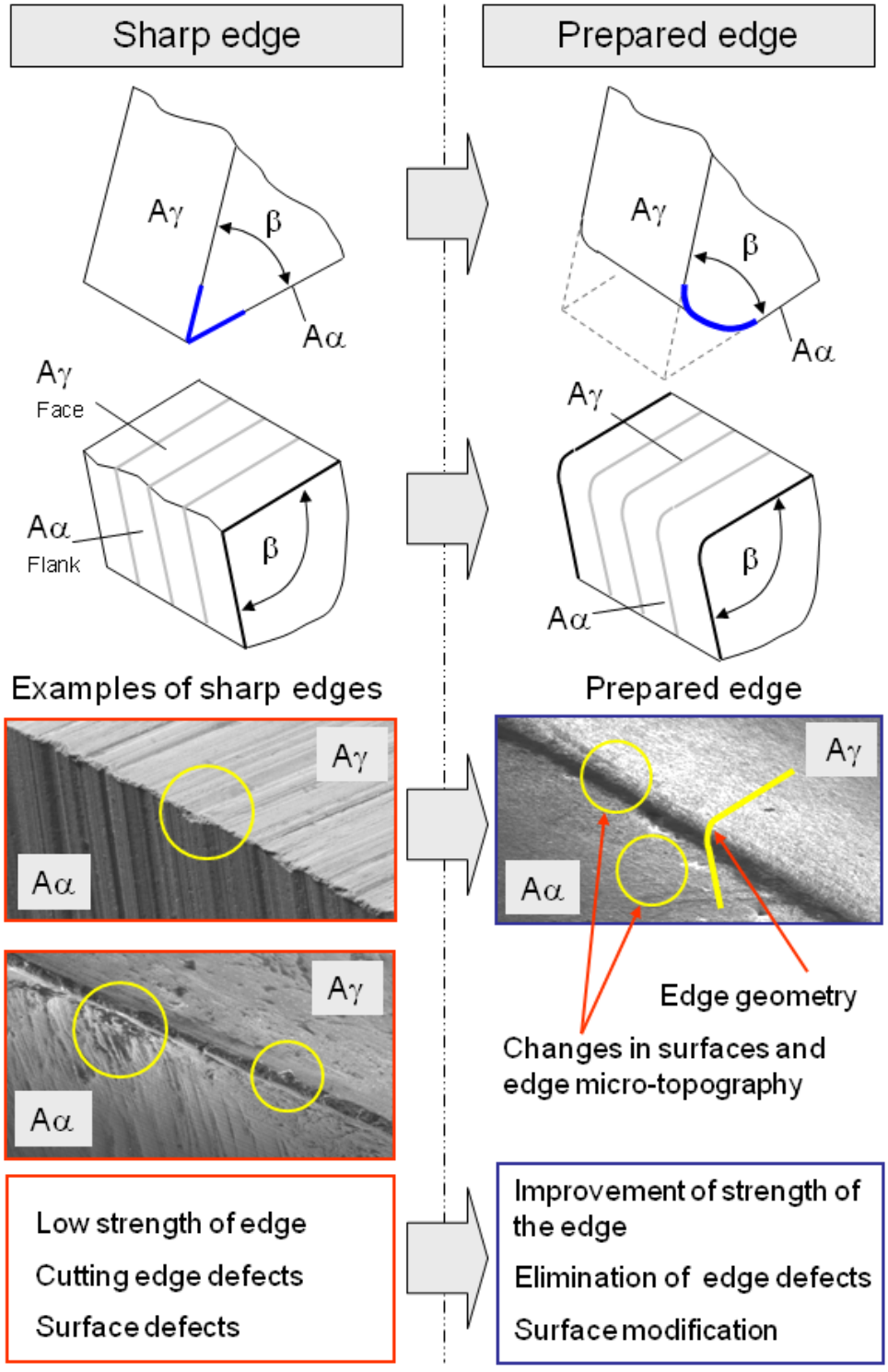

Figure 2-2: Input-output aspects of the cutting edge preparation process

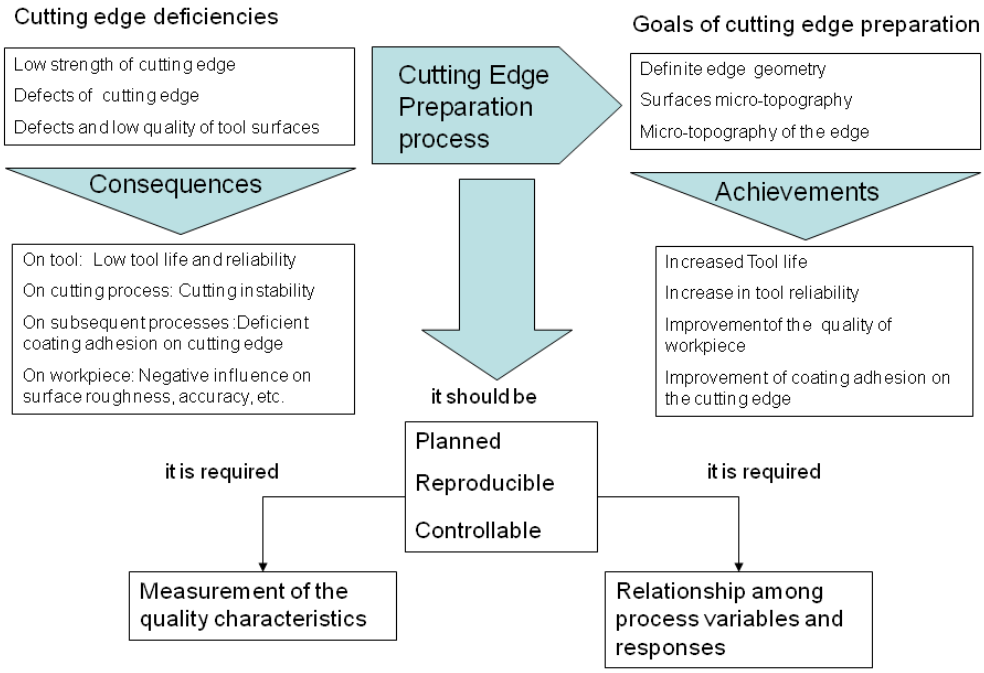

Figure 2-3: Aspects considered for a systemic cutting edge preparation

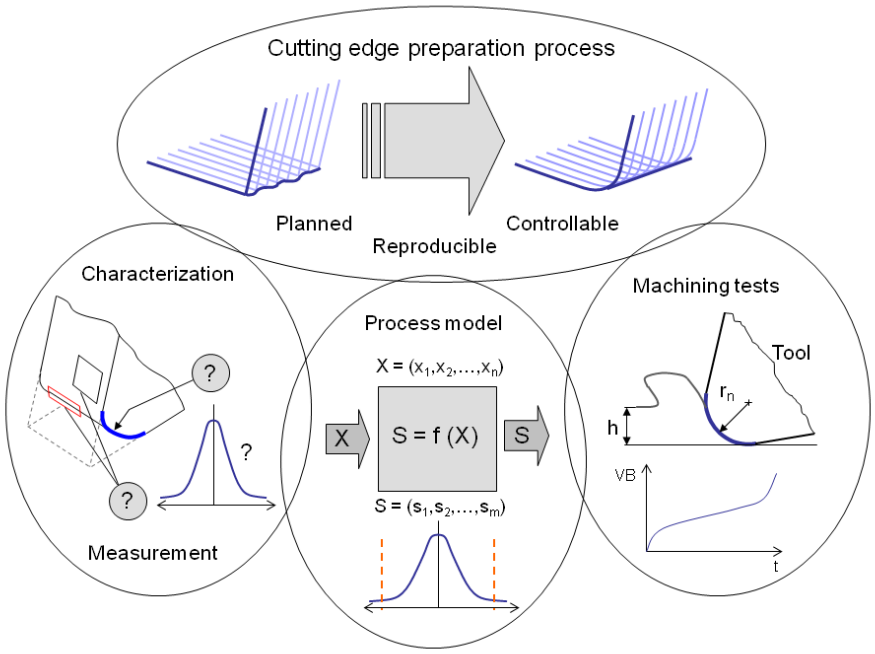

Figure 2-4: Aspects related with the problem definition

2.2 Research objectives

Considering the requirements that define the limit of the problem, the following objectives were proposed:

- To define the characterization of the cutting edge preparation.
- To propose a methodology and the appropriate measurement strategy for the characterization of the cutting edge preparation.
- To analyze experimentally, for the considered preparation processes, the effect of the process variables on removed material, final radius and roughness of tool surfaces.
- To propose a methodology for planning of the cutting edge preparation process.
- To evaluate the behavior of prepared cutting tools by means of machining tests, considering cutting forces and tool wear.

2.3 Methodology

Next the strategies used for the achievement of the proposed objectives are presented. For the characterization of the cutting edge preparation, concepts of differential geometry and curves fitting were considered for the characterization of the profile of the contour of the cutting edge and the determination of the cutting edge radius. Equally for the characterization of the surfaces and microstructuring, the existent normalization on 3D surface measurement and concepts of fractal geometry were used.

Regarding the measurement methodology, optical methods for the measurement of the cutting edge radius were used, specifically optical systems based on the principle of chromatic aberration. For the surface characterization, optical and stylus methods were considered.

For the experimental analysis of the considered processes, strategies of design of experiments (DoE) were used, especially fractional factorial designs for factor screening and for investigating main effects. Equally, regression analysis was considered to propose regressions models that relate the variables or more significant factors with the response variable of the processes. For each preparation process, a group of entrance variables (process parameters) and response variables (removed material, cutting edge radius and the roughness of the cutting surfaces of the cutting tool) were considered.

The process planning methodology was structured by means of the concepts of required removed area and area removal ratio combined with the information of the regression models for each cutting edge preparation process. The evaluation of the prepared precision cutting tools was carried out by means of machining experiments. As entrance variables, the cutting edge preparation processes and the cutting edge radius were considered, and as response variables the cutting forces and the flank wear were observed.

3 Fundamentals

3.1 Importance and purposes of the cutting edge preparation

The application of new cutting strategies to improve productivity in the machining process and quality of workpieces requires the development of modern precision cutting tools. For an integral and systemic development of a precision cutting tool, four related aspects are considered (see **Figure 3-1**):

- Cutting tool material (substrate); economically viable and meeting the requirements of a specific application.
- Coating technology ; economically viable in enhancing the properties of the substrate.
- Macro geometry ; technologically adequate for chip transportation, chip breaking, tool gripping and handling.
- Cutting edge preparation; precise, repeatable, controllable and compatible with a specific application and subsequent coating.

The control of each of these aspects affects the quality and reliability of the cutting tool that is subjected to extreme conditions in modern cutting technology; with local pressures between tool and workpiece material between 100-10000 N/mm^2, temperatures between 300-1200°C and velocities between 100-6000 m/min.

Regarding the cutting tool material, the current development offers the possibility of selecting among others; high speed steels, different types of cemented carbides, ceramics, polycrystalline cubic boron nitride, polycrystalline diamond and single-crystal diamond [55, 129, 172, 177]. The application defines the required mechanical and thermal properties and the adequate balance between wear resistance and toughness.

Coating technology and general surface technology applied to cutting tools have been areas of great development in the last two decades [55, 133]. Coatings have been applied principally to high speed steel and cemented carbide tools to improve wear resistance, to increase tool life and to achieve higher cutting speed. Principally based on PVD (physical vapor deposition) and CVD (chemical vapor deposition) processes, different coatings are currently available. Among others, TiN, TiC, Ti(C,N),(Ti,Al)N, Al_2O_3, polycrystalline

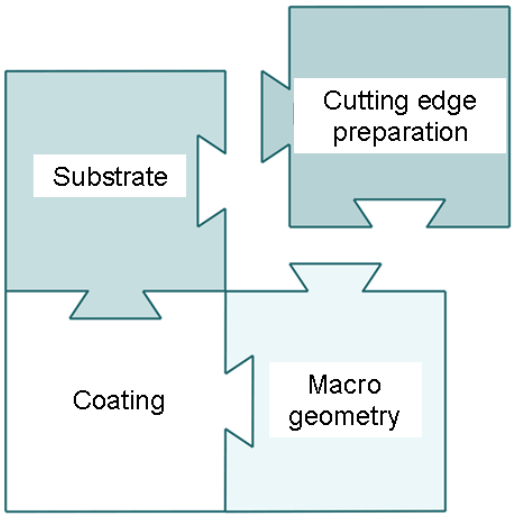

Figure 3-1: Linked aspects in the development of precision cutting tools

diamond coatings and boron nitride coatings (in development). Recently the application of nanotechnology techniques to surface engineering has offered new perspectives in coating technology for precision cutting tools.

The development of the macro geometry of the cutting tool is related to the design and optimization of shape and dimensions [36]. Among others, these includes cutting angles (α, β and γ), tool flank (A_α) and tool face (A_γ), reduced flank and face, rounded corner, chamfered corner, functional surfaces, cavities, and chip breakers, principally to achieve the requirements of the required cutting process and additionally to support the mechanical and thermal demands generated in the cutting process, to facilitate the chips flow and evacuation, to allow adequate refrigeration and lubrication during the process and to guarantee a sure operation.

Cutting edge preparation consists of generating the cutting edge geometry (see **Figures 3-2** and **3-3**) and modifying the micro topography of the edge (change in notchedness) as well as the change in roughness and texture of the tool surfaces (face and flank) in the vicinity of the edge, with the consequent elimination of edge defects and strength improvement, in order to improve the performance and reliability of the cutting tool and the quality of the workpiece. In addition to the design of macro geometry, research and practical applications have shown that cutting edge geometry have also a big influence on the performance and on the reliability of the precision cutting tool. This aspect is especially of high importance for cutting tools destined for mass production plants. Additionally, the consequences of applying the edge preparation process require on the one hand the coating adhesion and on the other hand the reinforcement of the cutting edge to avoid unpredictable cutting edge chipping.

Edge defects are present in nearly all tools prior to edge preparation. The defects are originated after pressing, EDM (electrical discharge machining) and grinding. Although

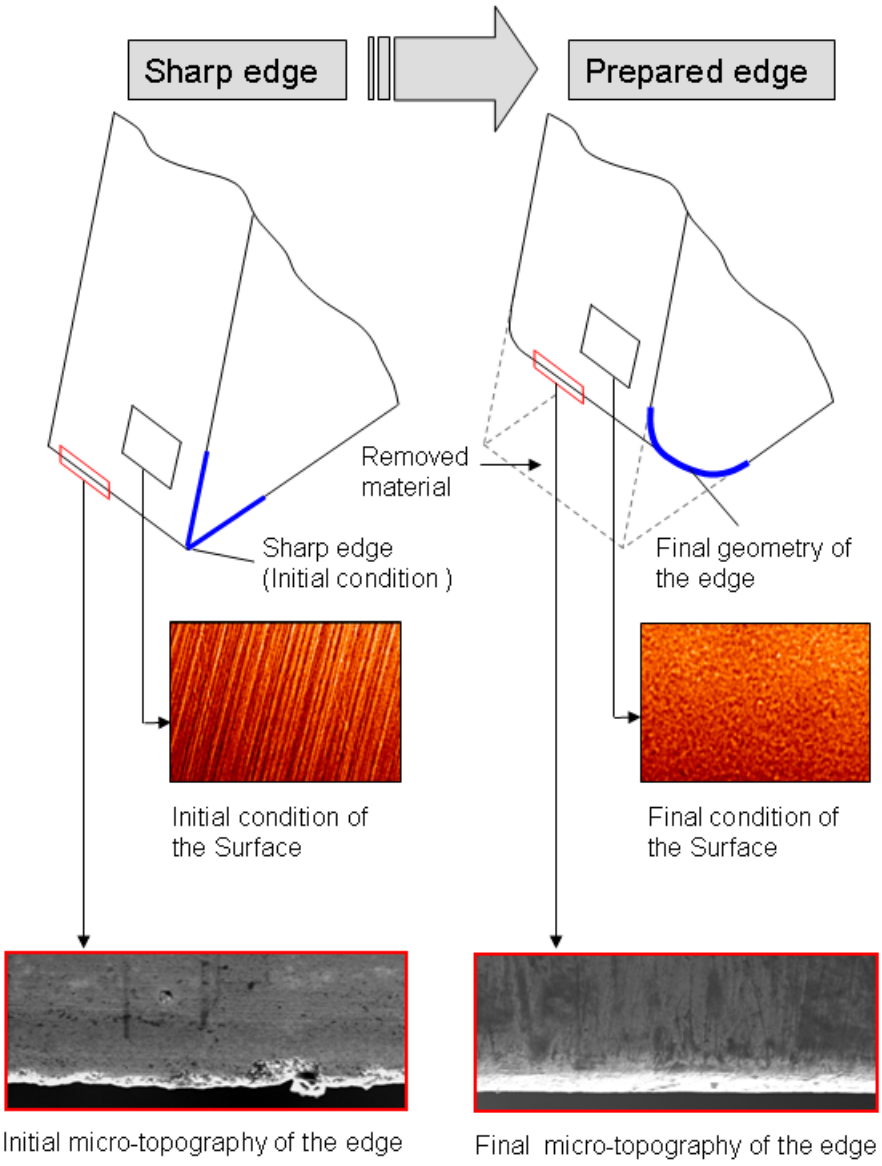

Figure 3-2: Aspects to consider in cutting edge preparation

microscopic in size, such defects lead to erratic tool performance and premature tool failure. Typical edge defects in a sharp cutting edge (without preparation) may be micro-breakages, burrs, burns, poor surface roughness and irregularities, which generate low mechanical resistance, susceptibility to chipping and unstable cutting. Therefore, these defects must be eliminated to achieve optimum tool performance.

Proper selection and application of cutting edge preparation is one of the basic ingredients for a successful development of the cutting tool. As proposed in [170], the cutting edge preparation and its characteristics associated with edge geometry and micro-topography of tool surfaces play an important role in the development of precision cutting

tools. In recent years, the interest in understanding the effects of the edge preparation has increased in response to a variety of emerging machining techniques, such as finish hard turning [172] and micromachining [40]. In these machining operations, the uncut chip thickness is often on the same order of magnitude as tool edge dimension. Additionally, the role of the cutting edge geometry (especially the rounding radius) is considered in HSC (high speed cutting)[9]. On the other hand, in the context of the conventional machining, it is very important to consider the effect of the cutting edge on the cutting process, because the geometry of the edge influences, among other characteristics, the tool life and the quality of the workpiece. Recently, cutting edge geometry and preparation processes have been intensively studied, because it is possible to have a large relative improvement in the reliability of the cutting tool and quality of the workpiece by applying an adequate cutting edge preparation process. In general, these have a low initial investment and low relative operation costs compared with the rest of the processes used in the manufacturing chain to produce coated precision cutting tools.

The systemic and controlled application of the the cutting edge preparation process has several main purposes:

- To add strength to the cutting edge
- To minimize the edge chipping
- To eliminate previous defects of the cutting edge
- To increase tool life
- To prepare the tool surfaces for coating deposition
- To improve part quality (accuracy, surface finish)

The above-mentioned can be achieved due mainly to the influence of the cutting edge geometry on the thermomechanical aspects of the cutting process. Moreover for the effect of the cutting edge preparation process on the micro topography of the edge and on the surfaces of the cutting tool. Regarding the thermomechanical aspects of cutting, the cutting edge geometry influences the shape of the deformation zones, the distribution of temperatures, the cutting forces and the distribution of stresses. These effects in turn affect chip formation and flow, surface integrity of the workpiece (e.g. residual stresses), surface roughness of the workpiece, tool wear resistance and tool life. Additionally, the cutting edge preparation process affects the micro topography of the cutting edge surface (notchedness) and the roughness and texture of the tool flank and tool face in the vicinity of the edge, as well as the surface integrity of the cutting tool. These effects produce changes that influence the friction coefficient between tool and chip and workpiece and additionally generate a microstructuring to guarantee the adequate adhesion of the coating.

Tool edge preparation is a prominent area to pursue. The overall confidence in new tool materials and coatings will grow if users can be certain that no catastrophic failures will occur. In such a case an appropriate cutting edge preparation can be a decisive factor.

3.2 Cutting edge preparation geometries

To specify the form of the cutting edge, tool designers and manufacturers provide various possibilities of tool edge geometries, which are commonly referred to as tool edge preparation. **Figure 3-3** illustrates the major types of edge preparation design that are used in most commercial precision cutting tools. In general there are three types: sharp edge, rounded edge and chamfered edge in addition to combinations between chamfered and rounded edges.

The sharp edge is defined theoretically by the intersection of the tool face A_γ and tool flank A_α. The rounded edge can have variants depending on the form of the profile that connects A_γ and A_α. If the curvature of the rounded profile, that joins A_α and A_γ, is relatively uniform without strong variations along the profile, a nominal single radius r_n is considered. On the other hand, if the rounded profile has a strong curvature variation, two geometries are considered: trumpet form or waterfall. In the trumpet form, the curvature is bigger at the end of the profile that connects with the tool flank A_α and the curvature is smaller at the end of the profile that connects with the face A_γ. In contrast, in the waterfall geometry, the curvature is bigger at the end of the profile that connects with the tool face A_γ and the curvature is smaller at the end that connects the tool flank A_α. The rounding lengths s_α and s_γ delimit the joint points of the rounding profile with tool flank and tool face.

Regarding the chamfered edge, the geometry is generated by a plane surface (chamfer or land) that join the tool flank A_α and the tool face A_γ. The chamfer or land, is delimited by the length of the chamfer b_n or length of land b_γ and the chamfer angle γ_b. In addition, combinations of rounded and chamfered edge are used. **Figure 3-3** shows an example of rounding added to a single chamfer. Likewise, designs of rounding added to double chamfer have been used for precision cutting tools.

Commonly applications of rounded cutting edges are finish cutting, semi-finish cutting, precision machining, and micromachining. In contrast, chamfered cutting edges are often used in hard turning, heavy rough cutting, and interrupted cutting [23, 52]. Chamfered edges are commonly employed on CBN (cubic boron nitride), PCBN (polycrystalline cubic boron nitride) and ceramic tools. Rounded edges are commonly employed on diamond, PCD (polycrystalline diamond), HSS (high speed steel) and cemented carbide tools.

It is usual for a sharp edge obtained by grinding of HSS or cemented carbide tools to have radius $r_n \leq 5$ μm, but greater values can be obtained depending on the grinding process parameters. As a general reference, prepared rounded edges obtained for typical

preparation processes (micro blasting, brushing or drag finishing) can have radii in the interval of 5 μm $\leq r_n \leq$ 50 μm, although greater values are also possible ($r_n \approx 100$ μm) depending on the application. Cutting edge radii are usually much smaller for HSS tools than the one applied on carbide tools because of the higher bending strength (4800 MPa for HSS against 1600 MPa for cemented carbides) [134]. In the case of CBN tools, the bending strength is quite inferior to one of carbide substrates (570 MPa for CBN versus 1600 MPa for cemented carbides). Under such conditions, the prepared geometry of the cutting edges must induce compressive stresses inside the substrate, and these stresses should be oriented to the bulk material. As a reference, the length of chamfer (or land) is in an interval of 30 μm $\leq b_n \leq$ 300 μm and the chamfer angle in an interval of 10° $\leq \gamma_b \leq$ 45°. A typical example of edge geometry of a CBN tool would be a chamfered edge with b_γ = 150 μm and γ_b = 15° or double chamfered edge with b_γ = 150 μm, b_n = 35 μm, γ_{b1} = 15° and γ_{b2} = 30°. Additionally, a rounding of $r_n \approx$ 20 μm can be added to the chamfers.

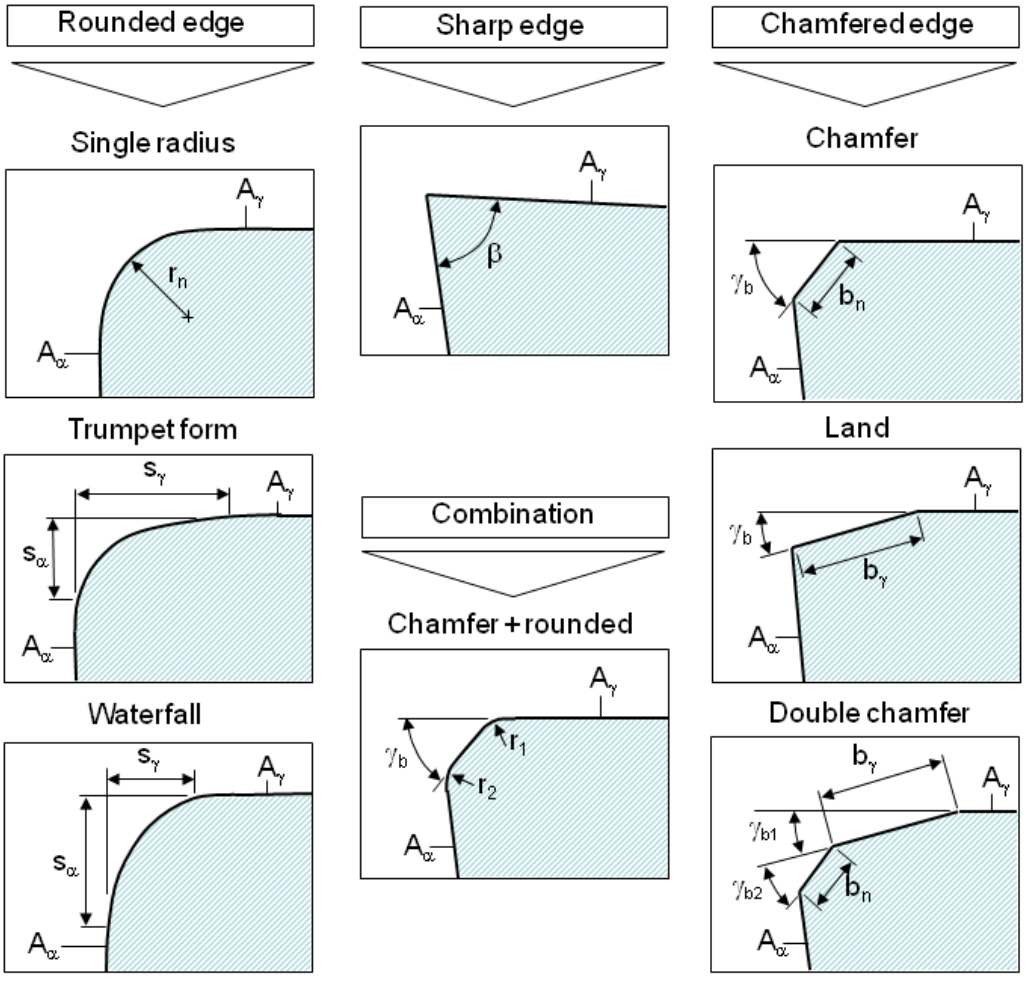

Figure 3-3: Typical cutting edge preparation geometries

3.3 Factors influencing the cutting edge geometry

In order to define the adequate cutting edge geometry and preparation for a specific application, it is required to consider the following aspects (see **Figure3-4**): initial condition of the cutting edge, type of machining process, process parameters, size effect and/or micro-machining aspects, workpiece material, tool material (substrate), tool macro geometry and required coating.

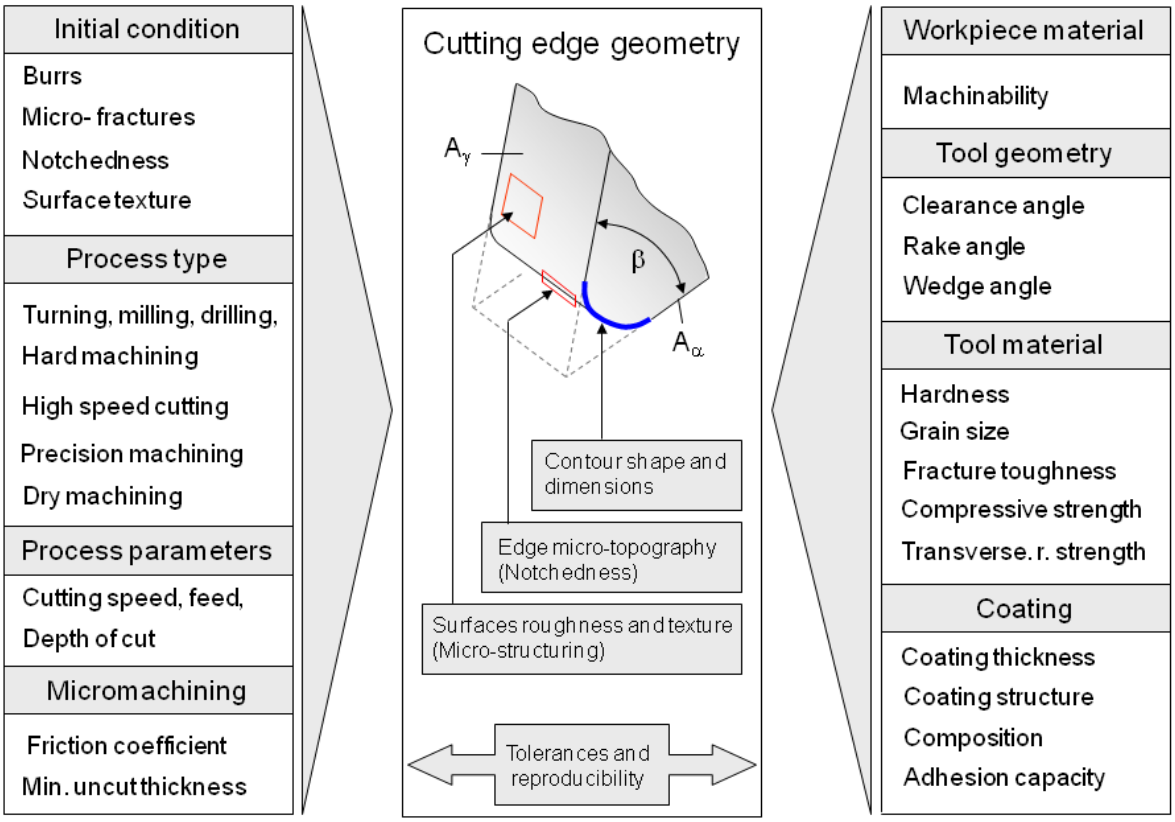

Figure 3-4: Factors influencing the selection and design of the cutting edge geometry

The selected or designed cutting edge preparation should satisfy several requirements. Considering the initial condition of the cutting edge, edge defects and irregularities and surface defects should be eliminated, hence the removed material in the preparation process should be enough to correct the most important defects that influence the final performance of the cutting edge. Additionally, the geometry of the edge contour should be adequate to support the forces and dynamics loads generated by the machining process and the combination of cutting parameters. The above-mentioned aspects of designing the edge contour are also related with the properties of the tool material and the machinability of the workpiece material.

The friction coefficient and the shape and dimensions of the contour determine the

minimum uncut thickness available. Therefore in addition to the contour design, the micro-topography of the edge and the micro structuring of the face and flank should be considered in order to define the conditions of the tool-chip and tool-workpiece contact and friction.

The edge geometry should be in accordance with the macro geometry of the cutting tool. The angles α, β, and γ limit the geometry of the contour. For example, with a small value of γ there is a more severe stress distribution on the edge compared with the stress distribution on the edge for a big value of γ as a result the shape and dimensions of the edge contour can be used to reach an adequate condition of distributed load on the edge.

The coating composition and structure of the layers and the required coating thickness define the dimensions and tolerances of the contour as well as the required micro structuring of the tool surfaces to guarantee the required adhesion.

3.4 Influence of the cutting edge preparation in machining

The cutting edge preparation process generates the contour of the cutting edge, changes the micro topography of the cutting edge, and also modifies the micro-structuring of the surfaces in the vicinity of the edge. These aspects of the cutting edge preparation influence the cutting process. As a result consequences on the tool performance and workpiece quality are observed. **Figure 3-5** shows a chain of influences, effects and consequences of the edge preparation on the machining process.

The cutting edge preparation geometry influences the thermomechanical aspects of the cutting process:

- Shape of deformation zones
- Distribution of temperatures in cutting
- Cutting forces
- Distribution of stresses in cutting

These effects in turn affect:

- Chip formation and chip flow
- Surface integrity of the workpiece (e.g. residual stress)
- Surface roughness of the workpiece
- Tool wear resistance

The above-mentioned effects on the cutting process result in increasing the tool life, increasing the tool reliability and improving the workpiece quality.

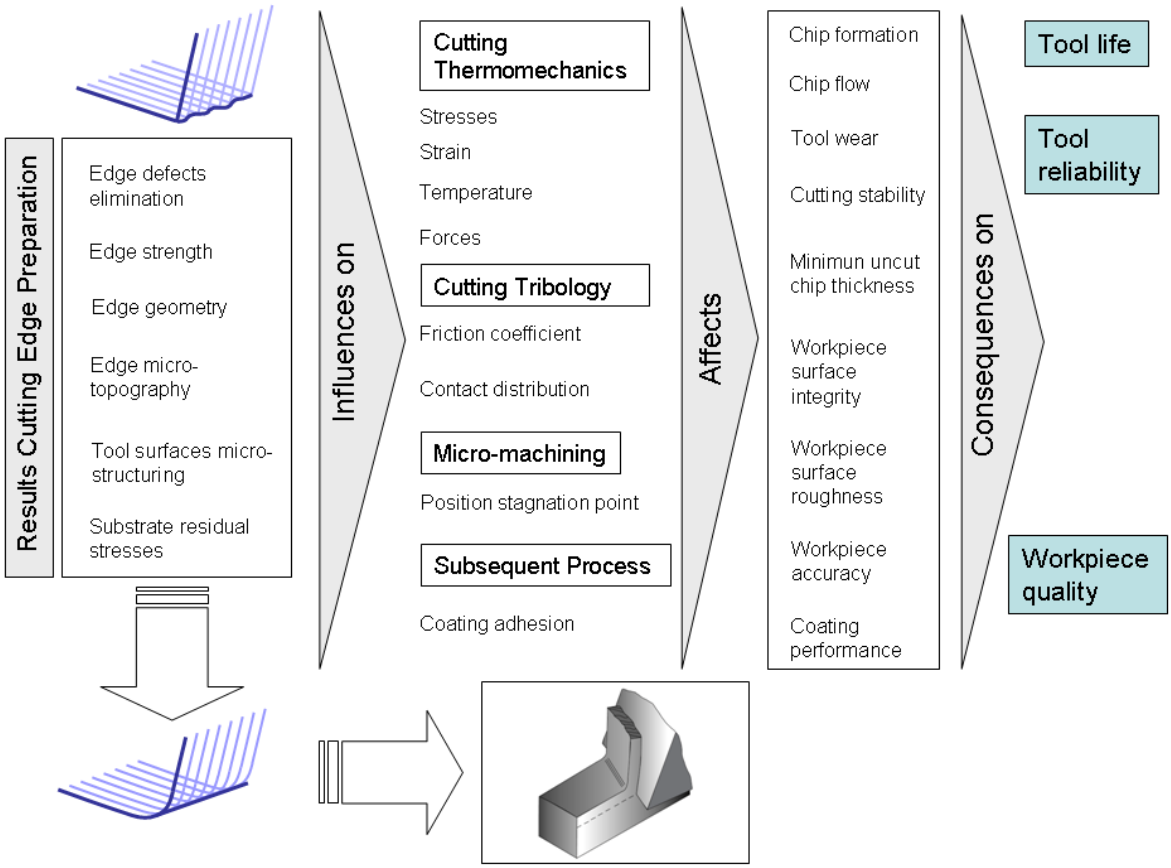

Figure 3-5: Influence of the cutting edge preparation on the machining process: chain of effects

3.4.1 Size effect and micromachining

Cutting tools commonly used in machining operations are never ideally sharp but always have some bluntness. The bluntness can often be approximated ideally as a circular radius between the flank and rake faces of the tool as illustrated in **Figure 3-6**. Since the cutting edge is closest to the root of the developing chip, the edge geometry can be expected to play a significant role in affecting the deformation process occurring at the chip-root. Most of the reported models of cutting are based on the assumption that the cutting tool edge is perfectly sharp [4, 14, 25, 124, 177]. The application of these models is sufficiently valid for a case in which the magnitude of the cutting edge radius r_n is quite small compared with the uncut cutting thickness h (the ratio r_n/h tends to zero). Otherwise, it is required to consider the effects of the geometry of the cutting edge to predict the behavior of the cutting process.

Alternatives to include the ratio r_n/h and the effect of the cutting edge geometry in the modeling of the cutting process have been proposed. A slip-line model for machining considering the effect of tool roundness has been proposed in [49, 50, 51]. This model

simultaneously accounts for other effects that commonly occur in machining such as shear zone, chip up-curl, tool chip contact, chip-groove, material pre-flow (pre-deformation) and size effect. In addition, other machining variables can be simultaneously predicted such as cutting force, plowing force, chip thickness, shear strain and shear strain rate. Specifically the analysis of the size effect [50] is suggested that the cutting tool edge roundness be comprehensively defined by four variables: edge radius r_n, position θ_s of the stagnation point on the tool edge (see **Figure 3-8**), and the tool-chip frictional shear stresses above and below the stagnation point. Likewise, a model of the effects of chamfered and honed tool geometry has been proposed in [52], in order to cover different possibilities of cutting edge preparation.

In addition, finite element models have been applied to study the effect of the rounded cutting edge in the machining process. A model to analyze the chip formation and growth in micromachining to obtain the Von Misses effective stresses, maximum shear stresses, hydrostatic stresses and deformation during the cutting process was proposed [197]. In this study, it was found using the arbitrary Lagrangian-Eulerian method that chip is formed through material extrusion upper critical $r_n/h > 1$. The changes in chip formation behavior are driven by intense deviatoric and hydrostatic stresses that are highly localized around the deformation zone. The onset on such chip formation mechanism is signified with a constantly changing negative effective rake angle γ_e that becomes stable in a later stage when chip formation reaches a stable tool-chip contact length.

The size effect in metal cutting is characterized by a nonlinear increase in the specific cutting energy u_c, i.e. energy per unit volume with decrease in uncut chip thickness h. These aspects are analyzed by a finite element model[105] that considers the size effect in orthogonal micro machining, principally the influence of the cutting edge radius r_n, which purportedly affects the micro-cutting process by altering the effective rake angle γ_e, enhancing the plowing effect or introducing an indenting force component. Similarly, finite element method and experimental analysis [86] were used to observe the effect of the edge radius in the cutting forces, effective strain rate and temperature distribution in orthogonal cutting for carbon steel.

The effects of different cutting edge preparation of the cutting tool (round/hone edge and T-land/chamfer edge) upon chip formation, cutting forces, and process variables (temperature, stress, and strain) in orthogonal cutting were simulated with finite element method [203]. The results obtained from this study provide a fundamental understanding of the process mechanics for cutting with realistic cutting tool edges and may assist in the optimization of tool edge design. Also, using finite element simulation was observed the influences of the cutting edge radius on the cutting forces, temperatures and maximum temperature allocation [25]. Additionally, finite element analysis for specific process modeling [149], considering edge preparation, has been proposed to predict process variables in two-dimensional orthogonal turning and three-dimensional face milling operations and to compare with published experimental data.

Modeling and experimental research has been reported for specific processes consi-

dering edge preparation. For example for drilling, [93] and micromilling [81, 99], among other aspects, the size effect, chip formation, minimum chip thickness and material strengthening are studied.

Considering the application in precision machining, a model of micro-cutting [84] was proposed and compared with the well-known Merchant′s model. The effect of the edge radius on crack initiation and cutting conditions as well as the influence of the ratio r_n/h in nano-cutting have been analyzed by means of molecular dynamics [21].

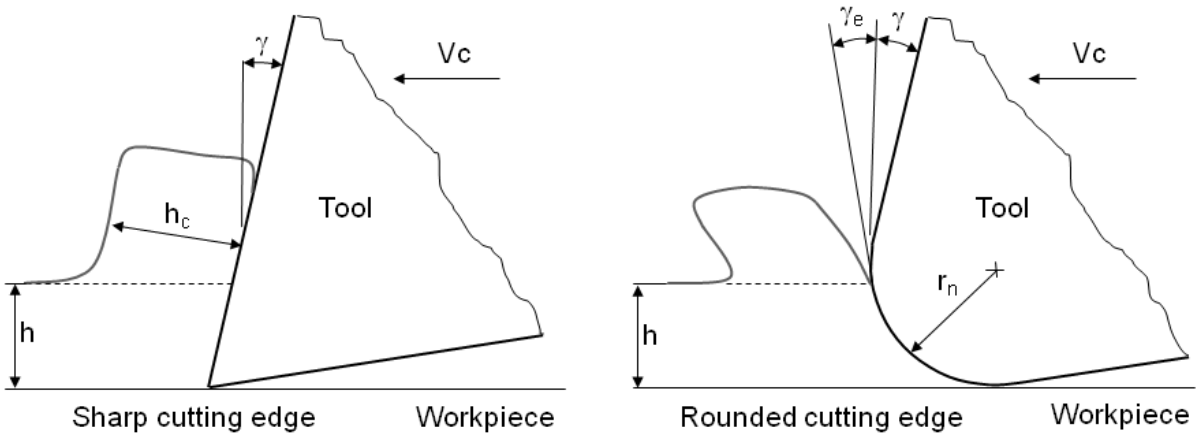

Figure 3-6: Theoretical assumptions about the cutting edge geometry

When the magnitude of the uncut chip thickness h is comparable to the cutting edge radius r_n, the effective rake angle γ_e is always negative, as is apparent in **Figure 3-6**, regardless of the nominal rake angle γ. Either it is positive, zero or negative. Because of the cutting edge radius effect, the effective rake angle γ_e of the cutting tool (see **Figure 3-6**) can be derived with the following equation [48]:

$$\gamma_e = -\frac{\pi}{2} + \cos^{-1}\left(1 - \frac{h}{r_n}\right) \tag{3-1}$$

An alternative equation for the effective rake angle γ_e is proposed in [172] for hard-turning:

$$\gamma_e = \arcsin\left(\frac{r_n - h}{r_n}\right) \tag{3-2}$$

In the cutting process, the resultant tool force F_r (see **Figure 3-7**) is distributed over the areas of the tool that contact the chip and workpiece. A cutting edge is not perfectly sharp and in the picture shown in **Figure 3-7**, the cutting edge is idealized by a cylindrical surface joining the tool flank and the tool face. As the cutting edge plows its way through the surface of the workpiece, the force that acts on the cutting edge is only a small proportion of the cutting force at large values of the undeformed chip thickness

h, but at small values of h, the force that acts on the cutting edge is proportionally large and must be considered [14].

Due to the high stresses acting on the cutting edge, deformation of the tool material may occur in this zone. This deformation causes contact between the tool and the new workpiece surface over a small area of the tool flank. When a sharp tool is used, a small frictional force acts in the tool-flank region. This force is a small proportion of the cutting force at high feeds. The force acting on the cutting edge and the force on the tool flank do not contribute to the removal of the chip. These forces are jointly called the plowing force F_p.

The existence of the plowing force F_p can explain the so called size-effect. This effect refers to the increase in specific cutting energy (the energy required to remove a unit volume of material) at low values of undeformed chip thickness h, corresponding to a high ratio r_n/h.

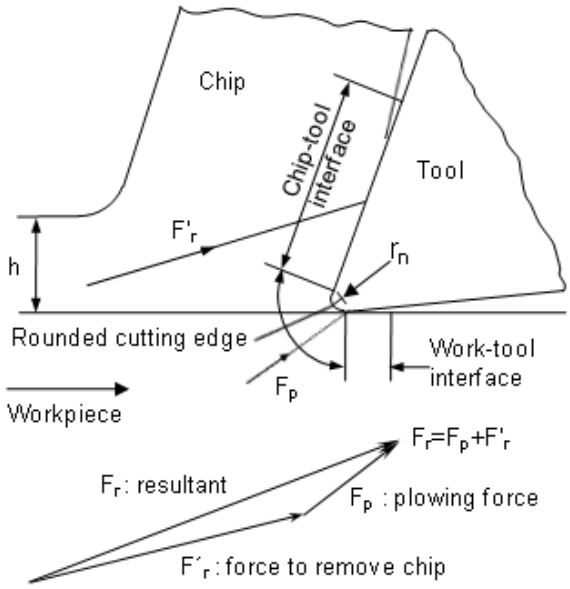

Figure 3-7: Plowing force and size effect (from [14])

The presence of the cutting edge radius r_n generates during the cutting process a material flow field (see **Figure 3-8**), in which is presented a stagnation point S. Above this point, material is assumed to flow into the chip, while below the stagnation point, it is considered to flow into the workpiece to form the newly-machined surface [164].

In micromachining, the cutting edge radius r_n tends to be the same order-of-magnitude as the uncut chip thickness h. Thus, a small change in the depth of cut a_p has great influence in the cutting process. The ratio r_n/h defines the active material removal mechanism either cutting, plowing or slipping, and in consequence the tool life and the resulting quality of the workpiece [40]. The concept of a limit or minimum chip thickness h_{min}, below

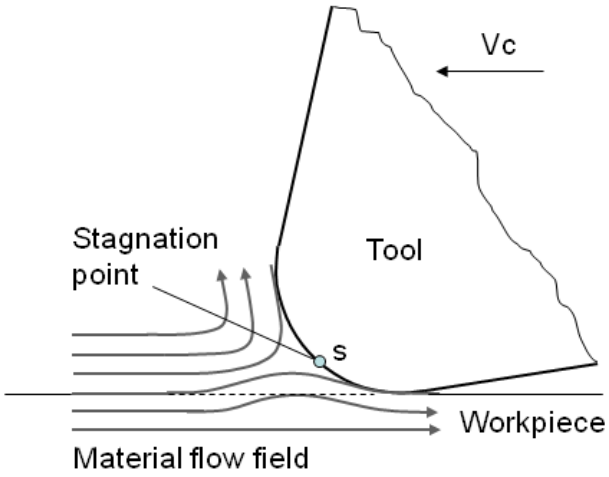

Figure 3-8: Concept of stagnation point

which no material removal occurs, has been considered in the research of the cutting process [157, 208].

The minimum cutting thickness available h_{min} depends on the cutting edge radius r_n and the physical relationship that occurs during the contact between tool and workpiece. **Figure 3-9** shows the relationship between h_{min}, the radius r_n the stagnation point S and the stagnation angle θ_s. During the cutting process, there are two forces acting at the stagnation point S: the horizontal force F_x and the vertical force F_y. These two forces can be divided into normal force N and tangential force μN, where μ is the friction coefficient between the cutting tool and the workpiece material. The minimum cutting thickness h_{min} is given by [208]:

$$h_{min} = r_n \left[1 - \frac{F_y + \mu F_x}{\sqrt{({F_x}^2 + {F_y}^2)(1+\mu^2)}} \right] \tag{3-3}$$

In the cutting process, the ratio F_y/F_x at stagnation point S depends on the mechanical properties of the workpiece material and the position of the point S. An empirical value of F_y/F_x is 0.8 to 1.0.

Measurements of the friction coefficient have been reported. For example, between Al-alloys and diamond, the measured value is 0.06 to 0.13 (varying with different crystal planes and different friction directions). It is important to note that there is a difference in the friction condition between a friction test and actual cutting process. For example, the value of μ in diamond cutting process can be considered twice as much as the measured friction test, therefore $\mu = 0.12$ to 0.26. Considering, for example, $F_y = 0.9\ F_x$ y $\mu =$ 0,12, it is obtained that $h_{min} = 0.322\ r_n$.

For cutting of steel with High Speed Steel (HSS) tools, h_{min} is 0.248 r_n to 0.274 r_n, and for cutting steel with cemented carbide tools, h_{min} is 0.350 r_n to 0.377 r_n. As general

reference, the minimum cutting thickness h_{min} is about 1/5 to 2/5 of the radius r_n of the cutting edge [208].

Furthermore, models of minimum cutting thickness have been proposed [157]. This model focus on the relationship between the friction coefficient of a tool-workpiece and the minimum cutting thickness. The theoretical model indicates that a smaller edge radius and a higher friction coefficient result in a thinner cut. As result of the model, a relationship is proposed among minimum cutting thickness h_{min}, edge radius r_n, and the friction angle ρ (associated with the friction coefficient μ). This friction angle has the same meaning that is given in the model of Merchant for orthogonal cutting (see **Figure 3-10**) [129, 172]. The minimum cutting thickness h_{min} can be written as [157]:

$$h_{min} = r_n \left[1 - \cos\left(\frac{\pi}{4} - \frac{\rho}{2}\right)\right] \tag{3-4}$$

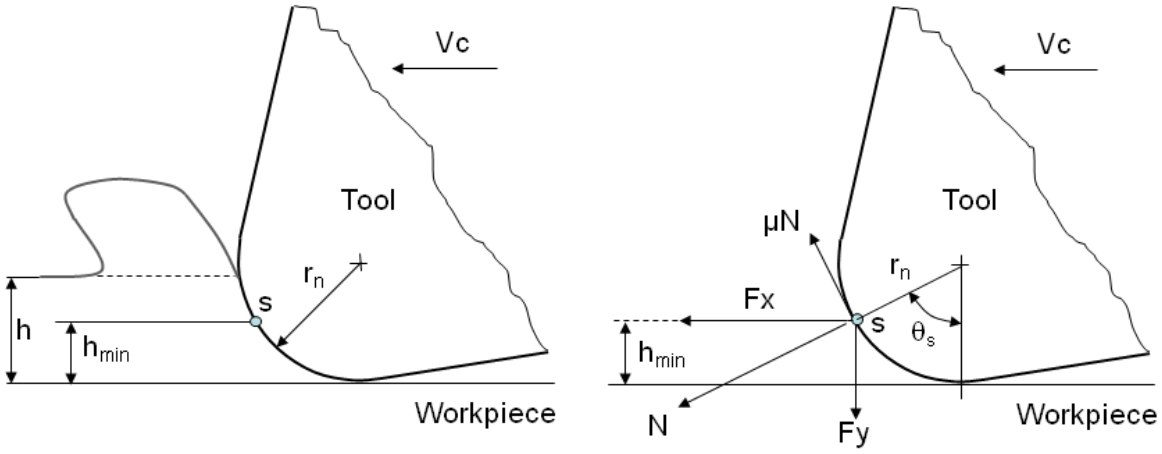

Figure 3-9: Minimum cutting thickness

3.4.2 Chip formation

The Merchant's model of cutting process (see **Figure 3-10**) considers a perfectly sharp tool and that the mechanism of chip formation is the shearing effect in the cutting zone (characterized by the shear plane), where the shear angle Φ is given as [124]:

$$\Phi = \frac{\pi}{4} - \frac{\rho}{2} + \frac{\gamma}{2} \tag{3-5}$$

Likewise, the shear angle Φ can be obtained as function of the rake angle γ, and the undeformed chip thickness h and the chip thickness h_c [129]:

$$\tan\Phi = \frac{\cos\gamma}{(h_c/h) \; - \; \sin\gamma} \tag{3-6}$$

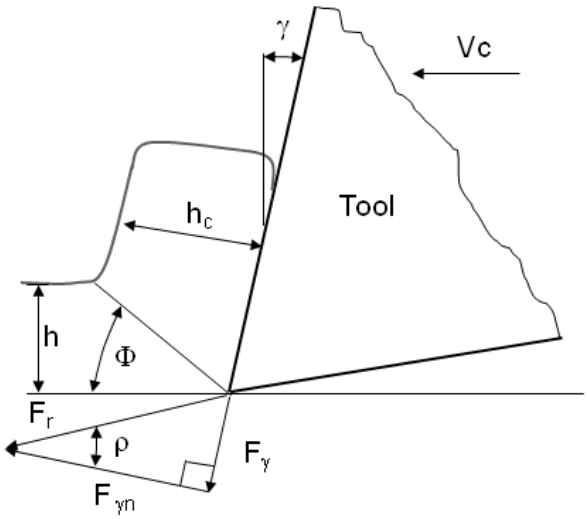

Figure 3-10: Cutting model according to Merchant

as a result, the chip thickness h_c is given as:

$$h_c = \ h \ \left[\frac{\cos\gamma}{\tan\Phi} + \sin\gamma\right] \tag{3-7}$$

Assuming a perfectly sharp tool, a model of chip formation with a parallel-sided shear zone was proposed by Oxley [49] as shown in **Figure 3-11**, where ΔS is the thickness of the primary shear zone. ΔS will reduce to zero if a perfectly sharp tool is assumed. In this case, the shear zone ($EFCD$) actually turns into a single shear plane. The original model proposed in **Figure 3-11** does not identify the point to which D would extent. On the other hand, a slip-line field model considering a rounded edge and three major shear zones (see **Figure 3-12**) was proposed by Fang[49]. This model clearly shows that point D would extent to a certain point on the round edge of a tool where a complex flow of material occurs. The model assumes that the chip deformation occurs in a shear zone $[AIBB_1A_2A_1A_3A]$ rather than on a parallel-sided zone or on a single shear plane. Additionally the model accounts for the chip-curling affect that often occurs in machining. This effect is caused by the convex slip-line AI. Likewise the model accounts for the material pre-flow effect in the shear zone. This effect is caused by the slip-line region AA_2A_3 as shown in **Figure 3-12**.

Considering the slip-line model for rounded edge tools (see **Figure 3-13**), the chip thickness h_c is given as [51]:

$$h_c = SB \cdot \ \cos\zeta_{SB} + \frac{BH}{2}\left[1 + \sqrt{1 + \left(\frac{\tau_{rake}}{k}\right)^2} + \frac{\tau_{rake}}{k}\right] \tag{3-8}$$

Where τ_{rake} is the tool-chip frictional shear stress on the tool rake; k is the average material shear flow stress; and SB, BH and ζ_{SB} (factor for tool-chip friction) are

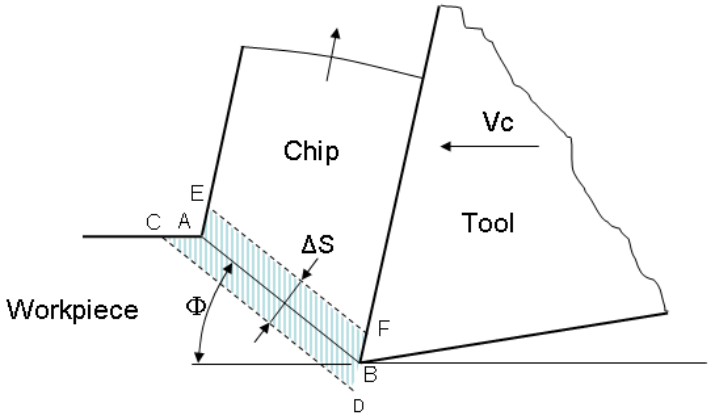

Figure 3-11: Parallel-sided shear zone (adapted from [49])

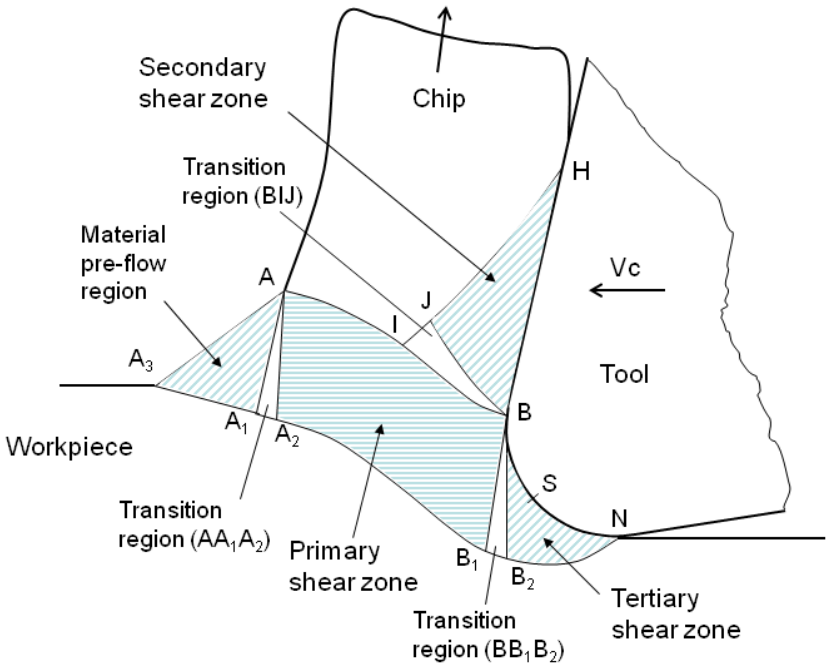

Figure 3-12: Shear zones (adapted from [49])

calculated as:

$$SB = 2 \cdot r_n \cdot \sin\left(\frac{\pi}{4} + \frac{\gamma}{2} - \frac{\theta_s}{2}\right) \tag{3-9}$$

$$BH = \frac{h + \sqrt{2} \cdot (\Delta S + SB \cdot \cos\zeta_{SB}) \cdot \sin\delta - r_n \cdot (1 + \sin\gamma)}{(\cos\zeta_{rake} + \sin\zeta_{rake}) \cdot \sin\left(\gamma + \zeta_{rake}\right)} \tag{3-10}$$

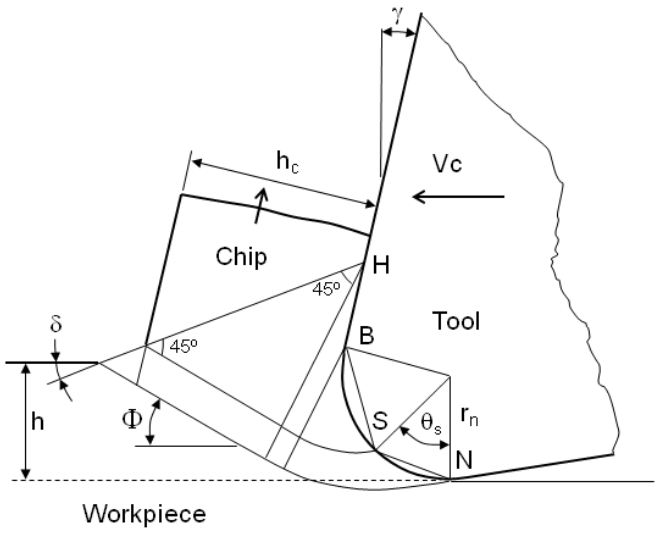

Figure 3-13: Cutting model with rounded edge (adapted from [51])

$$\zeta_{SB} = \frac{\arccos\left(\tau_{SB}/k\right)}{2} \tag{3-11}$$

$$\zeta_{rake} = \frac{\arccos\left(\tau_{rake}/k\right)}{2} \tag{3-12}$$

Where ΔS is the thickness of the primary shear zone, τ_{SB} and τ_{SN} are tool-chip frictional shear stress above and below the stagnation point S on the cutting edge, respectively.

ΔS is given as [49]:

$$\Delta S = \sqrt{2} \cdot r_n \left[\sqrt{1 + \frac{\tau_{SB}}{k}} \sin\left(\frac{\pi}{4} + \frac{\gamma}{2} - \frac{\theta_s}{2}\right) + \sqrt{1 + \frac{\tau_{SN}}{k}} \sin\left(\frac{\theta_s}{2}\right)\right] \tag{3-13}$$

The equation 3-13 illustrates the effect of tool edge edge radius r_n, rake angle γ, tool-chip friction (τ_{SB}/k and τ_{SN}/k) and position θ_s of the stagnation point on the thickness Δ_s of the primary shear zone.

3.4.3 Forces, strain and stresses

As expected, a precision cutting tool with an up sharp edge (radius $r_n \leq 5\mu$m) makes the cutting easier than a tool with a higher radius does. Thus, the stresses in the tool should decrease with decreasing the edge radius. Nevertheless, this is not the case, because a sharp tool, as expected, should have more stress concentration, especially in the vicinity of the cutting edge, than a less sharp tool. This stress concentration is likewise the cause of edge chipping and breakage and is the reason why edge preparation is used to relieve the stress concentration and strengthen the cutting edge. Therefore, to minimize cutting

edge breakage and chipping, the shape of the cutting edge should be optimized based on the balance between the higher stress concentration and the easier cutting (less induced stress) of the sharp tool and the lower stress and more difficult cutting (higher induced stresses) of the rounded tool.

It has been found that the shape of the cutting edge has more influence on the feed force than on the cutting force [149]. Regarding the effective strain rate, the deformation region extends deeper an more widely in the workpiece, but the maximum value decreases with increased tool edge radius [86]. Moreover, the chip thickness for a tool edge radius of r_n=100 μm is nearly equal to that for a tool edge radius of r_n=10 μm, which explains why an increase in the tool edge radius does not change the shear angle Φ.

Using a slip-line model [50], it is observed that the cutting force remains nearly constant, while the trust force increases with increasing the ratio r_n/h. The varying trend of the forces agrees well with experimental observations. Also with increasing ratio r_n/h, the plowing force increases and may reach as much as 40% of resultant force if r_n/h is large enough. This indicates that the tool edge radius plays a significant role in tool-wear and tool life. On the other hand, with an increase of r_n/h the ratio h_c/h decreases significantly and the ratio Δ_s/h of the primary shear zone increases significantly. Moreover, the average shear strain in the primary shear zone increases slightly and the average shear strain rate in the primary shear zone decreases non-linearly.

Recently, there have been increasing attempts to apply the finite element analysis to modeling the cutting process with non-sharp tools, largely due to the new techniques in adaptive remeshing functions and computational power. As example in **Figure 3-14** nodal displacements plots illustrate the chip growth and material deformation for different ratios r_n/h, and in **Figure 3-15** the Von Mises effective stress distributions are shown [197]. The FEM analysis has shown that concentrated shear at the primary deformation zone is absent at r_n/h >1, and additionally that extruded-like chip formation behavior is driven by intense shear and hydrostatic stress distributions that are highly localized around the deformation zone.

A finite element analysis was used to determine the stress distribution for various edge loads and varying microgeometries of the cutting edge for a saw tooth [3]. Sharp edge and cutting edge radii of 5, 15 and 30 μm were considered. The results of the finite element analysis show that the maximum principal stress decreases with increasing cutting edge radius and increases almost linearly with increasing undeformed chip thickness.

In addition, experimental techniques are used in order to determine the ploughing force induced by cutting edge radius and /or tool flank wear [65] and to observe the size effect produced for rounded cutting edges [111]. In contrast, a molecular dynamics simulation approach was used to analyze the effect of cutting edge geometry of cutting tool in nanometric cutting [94]. Cutting edge radii of 1.81 to 21.72 nm and depth of cut of 0.36 to 2.17 nm were considered for machining brittle materials. The reported simulation shows that while the forces increase with tool edge radius especially at the smaller edge radius (this is more pronounced in the case of thrust force than the case of

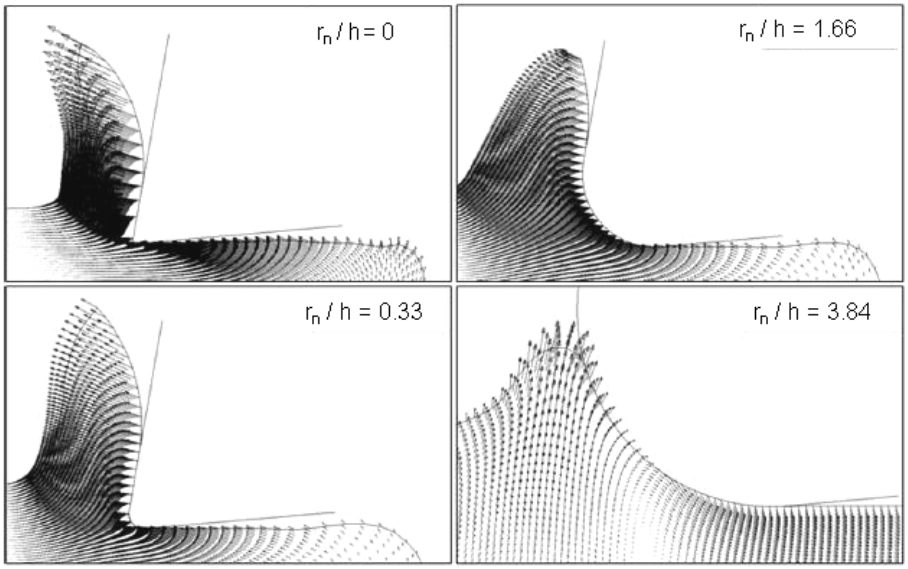

Figure 3-14: Chipgrowth at different r_n/h ratios (from [197])

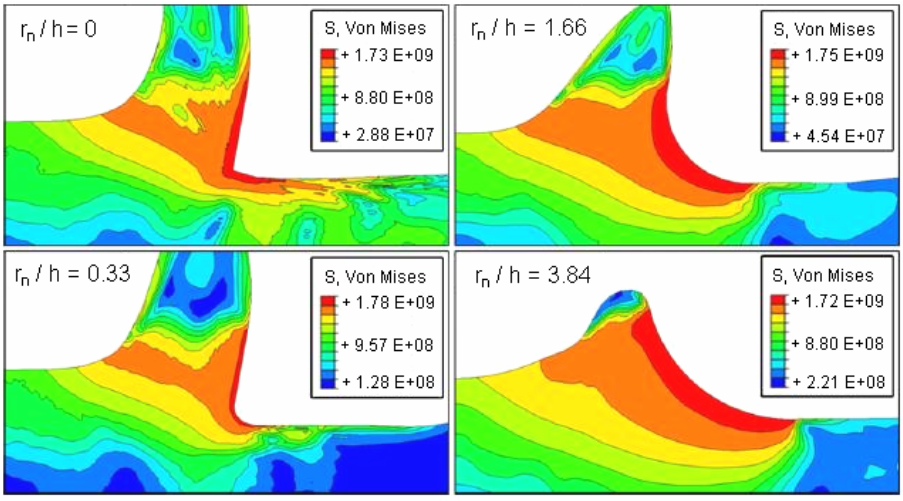

Figure 3-15: Von Mises effective stress distributions at different r_n/h ratios (from [197])

cutting force) they become independent of the edge radius at higher values of edge radius. This is because at higher values of tool edge radius, the equivalent negative rake angle is high and varies in a narrow range, while at the lower values of edge radius, it varies significantly. Also, at the higher edge radius, the ratio of the thrust to the cutting force remains constant, while at the lowest edge radius, they increase with increases in the edge radius.

3.4.4 Heat and temperature distribution

The ratio r_n/h can displace the maximum temperature field from the rake face to the clearance face [25]. Simulations using the finite element method considering an uncut chip thickness h= 50 μm, for different cutting edge radii r_n=5 μm, 60 μm and 120 μm, have showed that at r_n= 5 μm , with $r_n/h \ll 1$, the maximum temperature field is placed at the rake face. At r_n= 60 μm , with $r_n/h \approx 1$, the maximum temperature field is found on the cutting edge, and at r_n= 120 μm, with $r_n/h \gg 1$, the maximum temperature field is located on the clearance face. Similarly another study [86] concluded that increased cutting edge radius r_n causes change in the temperature distribution of the tool, particularly in the position of maximum temperature; the maximum temperature occurs along the cutting edge in a case in which the ratio r_n/h is comparatively greater. **Figure 3-16** shows the temperature ϑ in the cutting tool obtained by finite element analysis, considering a cemented carbide tool and 0.2% carbon steel as workpiece material.

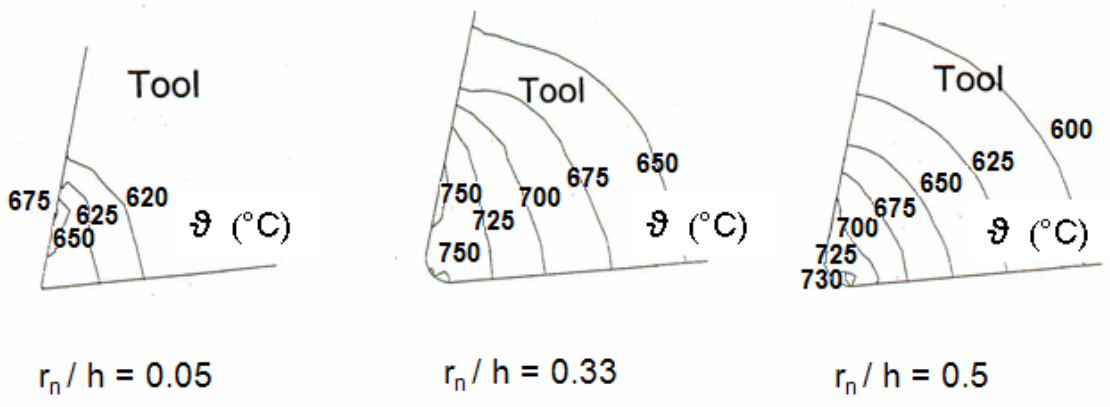

Figure 3-16: Tool temperature distribution for different r_n/h ratios (from [86])

Likewise, the effect of the cutting edge radius on the tool-chip interface temperature has been analyzed by cutting simulation [202]. Steel AISI- 1020 was used as workpiece material and uncoated cemented carbide was used as tool material, cutting edge radii of 10, 50 and 100 μm were considered, and a cutting speed of 130 m/min, feed of 0.2 mm/rev and uncut chip thickness of 200 μm were selected as cutting parameters. From the simulation can be observed that the magnitude of the maximum tool temperatures near the tool tip (∼650°C)is not sensitive to the size of edge radius. A minimum seems to appear at a moderate edge radius (r_n= 50 μm) while the average rake temperature is monotonically increasing with edge radius.

Additionally, a finite element model and a set of orthogonal cutting experiments were used to determine the effect of the cutting edge preparation of CBN cutting tools on orthogonal high speed machining of AISI-H13 steel (chromium hot work steel)[125]. The finite element model predicts temperatures developed at honed (r_n= 20 μm) and

chamfered (25°,100 μm) CBN tools. Results from the simulation show that honed CBN tools generate lower cutting forces, but higher rake face temperatures. On the other hand chamfered CBN tools resulted in lower temperatures on the rake face. The temperature generated at the chip-tool interface was found to be substantially higher than the other temperatures, an it is located about 0.10-0.15 mm distance from the cutting edge.

Finally, the effect of cutting edge preparation on tool temperature was observed by using the technique of mapping isotherms on the lateral face of the tool in single point turning using dedicated infrared CCD sensors [114]. Quenched and tempered steel was used as workpiece material in combination with a cemented carbide insert P20 as tool material. In all cases, the maximum temperature point was found on the rake surface. The investigation showed that the maximum temperature on the rake surface was higher for a tool with 150 μm flank land than for a round (r_n= 25 μm) and a sharp insert (r_n= 2 μm). The temperatures were 920°C , 860°C and 850°C, respectively. An increase in radius or flank land promotes an increase in secondary shear zone thickness. As a result of a larger plastic deformation zone will lead to more heat generation at the tool-chip interface and consequently higher temperatures.

3.4.5 Wear and tool life

The development of flank wear and tool life are affected by the geometry of the cutting edge, specially the cutting edge radius, and the preparation process used to round the cutting edge [15, 106, 135, 136]. The influence of the edge radius r_n on the tool life of sintered carbides was observed by turning steel (HBN=208) with a cemented carbide tool (P10) [20]. The results showed that the greater the radius r_n, the longer is the tool life until a limit value of the radius is reached. Moreover, the obtained results confirmed that the Weibull distribution is the best suited to describe the stochastic phenomenon of tool life, and the parameters of the distribution change with the edge radius. It can also be observed that sharp edges have a great scattering on tool life to fracture, and an optimum value of the radius exists allowing a maximum tool life.

In addition, the wear behavior of PM-HSS milling inserts with different cutting edge radii tested in industrial conditions was examined [136]. The radii were obtained by microblasting or by honing (by means of abrasive flow machining). The experimental results showed the effect of edge radius r_n on the performance of milling inserts. A radius on the cutting edge prevents fast and unpredictable wear. Moreover, the existence of an optimum value of the radius has been revealed experimentally. The performance of the PM-HSS inserts was analyzed experimentally by face milling in an annealed case-hardening steel. The modifications of the edge radius r_n and the modifications of the surface texture are the main criteria influencing the wear resistance. The best performance in dry milling was found for honed tools with a cutting edge radius of 10 μm, which can increase the tool life of a usual ground tool by a factor of 4-5. This cutting edge radius prevents the PM-HSS cutting tool from chipping of the substrate and from fatigue fracture

of the coating in high speed dry milling.

The influence of cutting edge preparation on the wear resistance of gear hobs made of PM-HSS was studied in the context of dry high-speed manufacturing [135]. The cutting edge preparation was carried out by means of microblasting and abrasive flow machining (AFM). The experimental results showed that a cutting edge radii r_n around 10 and 20 μm result an optimum tool life. On the contrary, smaller radii (around 5 μm) and larger radii (around 30 μm) seem to worsen the wear resistance. Moreover, considering the preparation processes involved, it seems that AFM yields better results compared to the microblasting process. Specifically, a comparison by testing cutting edges with r_n=10 μm, obtained by microblasting and AFM show very different results. This may be attributed to the influence of these processes on the surface texture. Indeed, the AFM process results in a better surface roughness. With a higher roughness of the cutting tool, the interface between the cutting tool and the work-material has a lower real area of contact compared to a perfect contact. Even if the average stress in the contact region can be considered equivalent, the local stress at the peaks of the surface are much higher in the rough surfaces. As a consequence, the improvement of the surface roughness allowed by the AFM process tends to lower mechanical stresses inside the coating and inside the substrate.

Likewise, the fatigue and wear behavior of PVD coatings on cemented carbide inserts with various cutting edge radii was investigated experimentally in milling [15]. The inserts with cutting edge radii from 8 up to 35 μm were prepared by honing and microblasting. The results of this study show ways to increase the cutting performance of PVD coated tools through size optimization and appropriate manufacturing of the cutting edge roundness. The focused microblasting causes carbide removals in the transient cutting edge region and worsens the wear behavior. On the other hand, the manufacturing of rounded cutting edges by honing, in combination with the fact that large cutting edge radii (r_n=35 μm) reduce the tool mechanical stresses, contributes to increasing the life of the coated tool.

3.4.6 Machined surface roughness

The influence of the cutting edge geometry on the surface roughness has been studied in combination with workpiece properties and machining parameters [42, 118, 126, 167]. The effect of the cutting edge radius on the roughness for precision turning was analyzed experimentally [42], considering different values of feed (0.05 ,0.033 and 0.021 mm/rev), cutting speed (150, 180 and 210 m/min), corner radius (0.4, 1.2, 1,5, 2,25 and 3,0 mm) and cutting edge radius (7, 14 and 28 μm) for a combination of C60 as workpiece material and HS10 (DIN EN 10027) as tool material. From this analysis, an empirical relationship between the roughness R_t , feed f and cutting edge radius r_n was obtained [42]:

$$R_t = f(r_n, f) = k_3 \cdot {r_n}^{k_4} = (12\,f + 1.60)\,{r_n}^{0.4} \tag{3-14}$$

The constants k_3 and k_4 are determined experimentally and their values depend on the combination between workpiece material and tool material.

Also, an experimental investigation was conducted to determine the effects of cutting edge geometry and workpiece hardness on the surface roughness and cutting forces by hard turning used to finish steel workpieces [167]. CBN inserts with various representative cutting edge preparations and through-hardened steel bars were used as the cutting tool and workpiece material, respectively. A statistical experimental design was applied to determine the affects of the workpiece hardness and cutting edge geometry on the surface roughness and machining forces. The study reveals that the effect of cutting edge geometry on surface generation in hard turning is significant. Increasing the edge hone radius tends to increase the average surface roughness because of the increase in the ploughing component compared to the shearing component of deformation. The effect of workpiece hardness and edge geometry interaction on surface roughness was also found to be very significant. The effect of edge hone on the surface roughness decreased with increases in workpiece hardness.

Likewise, the effects of cutting edge geometry, feed rate, workpiece hardness and cutting speed on surface roughness were studied [126]. CBN inserts with two distinct edge preparations (honed and chamfer) and hardened steel bars were used. Two level fractional experiments were conducted and statistical analysis of variance was performed. The results have indicated that the effect of cutting edge geometry on surface geometry is remarkably significant. Honed (rounded) edge geometry and lower workpiece surface hardness resulted in better surface roughness.

In addition, for micro- and nano-machining , experiments were conducted to observe the influence of different cutting conditions on the surface roughness [118]. Aluminium used in the mold making industry for creating prototype molds was employed as workpiece material in combination with single diamond cutting tools. The results show that the machined surface at an undeformed chip thickness smaller than the cutting edge radius (10-60 nm) is rougher than at larger undeformed chip thickness for the considered cutting speeds (10 m/min - 150 m/min).

For conventional machining, the cutting edge radius has influence on the machined surface roughness. In general, the smaller the cutting edge radius, the smaller the surface roughness [208].

3.4.7 Surface integrity of the workpiece

Residual stress in the surface layer is an important criterion of surface integrity. It has been found that the residual stress of the machined surface is largely affected by the cutting edge radius r_n [208]. At the same depth of cut, the absolute value of residual stress varies with the cutting edge radius. A large cutting edge radius corresponds to a big residual stress. It has also been found that in certain ranges of depth of cut, for a determined radius r_n, the residual stresses reduces as the depth of cut decreases. However,

when the depth of cut reaches a critical value, the magnitude of the residual stress goes up as the cutting depth decreases. This is caused by the size effect of the removed chip. When the depth of cut is at the same order of magnitude of the cutting edge radius, the material is actually removed by the tool with a large negative rake angle. In this case the cutting process is accompanied by severe rubbing or burnishing action. The specific machining energy will increase dramatically and the material near the vicinity of the tool edge will be subjected to a large plastic deformation. As a result the magnitude of residual stresses will increase greatly.

To evaluate the effect of tool edge radius on the work hardening of the machine surface layer, the micro hardness of the machined surface was measured considering different cutting edge radii [208]. It can be seen from the reported experiment that the cutting edge radius exerts a great influence on the machined surface hardness. The hardness of the surface machined with a sharp tool is less than that machined with a rounded tool.

The effects of the cutting edge preparation on the surface integrity of the workpiece have been studied for turning INCONEL at high cutting speeds [26, 130]. In general, the machining condition of the highest cutting speed (475 m/min) and lowest feed rate (0.05 mm/rev) and low moderated depth of cut (0.5 / 0.75 mm) with a honed cutting edge induces compressive residual stress condition in the machined surfaces. Likewise, the influence of cutting edge radius on the machined surface of brittle materials was simulated for orthogonal machining [85]. The results show that for brittle materials, surface cracks increased with the edge radius when the depth of indentation was constant. Similarly, the effects of cutting edge radius on residual stresses by orthogonal cutting of stainless steel were modeled by finite element analysis [115]. The analysis shows that larger edge radius induced higher tensile residual stresses in the near-surface layer while the thickness of tensile layer was unaffected. Higher tensile stresses are attributed to the increase in workpiece temperature with edge radius, as more heat is generated when the friction contact area between the tool tip and workpiece increases. Larger edge radius induced higher compressive residual stresses, far from the surface, and moved the location of their maximum magnitude deeper into the workpiece. This can be attributed to higher material plastic deformation and more material being ploughed into the new machined surface.

Furthermore, the effect of feed rate, workpiece hardness and cutting edge geometry on subsurface residual stress in the hard turning of bearing steel using chamfer plus hone edge geometry was investigated by using the X-ray diffraction/electropolishing method [74]. The results show that an increase in hone cutting edge radius facilitates the compressive residual stress in the subsurface, but it also causes an increase in tool temperature. The effect of chamfer is equivalent to increasing hone radius. Therefore medium hone radius (20-50 μm)plus chamfer angle of 20° is recommended.

Additionally, the geometry of the cutting edge was optimized by using the finite element method based on the machined residual stresses generated in diamond turning [215]. The analysis shows that a rake angle of 15°, a flank angle of 10° and a smaller possible edge radius (100 nm) are the optimal geometry for a diamond cutting tool for

machining ductile materials.

3.4.8 Cutting edge geometry and high speed cutting

Different studies have considered the influence of the cutting edge geometry (mainly the radius r_n) in several aspects of the high speed cutting (HSC). For machining of light alloys (aluminum and magnesium)[146], a radius of 10 μm appropriate for HSC was selected, considering a later coating that generates an effective radius of 30 μm. With greater radii, considering the selected uncut chip thickness (20-100 μm), a strong increase of the cutting force and a deterioration of the surface roughness of the workpiece were reported when working with cutting speeds between 1200 and 4500 m/min. On the other hand, the stagnation zone in high speed drilling of steel working with cutting speed between 100 and 500 m/min was observed [195]. Likewise, the effect of the cutting edge radius and friction coefficient on orthogonal machining was considered by means of finite element analysis applied to the HSC-chip formation process [9]. In this study, using a cutting speed of V_c = 1000 m/min and radii r_n between 10 and 50 μm, friction coefficients $\mu \leq 0.3$ and uncut chip thickness h = 100 μm, cutting and feed forces were determined. Likewise, a linear change of the chip thickness h_c related to the the friction coefficient μ for different edge radii r_n was observed. A change of the edge radius and friction coefficient also influences the workpiece temperature. The temperature field is not stationary, and increasing the edge radius means also increasing the maximum temperature.

3.5 Cutting edge preparation and coating process

The cutting edge preparation process influences the micro topography of the tool edge and surfaces and the tool surface integrity. These influences in turn affect the adhesion and reliability of the tool coating. Preliminary surface and edge preparation before coating is needed not only for the required relief formation on the substrate surface, but also for an increase in the contact area and activity intensification [178].

Recently, the effects of the cutting edge preparation process on the superficial structure and on film adhesion was studied [18, 19] considering the behavior of grains of tungsten carbide (WC) embedded in Cobalt (Co) as binder. In this study the effects of micro blasting, polishing by disc lapping and their combination were analyzed. **Figure 3-17** shows the effects of the different treatments on the substrate surface. The radius of the WC grains r_c is shown to compare with the WC carbide revelation from the Co-binder phase corresponding to each treatment. If the micro-roughness R_t exceed the WC grain radius r_c ($R_t > r_c$) the carbides embedded in the Co-binder are deteriorated and an adhesive coating failure during cutting is expected. Another parameter to consider is the mean spacing between successive profile peaks R_{sm}, which is used to evaluate, in combination with R_t, the mechanical interlocking between coating and substrate. The adhesion decreased through the micro-roughness R_t diminishing and the R_{sm} growth, both reducing

the mechanical interlocking in the coating interface.

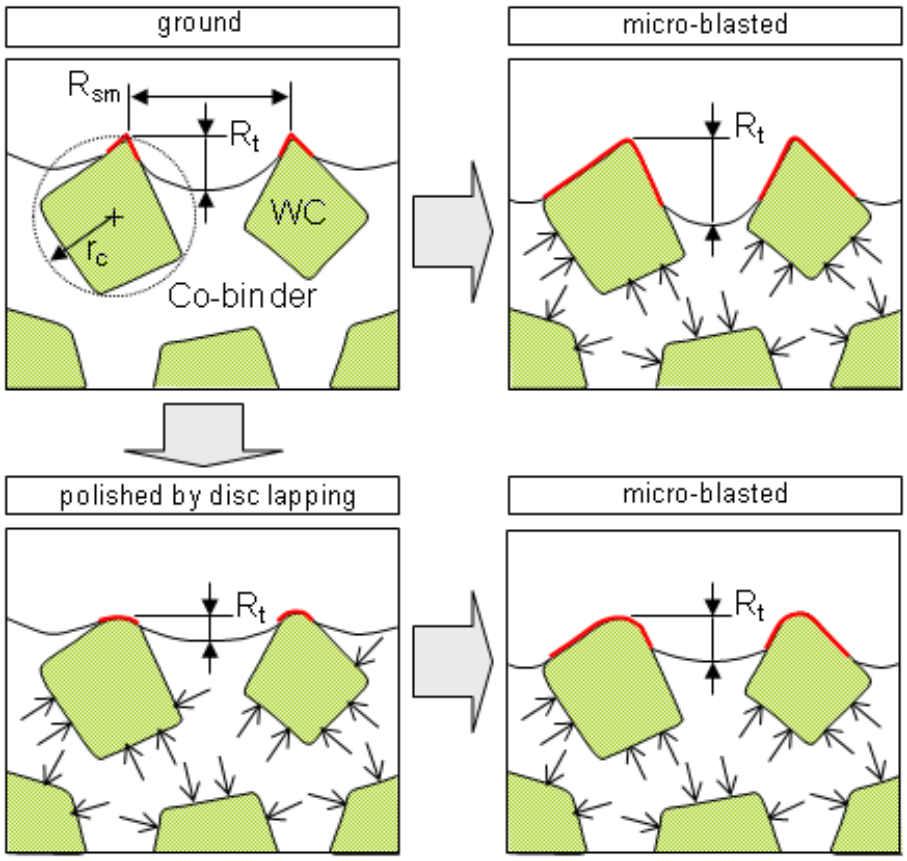

Figure 3-17: Effects of the cutting edge preparation on cemented carbide superficial structure and on film adhesion (adapted from [18])

Considering the different effects an increase of the R_t micro-roughness occurs by microblasting of ground surfaces because the individual WC carbides are revealed, through the Co-binder removal from the carbide surfaces. Moreover a lattice deformation of the WC-carbides is induced mainly by the Co-binder deformation. In this way, it can be assumed that during the film deposition, the nucleation rate of potentially formed transients junctions such as TiAlCN on the WC-carbide surfaces is increased, due to the WC lattice deformation, with accelerates the W and C atom movements in the film substrate interface. As a consequence, and adhesion improvement between the WC-carbides and the film, through potential transient junctions formation, acting as bonding material might occur. A corresponding mechanism was observed in the case of diamond coatings on carbide forming substrates, as for instance on tungsten.

On the other hand, after polishing by disc lapping, the carbides are rounded and Co-free WC surfaces restricted, moreover the R_t value decreases, thus deteriorating the film adhesion. Additionally, strong polishing increases the R_{sm} value of the ground surface, thus significantly reducing the film-substrate mechanical interlocking. However, through

micro-blasting of the polished surfaces, the described advantages of microblasting can be reobtained, but the micro-roughness R_t had to be less than the WC-carbide radius r_c ($R_t < r_c$) in order to attain a sufficient carbide embedment in the Co-binder. As complement, the R_{sm} value decreased after micro-blasting of ground and polished surfaces, resulting in a better mechanical interlocking between coating and substrate.

In brief, a fine balance between WC-carbides embedment and film-substrate mechanical interlocking is required. Through the control of the R_t and R_{sm} values it is possible to find the adequate combination in order to optimize the coating adhesion. Experimental and simulation analysis showed that microblasting of ground or polished substrate surfaces contributes to a coating adhesion improvement and a cutting performance increase [18]. The polished and microblasted substrate presented the highest wear resistance, and the poorest adhesion was obtained with the polished substrate, which had the most intense fracture propagation of the coating due to restricted film-substrate mechanical interlocking.

Similarly, other studies have been focused on the influence of the superficial structure obtained by microblasting on the formation of densely packed columnar grain structures within the coating and the reduction of delamination between the coating and substrate surface [103]. Moreover, the influence of the residual stress gradients generate by grinding, microblasting and water peening on the adhesion strength of hard coating has been analyzed [173, 176]. The study shows that steep residual stress gradients induced during grinding are modified by microblasting and water peening into flat residual stress depth profiles. This modified subsurface residual stress state is able to compensate higher tensile loads during cutting processes. An enhanced adhesion strength and better performance of the coated cutting tools can be achieved.

On the other hand, the improvement of the adhesion of diamond coatings on cemented carbides has been studied by using different surface and cutting edge preparation techniques. The application of microblasting has been analyzed using a surface morphology model [210] and experimentally by its application to milling tools [90]. Also, the use of water peening treatment as a preparation method for diamond coating has been reported [173]. Additionally, the effect of the microblasting on topography and adhesion of the coating has been analyzed by means of fractal analysis, in order to quantify the differences among the surfaces obtained by different combinations of process parameters [152].

Regarding the cutting edge geometry, the influence of the cutting edge radius of PVD coated inserts on the film fatigue failure was analyzed in order to find an optimum radius to avoid premature coating failure during milling [16].

3.6 Abrasion and erosion of cemented carbides

The mechanism for material removal of micro-abrasive jet machining (micro blasting) is erosion, and the mechanism for brushing-polishing and brushing with abrasive filaments is abrasion. In this section, some aspects of erosion and abrasion of cemented carbides are considered in order to understand the relationship among the variables to reach a systematic and controlled material removal required for cutting edge preparation.

Erosion is the gradual material removal from solid materials by means of fluids (gas or liquid) which may or may not transport external material as removal agent[27, 35, 53, 96, 180]. Abrasion is the gradual material removal that occurs when hard particles are rubbed across a surface [73].

When cemented carbides are subjected to particles carried in a low velocity air stream, the results suggested that erosion follows a rule of mixture; the erosion of the WC phase occurring by a Hertzian elastic fracture mechanism, and that of the Co phase by combined cutting and deformation mechanisms [10, 181].

The erosion rate, E, is commonly given in terms of mass or volume of material removed per unit mass of erodent impacted. E generally shows a power-law velocity dependence [96]:

$$E = k{v_a}^{n_v} \tag{3-15}$$

where k is a constant, v_a is the velocity of abrasive particles and n_v is a velocity exponent that generally depends on material and erosion conditions. The value of n_v falls in the range of 2 to 3.5 for metals, cermets, cemented carbides and ceramics.

Two major elastic-plastic theories of erosion have developed: the theory of Evans and the theory of Wiederhorn. The erosion rate predicted by Evans is given by [96]:

$$E \propto {v_a}^{3.2}{d_a}^{2/3}{\rho_a}^{1.3}{K_{IC}}^{-4.3}{H_m}^{-0.25} \tag{3-16}$$

while that predicted by Wiederhorn is [96]:

$$E \propto {v_a}^{2.4}{d_a}^{2/3}{\rho_a}^{1.2}{K_{IC}}^{-4.3}{H_m}^{0.11} \tag{3-17}$$

Where v_a , d_a, and ρ_a are velocity, diameter, and density of abrasive grains, respectively, H_m is the material hardness, and K_{IC} is the material toughness.

Regarding abrasion, the precise mechanism depends on the hardness of the abrasive particles relative to the bulk hardness of the cemented carbide. If the abrasive particle is hard, it can act as a cutting tool; it cuts craters or grooves in the surface that are much larger than the individual carbide grains. Material is removed by large plastic deformation that results in severe fragmentation of the carbide grains in the surface and in the extruded material [181].

There have been many attempts to predict abrasion rate. One of the most used is the Archard′s equation [43, 131]:

$$\frac{V}{S_d} = k\frac{L_a}{H_m} \tag{3-18}$$

This equation states that the volumetric abrasion rate, i.e. removed volume V per sliding distance S_d, is proportional to the applied load L_a and inversely proportional to the hardness H_m of the wearing material, where k is the dimensionless abrasion coefficient.

The properties of cemented carbide grades are predominately determined by their chemical composition and the grain size of the tungsten carbide in the sintered part [147, 44]. Abrasion resistance of cemented carbides decreases as cobalt content or grain size are increased [43, 140, 141]. The performance of carbides in erosion tests closely parallels their abrasion performance, although the effect of WC grain size is not strong as in straight abrasion. The erosion rate does, however, decrease slightly with increasing carbide grain size for cobalt percents greater than 15% [147].

3.7 Wear of hard metal cutting tools

For cutting tools, wear manifests itself primarily as crater wear and flank wear. Moreover, cutting tools may fail due to plastic deformation and fracture [82, 95, 172, 177, 195]. Three types of wear mechanisms generally accepted as major factors in cutting tool wear are abrasive wear, attrition wear, and diffusion wear.

For cemented carbides, the abrasive wear mechanism is most readily understood and has been studied in detail. Abrasive wear occurs when a hard particle is rubbed across a surface. Abrasive wear occurs in metal cutting when the material being cutting contains many hard particles. In steel and cast iron cutting, it is caused by carbides, nitrides, oxides, and non metallic inclusions present in the work-piece. When machining aluminium-silicon alloys, tool wear is almost entirely abrasive. Abrasive wear is very closely related to hardness of the tool material and, in consequence, to the composition and structural features that control hardness.

Attrition wear is associated to a wear process in which particles of microscopic size are detached from the tool surface and carried away in the stream of work material. Attrition wear is closely related to the more basic adhesive wear mechanism. It is due to the cold welding effect, which can occur readily in metal cutting especially at low speeds. Due to the cutting action, intermittent welding between tip and chip is inevitable under the high pressures produced. The motion of the work piece and chip continually breaks the resulting junctions formed and discrete particles of tool material are carried away. This type of wear seems to occur mainly by the plucking away of complete grains of WC. The wear rate is associated with grain size rather than hardness. A fine grain hard metal with 16% cobalt and hardness of 1265 HV shows better resistance to attrition wear than a coarser grain hard metal with 4.5% cobalt and a hardness of 1600 HV [181].

In diffusion wear the tool shape is changed by the diffusion of atoms into the work material, equivalent to a dissolution of the tool surface by the chip material flowing over

it. This depends on the solubility of tool material in the work material and the interface temperature obtained during cutting. The interface temperature is proportional to the cutting speed, and diffusion wear is a major factor limiting cutting speeds. The diffusion mechanism generates the cratering of the cutting tool. The cratering results from the diffusion of carbon from the cemented carbide to the steel chip sliding over the rake face of the cutting tool [181].

Wear can also occur as chipping along the cutting edge. Such chipping occurs more commonly when the cutting edge removes chips intermittently. This result in cycling impact and thermal loading of the cutting edge. These cyclic loadings can initiate small cracks and then propagate these cracks to form the chips [82].

Although adhesive and abrasive wear are predominant in flank wear, some diffusion also exists. There are different models proposed to calculate the tool flank wear rate that consider the effect of the combined mechanisms [108, 204]. Considering the complexity of the tool flank wear mechanism, an empirical model to determine the tool wear flank rate was proposed[108]. This model considers abrasive/adhesive and diffusion mechanisms, and it is expressed as:

$$\frac{d\,(VB)}{dt} = A \cdot \left(\frac{F_{cn} \cdot v_d}{H_t \cdot v_c \cdot f} \right) + B \cdot \exp\left(\frac{-E_a}{R \cdot T_f} \right) \tag{3-19}$$

Where A is the abrasive/adhesive wear constant and B is the diffusive wear constant, VB is the flank wear land width, F_{cn} is the normal cutting force, v_d is the sliding speed, H_t is the hardness of cutting tool material, v_c is the cutting speed, f is the feed rate, E_a is the process activation energy, R is the universal gas constant and T_f is the cutting temperature in the tool flank zone.

During the cutting process, the wear state of the cutting edge has a decisive influence in the structure of the surface of the workpiece. Form errors at the cutting edge and at the tool flank are reproduced on the surface thus a bad quality of the surface is generated [195]. The control of wear in cutting process is carried out by means of the adequate selection of cutting parameters, macro-geometry of the cutting tool, meso- and micro-geometry of the cutting edge, properties of the substrate, the topography of the tool flank and tool face, coating structure and coating materials and lubrication and refrigeration strategies.

4 State of the art

4.1 Measurement technology for the characterization of the cutting edge preparation

The detailed characterization of the cutting edge preparation implies the measurement of form characteristics in the order of micrometers and the topography and roughness in the order of one micrometer. The state of the art measurement technology of geometric characteristics (dimensions, forms and positions) and topography of the surfaces among 1 μm to 0.5 mm, includes tactile (stylus) as well as optical sensors and micro computer tomography [117].

Tactile sensors:

- Piezo-electric micro stylus
- Capacitive micro stylus
- Micro stylus with flat spring
- Micro stylus with solid joint
- Tactile optical micro stylus (fiber stylus)
- Ultrasonic micro stylus

Optic sensors :

a) Distance optic sensors

- Foucault sensor (Laser autofocus)
- White light chromatic sensor
- Spectral coherence interferometer (SCI)

b) Sensors for spatially distributed measurements

- Image processing sensor with video auto focus

- Color focus sensor
- Micro strip projector
- White light interferometer
- Confocal microscope
- X-ray micro computer tomography

For the analysis of the microstructuring of the tool face and tool flank, and for the description of the topography of the cutting edge, is required not only the information of the roughness profiles obtained by 2D profile sections, but also the information coming from 3D data that allows to determine the topography and elements of the structure and morphology of the surface from a functional perspective. The proposal of new parameters [148], obtained from 3D data and the development of the measurement technology that combines multi sensor approaches with image processing generates a new state of knowledge that allows the characterization of the cutting edge and the cutting tool surfaces.

The current development of optical methods based on chromatic sensors [56, 57, 58] in combination with other possibilities as confocal microscopy[189], white light interferometry and atomic force microscopy (AFM), allows a multi scale (mm, μm, nm) characterization by using a multi sensor approach to determine the 3D parameters that describes an engineering surface. With the 3D information it is possible to obtain contour and topography data.

Optical measurement devices, specially based on white-light interference microscopy and confocal microscopy [183] represent the state of the art in the 3D-measurement of workpieces in the microsystems technology [101]. For example, in [184], the characterization of a micro-tool by using scanning white light interferometry is reported. Additionally, the combined use of image processing and AFM, computer tomography and coordinate measurement allow the measurement from global object recording to local measurement, by means of multi-sensor technology, and a multi-scale strategy [191].

The measurement of cutting edge radius of micro end-mills in the order of 3 μm by means of SEM is reported in [47]. Likewise, the measurement of the cutting edge profile for a single diamond cutting tool by means of a combined sensor is achieved. An optical sensor based on a laser beam is used to align an AFM unit with the top of the diamond cutting tool edge [59]. By means of these sensor combination, cutting edge radii between 92 nm and 219 nm were measured. Similarly, a device based on a laser beam was used to characterize cutting edge radii smaller than 20 μm [166].

In [72] a method for measurement of the cutting edge of cemented carbides tool are presented. A confocal white light microscope was used for determining the cutting edge radius, the notchedness and wedge angle. Additionally, a method for determining the edge radius from 3D measurement data is reported.

The application of the computer vision for measurement of geometric characteristics has motivated the development of algorithms for the determination of the digital curvature [182]. Such algorithms can be applied to measure the curvature (or radius) of the cutting edge profile obtained by computer vision systems.

The application of the industrial 3D computer tomography [102] to measure the geometry of small components, is an interesting alternative for dimensional metrology applied to cutting edge characterization, principally to describe the contour.

The principle of stripe projection [196, 198] has been used to measure the geometric characteristics of relatively big components, with features in the order of millimeters to meters. With the recent advances in opto-electronics, the same principle has been used for measuring small characteristics in the order of magnitude of the roughness of the engineering surfaces. Specialized micro-stripe projection devices have been developed with the capacity to measure the cutting edge radius and the notchedness of the edge of precision cutting tools [61, 62, 209].

The white light chromatic sensor [56, 57, 58], micro strip projector [61, 62, 209] and the confocal microscope [72], represent, in their majority, the state of the art in the measurement of the cutting edge rounding for precision cutting tools, principally the geometry of the edge contour and the notchedness of the edge. Additionally, by means of these devices, can be observed the topography of the tool face and flank in the vicinity of the cutting edge.

The necessity to standardize the measurement of engineering surfaces in terms of areal parameters specially by using optical technology has generated the development of new definitions, concepts, measurement strategies, standards and calibration processes [75, 76, 77, 98], principally because the tactile and optical methods should be treated in different way. It is a serious mistake to try to calibrate optical instruments with tactile standards and vice versa. Both systems should be independently traceable to international standards [192, 193].

On some very fine surfaces, there is a considerable difference in value between an optical measurement and a stylus method. Invariable, the optical method gives a larger value than the stylus. This is because the stylus methods tends to integrate, whereas the optical method differentiates e.g. it enhances edges. These statements assume that the spot size of both methods is about the same [193].

It should be pointed out that neither of the methods is wrong or correct; they are both obeying their own physical laws. Also, when measurement ordinary engineering surfaces, the differences between the methods are small. It is only when very fine surfaces are being measured that the differences are significant [193].

The characterization of small features and complex geometries of the precision cutting tools has generated new approaches for determining the measurement of edges and radii [119], inside new measurement ranges that previously were not considered and where the optical measurement technology can be advantageous.

4.2 Approaches for the characterization of the cutting edge preparation

The cutting edge configuration is presented by DIN 6582 [36], which considers sharp cutting edge, rounded cutting edge with radius r_n and chamfered cutting edge. Additionally to the previous approach, for cutting edge preparation applications, a more detailed description of the geometry is required in order to characterize the cutting edge rounding. Principally, because not always the geometry of the generated profile of a rounded edge can be considered as an ideal circumference arc.

In [20, 30, 32, 34, 172] a method for the characterization of the cutting edge rounding is suggested. **Figure 4-1** shows the parameters S_γ, S_α,Δ_r, and φ used to describe the geometry of the cutting edge. Δ_r describes the value of the chamfer shape, the angle φ describes the shift of the cut point either to the rake face or the flank face, the parameters S_γ and S_α characterize the the sharp or obtuse run of the contour to the rake- or flank-face respectively. K is defined to describe the symmetry of the contour generated by the cutting edge rounding process.

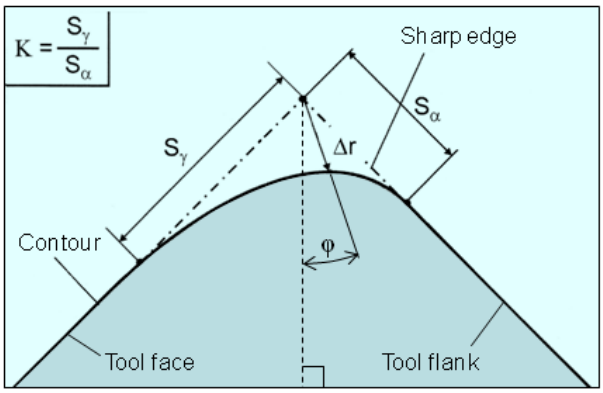

Figure 4-1: Parameters for the characterization of cutting edge rounding (adapted from [20, 30, 32])

Figure 4-2 shows examples of different rounded cutting edges in order to observe combinations of parameters and different values of the symmetry factor K [30].

Together with the rounding characterization parameters, three basic shapes for the cutting edge rounding are considered; profile with unique radius, waterfall (with two radii transition) and chamfers plus rounding [30]. There is also recommendations related with the tolerances for each characterization parameter. For example, for nominal radii the following tolerances are suggested; +/- 15% for radii smaller than 30 μm and +/- 10% for radii bigger than 30 μm.

Additionally to the cutting edge profile characterization, the irregularities and defects of the cutting edge as result of the grinding process and the preparation process

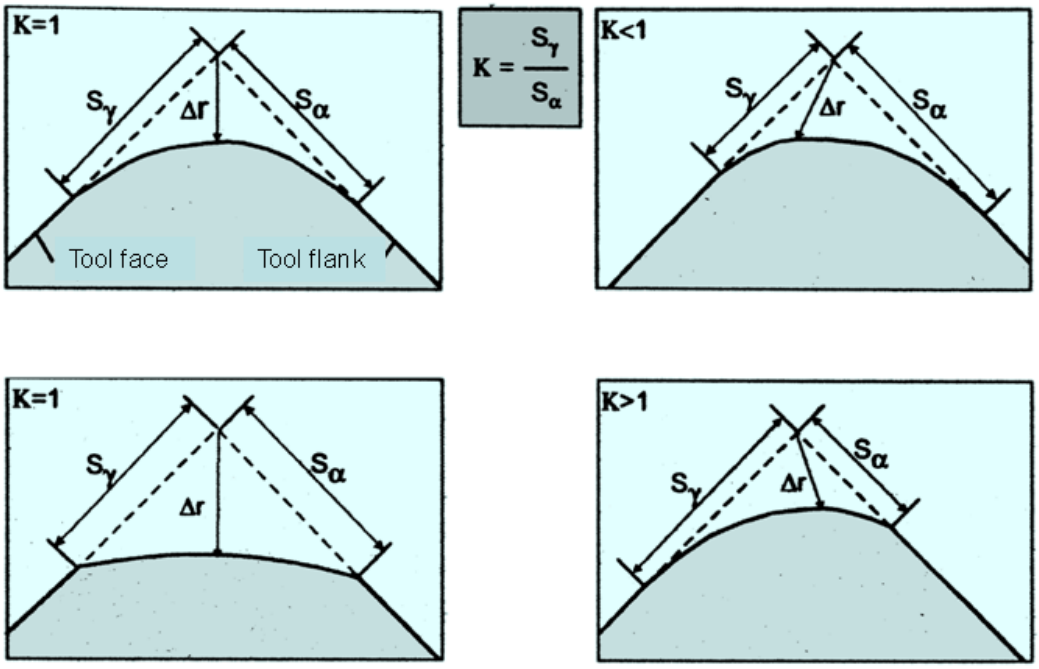

Figure 4-2: Examples of different cutting edge rounding (adapted from [30])

should be described. In [30], an approach to characterize the notchedness of the grinded cutting edge is reported. The characterization considers the depth of the irregularities and notches of the edge and the long of the irregularities and their separation in longitudinal direction to the cutting edge. Moreover, a limit value for the roughness of the grinded surfaces of the cutting tool is recommended ($R_{max} \leq 5\ \mu$m).

A characterization approach for the notchedness for a grinded cutting edge is referred in [97]. The estimation of the notchedness (as roughness depth of the cutting edge R_k) is based on the value of the wedge angle β, the roughness depth on the tool face R_s and the roughness depth of the tool flank R_f. The proposed equation for R_k is:

$$R_k = \frac{1}{\sin\beta} \cdot \sqrt{{R_z}^2 + 2 \cdot R_s \cdot R_f \cdot \cos\beta + {R_f}^2} \tag{4-1}$$

The equation is valid only if the cutting edge has no breakouts or no big irregularities produced by grinding, specially for an inadequate selection of the grinding direction on the tool flank and tool face combined with an inadequate selection of grit size and grinding strategy.

In [97], a strategy by using a tactile method for the measurement of the notchedness is presented. An special designed blade stylus adapted to a stylus arm was used. The stylus is mounted in a combined roughness-contour measurement device and the stylus is displaced along the cutting edge to obtain a longitudinal profile of the cutting edge. The notchedness is characterize by means of the parameters R_z and R_{max} obtained from the longitudinal roughness profile of the cutting edge.

4.3 Manufacturing of precision cutting tools

For the manufacturing of precision cutting tools of hardmetal (cemented carbide), in general the following steps are considered [55]:

- Pressing and sintering: to obtain the geometry and initial properties of the blank [150].
- Grinding: to obtain the definitive geometry of the cutting tool [174].
- Cutting edge preparation: to obtain the geometry of the cutting edges and to improve the characteristics of the surface of the cutting edges (notchedness) [33].
- Pre treatment of the surfaces: to prepare the surface before the coating and to improve the surface integrity of the cutting tool [152, 173, 175].
- Coating: to extend the tool life by protecting against the wear, corrosion, and oxidation [133, 142].
- Post treatment: to optimize the quality of the surface of the cutting tool after coating and to adjust the final geometry [16].

As reference, the linkage of the processes and a comparison of the corresponding proportionate costs for the manufacturing of precision cutting tools is presented in **Figure 4-3**.

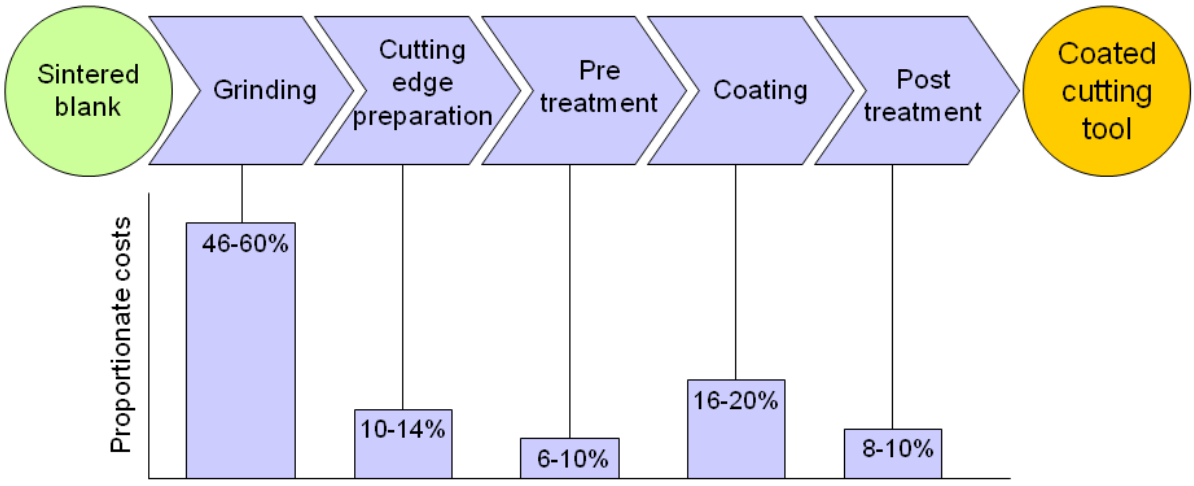

Figure 4-3: Manufacturing steps for precision cutting tools and proportionate costs (adapted from [55])

4.4 Processes for cutting edge preparation

The objective of a cutting edge preparation process is to remove material systematically in order to achieve the specified geometry of the cutting edge and the required micro topography of the edge surface (notchedness), as well as the modification of the functional surfaces in the vicinity of the edge. Additionally the preparation process should guarantee the necessary reproducibility to meet the quality requirements.

There are different technological possibilities for carrying out the cutting edge preparation of precision cutting tools. The considered processes utilize a variety of energy sources for removing the required material for the cutting edge preparation. Some of the most frequently used processes are shown schematically in **Figures 4-4**, **4-5** and **4-6**, grouped according to the energy source used (mechanical, thermal and chemical processes).

Some of the mentioned preparation processes come from deburring technology [143, 168] surface finishing [8, 155, 165] and precision manufacturing [28, 92]. The broadly used edge preparation process at the industrial level have been brushing [33, 156], micro-abrasive jet machining (or microblasting)[71, 190], drag finishing (or slip grinding or drag grinding) [122, 137], magnetic-finishing [22, 83, 113, 153, 154], and abrasive flow machining [8].

On a smaller industrial experimentally scale, laser beam machining [30, 79, 145, 132], electrochemical micro-machining [11] and ultrasonic machining are used [205]. Combinations of processes can also be made in order to achieve the cutting edge preparation, for example electro-polishing [128], electrolyte jet machining [116] and magnetic abrasive flow machining [154].

On the other hand, there are new processes of material removal, at the level of precision manufacturing, usable for cutting edge preparation such as: vibration-assisted magnetic abrasive finishing [206], micro-ultrasonic assisted lapping [211], nano-grinding [60] and ion-beam machining [110]. For the preparation of diamond coated cutting edges with sharp wedge angle (β smaller to 20°) a plasma based process has been developed that allows manufacturers to achieve radii of 0.5 μm [54].

Micro-abrasive jet machining (with air or water as transport fluid) , brushing (with abrasive filaments or polishing with diamond paste), drag finishing, magnetic finishing, abrasive flow machining and ultra-short pulse laser beam represent the state of the art for the cutting edge rounding of precision cutting tools. Recently, the development is focused toward the control of the process parameters to reach a repeatable material removal and the automatization of the kinematics and the precise positioning an referencing of the edge as strategies to obtain process reproducibility and productivity in the cutting edge preparation.

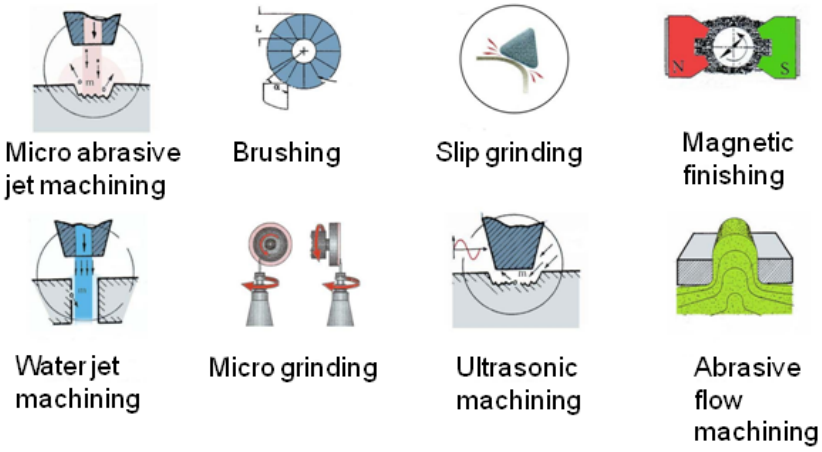

Figure 4-4: Mechanical preparation processes

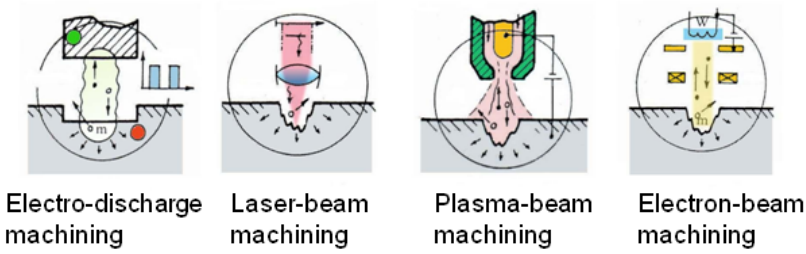

Figure 4-5: Thermal preparation processes

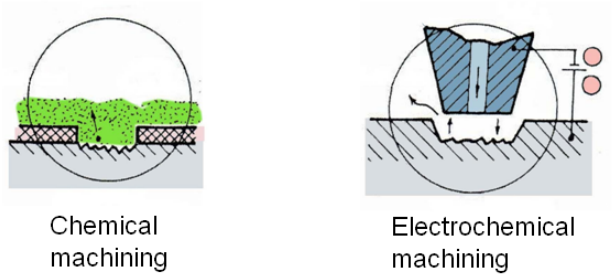

Figure 4-6: Chemical preparation processes

4.4.1 Micro-abrasive jet machining

Micro-abrasive jet machining (MAJM) removes material through the mechanical action of a focused stream of abrasive-laden gas (see **Figure 4-7**). Applied to cutting edge preparation, an abrasive jet is formed when micro-abrasive particles (10 to 50 μm of diameter) are entrained by an inert gas and propelled through a small nozzle (0.4 to 1.2

mm of diameter) at pressures of up 6 bar. The resulting jet of abrasive particles travels at a velocity of approximately 150 to 300 m/s [78, 91, 163]. When directed at a workpiece, material removal occurs as a result of chipping action. The impact of single solid particles is the basic event in the material removal by abrasive jets. The most commonly used abrasives are aluminium oxide and silicon carbide. Nozzles are made of either tungsten carbide or sapphire. The major process variables affecting MAJM removal rates are type and size of abrasive, nozzle-workpiece distance, gas pressure and abrasive flow rate.

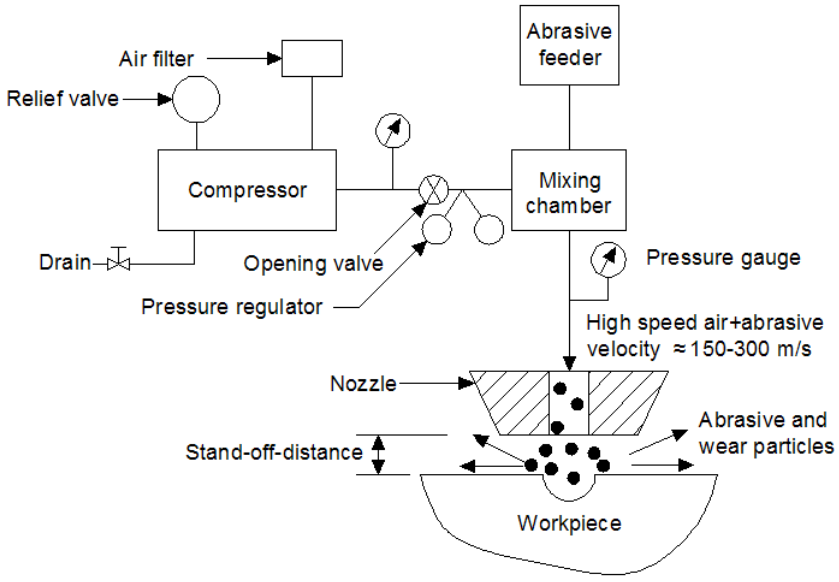

Figure 4-7: Typical system for micro-abrasive jet machining (adapted from [78])

There are variants of the MAJM depending on the transport fluid. By including water as transport fluid for the abrasive particles, with a volume ratio (volume of fluid : volume of abrasive) of 7:1 to 10:1, a technological variant is obtained. The mentioned process is called wet micro-abrasive jet machining or jet-lapping [29, 67, 91]. In **Figure 4-8** the basic components of the wet micro-abrasive jet machining are shown.

Material in MAJM is removed due to erosion action caused by impingement of a high velocity abrasive jet on the work material surface. Different mechanisms of material removal, for both ductile and brittle materials, have suggested by various investigators [78]. In the case of ductile materials, material is removed by plastic deformation and cutting wear, or plastic strain and deformation wear. In the case of brittle materials, it may take place due to indentation rupture, elastic-plastic deformation, critical plastic strain theory, radial cracking and propagation of surface energy criterion.

There are different analytical models proposed to determine the material removal for MAJM [78]. For example for brittle materials, considering abrasive grains as identical spheres, material to be removed as rigid perfectly plastic and abrasive particles as inelastic

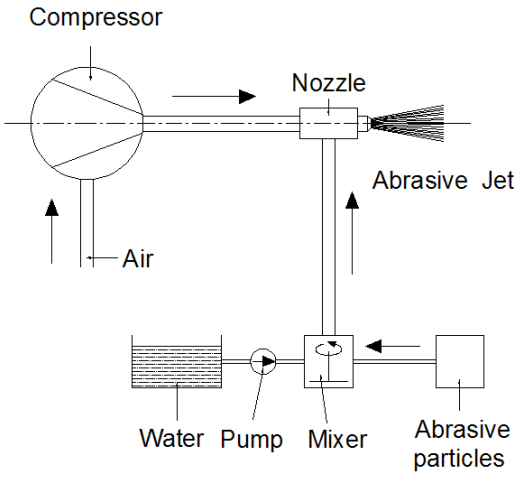

Figure 4-8: Typical system for wet micro-abrasive jet machining (adapted from [67])

and Hertz′s equations valid for fine abrasive particles, the following model is proposed [78]:

$$MRR = \frac{2}{3}\pi {d_a}^3 {v_a}^{1.5} \left[\frac{\rho_a}{12 \times 10^3 \sigma_{yw}}\right]^{0.75} N_a \tag{4-2}$$

Where MRR is the material remove rate, d_a is the diameter of the abrasive particles, v_a is the velocity of abrasive particles, ρ_a is the density of the abrasive, σ_{yw} is the flow stress of the workpiece or target material and N_a is the effective number of abrasive particles impacting per unit time.

Another practical aspect to consider is the coverage of a surface (area of the surface affected by the impingement of the abrasive particles) generated by an abrasive jet. The coverage is related to the coverage obtained by an individual passing and the number of passings applied. The following equation express this concept [71]:

$$C = 1 - (1 - C_1)^{n_p} \tag{4-3}$$

Where C is the coverage (expressed as % of the considered target surface) corresponding to n_p passings executed in a specific time. And C_1 is the coverage (in %)corresponding to an individual passing.

There are research works focused on the characterization and optimization of the MAJM principally oriented to find the relationship between the process parameters and the material remove rate and the generated surface finishing. In [7], the shape of the surface generated by abrasive jet machining is analyzed considering the effect of particle size, stand-off distance, center line and peripheral velocities of the jet. By means of proposed semi-empirical equation, it is observed that the generated surface by means of MAJM, when the jet impacts a plane surface, is a reverse bell mouthed in shape with an edge radius at the entry size of the target surface.

In [5, 6], experimental investigations to observe the influence of the process parameters on the quality of abrasive jet deburred components are reported. Taguchi′s orthogonal arrays were used to systematically measure the influence of the major process parameters on the deburring of stainless steel workpieces [5]. Also a statistical model was developed for the magnitude of the edge radius generated. The mathematical modeling study reveals that the stand-off distance is the most significant parameter in generating an edge radius.

The effect of workpiece properties on machinability in MAJM of ceramics is presented in [185, 186]. An important aspect to consider is that due to the fact that the size of the particles employed in MAJM is usually much smaller than those used in erosion tests, it is doubtful whether the established theories can also be applied to the MAJM. The obtained results from the experimentation shows that the fracture toughness K_c and hardness H_w of the target materials, are critical parameters affecting the removal rate in MAJM. However their influence on the machinability varied greatly with the employed abrasives, and therefore, it was not possible to generalize the obtained data of the material removal rate into the form of the erosion models. In general, the erosion models are described as a function of the experimental parameters in terms of jet (velocity v_a, diameter of abrasive particles d_a, density of abrasive ρ_a) and workpiece materials (toughness K_c, hardness H_w) as follows [185]:

$$E \propto {v_a}^{e_1} {d_a}^{e_2} {\rho_a}^{e_3} {K_c}^{e_4} {H_w}^{e_5} \tag{4-4}$$

Where E is the dimensionless erosion rate expressed as the ratio of the eroded weight/erodent weight and e_1,e_2,e_3,e_4 and e_5 are the exponents associated to the parameters.

The physical aspects and fundamentals of erosion by micro-abrasive jet machining have been studied [66]. The fluid dynamic mechanisms of particle flow causing ductile and brittle erosion are analyzed by a 2D numerical model which allows to estimate the erosion for dense flows. Likewise, a three dimensional vortex simulation of particle-laden jet is reported in [179]. With this model the radial profile on mean velocity was obtained for the two-phase jet for particles of 60, 80 and 100 μm for a rounded nozzle. Equally it was observed that the mean velocities for air and particle on jet centerline change as function of the axial distance from the nozzle exit. Additionally, the results of the analysis show that there is a significant difference in the velocity profile between the single-phase jet and the two phase-jet, principally due to turbulence effects.

The development of a rectangular Laval nozzle to improve the MAJM is reported in [1] and the influence of the nozzle geometry in the quality of the generated surface is analyzed in [2] . Models to predict the performance of such nozzles are presented. They can be applied successfully in the selection and of the process parameters and the machining strategy. The model for the jet shows that its energy intensity is more evenly distributed and a substantial higher compared to conventional nozzle concepts. Additionally, a model for the contour generation predicts the shape and roughness of the blasting profile and a scanning strategy have developed which enables a significant

reduction of the processing time. The results of this investigation opens the possibility to derive new rules for the design of microstructures.

4.4.2 Brushing-polishing

A combination of polishing and brushing is used for cutting edge preparation. The process uses a soft brush (with natural or polymeric fibers as filaments) which configures the polishing pad, and diamond past as slurry with diamond particles or granules (grit size between 5μm and 8μm)as solid phase. The process can be described as four component systems and that mechanisms involved in brushing-polishing (BP) can be grasped by first understanding the interactions among those components : workpiece, fluid, granules and brush-lap. The brush-lap imposes relative motion between the granules and the work and affects slurry and swarf transport through the contact. The process combination brushing-polishing can be considered as a special case of polishing, with the particularities related to the brush-lap. **Figure 4-9**, shows the principle of brushing-polishing applied to a workpiece surface.

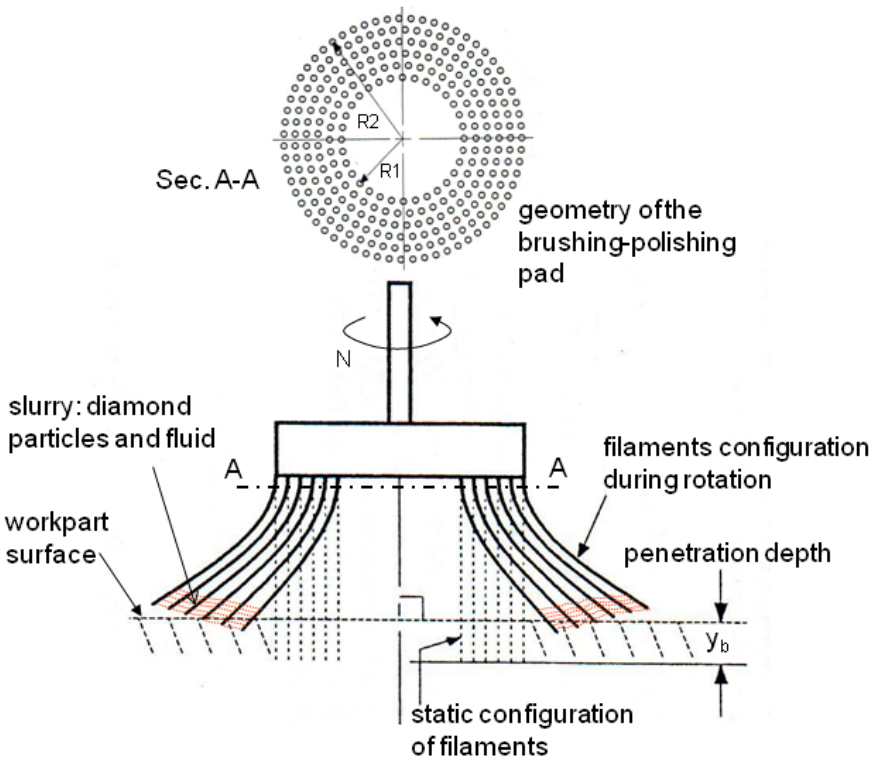

Figure 4-9: Principle of brushing-polishing

Different analysis of the material removal mechanisms in polishing are reported in [45, 158]. The mechanisms can be catalogued en terms of the interactions of the workpiece,

fluid, granules and lap. Likewise, in [91, 120], different hypotheses to explain the material removal mechanisms are presented; mechanical hypothesis, flux-based hypothesis and chemical hypothesis.

A model to estimate the volumetric removal rate is reported in [91, 120, 171]. The model considers the removed volume V, the polishing pressure p, the relative velocity between the workpiece and the lap v_{wl}, and a constant K is defined as [91, 120, 171, 187]:

$$\frac{dV}{dt} = K \cdot p \cdot v_{wl} \tag{4-5}$$

Another material removal rate model is presented in [87]. The concept used and developed is that slurry movement in the lap-work (or pad-work) interface is relatively free, compared to the well-controlled movement of abrasive grits in a grinding wheel. This freedom of abrasive movement implies that abrasive grits move into and out of the polishing area and also that they can move into and become lodged in the polishing pad. The amount of material removed from the surface as a function of time is called $A(t)$. The material removal rate is expected to depend on the slurry flow rate and the effectiveness of the abrasive grains in removing material. That is, material removal rate depends on the number of abrasive grits acting and the ability of the abrasive grits to remove material. As material is removed from the workpiece, some polishing debris and abrasive particles move out of the pad-work interface region and some remains attached to the pads. Experience and the results show that the material removal rate decreases with the amount of material removed. A general description of this effect is that the material removal effectiveness decreases with amount of material removed. An expression to describe the decrease in material removal effectiveness is [87]:

$$E(A(t)) = E_{A_0} - \exp\left[-a_A\, A(t)^{b_A}\right] \tag{4-6}$$

Where $E(A(t))$ is the effectiveness for a material removal $A(t)$ in time t, E_{A_0} is the initial effectiveness and a_A and b_A are determined from the experimental data.

A theoretical model to predict the relationship between the polishing parameters and the wear rate for the case of abrasive particles sandwiched between a soft pad and a workpiece, are reported in [201]. Experimental results and theoretical predictions indicate that the wear rate increases with an increase in the particle size, hardness of polishing pad and nominal contact pressure, and with a decrease in elastic modulus of the polishing pad. Surface roughness increases with an increase in particle size and hardness of polishing pad, and nominal contact pressure has little effect on the roughness. A dimensionless parameter, wear index which combines all of the preceding parameters, was introduced to give a semi-quantitative prediction for the wear rate in free abrasive polishing. The wear index is defined as [201]:

$$\frac{p}{E_p}\left(\frac{R}{\sigma_p}\right)^{0.3}\left(\frac{H_p}{H_w}\right)^{1.5} \tag{4-7}$$

Where R is the radius of the particle, H_p is the hardness of the pad, H_w is the hardness of the workpiece, E_p is the elastic modulus of the polishing pad, p is the normal polishing pressure and σ_p is the standard deviation of the height distribution of the polishing pad.

4.4.3 Brushing with nylon abrasive filaments

Brushing can be commonly made with two main filament types: nylon abrasive filaments (NAF)[156] and steel wire [100, 156, 168]. Brushing with NAF is used in applications involving specific edge-radius requirements, and surface finish improvements [156]. Because NAF are filamentary in nature, they do not function like grinding wheels or coated abrasive products. During use sharp new abrasive grains are constantly being exposed as nylon wears against the work surface. This provides consistent brushing action throughout the brush life. NAF brushes only remove small amounts of material and improve surface finish. The compliance of the filaments and the manner in which abrasive grains are held in the nylon carrier govern their material removal and surface-finishing capabilities. NAF brushes can be used either on manual/off-hand setups like bench and pedestal grinders, drill presses, or in automated setups involving CNC machining centers, robots and automated workstations. Abrasive grits commonly used in nylon filaments are silicon carbide and aluminum oxide. Other alternatives are CBN (cubic boron nitride) and PCD (polycrystalline diamond). **Figure 4-10** shows the principle of brushing with nylon abrasive filaments (BNAF).

The material removal mechanics of brushing is not clear. The absence of technical information concerning material removal mechanics of brushes, is in part, attributed to difficulties associated with modeling the complex interaction that occurs at the interface of the filament/workpiece material system [159]. It has been observed that polymer(i.e.,nylon)/abrasive brushing can exhibit a time dependence force response that is solely due to the increased temperature caused by rapid cyclic loading of filaments and the corresponding reduction of stress relaxation module.

The morphology of the surface generated by BNAF applied to surface finishing and edge-rounding was observed for nylon/SiC filaments [123, 160]. The surface topography generated during orthogonal brushing of aluminium (6061-T6) was observed using scanning electron microcopy. Also, the microscopic morphology of nylon/SiC filaments was examined as-received and steady-state configurations. This information is used to propose a qualitative model for material removal mechanisms and the wear/attrition characteristics of the filament material.

The analysis of the contact problem associated with the filament/workpart interaction that arises during brushing processes is reported in [151]. A discretized model of a filament within the brushing tool is developed by employing equations of Lagrange in conjunction with special constraint equations that are appropriate for the impact and impending large displacement of a flexible fiber whose tip traverses a flat, rigid surface.

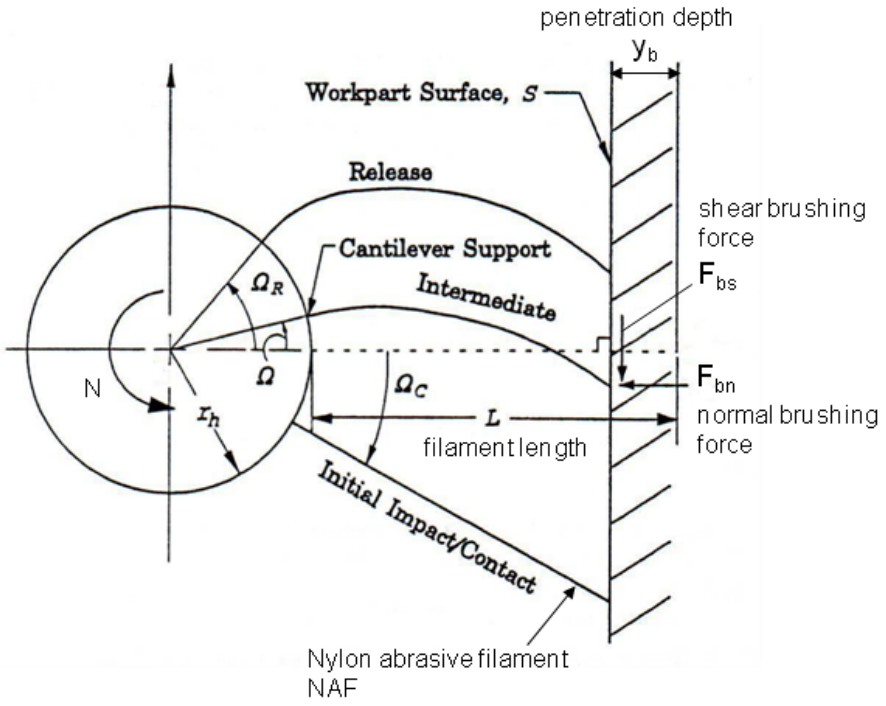

Figure 4-10: Principle of brushing with nylon abrasive filaments (adapted from [151])

This formulation leads to the identification of five nondimensional parameters which fully characterize the filament/workpart contact problem. A damping mechanism is also included which can be used for modeling complex filament interactions that arises during the actual brushing operation.

The design of the NAF brush plays an important role in the performance of the process and the quality obtained of the surface and rounded edge of the workpieces. A methodology for the design of advanced brushing tools is presented in [162]. The proposed methodology considers the dynamic properties of the filamentary brush system associated with the geometry of the brush, filament material properties, filament stress, filament contact force, overall brush response, and corresponding material removal/surface finish performance. Additionally, an analytical procedure is developed to facilitate the design of brush stiffness and brush compliance. On the other hand, to complement the aspects associated with the design of brushes, a mechanics-based method for evaluating large deformation of filaments for rotating brushes is presented in [161].

The precision machining of metallic workpieces by using BNAF is reported in [100]. Experiments mounting a NAF brush in a combined CNC turning-milling center show that there is a significant improvement of the roughness (R_z)of previous turned surfaces of steel (42CrMo4) and aluminium (AlCuMgPb). The influence of the grit size of the abrasive particles for different cutting velocities was analyzed. By changing the grit size from F80

to F320 for SiC as abrasive and Aluminium as workpiece material, the roughness R_z falls from 9 μm to 1 μm respectively, considering a cutting velocity of 500 m/min. Likewise, the decrease of the roughness of the surface by brushing the turned surfaces was observed. The behavior is non linear falling von 7 μm to less than 1μm for two minutes of effective working time. These non linear falling behavior of the roughness R_z, depending on the cutting time, was observed for different workpiece material and cutting velocities.

4.5 Research about processes for cutting edge preparation

The influence of the parameters of water-abrasive jet machining and brushing upon the size of the generated cutting edge radius and the roughness R_z of the tool surfaces was reported in [33] for cemented carbide cutting tools. The parameters considered for water-abrasive jet machining were type of abrasive, grain size of abrasive, jet feed, jet pressure, and jet angle. It is observed an increase of the roughness R_z and edge radius with a increase of the jet pressure. The edge radius decreases with an increase of the jet feed and the roughness decrease with a decrease of the grain size of the abrasive, and additionally the quality of the surface improves by using small grain size of abrasive. The abrasives considered were different types of corundum and silicon carbide. For the brushing process were considered as parameters; brushing time, brush angle, cutting speed, and penetration depth. The edge radius increase with a increase in brushing time, cutting speed and penetration depth. The edge radius presents a maximum for a brushing angle of 45°. Brushes with Nylon filaments and silicon carbide were mounted in a plane grinding machine in order to obtain the kinematics of the preparation process.

In [34], the application and general characteristics of brushing, magnetic finishing, and ultra-short pulse laser for cutting edge preparation are presented. The results of the research with the mentioned processes show that it is possible to obtain reproducible complex geometries for cutting edge preparation by applying the considered processes, controlling their process parameters, kinematics and positioning.

Regarding the notchedness of sharp cutting edges obtained by grinding, in [97] is reported the influence of the wedge angle β in the values of R_z and R_{max} for cutting edges with wedge angle varying from β =30° to β =135°. The results show that there is an inverse relation between notchedness and the wedge angle β. The notchedness diminishes as β increases. Moreover, as tendency, the decrease in notchedness is more notorious for values of β <90°. For values of $\beta \geq$90° the decrease in notchedness are not very strong with the increase of β.

The behavior of the cutting edge rounding and the edge notchedness by using wet micro-abrasive jet machining (with water as transport fluid for the abrasive particles) as edge preparation process, is reported in [97]. A comparison of the obtained rounding and notchedness for six different tool materials with the same jet machining parameters and

abrasive material, shows for example that a maximal rounding of 105μm for cemented carbide (HW-K05) and a minimal rounding of 12μm for PCBN (hard phase: C, bounding phase: TiC, particle size: 2μ) were obtained. On the other hand, the notchedness, by using the same experimental conditions, is lower (in terms of R_{max}) for the cemented carbide tools than for the PKD and PCBN tools. Moreover, the difference between the notchedness parameters R_z and R_{max} (expressed as the ratio R_{max}/R_z), is more remarkable for PKD and PCBN than for cemented carbides.

Additionally, the influence of the parameters of the micro-abrasive jet machining process on the edge rounding and the edge notchedness is presented in [97]. A decrease of the size of the abrasive particles, produces a decrease in the radius of the prepared cutting edge, these behavior has non linear tendency. Regarding the notchedness, the decrease in particle size generates a decrease in the notchedness, and the tendency is non linear too, but after a critic grit size (F150 for the reported experiment), there is not a notorious decrease in notchedness. Likewise the influence of jet pressure, feed speed of the jet, and wedge angle was analyzed. In general, an notorious increase of the radius generated is observed by increasing the jet pressure. On the other hand, for the considered range of pressures (5-10 MPa), the notchedness (in terms of R_z) increases with the increase of pressure. For example, for a cemented carbide HW-P25, this increase is between 9μm and 12μm. Another important aspect to consider is the variation of notchedness with the increase of wedge angle β. The results show that there is a decrease of the notchedness with the increase of β, but there is a critic wedge angle (β =90°), after which the decrease of the notchedness is not notorious.

In [190], the effect of the MAJM process parameters on the generated cutting edge radius and the edge notchedness are analyzed. Likewise, the application of the MAJM (with water as transport fluid) to the preparation of hardmetal drill of 12 mm of diameter is presented. A tendency to significant improvement of the notchedness and high reproducibility and accuracy of the cutting edge rounding were observed.

MAJM applied to ground or polished surfaces, can increase the cutting performance of coated tools, mainly due to film adhesion enhancement [17]. Additionally the application of MAJM to increase the cutting performance of coated cemented carbides tools is analyzed by experimental and computational investigations (finite elements). The results revealed that a significant tool life increase through MAJM of films, deposited on micro-blasted polished surfaces. On the other hand, a comparable lower enhancement of the wear resistance can be attained through micro-blasting of films on ground micro-blasted surfaces.

4.6 Evaluation of prepared precision cutting tools

The influence of the form of the cutting edge contour upon the cutting forces was observed for orthogonal turning by using hard metal inserts [32]. The results show that the contours

with $\varphi = 0$ (see **Figure 4-1**) generate bigger cutting forces than the contours with $\varphi < 0$ or $\varphi > 0$. This tendency is even observed considering variations in cutting speed and Δ_r.

It was observed that the K factor has effect on the tool life [31]. Experiments of external turning of CK45 using inserts of coated cemented carbide showed that a value of $K = 0.5$ combined with high values of S_α produces lower tool life of the cutting tool than tools with $K = 1$ and $K = 1.8$ with low values of S_α ($S_\alpha < 40\mu$m). As tendency, the best results were obtained considering $K = 1.8$ and $S_\alpha \approx 20\mu$m.

Additionally, the effect of the cutting edge radius on the generated residual stresses in the workpiece is reported [31]. Results from machining experiments considering cutting edge radii from 20μm to 300μm and $K = 1$, show a clear linear tendency in the relationship between cutting edge radius and residual stress in the workpiece. The residual stress on the surface increase with the increase of the cutting edge radius and the minimum residual stress values diminish with the increase of the cutting edge radius. However, an important aspect to observe is that the residual stresses on the surface are negative (compressive) for cutting edge radii lower than 100μm, but for bigger radii the generated residual stresses are positive (tensile), thus, there is a critical radius that represents the transition point from compressive residual stress to tensile residual stress.

In [12], the importance of different aspects of manufacturing of cutting tools are considered. The development of cutting tool materials and coating technology should be complemented with the consideration of the manufacturing technology used to generated the macro and micro-geometry of the cutting tools. The parameters of the grinding process and the macro- and micro-characteristics obtained by the subsequent cutting edge preparation process play an important role in increasing the productivity of the cutting process. The influence of the grinding parameters in the wear behavior of twist drills and hard metal inserts was observed. Likewise, the influence of the cutting edge preparation in the wear of the cutting tool and in the quality of the workpiece surface surface quality was analyzed.

An analysis of the scale effect in micro-machining is reported in [107], by using drills and end-milling tools. Among other aspects, the effect of tool diameter in the specific feed force and the influence of the cutting edge rounding were observed, principally the relationship between the specific cutting energy and the ratio h/r_n.

An experimental research that considers the influences of the microgeometry of the cutting edge of drills on the cutting edge process is reported in [137]. Drills of cemented carbide (HW-K20) with external diameter d of 1 mm to 10 mm and cutting edge radius r_n of $0.004{\cdot}d$ prepared by drag finishing were used to drill workpieces of steel (C45E+N) by using the following cutting parameters: cutting speed $v_c = 35$ m/min, feed $v_f = 133.7$ mm/min and drilling depth of $2{\cdot}d$. The results of the tests show that the rounding of the cutting edge with r_n/d=0.004 has the tendency to increase in 5% the specific feed forces and the related cutting torques. Moreover, the data from the tool-life experiments with uncoated 1 mm drills with $v_f = 133$ m/min, show an increase of the tool life of 360% for the cutting tools with cutting edge rounding in comparison to the sharp cutting tools (without

rounding). Complementary experiments using v_f =601.7 mm/min with sharp coated tools lead to outbreaks along the cutting edges in the first drilling. On the contrary, with rounded cutting edges, 300 bores can be produced. Regarding the dimensional tolerances and the quality of the surface, drill holes obtained by using rounded cutting edges show less diameter deviations and smaller scattering ranges of peak-to-valley heights than drills obtained by sharp cutting edges. With respect to the subsurface areas of the workpiece material, considering the used experimental conditions, there is no significant differences in the structure after machining with sharp or rounded cutting edges. The observed aspects from this research allow to see that there is a lot of potential for improving the tool life by means of a defined cutting edge rounding.

In [97], the evaluation of the behavior of cutting tools prepared by micro-abrasive jet machining (water as transport fluid) is presented. Hardmetal drills prepared and coated by PVD (TiAlN), were tested by drilling steel (CK45). A comparison between drills with sharp edges and drills with edge radius of 43.5μm, shows that there is a significant improve of the roughness R_z of the machined surface. Likewise, turning inserts of cemented carbide (HW-P25)coated by PVC (TiAlN) were tested by orthogonal turning of steel (CK45). The cutting force vs volume of material removed was observed for sharp edges and rounded edges with radii of 10μm and 20μm. The experiment evidences that in the first stage of machining the cutting force is smaller for the sharp edge, but after a critical point the force begins to be smaller for the edge with 10μm and later appears another critical point where the force for the edge with 20μm radius begins to be lower than the force for the sharp edge. After that, the cutting forces for the edges with radii of 10μm and 20μm are lower than the cutting force for the sharp edge. Another important observation, considering the roughness R_z of the machined surface vs the volume of material removed, is that R_z has the tendency to be smaller when increasing the cutting edge radius.

Orthogonal turning tests by using prepared hardmetal inserts were reported in [30]. The turning inserts were coated with TiNALOX and casting (GJS400) and steel (CK45) and were considered as workpiece materials. The influence of the cutting edge geometry (S_α,S_γ,Δ_r and K) on the cutting forces was observed. Likewise, the effect of K and S_α on the tool life was analyzed. Additionally, a simulation by finite element analysis was used to observe the influence of the edge geometry on the cutting temperature. Parallel to the turning tests and simulation, the behavior of prepared hardmetal drills (coated with TiAlN) was observed by using steel (42CrMo4) as workpiece material. The tool life has the tendency to be less for K=0.7 than for K=1.0 and 1.3, considering values of Δ_r of 30μm,40μm and 50μm. Additionally, it was observed that there is no significant differences in the wear (VB) for different values of K maintaining Δ_r constant.

Prepared end-mills of hardmetal were tested by using CK45N as workpiece material [30]. The experimental results show that for values of S_α between 22μm and 75μm, with K =1.25, the biggest tool life corresponds to S_α=45μm. Additionally, a finite element simulation considering the same parameters showed that the biggest maximal cutting temperature corresponds to S_α=70μm. Based on the experimental observation of the tool

wear (VB) for different values of K (0.7, 1.0, 1.4 and 1.8), can be concluded that there is no significant difference in the behavior of wear by changing the parameter K. Regarding on the cutting forces, by end-milling, there is no significant difference considering changes in the parameters S_α,S_γ, Δ_r and K.

The development of an experimental system for the cutting edge preparation and measurement of precision cutting tools , by using laser, is reported in [30]. The system was designed with six degrees of freedom to allow the orientation of the laser beam on the complex 3D workpiece geometries. Three linear axes allow the 3D-positioning, and two rotation axes are used to rotate the cutting tool during the measurement and preparation process and the other axe is used in combination with optical components to focus the laser beam for the material removal process. Three types of lasers (solid state laser, excimer-laser and ultra-short pulse laser) were tested to define the best alternative for edge preparation. The laser with pulse length less than 20 ns (ultra-short pulse laser) was not considered, because the results in terms of roughness and surface affectation were not reproducible and acceptable. Finally, a solid state laser ($Nd : YVO_4$) was considered. Regarding the measurement technology, the system has an optical measurement device based on a camera to obtain the relative positioning between the laser beam and the cutting edge. Additionally, to measure the cutting edge position and the cutting rounding, an optical sensor was used.

The cutting edge preparation with the laser system presented in [30] was evaluated by analyzing the influence of the laser on the substrate of the cutting tool by means of XPS technique. A oxidation layer of several nanometers was observed which can be removed with a subsequent micro-blasting treatment previous to the coating process. Additionally, a comparison between cutting edges obtained by conventional preparation process and laser was reported. The results show that there is no significant difference between the laser and conventional preparation process in terms of cutting forces and tool life.

5 Proposed characterization of cutting edge preparation and measurement

To analyze the cutting edge preparation processes and to describe the quality of the preparation, it is important to define the geometric characteristics of the cutting edge and the corresponding measurement technology. In this chapter, the fundamentals for the geometric description of the cutting edge are presented.

The description of the tool geometry of a precision cutting tool is considered at various scales: macro-geometry (cutting angles, chip breakers, etc.), meso-geometry (cutting edge radius, contours of the cutting edge; order of magnitude: 1-100μm), and micro-geometry (surface texture and notchedness; order of magnitude: less than 2μm).

This work is centered in the preparation by rounding the cutting edge, therefore emphasis will be made in the characterization of the rounding of the cutting edge by means of systematic geometric parameters that will be defined presently. Such parameters are related to the description of meso- and micro-geometry of the cutting tool.

5.1 Measurement technology

To measure the cutting edge geometry and to characterize the surface in the vicinity of the cutting edge, a white light chromatic sensor was used [56, 57, 58]. In a chromatic sensor, polychromatic white light is focused onto the target surface by a multi-lens optical system. The lenses are arranged so that the white light is dispersed into a monochromatic light by controlled chromatic aberration (see **Figure 5-1**). A specific distance to the target is assigned to each wavelength by a factory calibration. Only the wavelength which is exactly focussed on the target is used for the measurement. This light reflected from the target surface is passed through a confocal aperture onto a spectrometer which detects and processes the spectral changes (see **Figure 5-2**).

The measurement range of the sensor is equal to the axial chromatic dispersion registered between the shortest and longest wavelength by the detector. The sensor is able to achieve vertical ranges from several tens of micrometers to several millimeters, depending on the objective lens (see **Figure 5-2**).

Because the chromatic sensor measures the height at a single point on the workpiece, it is possible to use it to measure a profile or a surface. It will be necessary to scan in a horizontal direction to get a profile (different points in the vertical direction), and in the

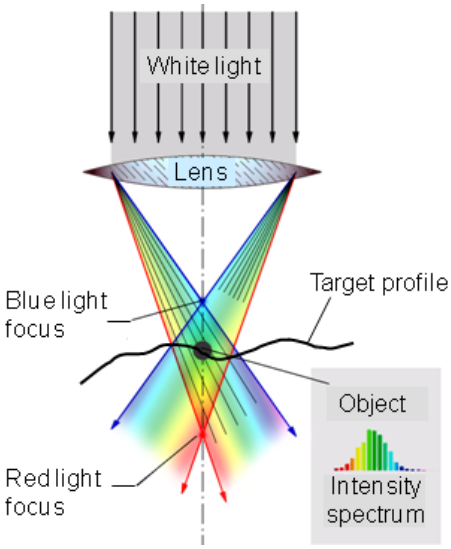

Figure 5-1: Principle of white light chromatic sensor

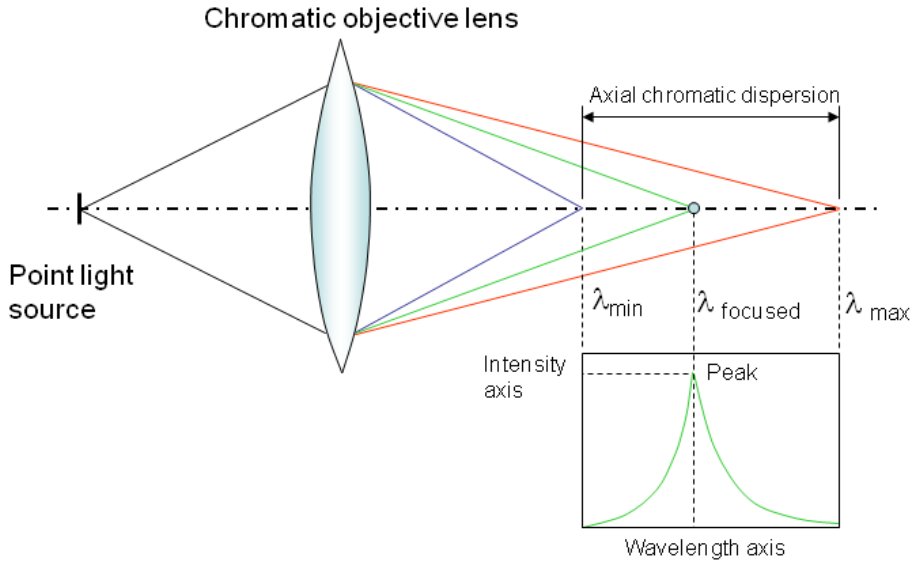

Figure 5-2: Axial chromatic dispersion and intensity peak on the spectrometer curve

two horizontal directions to get an areal topographic image.

Figure 5-3 shows an example of a scanned cutting edge obtained with a chromatic sensor used to characterize the edge rounding. The used sensor works with a horizontal resolution of 1 μm and a vertical resolution of 60 nm.

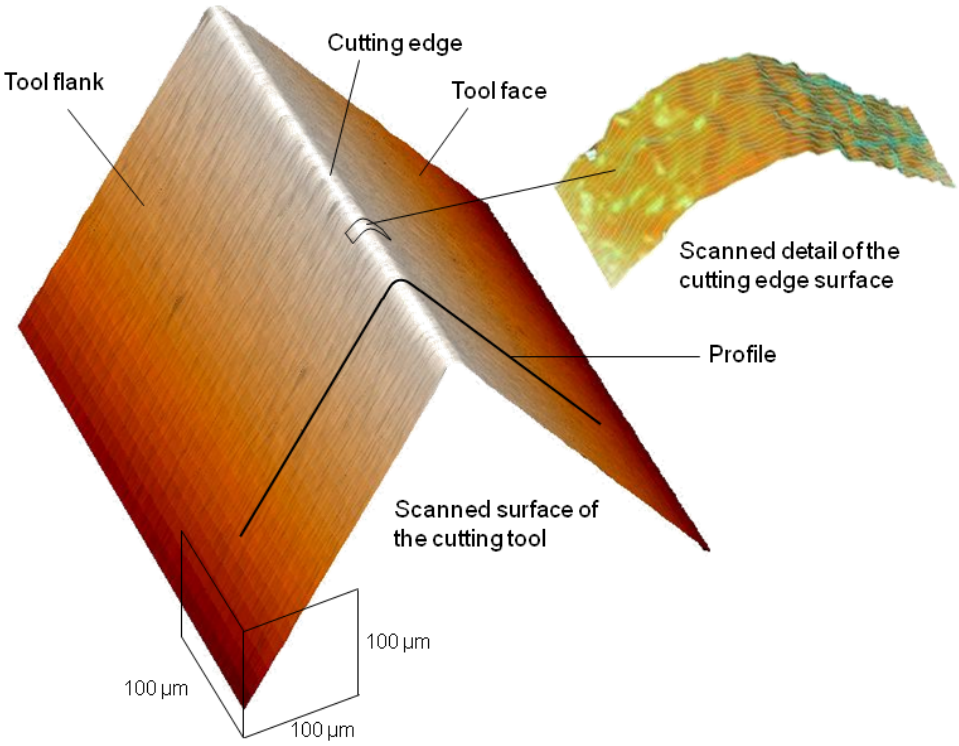

Figure 5-3: Cutting edge scanned by means of a chromatic sensor

5.2 Definition of rounding of the cutting edge

Rounding of the cutting edge, is defined as the process of generation of a convex surface that connects the flank and face and configures the geometry of the cutting edge (see **Figure 5-4**). The generation of the convex surface is achieved by means of precision material removal processes. The successive cuts applied to this convex surface by means of a normal plane to the longitudinal direction of the cutting edge generate contours that describe the rounding of the cutting edge.

The realization of the rounding process by means of some of the available manufacturing techniques generates not only the convex surface that configures the cutting edge, but rather also changes are caused in the micro topography of the cutting edge surface and in the microstructuring of the flank and the face of the cutting tool in the proximity of the cutting edge. For this reason, it is necessary to consider in the characterization of the cutting edge preparation, not only the geometry of the contours of the cutting edge but also the description of the micro topography of the cutting edge (notchedness) and the micro topography (microstructuring) of flank and face in the proximity of the cutting

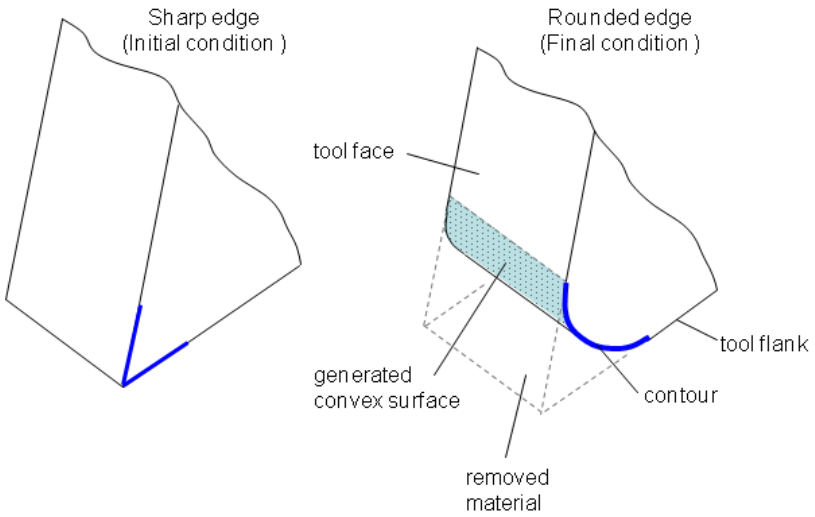

Figure 5-4: Definition of rounding of the cutting edge

edge.

From this perspective, the result of a planned cutting edge rounding is the generation of a convex surface with an specific curvature or profile and the modification of the micro topography of the cutting edge and the microstructuring of the flank and face to improve the behavior of the edge during the cutting process. Such an improvement is associated with the increase of the tool life and the quality of the surface of the workpiece. Moreover, an additional objective of the cutting edge preparation is to improve the characteristics of the edge surface to increase the quality of the subsequent edge coating.

5.3 Detailed description of the geometry of the cutting edge

The geometry of a precision cutting tool can be divided in macrogeometry and cutting edge geometry, which can be separated in mesogeometry and microgeometry (see **Figure 5-5**). The macrogeometry includes cutting angles, corner radius, chip breakers and other functional surfaces and geometric characteristics related to chip flow, cooling and lubrication, etc. In the mesogeometry are considered the contours corresponding to the convex surface of the edge generated by edge preparation process. In the microgeometry are included the microtopography of the cutting edge (notchedness) and the microtopography of the surfaces (flank and face) in the vicinity of the edge.

In **Figure 5-6** the categories used for the definition of the geometry of the cutting edge are shown. These categories allow the characterization of the cutting edge prepara-

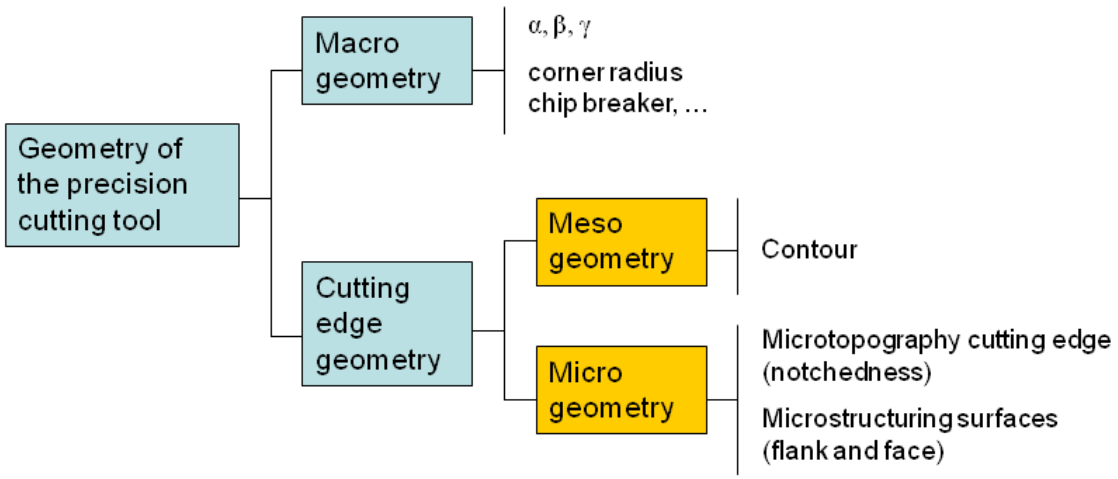

Figure 5-5: Aspects of the cutting edge geometry

tion by means of quantifiable parameters using the appropriate measurement technology. The characterization of the contours that describe the convex surface generated by the rounding process is considered an important aspect. The characterization of these contours can be carried out by means of a nominal radius of rounding r_n that corresponds to the best fit of the contour to a circumference arch, or more detailed through the curvature function that represents the curvature and the radius in each point of the contour. The microtopography of the cutting edge (notchedness) is described by using normalized roughness parameters and the material ratio corresponding to profiles in the longitudinal direction of the edge convex surface. Finally, the microtopography of the face and flake in the vicinity of the cutting edge is considered by means of normalized areal parameters and polar diagrams to observe the anisotropy of the microstructuring generated by the preparation process. In addition to these parameters, the roughness in specific directions (for example chip flow direction) can be considered. In the following sections the proposed characteristics of the cutting edge preparation are described.

5.3.1 Mesogeometry of the cutting edge

The mesogeometry of the cutting edge is represented by the contours that describe the convex surface. The geometry of the contours generally is expressed as rounding of the cutting edge. The observation of a typical contour ϕ (see **Figure 5-7**), allows appreciating that in general this contour does not have form of circumference arch and therefore the description of the rounding by means of a only radius r_n, was only used in nominal terms. The characterization of the geometry of the contour ϕ should be expressed by means of a series of parameters that allow its detailed description oriented toward the edge preparation process planning and the machining process. The contour ϕ among points c and d, describes the rounding of the cutting edge in a specific point of edge.

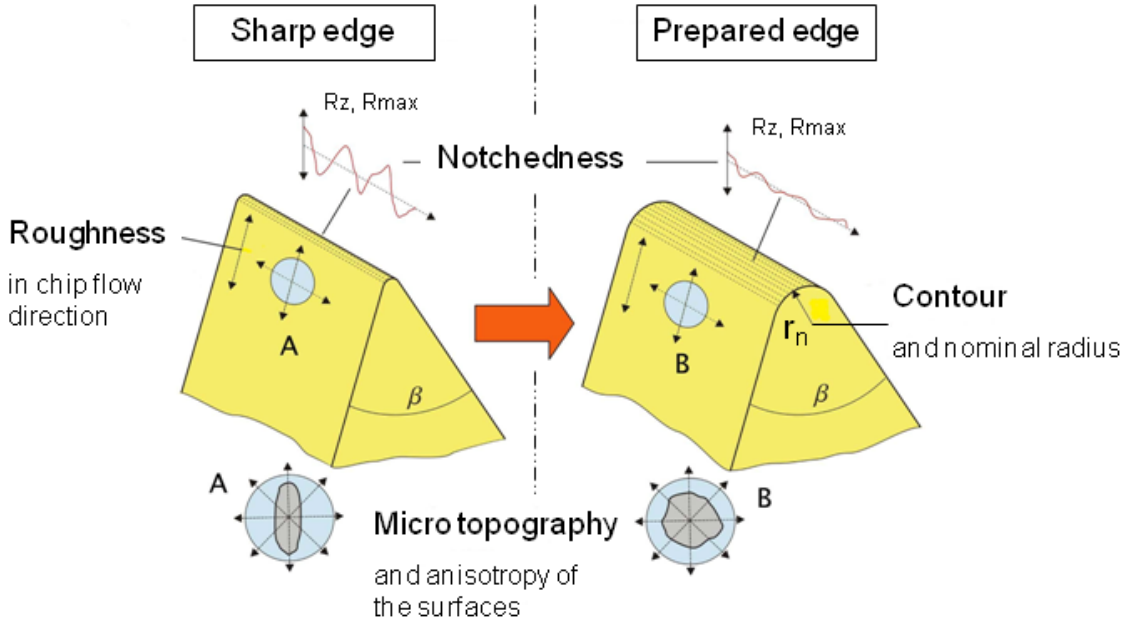

Figure 5-6: Characterization of cutting edge preparation

The points c and d represent the joint between the contour and the tool flank and tool face respectively. The **Figure 5-7** shows also the coordinate system used to describe the contour. The position of the contour, with reference to axes x and y, with the axis of symmetry of the contour coinciding with the vertical direction y (defining the two angles $\beta/2$), is defined as measurement position of the contour (see right side of **Figure 5-7**).

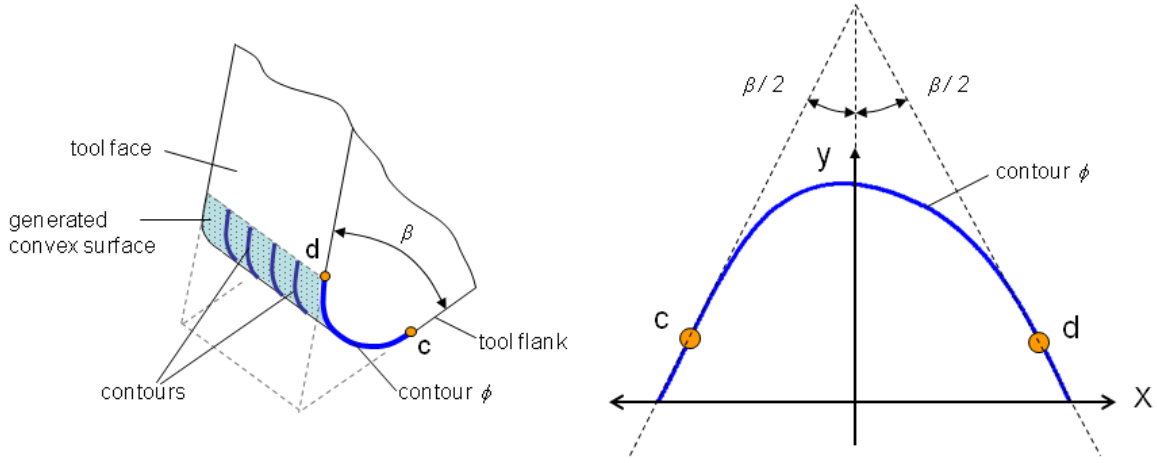

Figure 5-7: Generated convex surface and contours

A detailed observation of the contour ϕ, allows the analysis that for each point of

the contour exists a curvature and a specific radius. In the **Figure 5-8** a typical contour is shown. For the points a and b , there are two radii r_a and r_b, substantially different, corresponding to the coordinates x_a and x_b, whose separation is usually of the order of some micrometers. For these reasons a characterization approach is necessary to describe the curvature and radius for each point of the contour.

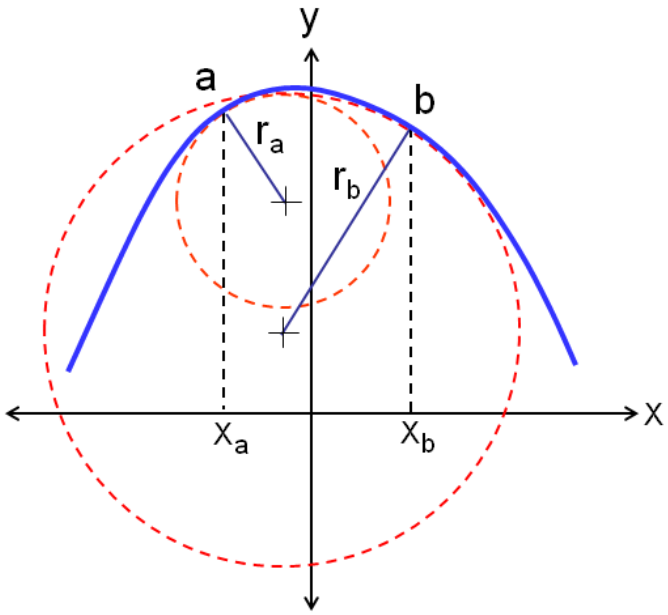

Figure 5-8: Contour and radii

Likewise, in order to relate the geometry of the contour with the macrogeometry of the cutting tool, for example to determine the effective rake angle γ_e, or the position of the contour during the cutting process, it is necessary to fit the slopes of the tangents to the contour, which are described by means of the concept of turning angle θ just as it is shown in the **Figure 5-9**. The turning angle θ measures the inclination of the slope of the tangent in each point of the contour with regard to the reference horizontal line parallel to the axis x [64]. θ is always measured leaving from the tangent line to the contour until the horizontal reference. When the direction of θ is clockwise, θ is defined as positive, in the event of being counterclockwise θ is defined as negative.

Figure 5-10 shows the methodology used to characterize the mesogeometry of the cutting edge. From the measurement of the cutting edge surface, points that describe the contours are obtained. Then the points are fitted to a polynomial function that describes the contour mathematically. Starting from this mathematical description and using concepts of differential geometry, the curvature function, the radius function, the turning angle function, the effective contour, the effective rake, the nose radius, and the asymmetry of the contour are obtained. Additionally, from the measurement data, the nominal radius that represents the best fit of the contour to a circumference arch is

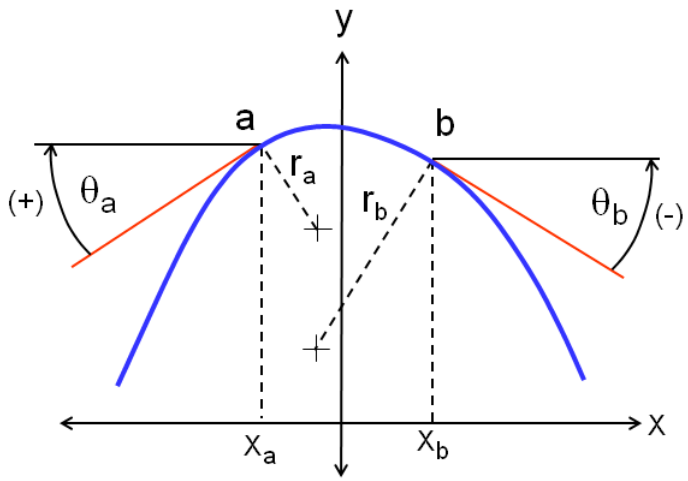

Figure 5-9: Turning angle definition

obtained.

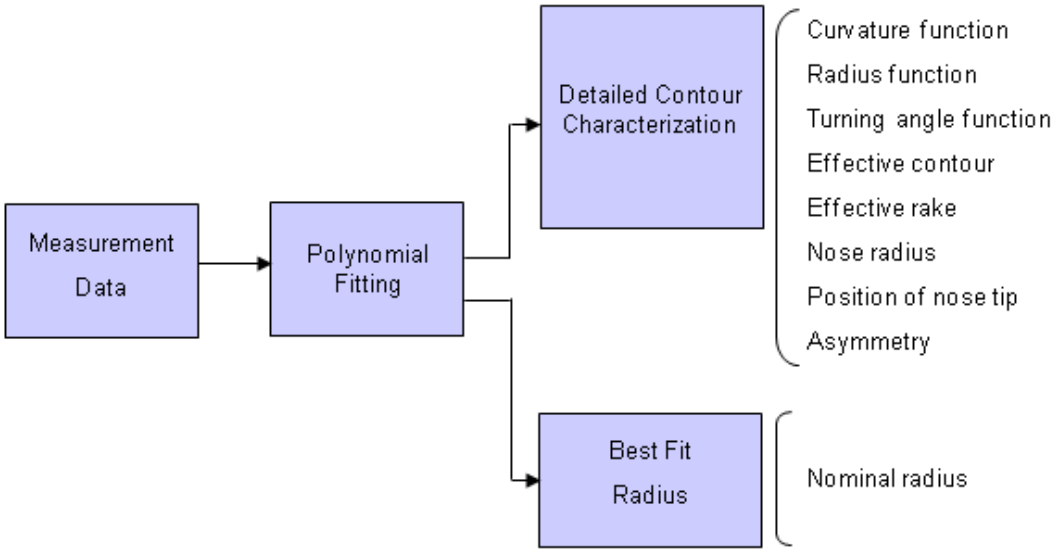

Figure 5-10: Methodology for contour characterization

The measurement data comes from information obtained by scanning the edge surface by means of a white light chromatic sensor [57, 117]. The surface of the cutting edge (convex surface generated by the preparation process) is scanned to obtain contours by cutting the surface with orthogonal planes to the longitudinal direction of the cutting edge (see **Figure 5-11**). **Figure 5-12** shows the data for a contour obtained from the information of the scanning process.

The measurement data obtained from the sensor for each contour can be represented in a coordinate system xy and fitted to a polynomial function $y = f(x)$ (see **Figure 5-13**).

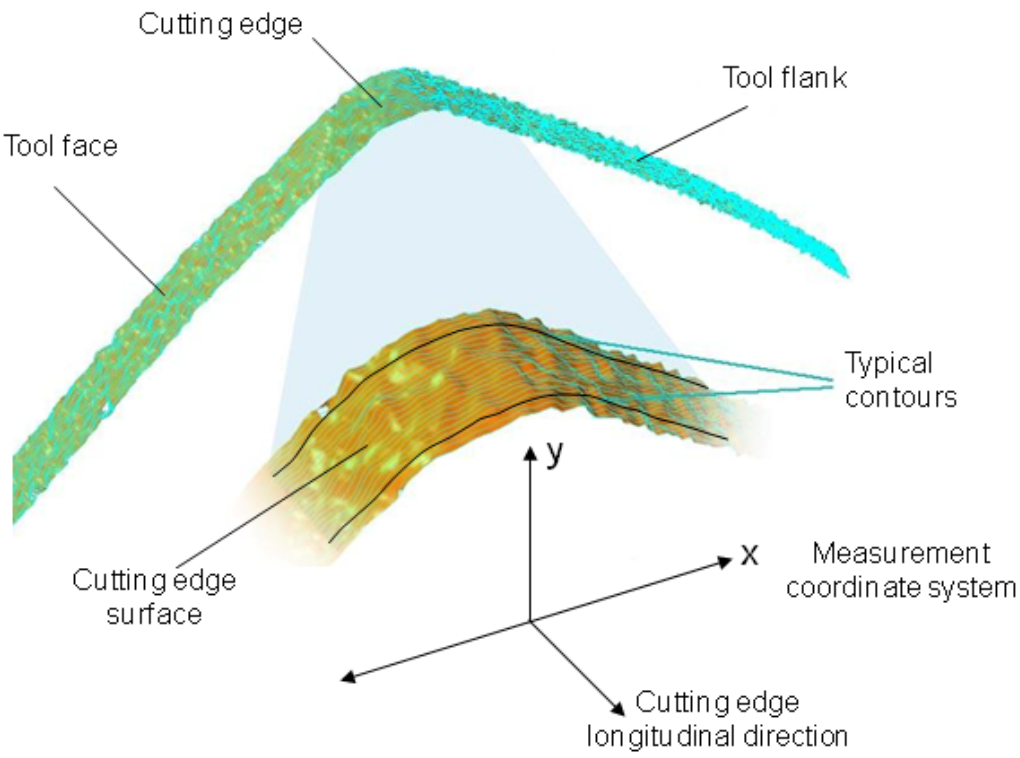

Figure 5-11: Scanned cutting edge surface

A contour can be described in a specific point of the cutting edge or a representative unique contour can be outlined considering a group of contours in a certain longitude of the cutting edge or in the entirety of the cutting edge. To obtain the representative contour of the cutting edge, the median or the average of the contours are considered.

The polynomial function $y = f(x)$ expresses the contour ϕ in cartesian coordinates. To find the curvature function, the radius function and the turning angle function, concepts of differential geometry are used [64]. In this case, it is convenient to express mathematically the contour ϕ as a parametrized curve in the plane R^2:

$$\phi = \phi(t) = (x(t), y(t)) \tag{5-1}$$

The curvature function $\kappa 2[\phi]$ of ϕ is given by[64]:

$$\kappa 2[\phi](t) = \frac{\phi''(t).J\phi'(t)}{\|\phi'(t)\|^3} \tag{5-2}$$

J is the complex structure $J(p_1, p_2) = (-p_2, p_1)$. Where $\mathbf{p} = (p_1, p_2)$ is a point in the plane R^2, which can be considered as a complex number $p_1 + ip_2 = \Re(\mathbf{p}) + \Im(\mathbf{p})$.

An alternative formula for $\kappa 2[\phi]$ is [64]:

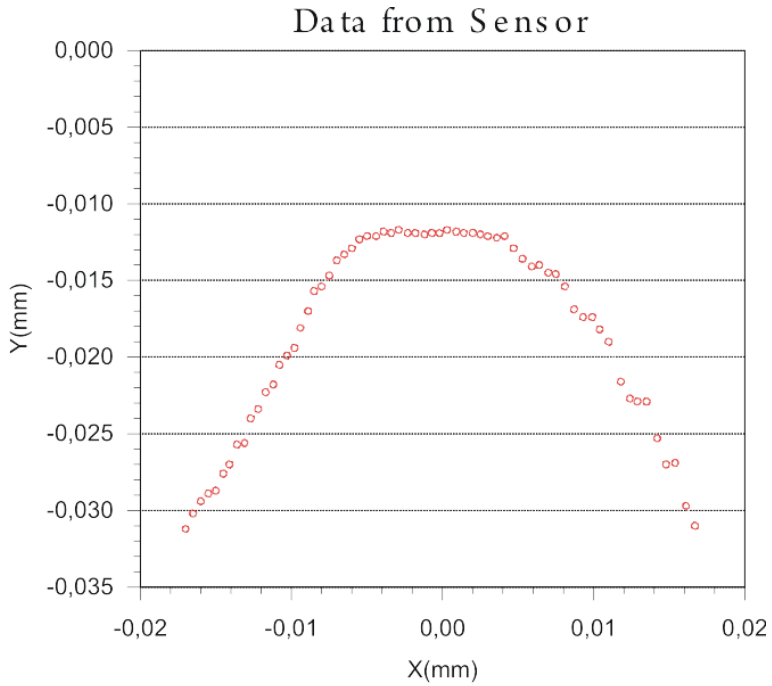

Figure 5-12: Data from chromatic sensor

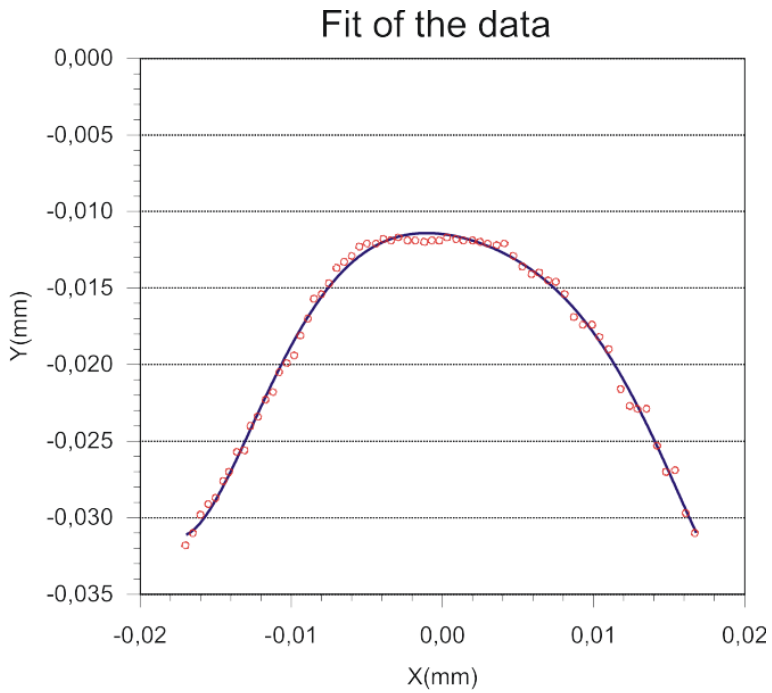

Figure 5-13: Fit of the contour data

$$\kappa 2[\phi](t) = \frac{x'(t)y''(t) - x''(t)y'(t)}{[x'^2(t) + y'^2(t)]^{3/2}} \tag{5-3}$$

The function $1/|\kappa 2[\phi]|$ is called the radius of curvature of ϕ.

The turning angle function is expressed in terms of the parameterized contour ϕ, considering that geometrically, the turning angle $\theta[\phi](t)$ is the angle between the horizontal and $\phi'(t)$. The turning angle and the curvature of a regular curve $\phi](t)$ in the plane are related by [64]:

$$\theta[\phi]'(t) = \|\phi'(t)\| \, \kappa 2[\phi](t) \tag{5-4}$$

To obtain the curvature function, the radius function, and the turning angle function, an algorithm was developed. The algorithm, implemented in the software *Mathematica*®, takes the points obtained by means of the chromatic sensor, and carries out a polynomial fitting (of sixth grade) of the measured contour. The polynomial fitting of the contour, expressed as $y = f(x)$, is parametrized (as in equation 5-1) to calculate the curvature function according to equation 5-2. From this curvature function, the radius function is obtained. Equally, considering the equation 5-4 the function for turning angle in each point of the contour is determined.

As example, considering the data from the chromatic sensor showed in the **Figure 5-12**, the implemented algorithm was applied. As result, **Figure 5-14** shows a parameterized contour after having carried out a polynomial fitting of sixth grade. The curvature, radius and turning angle functions corresponding to the contour of the **Figure 5-14** are shown in **Figures 5-15** , **5-16** and **5-17** respectively.

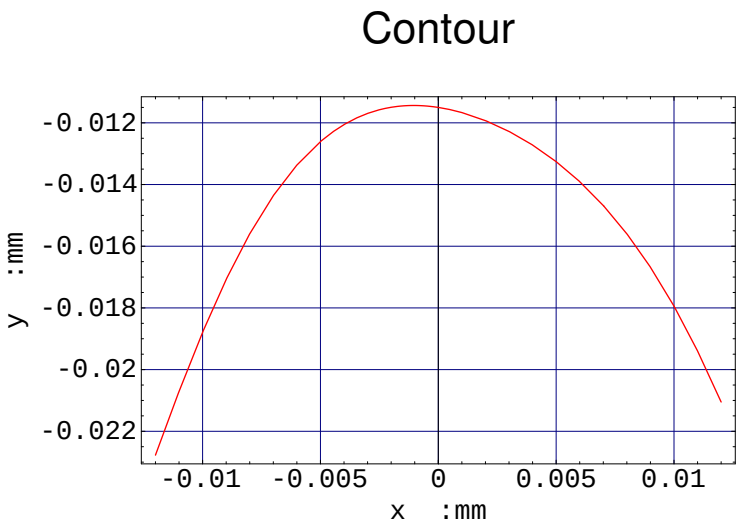

Figure 5-14: Contour of the cutting edge

Considering the contour in working position (see **Figure 5-18**), and relating the geometry of the contour with the macrogeometry of the cutting tool and with the required uncut chip thickness h, it is possible to determine the effective working contour or effective contour ϕ_e among the points 1 and 2. The effective contour ϕ_e represents the geometry

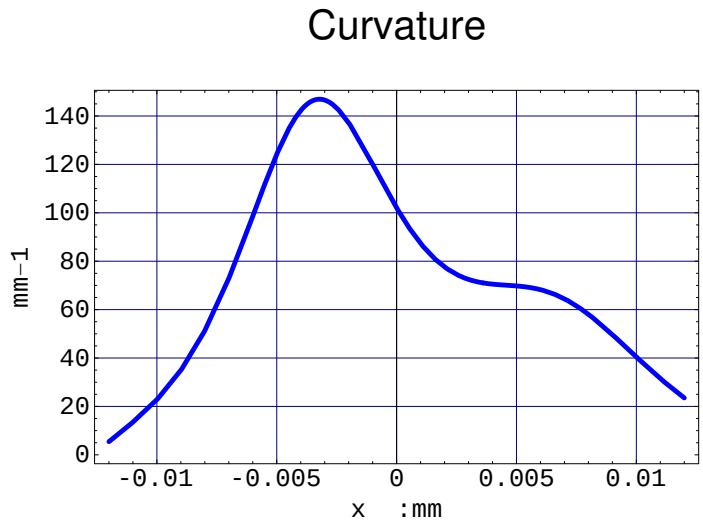

Figure 5-15: Curvature function

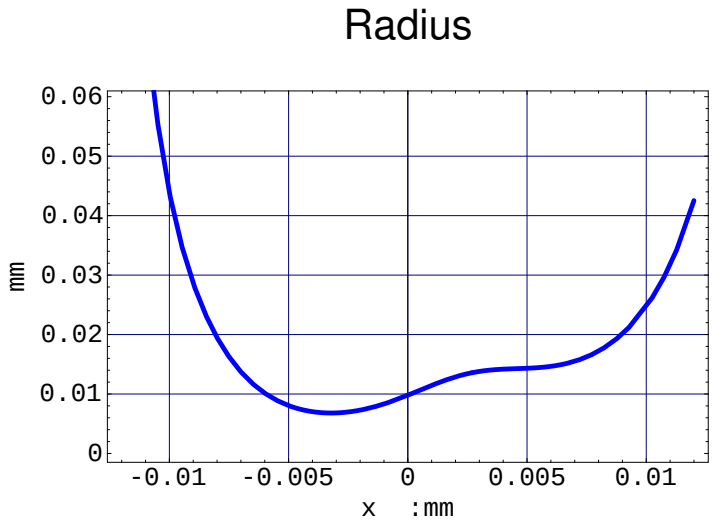

Figure 5-16: Radius function

of the contact between the cutting tool and the workpiece when beginning the cutting process. The Point 1 is the contact point between the tool flank and the machined surface, and the point 2 is the highest contact point between the material to be removed and the cutting tool considering the selected uncut chip thickness h. In the **Figure 5-19**, the contour in measurement position is showed to observe the relationship among the different parameters and the measurement reference system xy.

From the information of the polynomial fit of the contour expressed as $y = f(x)$, the turning angle function $\theta = \theta(x)$, the macrogeometry (α, β and γ), and the uncut chip thickness h, it is possible to determine the effective contour ϕ_e (through the coordinates

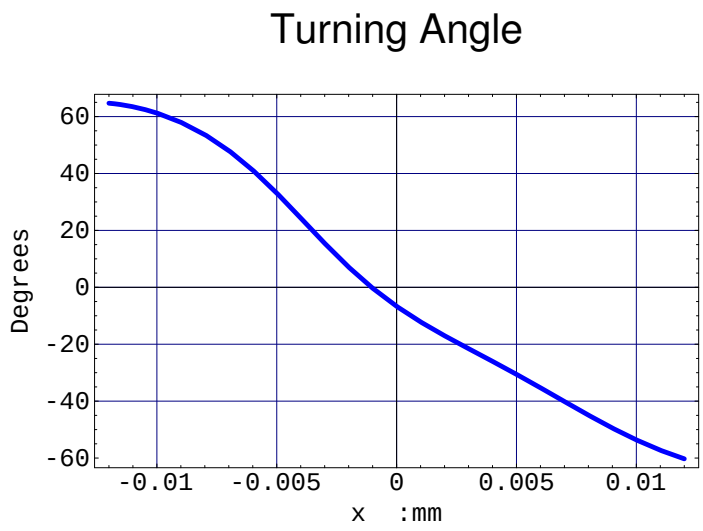

Figure 5-17: Function turning angle

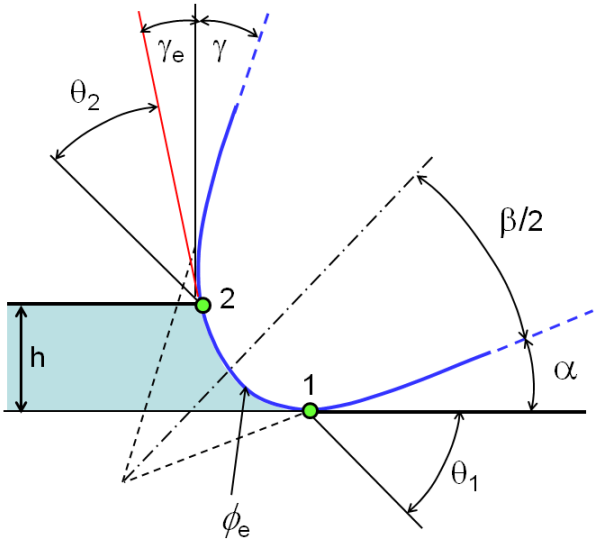

Figure 5-18: Contour in working position

of the limit points 1 and 2), and the effective rake γ_e.

For the above-mentioned the following relationships are considered:

To find the turning angle θ_1:

$$\beta/2 \; + \; \alpha \; + \; \theta_1 \; = \; 90° \tag{5-5}$$

To determine the coordinates of point 1:

$$\theta_1 \; = \; \theta(x_1) \tag{5-6}$$

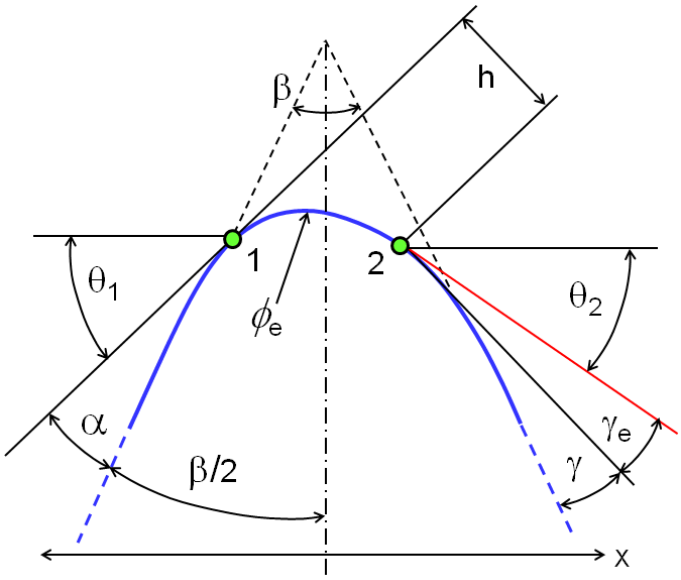

Figure 5-19: Contour in measurement position

$$y_1 = f(x_1) \tag{5-7}$$

To find the coordinates of point 2:

$$x_2 = x_1 + h \cdot \sin\theta_1 + \frac{y_2 - y_1}{\tan\theta_1} \tag{5-8}$$

$$y_2 = f(x_2) \tag{5-9}$$

To determine the turning angle θ_2:

$$\theta_2 = \theta(x_2) \tag{5-10}$$

To find the effective rake γ_e:

$$\theta_2 + \gamma_e + \gamma + \beta/2 = 90° \tag{5-11}$$

Likewise, from the information of the contour; the nose radius r_d is determined. r_d corresponds to the radius of the highest point of the contour with coordinate $n = (x_n, y_n)$ and with turning angle $\theta_n = 0$ (see **Figure 5-20**). Additionally, with the position of the nose tip n, the asymmetry of the contour S_c can be characterized by means of the quotient of the distances p and q measured on a horizontal reference line that intersects the profile of the tool flank and the tool face.

$$S_c = \frac{p}{q} \tag{5-12}$$

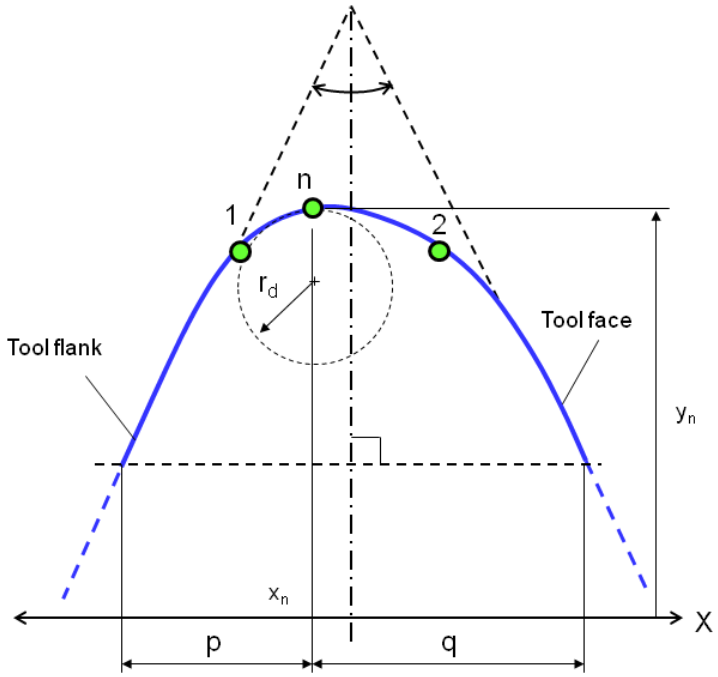

Figure 5-20: Nose radius and asymmetry

If $S_c = 1$, the point m is in the axis of symmetry of the contour, if $S_c < 1$, n is near the tool flank and if $S_c >= 1$, n is near the tool face. The position of the point n (and therefore the form of the contour) has influence in the position of the stagnation point and in the conditions of material flow during the cutting process.

Figure 5-21 shows the contour in working position and the position of the nose tip n represented by h_n compared with the uncut thickness h. From data of the effective contour, h_n is determined as:

$$h_n = \sqrt{(y_n - y_1)^2 + (x_n - x_1)^2} \cdot \left[\sin\left(\theta_1 - \arctan\left(\frac{y_n - y_1}{x_n - x_1}\right)\right)\right] \tag{5-13}$$

If the contour is relatively symmetric $S_c \approx 1$, a nominal radius r_n of the complete contour is considered. The fitted circle arc with radius r_n, is tangent to the generatrices of the tool face and tool flank and its center is on the symmetry axis of the measured contour. An iterative process determine the least square error between the coordinates of the contour points and the coordinates of the points of different circle arcs. **Figure 5-22** shows an example of a best fit estimation of r_n. The contour and the arc which represented the best fit are shown.

The previous characterization, using curvatures, radii, turning angles, effective contour, effective rake angle, nose radius, asymmetry of the contour and nominal radius, allows the relation of the geometric parameters obtained from the measurement process with the macrogeometry of the cutting tool and the working conditions during the cutting

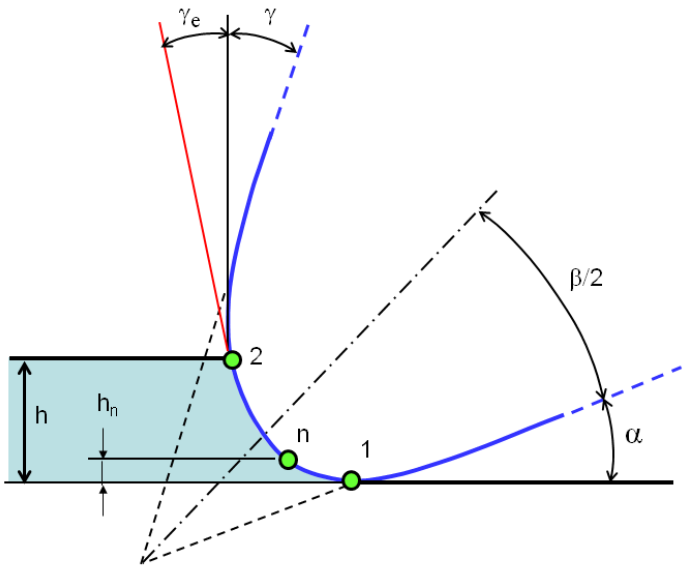

Figure 5-21: Position of nose tip and uncut chip thickness

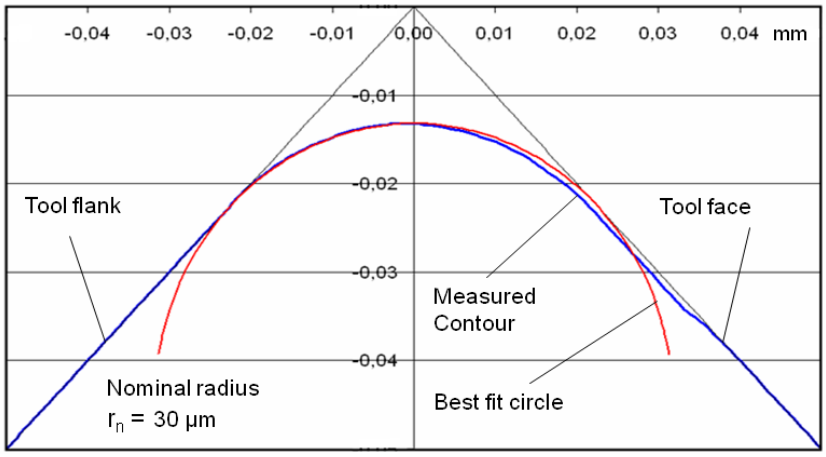

Figure 5-22: Best fit radius for a measured contour

process. Thus, the detailed description of the contour and its relative position during the cutting process is obtained. Such a characterization is useful for quality control, edge preparation process planning, modeling, simulation and experimentation.

5.3.2 Microgeometry of the cutting edge

Definition of Notchedness (*Schartigkeit*)

The quantification of the notches and microtopography irregularities on the surface of the cutting edge is considered as notchedness. The notchedness of the cutting edge, for

a hardmetal cutting tool, is originated by factors associated with the material substrate (metalographic structure: grain size of carbides, thermal and mechanical properties of the substrate: fracture toughness, plastic behavior, creep behavior, thermal conductivity), the macrogeometry of the cutting tool (principally β, shape of the edge: curved or right), the grinding parameters to obtain a sharp edge (type and grain size of abrasive, density of abrasive, bonding material, speed, feed, grinding direction: direction of lay of face and flank, cutting fluid: type and quantity), and/or the parameters of the preparation process to obtain a rounded edge (if it is considered the notchedness of a prepared cutting edge).

From a functional perspective, the characterization of notchedness of the edge surface is required for its importance in the definition of the contact between the edge and the workpiece during the cutting process and therefore the condition of the material flux and wear during the process, and additionally, in the determination of the previous microtopography, exactly on the cutting edge, for the subsequent coating process of the cutting tool.

The characterization of the microtopography of a surface of high curvature represents a complex measurement process, either using stylus or optical measurement methods. For this reason, the characterization of notchedness is made by means of the description of a longitudinal profile on a orthogonal plane to the tangent of the edge contour in the point of interest (see **Figure 5-23**).

The measurement of the longitudinal profiles can be made by means of a special tactile device based on a sharp blade [97] with right edge oriented so that it coincides with the direction of the tangent to the contour at the required point. The tactile device is mounted in to conventional tactile roughness measurement equipment. Likewise, measurement equipment with distance optic sensors can be used. For example, a white light chromatic sensor [57, 117] with the beam oriented orthogonal to the tangent of the contour.

The description of the topography of a surface profile at the most prominent point (nose tip n) of the contour that describes the cutting edge is considered as nominal notchedness (**Figure 5-23**).

For their importance in the definition of effective contact between the cutting tool and the workpiece during the cutting process, it is also considered the notchedness in the points 1 and 2 that correspond to the ends of the effective contour (**Figure 5-23**). A detailed description considers the notchedness in different points of the contour, since the turning angle is known for each point of the contour, it is possible to define the orientation of the orthogonal planes to obtain the different profiles.

The notchedness is quantified through the roughness of the profile, by means of the parameters R_z and R_{max} [13, 41, 188],and through the parameters of the material ratio curves (Abbott′s curves) mainly R_{pk}, $R_k$and, R_v according to international standards (DIN-EN-ISO)[37, 38, 39]. Additionally the ratio R_{pk}/R_z is considered because it gives a measure of the proportion of picks of the profile in relationship with the roughness. A profile with high ratio R_{pk}/R_z implied high susceptibility to initial failure and chipping

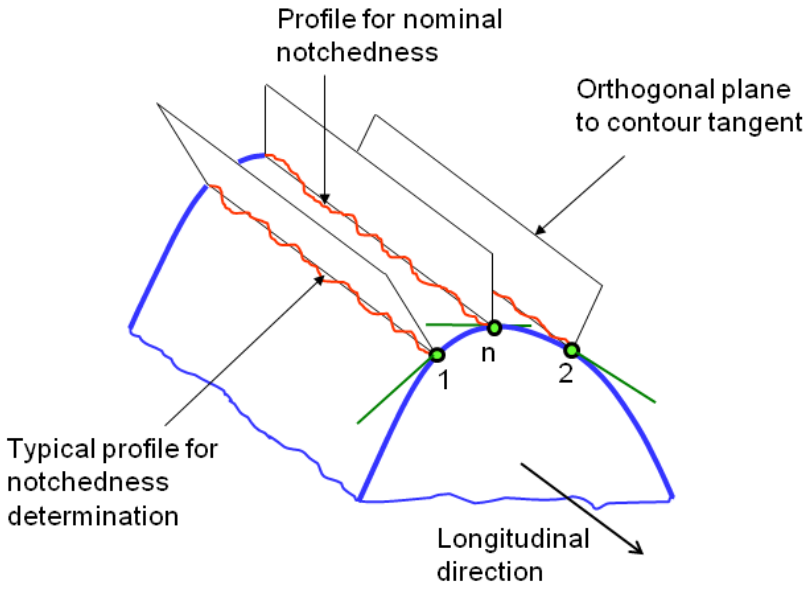

Figure 5-23: Notchedness characterization

because of its little capacity to support loads in the first contact at the beginning the cutting process.

Figure 5-24 shows the characterization of the nominal notchedness of a cutting edge with $\beta = 65°$ obtained by grinding. The profile was obtained by means of a tactile device based on a sharp blade (as reported in [97]). In **Figure 5-24** are shown the parameters of the profile and the material ratio curve with its corresponding parameters R_{pk},R_k, and R_{vk} and the ratio R_{pk}/R_z.

In **Figure 5-25** is considered a complete characterization of the notchedness of a rounded cutting edge obtained by micro-abrasive jet machining. The macrogeometry of the cutting edge is given by; $\beta = 65°$, $\gamma = 10°$ and $\alpha = 15°$, and as example a chip thickness is h =10μm is considered, in order to define the effective contour. The notchedness is observed in three points, in point n corresponding to the nominal notchedness, and at points 1 and 2, that are the limits of the effective contour. The turning angles at the points 1 and 2 are showed. They are used as reference for the measurement of the notchedness in these points. **Figure 5-25** shows also the results of the notchedness at the considered points, in terms of R_z, R_{pk} and the ratio R_{pk}/R_z.

An important aspect of the proposed notchedness characterization is the possibility to compare quantitatively the topography of the resultant cutting edge surface obtained by different combinations of grinding and cutting edge preparation parameters and to observe the evolution of the nominal notchedness during the preparation process. **Figure 5-26** shows a sequence from sharp edge to prepared edge with an intermediate condition during the preparation by using micro-abrasive jet machining. The material ratio curves are

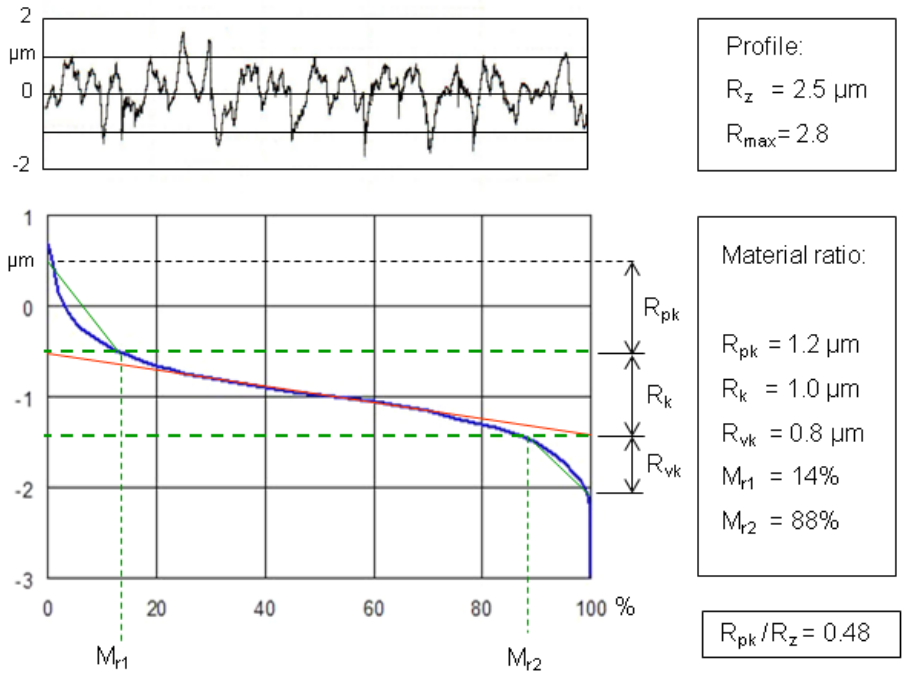

Figure 5-24: Material ratio curve parameters for nominal notchedness of a grinded sharp edge

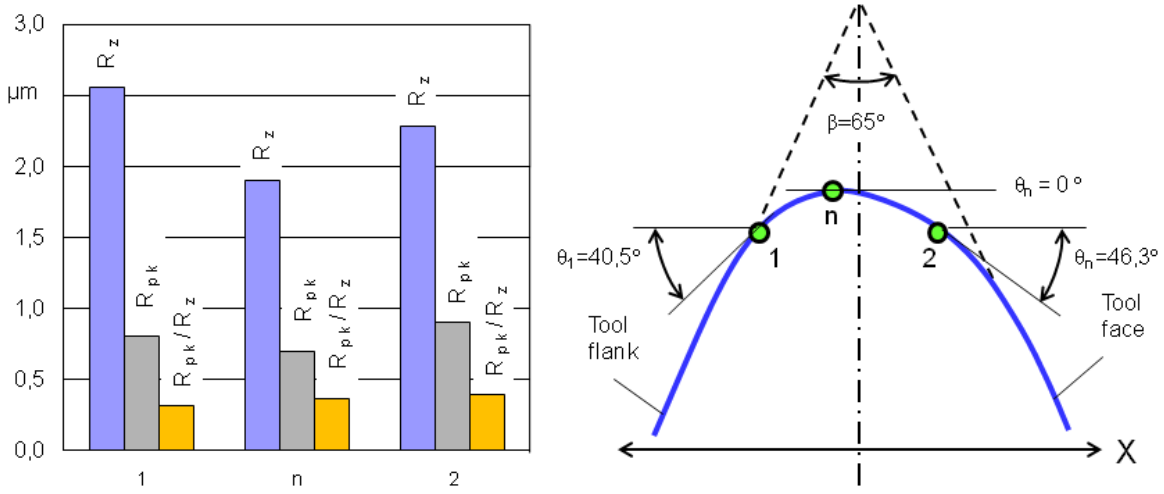

Figure 5-25: Notchedness for three relevant points of the effective contour

shown for the grinded cutting edge and for two conditions of the cutting edge during the preparation process. Considering the ratio R_{pk}/R_z, an improvement in the notchedness is observed by progressive application of micro-abrasive jet machining, which is expressed in the decrease of the picks related with the nominal roughness R_z. To observe quantitatively

the improvement of notchedness, a visual comparison is shown by using scanning electron microscopy (SEM).

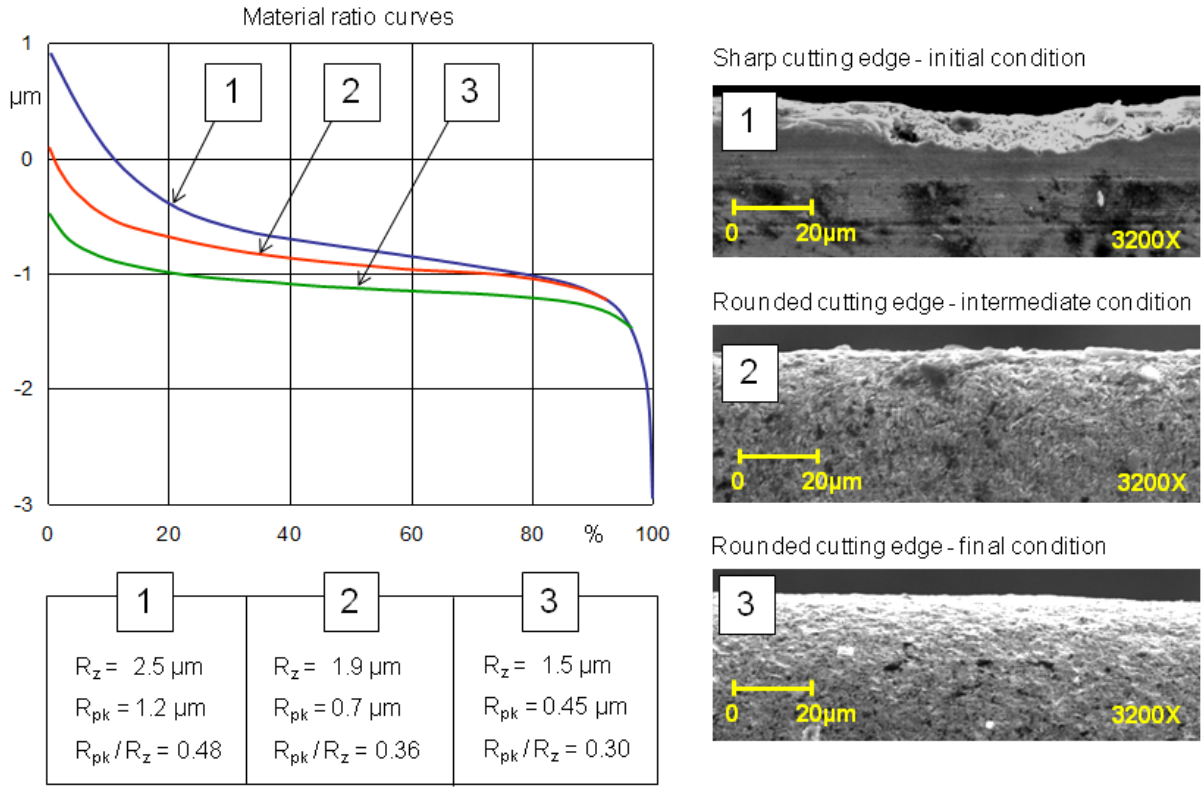

Figure 5-26: Nominal notchedness for different conditions of an edge rounded by micro-abrasive jet machining

Figure 5-27 shows the comparison of the nominal notchedness for three cutting edges obtained by grinding, micro-abrasive jet machining and brushing-polishing respectively. The grinded cutting edge represents a sharp edge and the cutting edges obtained by micro-abrasive jet-machining and brushing-polishing were rounded to obtain the same nominal radius r_n=20μm. It is observed an improvement of the notchedness for the two rounded cutting edges in terms of decrease of R_z and principally by the decrease of the ratio R_{pk}/R_z. Additionally, a visual observation by using SEM, is presented in order to compare the cutting edge surfaces and their improvement in notchedness.

Characterization of microstructuring of the tool face and tool flank

The microstructure of the surfaces in the chip-tool and workpiece-tool interfaces influences tribological aspects of the cutting process, principally the wear in the face and flank. Such microstructuring of the tool flank and face is relevant for the lubrication strategy or for the dry cutting process behavior. The microstructure of the face has special influence upon chip flow and chip transport, which is vital in different processes as deep drilling

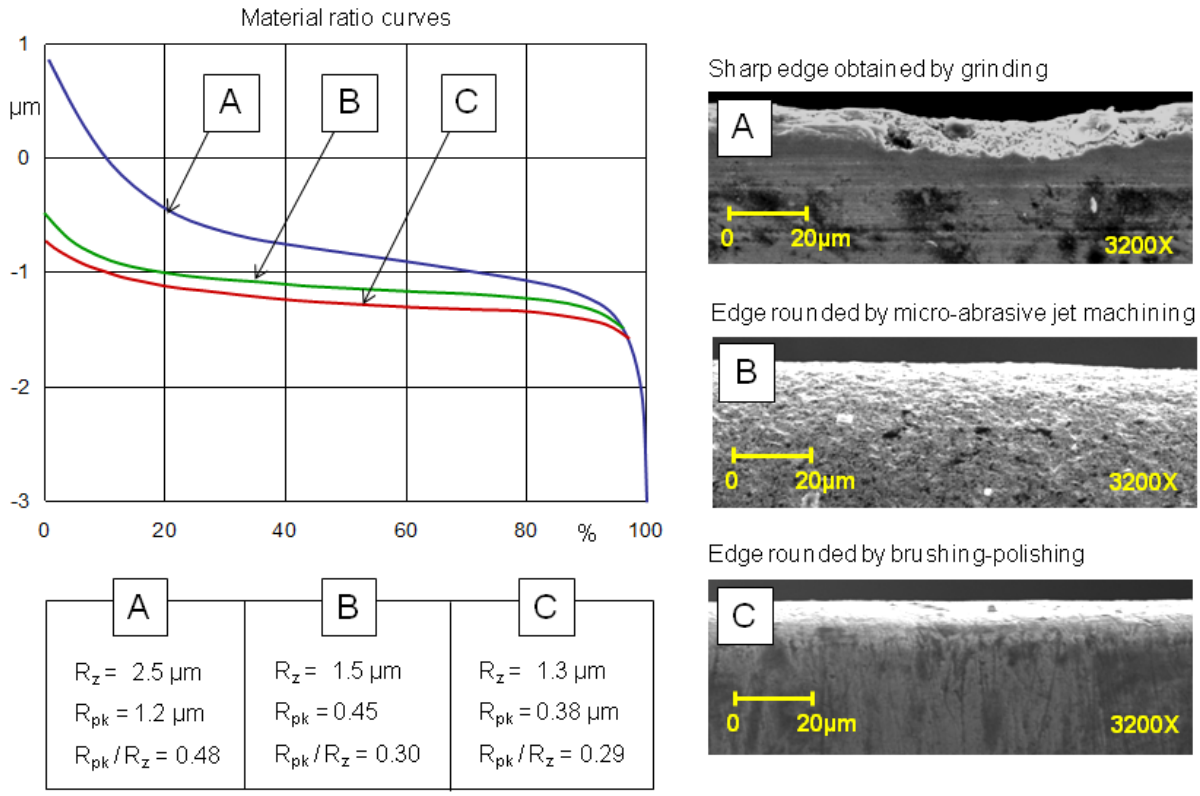

Figure 5-27: Comparison of nominal notchedness of a cutting edge obtained by different processes

and high speed cutting. On the other hand, the microtopography of the surfaces of the cutting tool affects the quality of coating when it is applied as subsequent process to the cutting edge preparation process. For these reasons an adequate characterization of the microstructuring of the tool face and flank is required.

For the characterization of the microstructuring of the tool face and tool flank in the vicinity of the cutting edge, in this work, two approaches are used. Firstly, the new concepts and international norms related with three dimensional surface texture characterization are applied. Secondly, for the analysis of the anisotropy of the microstructuring, concepts of fractal geometry, applied to engineering surfaces, are considered.

3D surface texture characterization

Because of requirements for characterizing the microstructure of the engineering surfaces for applications in surface engineering (coating processes) and tribology (friction, wear), areal parameters for three dimensional description of the surfaces have been proposed [109, 193].

Additionally, with the development of new optic and tactile technology for measuring the microtopography of the engineering surfaces, it is possible to obtain, with

enough resolution and precision, three dimensional information of the surface topography expressed as heights in vertical direction z, corresponding to points on a horizontal plane xy. In this work the information upon the 3D microtopography of the surfaces is obtained by using a white light chromatic sensor and following international norms [75, 76, 77].

The concept of electromagnetic surface is proposed in the international norms [75, 76, 77], and it is related with scanning of the surface by using electromagnetic radiation with a specific wavelength, as it is the case of scanning with optical devices. In **Figure 5-28** the locus of three different surfaces obtained by scanning with a light chromatic sensor are showed. The surfaces were obtained by grinding, micro-abrasive jet machining and brushing-polishing. Equally, **Figure 5-28** shows the considered area to analyze the microstructuring of the tool face in the vicinity of the cutting edge before and after applying the preparation process.

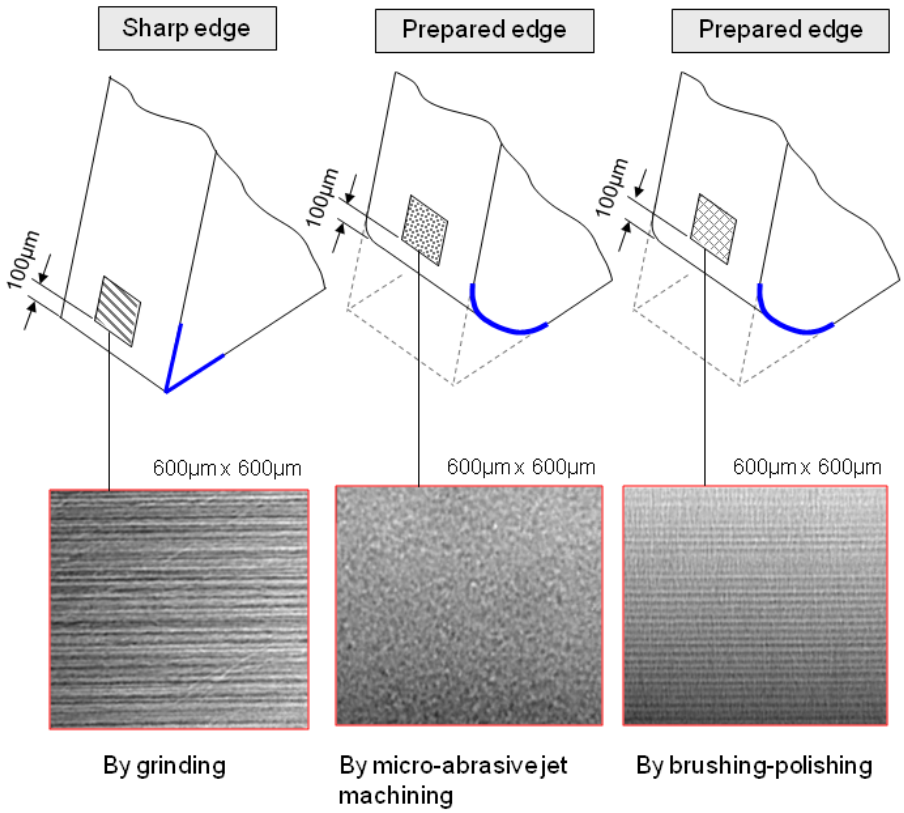

Figure 5-28: Electromagnetic surfaces (600μm x 600μm) for different processes obtained by scanning with a white light chromatic sensor

With the information obtained by scanning with a white light chromatic sensor, the 3D amplitude parameters [75]; arithmetical mean height S_a, root mean square height S_q, maximum height S_z, maximum peak height S_p, maximum pit height S_v, skewness S_{sk} and

kurtosis S_{ku} are determined. Equally, the parameters of the areal material ratio [37, 75]; S_k, S_{pk}, S_{vk}, S_{mr1} and S_{mr2} are considered. Additionally, to observe the tendency of the microstructuring in terms of isotropy, the autocorrelation function of the surface is calculated [75]. An autocorrelation function with a central peak shows a surface with an isotropic tendency, otherwise the form of the autocorrelation function shows the direction or main directions of the texture.

Figure 5-29 shows the characteristics of a surface obtained by grinding corresponding to the tool face of a sharp tool. The surface parameters (amplitude and material ratio) are listed and additionally the autocorrelation function of the surface is shown. The autocorrelation function evidences a strong anisotropy with a clear main direction of the texture generated by the grinding process.

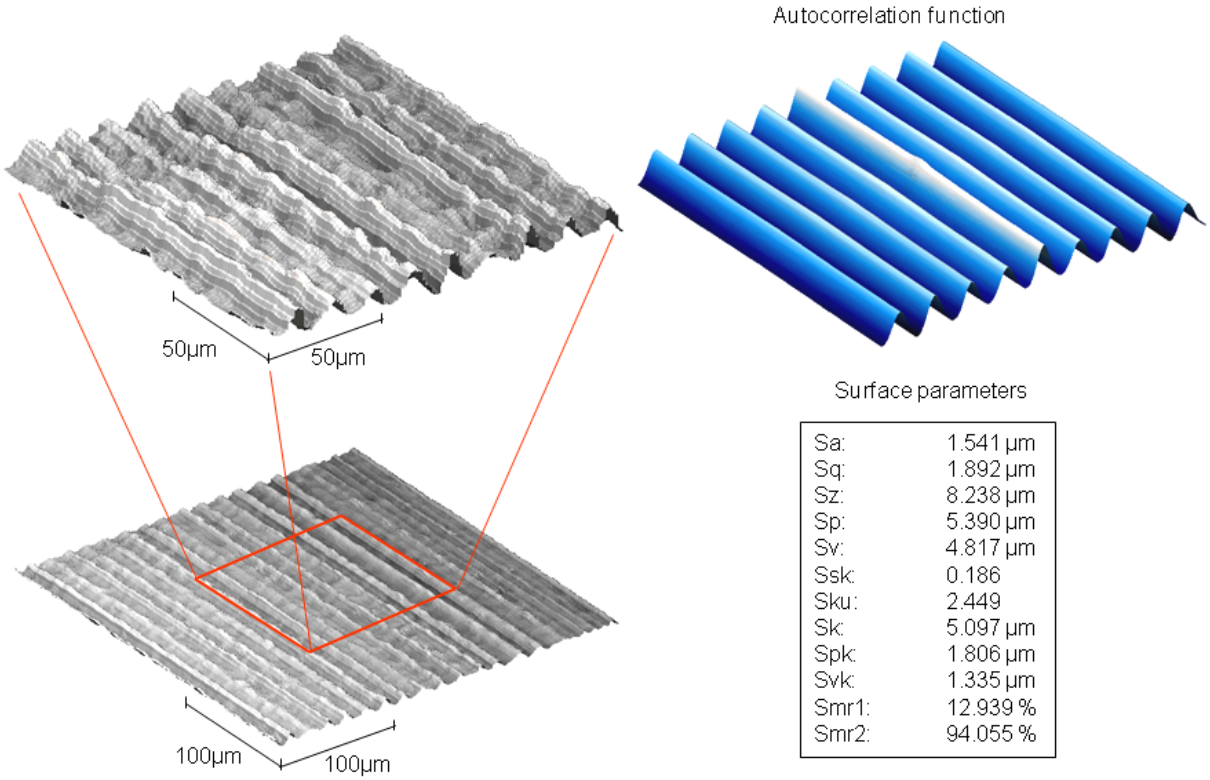

Figure 5-29: Parameters to characterize the microstructuring of a tool surface obtained by grinding

Figure 5-30, shows the characterization of a surface obtained by micro-abrasive jet machining corresponding to the tool face of a rounded cutting edge. The surface parameters are listed and the autocorrelation function shows a peak that evidences an isotropic tendency. This isotropy is caused by the prints generated by random impacts of the abrasive particles of the jet on the surface. Although the jet was not applied orthogonal to the tool face surface, because the it was applied attacking the edge in a

symmetrical direction (see **Figure 7-2**), anyway the effect of the impacts generates a surface with isotropic tendency.

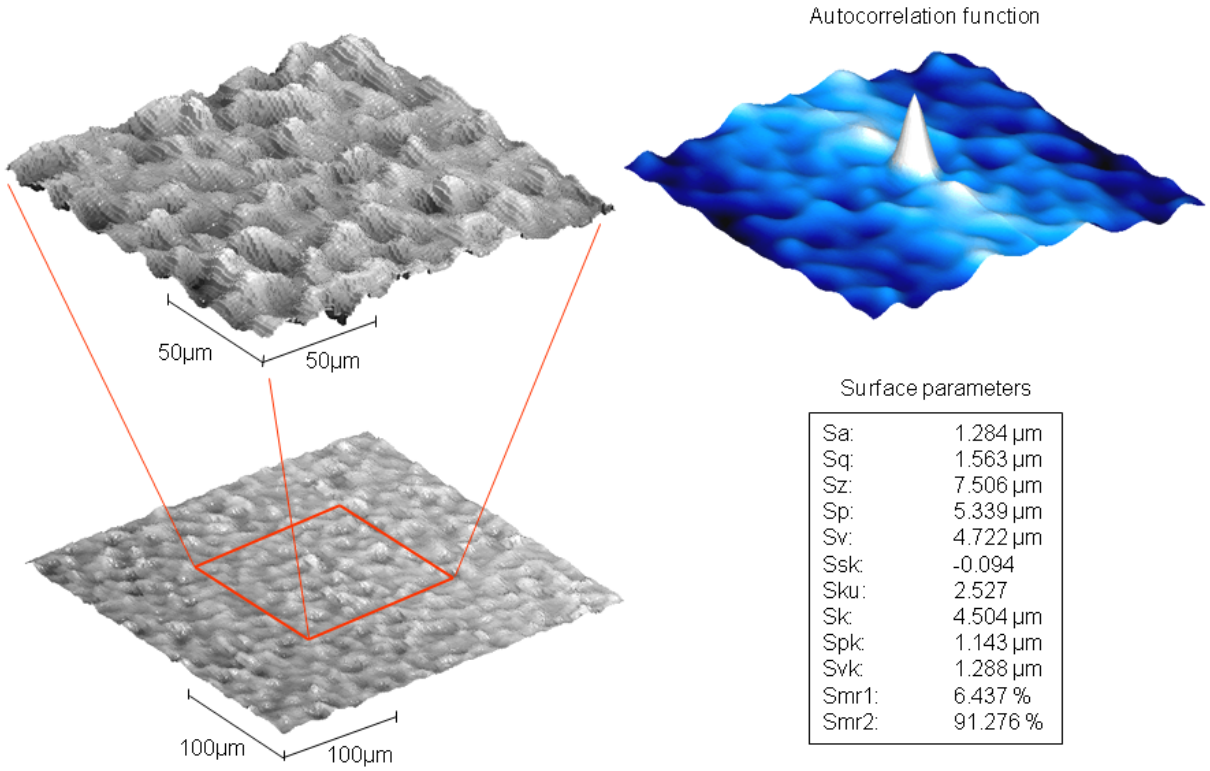

Figure 5-30: Parameters to characterize the microstructuring of a tool surface obtained by micro-abrasive jet machining

Figure 5-31 shows the characterization of a surface obtained by brushing-polishing corresponding to the tool face of a rounded cutting edge. The surface parameters are listed and the obtained autocorrelation function evidences an anisotropic tendency. This anisotropy is originated from the combination of the texture direction of the previous grinding process and the texture generated by the kinematics of the brushing-polishing process, giving as a result a crossed structure, which can be appreciated in the image of the scanned surface and in the corresponding autocorrelation function.

The characterization using 3D surface parameters (amplitude and material ratio) and the autocorrelation function, is proposed for the tool face and the tool flank surfaces to describe the effect of the cutting edge preparation process on the microstructuring. An important objective is the control of the surface generated and the comparison before and after the preparation process.

Fractal characterization of anisotropy of the tool face and flank surfaces

To describe the texture of the surfaces in the proximity of the cutting edge, concepts of Fractal geometry were used, specifically for the characterization of the anisotropy of the

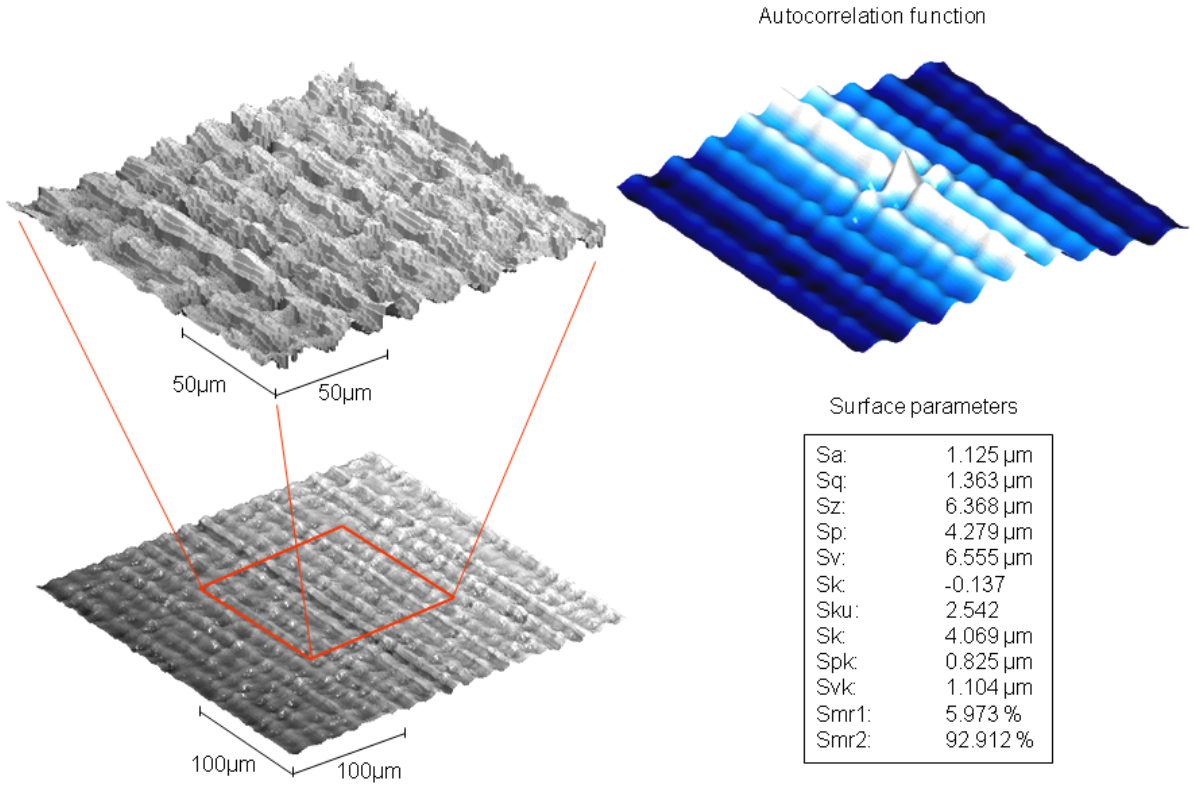

Figure 5-31: Parameters to characterize the microstructuring of a tool surface obtained by brushing-polishing

surfaces of the cutting tool (flank and face). Fractal geometry is used to describe shapes where the same basic structural pattern appears upon increasing magnification of the object [24, 68, 104, 192, 213].

Fractals are functions which are continuous but not differentiable [109]. They possess the property of self-similarity, that is they appear the same at any scale of magnification (see **Figure 5-32**). Self-similar fractals can be completely characterized by a single parameter, the fractal dimension D. For ideally self-similar fractals, there is no preferred direction and scaling of details is either exactly or statistically the same in all directions. However, self-similarity of surface detail implies that there can be undercuts that are not imaged by top-down measurement systems, which return only the elevation of the highest point at each location. In this case, even an ideally self-similar fractal surface will produce a data set that is self-affine. Self-affine means that the data contains a hierarchy of data that scale at different rates and in different directions.

For many engineering surfaces, it is observed that if the surface profile is repeatedly magnified, more roughness keeps appearing (see **Figure 5-33**), then this means that the profile can be self-similar or self-affine. A surface profile $z(x)$ is known as self-similar if $z(bx) \sim b$ and is known self-affine if $z(bx) \sim b^d$, where b is the horizontal scaling factor

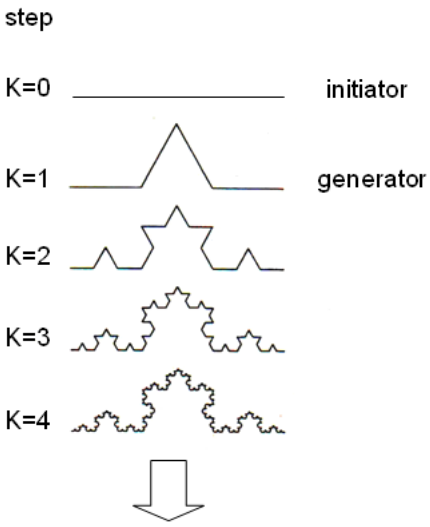

Figure 5-32: Example of self-similar structure (Koch′s curve)

and d some real number. Surfaces that are self-similar or self-affine are never smooth at any length scale. In this sense, local slopes (dz/dx) are undefined.

The difference between the self-similar property and the self-affine property is that the self-similar fractals require only one parameter to define them, the fractal dimension D, whereas self-affine surfaces require an additional one which relates to the scale being viewed. In terms of roughness description, it is necessary to specify, in addition to D, the way in which the ratio of vertical to horizontal magnification has to be changed in order to preserve self-similarity. The name given to this other parameter is topothesy. The topothesy Λ is formally defined as the distance along the profile for which the expected angle between two points would be one radian.

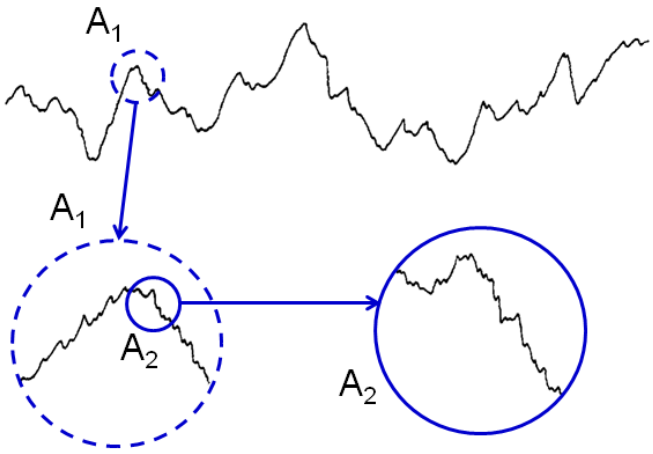

Figure 5-33: Surface fractal profile (adapted from [109])

To analyze the engineering surfaces by means of fractal geometry, there are different methods for surface profile fractal calculation [68, 138, 169, 194, 199, 200, 207, 213, 214]:

- Horizontal dilation(Mikowski method)
- Variance or RMS (root mean square) vs. sampling length
- Hurst analysis
- Fourier power spectrum
- Structure function

And for surface fractal calculation [104, 207]:

- Slit island method (SIM)
- Box counting method

In this work the Fourier power spectrum method was used for the characterization of the anisotropy of the surfaces. The method is applied considering an image obtained through the registration of the elevations of the surface by means of an optic sensor (white light chromatic sensor) that operates under the principle of chromatic aberration. The Fourier method has several advantages for studying fractal surfaces. It can reveal and allow the characterization of the anisotropy of the surface. Additionally the method is relatively insensitive to the presence of the noise in images due to the operation of the measuring instrument. Next the foundations of the method are presented.

Consider a surface profile $z(x)$, which has the mathematical properties of being continuous everywhere but not differentiable and self-affine in roughness structure. These properties can be satisfied for the Weierstrass-Mandelbrot(W-M) fractal function, which can be used to characterize the roughness of surface profiles.

The W-M fractal function is given as [68, 104]:

$$z(x) = G^{(D-1)} \sum_{n=n_l}^{\infty} \frac{\cos 2\pi\psi^n x}{\psi^{(2-D)n}} \qquad \psi > 1 \tag{5-14}$$

Where D is the fractal dimension, G is a characteristic length scale, ψ^n corresponds to a frequency term that is reciprocal to wave length $\psi = 1/\lambda^n$, in another way $\psi^n = \omega$, where the frequency ω is the reciprocal of wave length and n is called wave number. Also $\psi^{n_l} = 1/L$ where L is the sampling length.

The considered W-M function satisfies two important properties of a fractal surface: (i) although the summation series $z(x)$ converges, dz/dx diverges, implying that $z(x)$ is non-differentiable; (ii) the function is self-affine, because $z(\psi x) = \psi^{2-D} z(x)$, this means the scaling of $z(x)$ and x is unequal.

The power spectrum of W-M function is given as [68, 104]:

$$P(\omega) = \frac{G^{2(D-1)}}{2\ln\psi}\frac{1}{\omega^{(5-2D)}} \tag{5-15}$$

It can be seen that both G and D are independent of ω, therefore they are scale invariant. On the other hand, the power spectrum follows a power law behavior. If $P(\omega)$ is plotted versus ω on a log-log plot, then the power law behavior would result in a straight line. D relates to the slope m ($m < 0$) of the spectrum on log-log plot and G correlates with the intercept of the log-log plot.

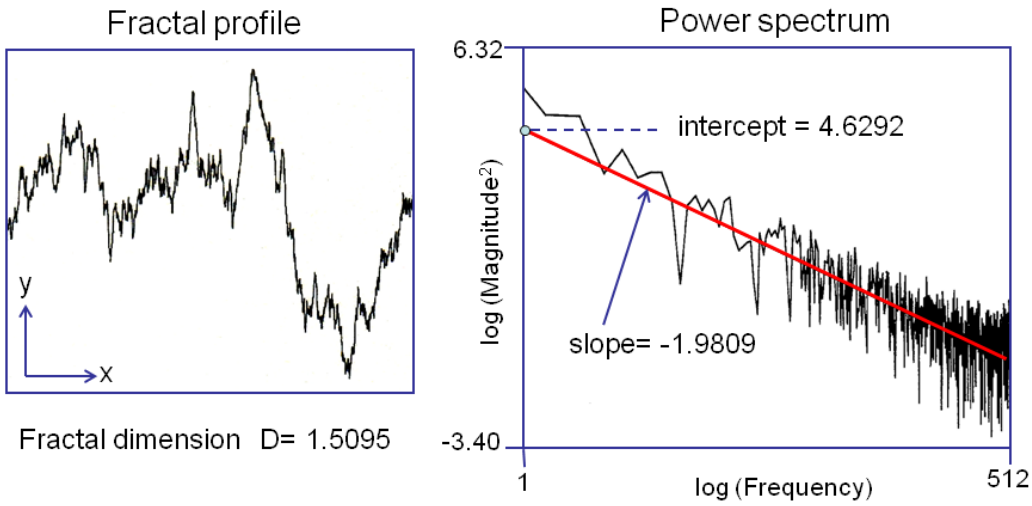

Figure 5-34: Fractal profile and its power spectrum on log-log axes

Another way to write the function $P(w)$(equation 5-15) in order to interpret the meaning of the terms is:

$$P(\omega) = \frac{A}{\omega^m} \tag{5-16}$$

The constant term A ,related with the intercept of the straight line in the log-log plot, contents G,D and ψ, and the term m ($m < 0$) is the slope of the straight line. Knowing the slope and intercept, the fractal dimension and topothesy are determined respectively. D can be given as follows :

$$D = \frac{1}{2}(5 + m) \tag{5-17}$$

The scaling constant G is related to topothesy by [192]:

$$\Lambda = \frac{G}{(2D-2)\sqrt{2\ln\psi}} \tag{5-18}$$

The slope of the log-log plot of the power spectrum an the resulting fractal dimension provides an additional surface characterization that describes the spatial organization of

the roughness in a way that descriptive statistics (for example, the root mean square RMS value) does not.

Generally used roughness parameters (R_a, R_z, R_{max}, etc.) are scale-dependent; the values will depend on the measurement scale and the sampling interval. On the contrary Fractal analysis is a scale-independent evaluation technique. The fractal dimension D is an intrinsic property of the surface, independent of the wavelengths measured, and thus independent of filtering.

Consider two profiles with the same fractal dimension, whose Fourier plots show the same slope but are displaced vertically, therefore they have different intercepts. The meaning of this offset is that the surfaces have a different magnitudes of roughness. The intercept can be used to describe the overall magnitude of the roughness. Through the application of Fourier analysis to both profiles and 2D range images, the constant that defines the vertical position of the line, which is independent of the slope, and represents the magnitude of the roughness directly, is determined. This parameter will represent the magnitude of surface roughness in a way that is independent of the measurement technique or the range of dimensions over which the measurement is performed [138].

Fractal calculation for surface analysis mainly includes the calculation of the profile fractal dimension and the calculation of surface fractal dimension [69, 80, 169]. This calculation is involved with computer assisted analysis of topography images in 2D or 3D of a surface obtained in analog or digital signals using profilometer, microscopy, etc.

In the calculation of the fractal dimension of an image, surface topography must be converted into a digital colorized image, then into a grey image that may be threshold optimally into a binary image. Finally, profiles are obtained through edge detection. Through tracking boundary, coordinates of all points on the profile are gained and the fractal dimension of profile with programming can then be worked out by using proper methods.

When a range image (in which each pixel value represents the highest elevation of the surface within the pixel area) of a fractal surface processed with a conventional 2D FFT (Fast Fourier Transforms), the $\log P(\omega)$ falls off linearly with $log(\omega)$[109]. Since the usual representation of the image in frequency space uses a linear scale of frequency , radial from the center of the image, with a logarithmic scale for the magnitude or power, the result is a transformed image showing the power spectrum in which in which the pixel brightness drops off smoothly but nonlinearly with the radius. For measurement purposes, it is important to average the values and plot $\log P(\omega)$ VS. $log(\omega)$ to determine the fractal dimension.

When the original surface image is anisotropic, the two dimensional Fourier transform (2DFT) reveals this [138, 139]. The slope of the $\log P(\omega)$ VS. $log(\omega)$ plot can be evaluated as a function of the direction by using all of the points within a pie-shaped wedge in the transform image. Performing a least squared fit to these data points provides a direct measure of the fractal dimension as a function of the direction . Plotting these values as a rose plot vs. orientation angle shows the degree and direction of the

anisotropy. For the case of a perfect isotropic surface, the rose plot is a circle.

To observe the proposed methodology to characterize the microstructuring of the tool face and tool flank of the cutting tool, in **Figure 5-35** the reference system used to define the fractal characterization is shown. The orientation is important to compare the changes in microstructuring after applying an specific preparation process. The data of the observed surfaces was obtained by using a white light chromatic sensor (with lateral resolution of 1 μm and vertical resolution of 60 nm). The data from the surface was converted to a *JPG* file as black and white picture, where the gray scale represent the height of each point of measurement. Using the algorithms proposed in [138], which were implemented in *Matlab*® by means of the function *fdsurfft* [212] (which calculates the fractal dimension of a fractal surface by fourier transform), the power spectrums of the profiles of the surface in different directions are determined. With this information, the intercepts and the slopes in each direction is computed, and the rose plot of intercepts and slopes is obtained.

Figure 5-36 shows a typical power spectrum obtained by processing an image from a tool face surface that was processed as result of a cutting edge rounding by means of micro-abrasive jet machining. The image of the surface was obtained by means of a white light chromatic sensor and converted to a *JPG* file as black and white picture. In **Figure 5-36** the power spectrum and the corresponding linear regression, by means of least squares, was presented. With the linear regression the slope and intercept are obtained.

Figure 5-37 and **Figure 5-38**, show the rose plot of intercepts and the rose plot of slopes (in absolute value), respectively, for a tool face surface (see **Figure 5-35**) obtained by grinding to generate a sharp cutting edge. The values of intercepts evidence that the roughness is greater at 90° and 270°, with a value of intercept of 27, in contrast, the roughness is lower at 0° and 180°, with a value of intercept of 22. This result is associated with the main grinding direction which is parallel to the direction of the 0°-180° axis. Likewise, the rose plot of slopes show the spatial organization of the roughness of the surface in each direction. In each direction there is a value of slope m that is associated to the fractal dimension D according to equation 5-17. For the considered surface, the minimal slope is 1.3 at 0°, and the maximal is 2.25 at 90°. These values of slopes and the general distribution of slopes evidence a strong anisotropy associated with the grinding kinematics used to generate the microstructure of the surface.

Figure 5-39 and **Figure 5-40** show the rose plot of intercepts and the rose plot of slopes, respectively, for a tool face surface (see **Figure 5-35**) obtained by micro-abrasive jet machining in order to round a cutting edge. The general distribution of intercepts shows that the roughness of the surface has not strong differences depending on the direction, and in general the values of intercepts, varying between 24 and 25, evidence uniformity in the roughness that can be caused by random impacts of the abrasive particles of the jet on the surface. Regarding the rose of slopes, there is no complete radial

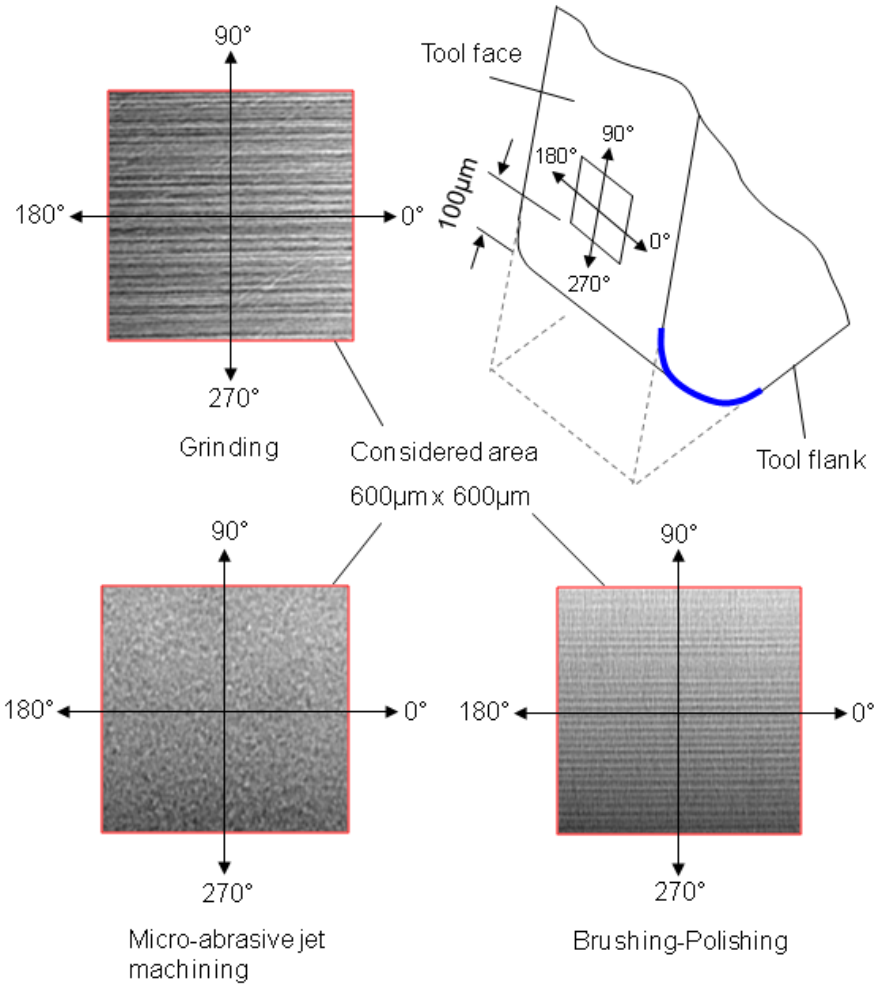

Figure 5-35: Reference system for fractal characterization of the surface obtained by different processes

symmetry in the spacial distribution of the roughness, because the abrasive jet was not applied orthogonal to the tool face surface, but directing to the cutting edge in symmetrical direction, attacking the tool face and the tool flank with the same angle in the same operation.

Figure 5-41 and **Figure 5-42**, show the rose plot of intercepts and the rose plot of slopes, respectively, for a tool face surface (see **Figure 5-35**) obtained by brushing-polishing in order to round a cutting edge. The intercepts evidence a relative uniformity in the roughness, varying the intercepts between 21 and 25. The structure is the result of a combination of the previous grinding microstructuring and the microstructuring resulting from the kinematics of the brushing-polishing process. The corresponding rose plot of slopes, in which the slopes varying between 1.1 and 1.7, evidences a relative radial symmetry in the spatial distribution of the roughness.

The fractal characterization by means of Fourier power spectrums, obtained from

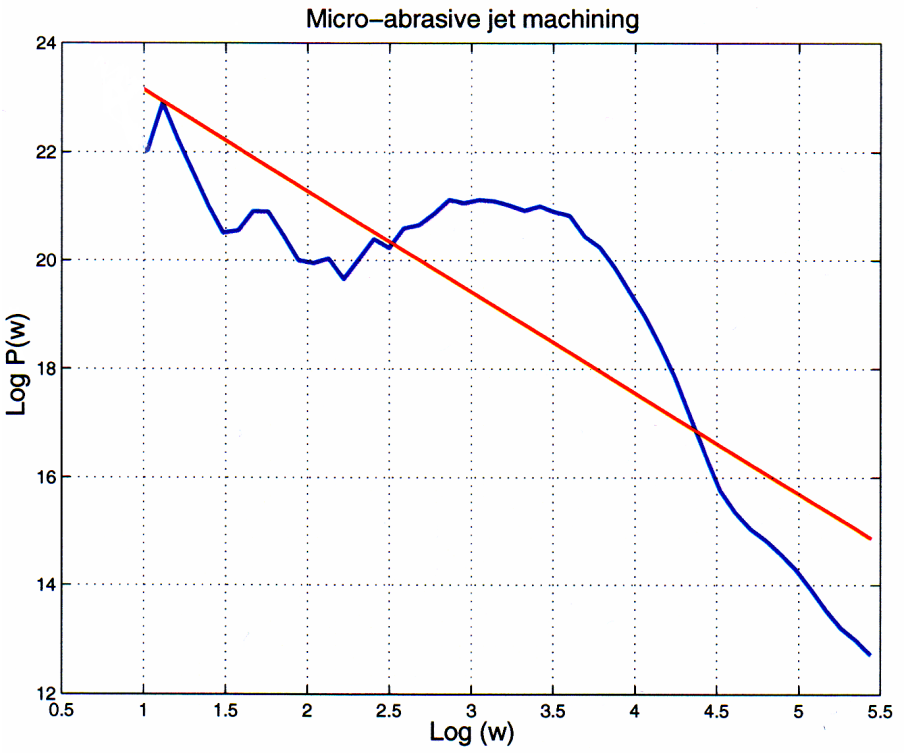

Figure 5-36: Example of power spectrum of a profile for a tool surface obtained by micro-abrasive jet machining

scanned surfaces by using a chromatic sensor, allows determining the microstructuring of the tool face and flank, resulting from a cutting edge preparation process. The characterization defines the radial distribution of two parameters (intercept and slope) to observe the roughness in each direction of a polar plot and also the spacial distribution of the roughness. Additionally, it is possible the quantitative comparison of microstructuring obtained with different preparation processes or combination of process parameters.

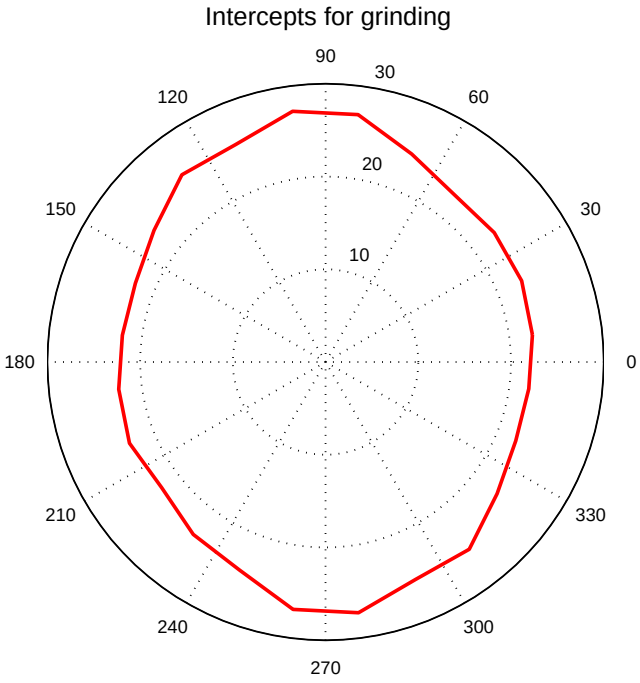

Figure 5-37: Rose plot of intercept for a tool surface obtained by grinding

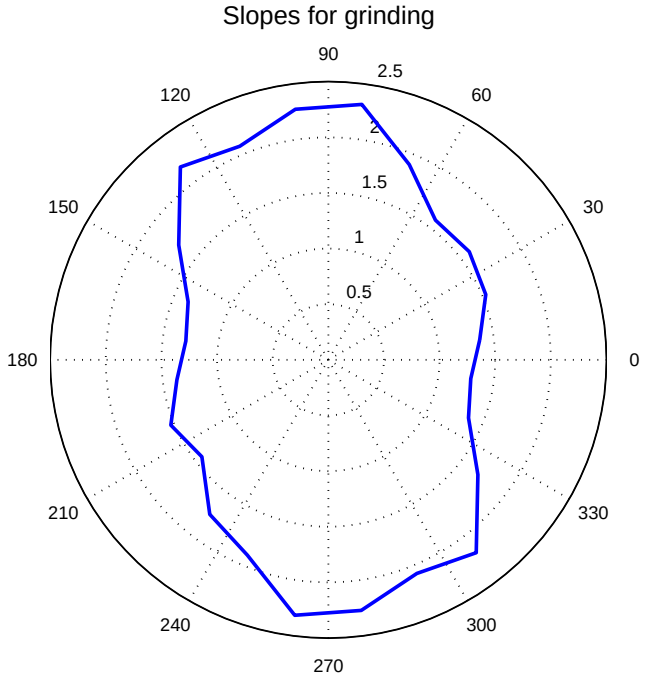

Figure 5-38: Rose plot of slope for a tool surface obtained by grinding

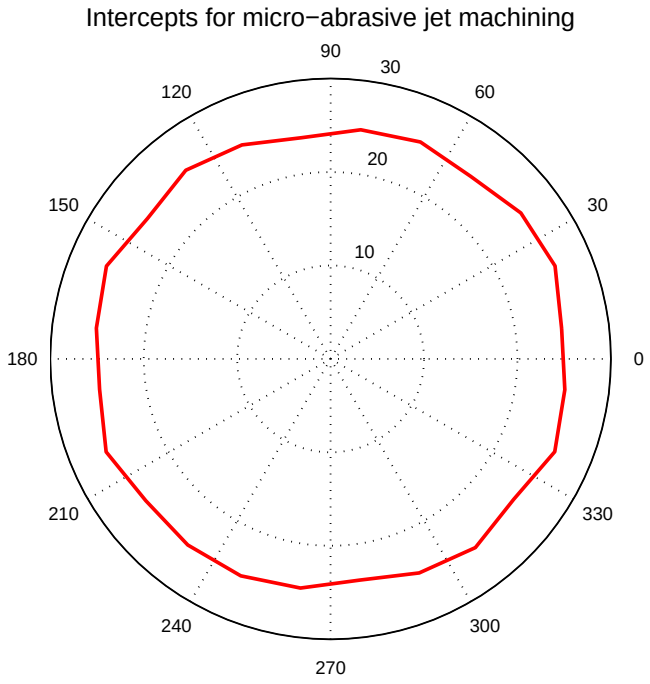

Figure 5-39: Rose plot of intercept for a tool surface obtained by micro-abrasive jet machining

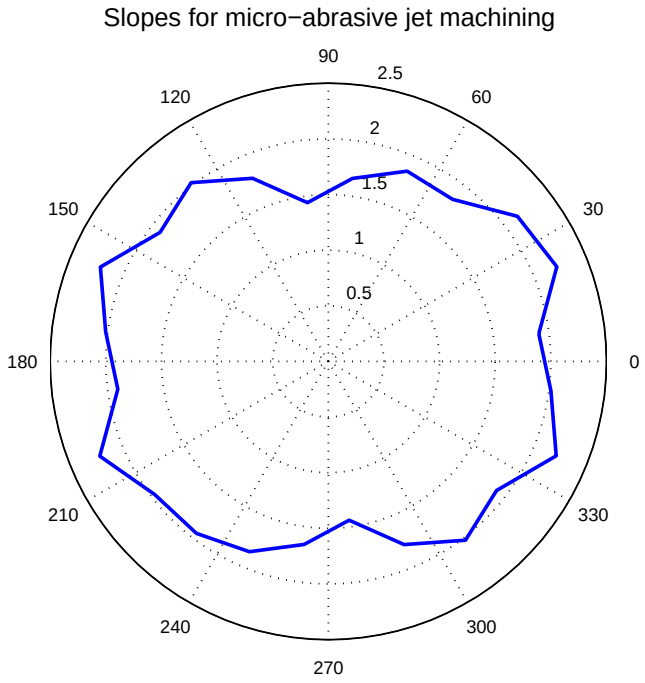

Figure 5-40: Rose plot of slope for a tool surface obtained by micro-abrasive jet machining

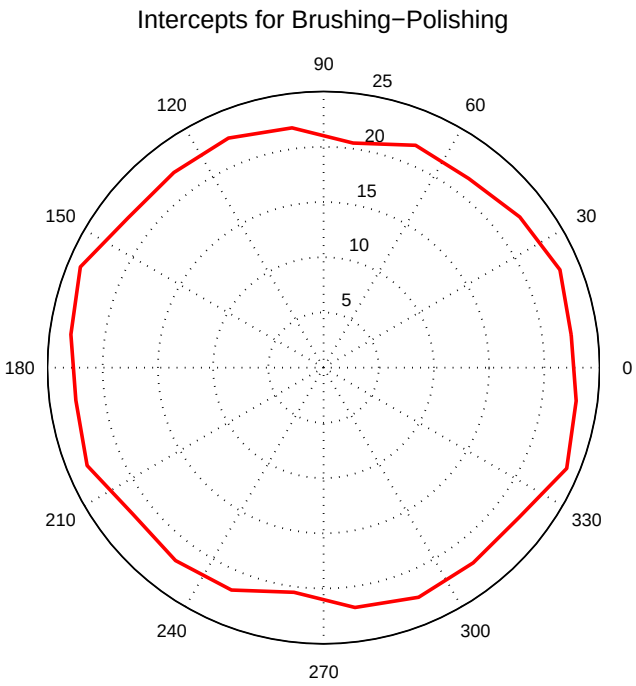

Figure 5-41: Rose plot of intercept for a tool surface obtained by brushing-polishing

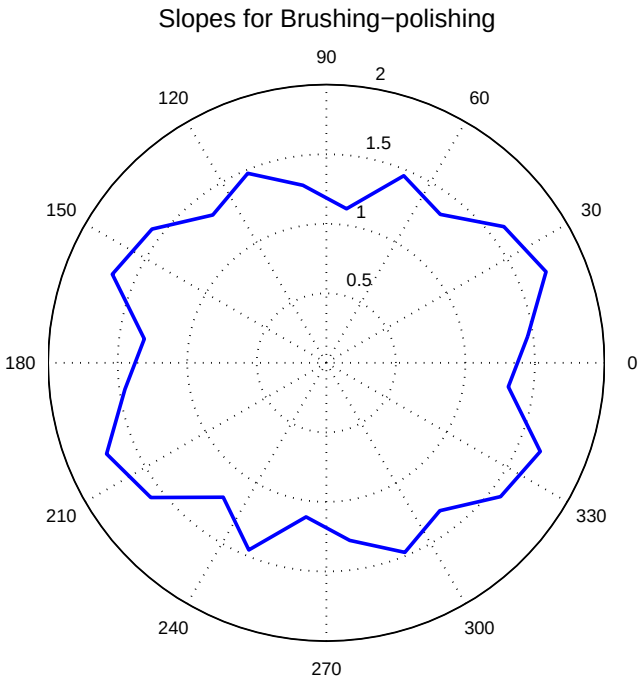

Figure 5-42: Rose plot of slope for a tool surface obtained by brushing-polishing

6 Process planning aspects

For the process planning of the cutting edge preparation, the determination of the removed material to obtain a required cutting edge rounding is considered. Beginning from an initial nominal radius r_{1n}, a final nominal radius r_{2n} should be obtained by using a precision material removal process. To determine the material removal, the concepts of nominal removed area A_r and area removal ratio A_t are introduced. Likewise, the origin of the variability of the process is analyzed.

6.1 Required material to remove

To characterize the precision removal process for cutting edge preparation, it is necessary to define a parameter that considers the quantity of removed material independently of the length of the cutting edge, of the number of cutting edges and also of the number of tools that are been processed at the same time. **Figure 6-1** shows the nominal removed area A_r (transversal removed area) proposed as parameter to determine the removed material in the cutting edge preparation. A_r represents the transversal section (orthogonal to the edge longitudinal direction) of the removed material to reach the nominal final radius r_{2n} beginning with a nominal initial radius r_{1n}.

As shown in **Figure 6-2**, the required nominal removed area to round a cutting edge depends on the value of the wedge angle β and the values of the initial radius r_{1n} and the required final radius r_{2n}. In **Figure 6-2**, the removed area for two values of β, with the same increase of radius, are presented. In both cases it is required to obtain a radius of 20μm beginning from an initial radius of 10μm. In the left cutting edge with β=60° the required removed area is A_r=205.7 μm^2, whereas in the right cutting edge with β=80° the required area is A_r=95.9μm^2. This aspect is important in terms of process productivity and for process planning.

Considering the application for planning the cutting edge preparation process, next an expression to determine the nominal removed area of material is proposed. For this expression, the change of radius (from r_{1n} to r_{2n}), and the wedge angle β are considered.

The nominal removed area, or simply removed area A_r, can be written as follows:

$$A_r = K_\beta[\ {r_{2n}}^2 - {r_{1n}}^2] \tag{6-1}$$

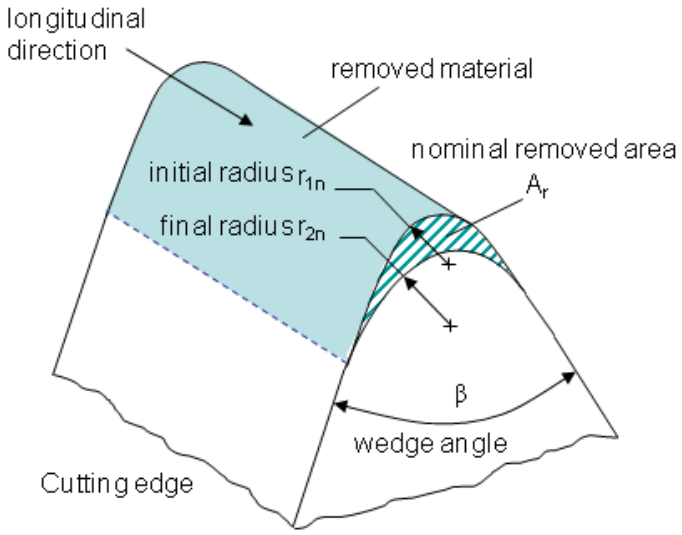

Figure 6-1: Concept of nominal removed area A_r

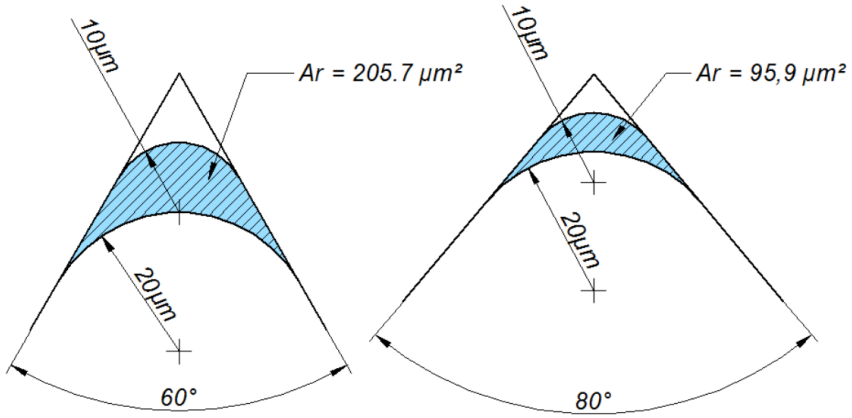

Figure 6-2: Comparison of removed area for $\beta = 60°$ and $\beta = 80°$

Where K_β is:

$$K_\beta = \frac{\sin^2(90° - \frac{\beta}{2})}{\tan\frac{\beta}{2}} - \frac{\pi}{2}\left(\frac{180° - \beta}{180°}\right) + \sin(180° - \beta) \tag{6-2}$$

Figure 6-3 shows the value of the coefficient K_β as function of the wedge angle β and **Figure 6-4** shows K_β for typical values of β used in the design of the macrogeometry of precision cutting tools.

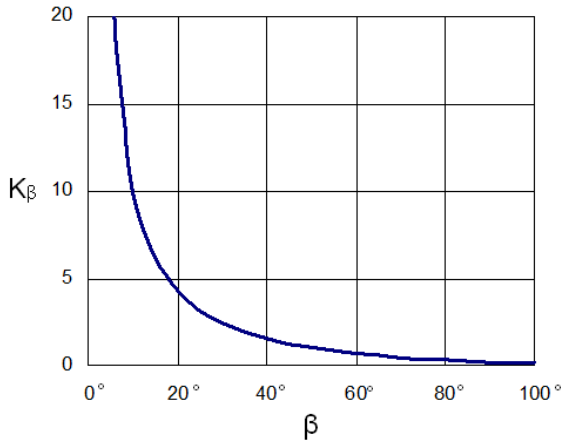

Figure 6-3: Coefficient K_β as function of the wedge angle β

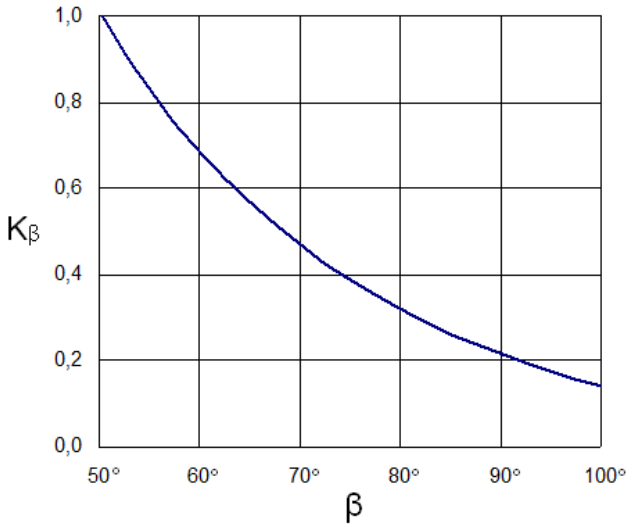

β	Kβ
50°	1,01
55°	0,83
60°	0,69
65°	0,57
70°	0,47
75°	0,39
80°	0,32
85°	0,26
90°	0,21
95°	0,17
100°	0,14

Figure 6-4: Coefficient K_β for typical values of β for precision cutting tools

Applying the equation 6-1, in **Figure 6-5** the removed area A_r for β=60° and β=80°, beginning with initial radius r_{1n}=10μm to obtain different final radii r_{2n} from 10μm to 40μm is presented. It can be observed that the value of A_r for β=60° is approximately twice as the value of A_r for β=80° for any value of increment of radius.

In **Figure 6-6**, a three dimensional plot to visualize the effect of changing the wedge angle β and the combination of r_{1n} and r_{2n} on the nominal removed area A_r is presented. Three angles β are considered, corresponding to each surface. In the horizontal plane, the combination of initial an final radii is considered, and depending on the angle β, a surface that represents the removed area A_r is obtained.

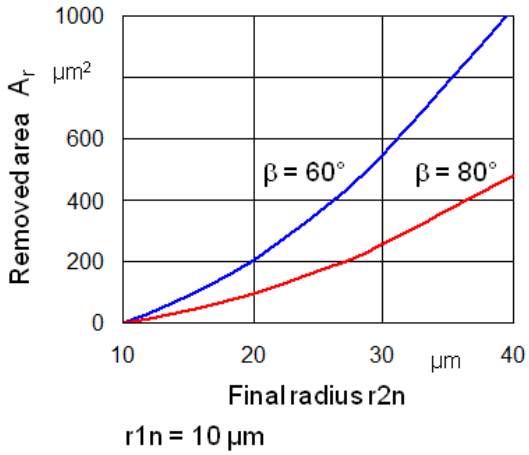

Figure 6-5: Removed area for two values of β considering r_{1n} =10μm and different radii r_{2n}

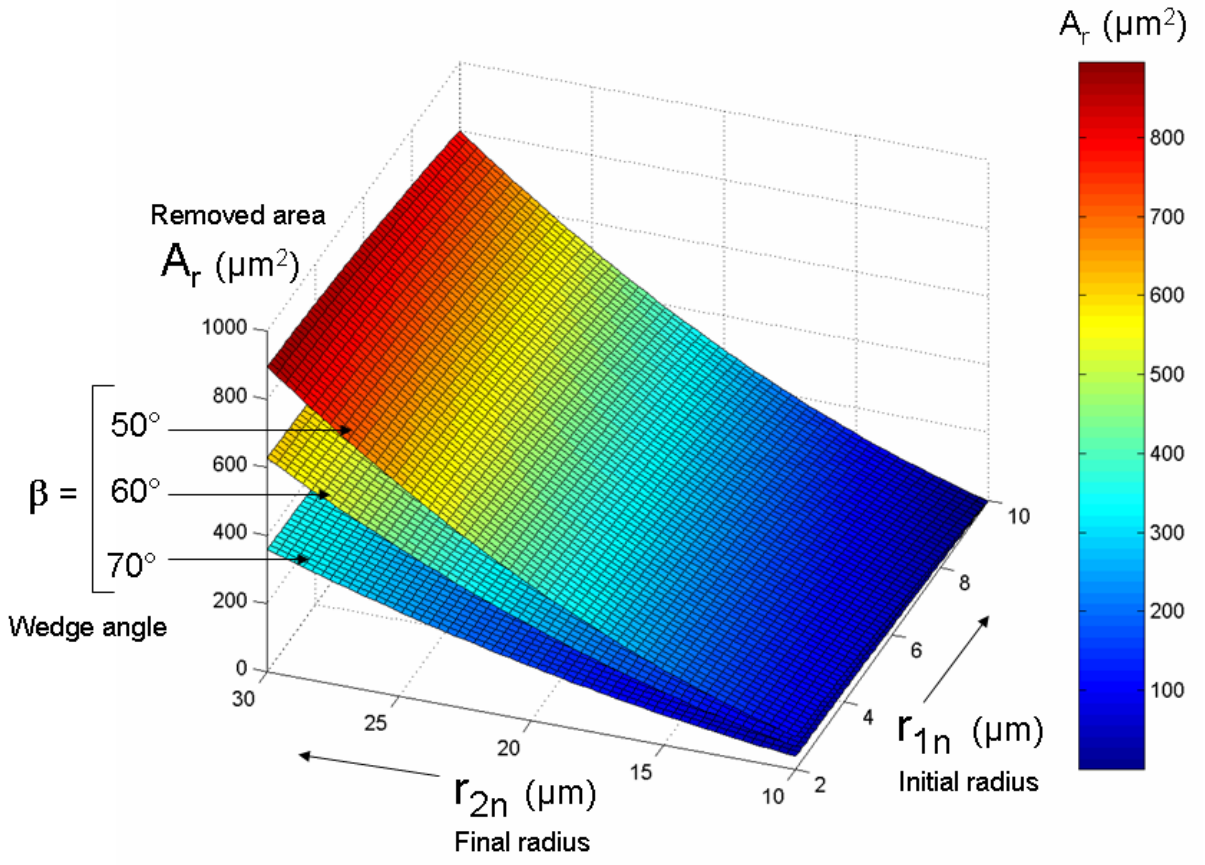

Figure 6-6: Removed area considering different β angles and combinations of r_{1n} and r_{2n}

6.2 Process planning to obtain the final radius

The planned preparation of cutting edges by means of precision material removal process requires the determination of the material removal capacity per unit time for the considered process. In consequence, for cutting edge preparation processes the area removal ratio A_t is defined. $A_t = dA_t/dt$ is the nominal removed area per unit time expressed in $\mu m^2/s$. This characteristic is related with the preparation process parameters and the properties of tool material associated with the physical-chemical principle of the removal process (erosion, abrasion, chemical, thermal principles, etc.). To remove A_r with an area removal ratio A_t, a specific process time t is required. This can be expressed as:

$$A_r = A_t \cdot t \tag{6-3}$$

A_t can be determined experimentally considering values of A_r obtained for different process time t. With the measurements of r_{1n}, r_{2n} and β and by means of equations 6-1 and 6-2, A_r can be determined for each process time t. With the experimental data, and applying regression to obtain an expression for $A_r = f(t)$, the slope dA_t/dt can be determined for each time t.

The nominal final radius r_{2n} can be estimated as process time function. By combining equations 6-1 and 6-3 the following expression is obtained:

$$r_{2n}(t) = \sqrt{\left[\frac{A_t}{K_\beta}\right] t + (r_{1n})^2} \tag{6-4}$$

Where A_t depends of the removal mechanism of the process and the properties of the tool material, and for practical application can be assumed as constant if a linear regression of the experimental data of $A_r = f(t)$ can be fitted in consistent form. K_β is associated with the wedge angle β (see equation 6-2) and r_{1n} is the nominal initial radius.

Figure 6-7 shows the influence of the wedge angle β on the final radius r_{2n} considering for analysis a constant area removal ratio A_t= 4 $\mu m^2/s$ and initial radius r_{1n}= 7μm. It can be observed, for example, that for obtaining a final radius of 20 μm for a cutting edge with β= 90°, 20 seconds are required, whereas for β= 60°, 60 seconds are required. Considering 100 seconds as process time, for β= 60°, 70° 80° and 90°, radii of 25, 28, 36, and 44 μm are obtained respectively.

In **Figure 6-8** the effect of the area removal ratio A_t on the final radius r_{2n} is presented. Initial radius r_{1n}= 7 μm and β= 80° are considered. For process time of 100 seconds, removing material with A_t= 4 $\mu m^2/s$, 6 $\mu m^2/s$ and 8 $\mu m^2/s$, final radii of 36, 44 and 50μm are obtained respectively. The different values of A_t corresponds to different process parameters and/or cutting tool material properties.

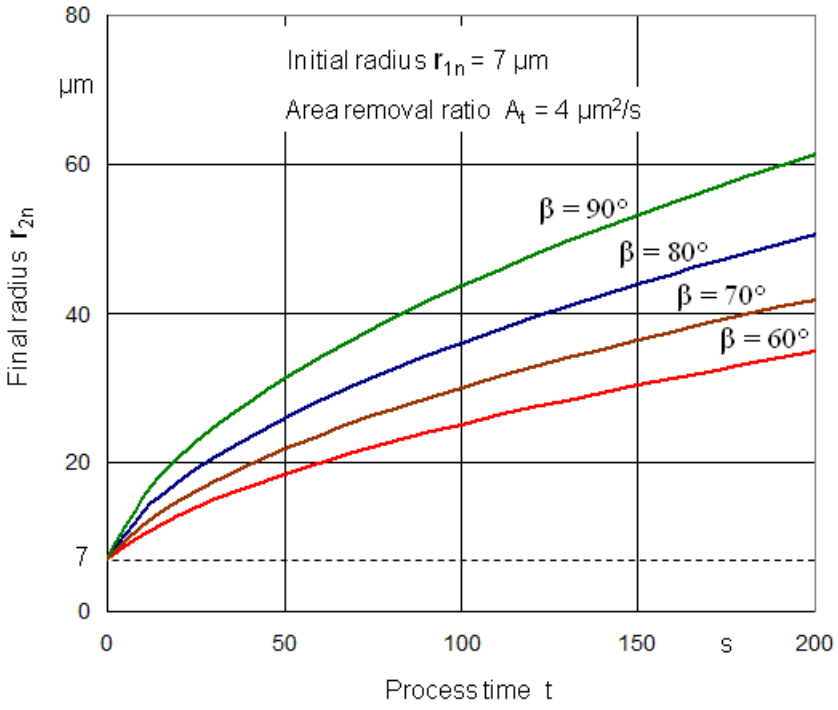

Figure 6-7: Comparison of obtained final radii for different values of β

6.3 Process variability

The variability in the cutting edge preparation process is a complex aspect to consider. There are different sources of variability that cause high variability of the final nominal radius obtained by the precision removal processes used for cutting edge preparation. For analysis and practical application the sources of variability are considered in two groups corresponding to the previous processes (used to obtain the macrogeometry of the cutting tool) and the preparation process (see **Figure 6-9**). As result of the previous processes (sintering and grinding) the variabilities of the initial radius r_{1n} and in wedge angle β are generated. The variability of the removed area (or removal ratio) comes from the variability of the process parameters (depending of the specific removal mechanism, process set-up and specific process conditions) and the variability of tool material properties (related with the material removal mechanism). To reach a specified tolerance for the final radius, a precise balance of the sources of variability is required.

In **Figure 6-10**, the effect of the variability of the area removal ratio A_t on the obtained final radius r_{2n} is presented. The variation of the final radius r_{2n}, can be observed considering variations of ±20% and ±10% regarding to the average A_t= 4 μm^2/s. The initial radius r_{1n}= 8μm and the wedge angle β= 65° were considered as constants.

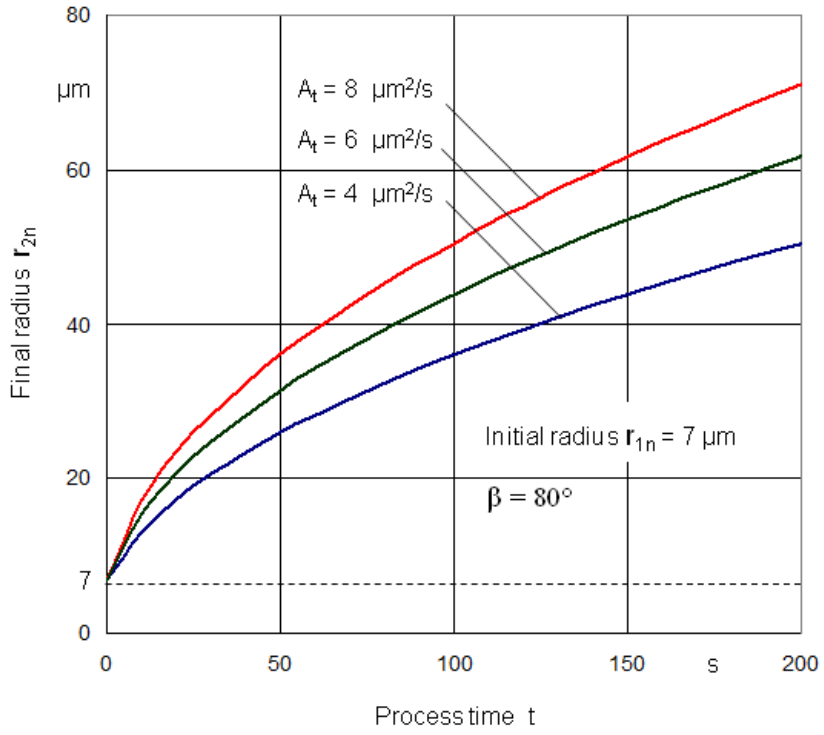

Figure 6-8: Comparison of obtained final radii for different values of A_t

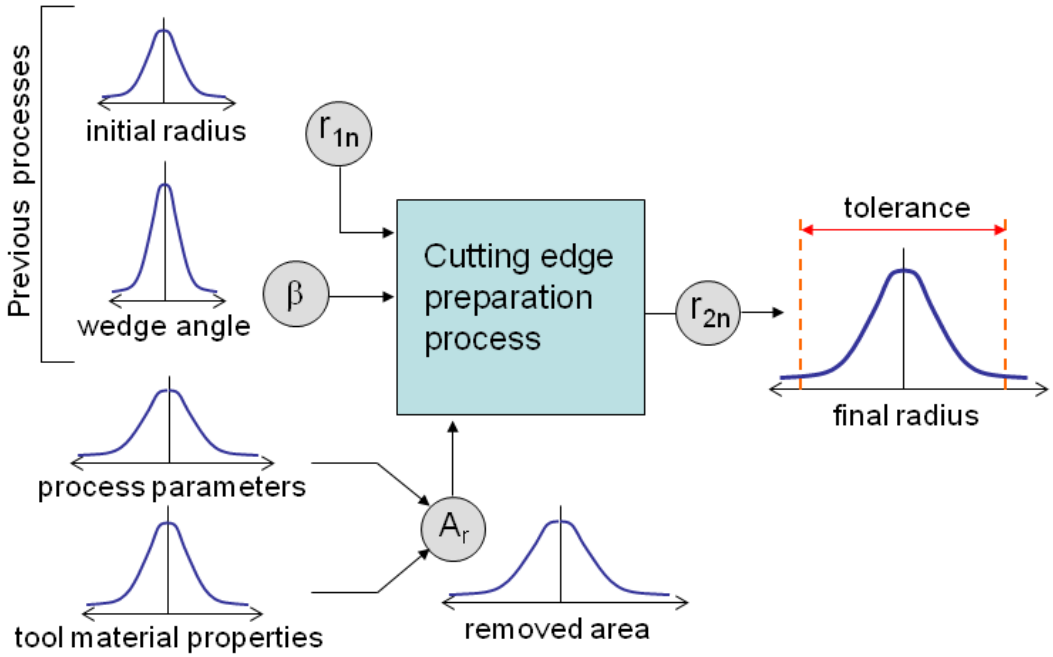

Figure 6-9: Sources of resultant variability for nominal final radius

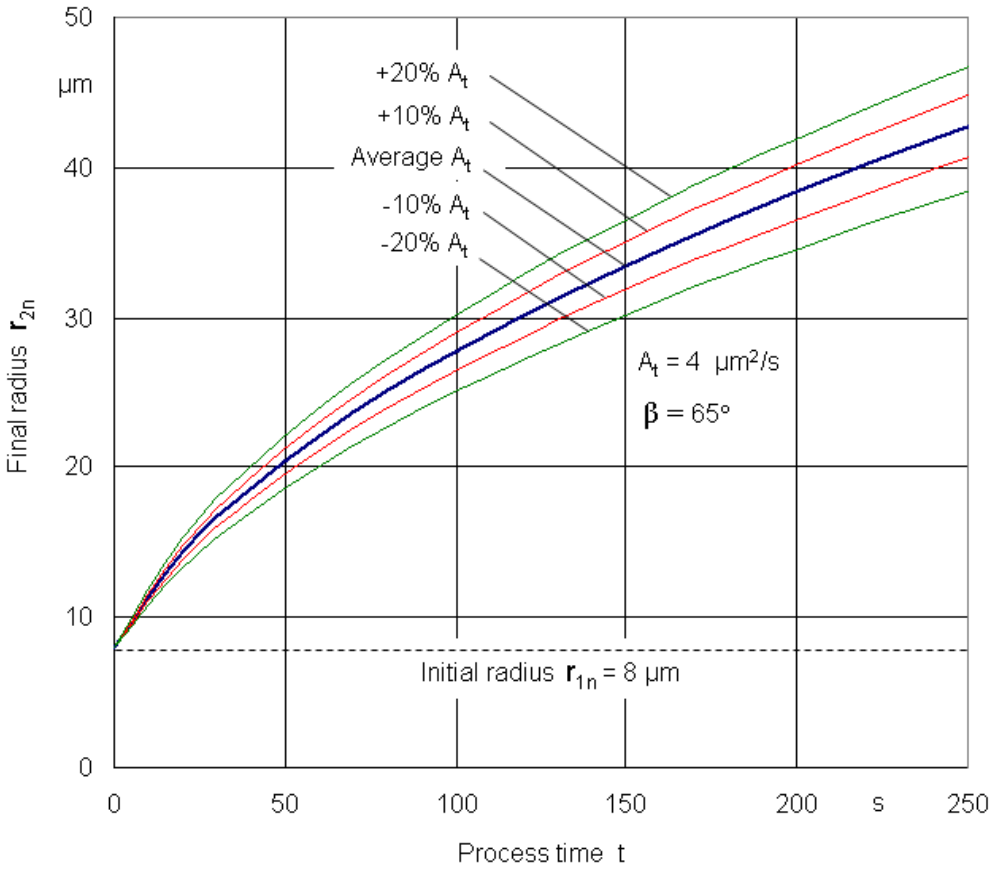

Figure 6-10: Obtained final radius according to variability of A_t

A more general description of the resultant variability can be expressed by using the error propagation equation proposed by Gauss and presented in [88, 127]. Considering a function $y = f(x_1, x_2, ..., x_n)$, the error propagation is expressed as [88, 127]:

$$S_y{}^2 = \left(\frac{\partial f}{\partial x_1}\right)^2 \cdot S_{x_1}{}^2 + \left(\frac{\partial f}{\partial x_2}\right)^2 \cdot S_{x_2}{}^2 + \cdots + \left(\frac{\partial f}{\partial x_n}\right)^2 \cdot S_{x_n}{}^2 \tag{6-5}$$

Where $S_y{}^2$ is the variance of y, $S_{x_i}{}^2$ are the variances of the independent variables x_i, and $\partial f/\partial x_i$ are sensitivity coefficients.
Considering the nominal final radius expressed as $r_{2n} = f[A_r, K_\beta, r_{1n}]$ by means of the equation:

$$r_{2n} = \sqrt{\left[\frac{A_r}{K_\beta}\right] + (r_{1n})^2} \tag{6-6}$$

And applying the error propagation concept to this expression, the following equation is obtained:

$$S_{r_{2n}} = \sqrt{\left(\frac{1}{2K_\beta \cdot r_{2n}}\right)^2 \cdot {S_{A_r}}^2 + \left(\frac{-1}{2{K_\beta}^2 \cdot r_{2n}}\right)^2 \cdot {S_{K_\beta}}^2 + \left(\frac{r_{1n}}{r_{2n}}\right)^2 \cdot {S_{r_{1n}}}^2} \qquad (6\text{-}7)$$

Where $S_{r_{2n}}$ is the standard deviation of the nominal final radius, S_{A_r}, S_{K_β} and $S_{r_{1n}}$ are the standard deviations of the removed area, of the coefficient K_β and of the initial nominal radius respectively.

Considering a cutting edge preparation process with a required final nominal radius r_{2n}= 20μm, and with the following conditions of average and standard deviation of the variables: for initial radius r_{1n}= 8μm, $S_{r_{1n}}$= 1μm, for wedge angle β= 65°, S_β= 0.3°, or K_β= 0.5668 , S_{K_β}= 0.0065 and for removed area A_r= 190.46μm^2, S_{A_r}= 10μm^2, the resultant standard deviation of the final radius is $S_{r_{2n}}$= 1.16μm, calculated by using equation 6-7.

6.4 Selection of process parameters

The adequate selection of process parameters is the result of a delicate balance between the requires production rate and the quality of the cutting edge preparation (in terms of required meso- and micro-geometry). With a high area removal rate A_t, lower process time is required to reach a final radius r_{2n}, but inadequate effects on the micro-topography of the cutting edge and the tool flank and tool face, can be produced. **Figure 6-11** shows examples of two cutting edge preparation strategies in order to obtain a final radius r_{2n}= 30μm by means of micro-abrasive jet machining. Considering a cutting edge with β= 65° and beginning with initial radius r_{1n}= 7μm (point A), the first strategy, from point A to point B, uses an area removal ratio A_t= 8μm^2/s and the second strategy, from point A to point C, uses an area removal ratio A_t= 4μm^2/s. For the first strategy the process time is 60 seconds whereas for the second strategy the process time is 120 seconds. In the right side of **Figure 6-11** three pictures obtained by SEM (scanning electron microscopy) show the condition of the cutting edge at points A, B, and C. At picture A, the initial condition of the edge are presented. Observing pictures B and C, it is possible to see the differences in obtained micro-topography resulting from an aggressive material removal by using the first strategy (picture B) and a moderate removal material of the second strategy (picture C).

Figure 6-12 shows the final radius and notchedness obtained after applying a group of selected process parameters associated with the area removal rate A_t= 4μm^2/s. At the lower diagram the typical behavior of the obtained notchedness vs process time is presented. The curve presents a strong decay of notchedness (in terms of R_z) in the first stage of the cutting edge preparation process. After that the improvement of notchedness is not appreciable.

The typical behavior of the obtained notchedness (in terms of R_z) as function of process time t can be modeled by means of a exponential decay as:

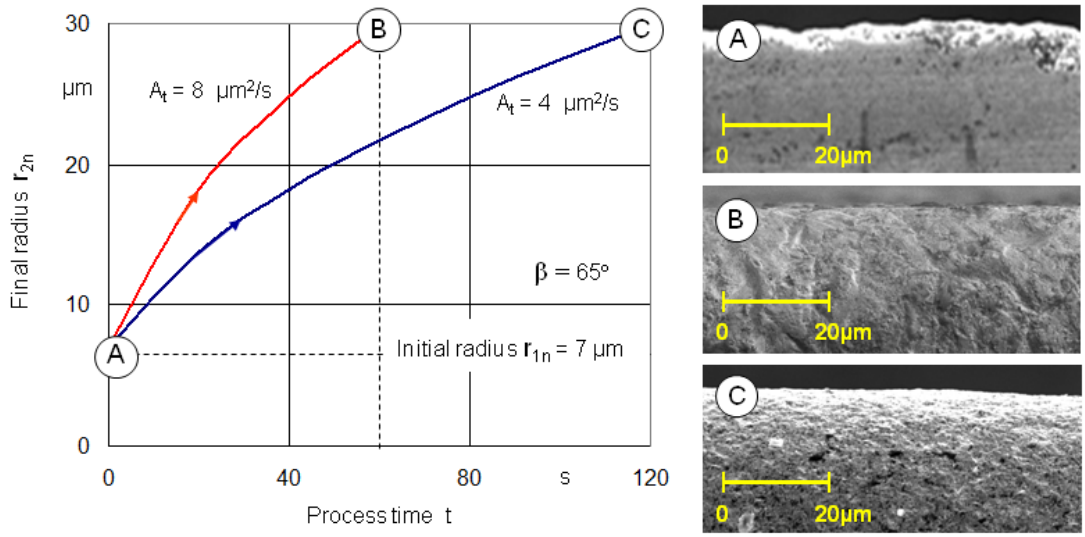

Figure 6-11: Two possibilities to reach the same final edge radius and differences in obtained micro-topography

$$R_z(t) = c_1 + e^{-c_2\,(t-c_3)} \tag{6-8}$$

Where c_1, c_2, and c_3 are constants determined by non-linear fitting of the measured notchedness.

Considering the curves in **Figure 6-12**, the final cutting edge radius r_{2n} and the notchedness in terms of R_z can be represented as function of process time t with the following expressions:

$$r_{2n}(t) = \sqrt{\left[\frac{4}{0.57}\right]t + (7)^2} \tag{6-9}$$

$$R_z(t) = 1.77 + e^{-0.05\,(t-25.30)} \tag{6-10}$$

6.5 Detailed estimate of removed material

In the previous analysis, the nominal cutting edge radii r_{1n} and r_{2n}, and the wedge angle β were considered to estimate A_r. The nominal radii are obtained by using the best fitting of the representative contour of the rounding, as showed in **Figure 5-22**. If the contour is highly asymmetric, or a special geometry of the convex contour, different to a circumference arc, is considered, A_r can be estimate by means of the fitting of sensor data of the contours, as described in section 5.3.1. If the measurement of the initial contour and the final contour were made with the same measurement reference that guaranties

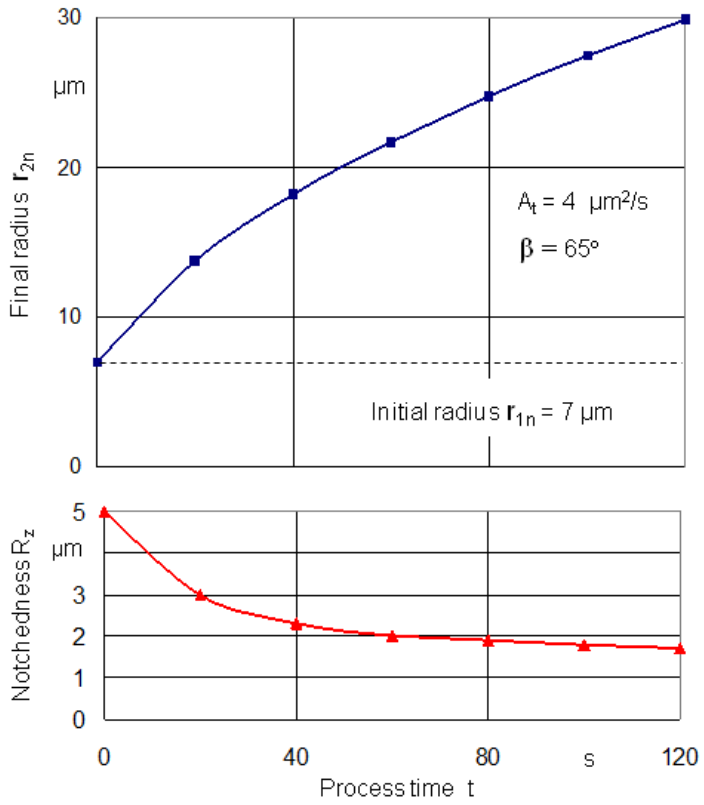

Figure 6-12: Final radius- and notchedness vs process time

the same position of the coordinate systems for the two contours, the estimate of A_r can be expressed as:

$$A_r = \int_{x_c}^{x_d} (\phi_1 - \phi_2) dx \tag{6-11}$$

Where ϕ_1 and ϕ_2 are the fittings of initial and final contours respectively, and x_c and x_d are the coordinates on the x axis of the considered limit points c and d for the contours, as showed in **Figure 5-7**.

7 Micro-abrasive jet machining for cutting edge preparation

7.1 Description of the process and set-up

Micro-abrasive jet machining (MAJM) uses the energy of an abrasive jet formed by pressurized air and micro-abrasive particles to remove material by erosion (see sections 3.6 and 4.4.1). The experimental set-up for cutting edge preparation by MAJM is illustrated in **Figure 7-1**. The cutting tools to be prepared are fixed and positioned by means of a fixture mounted on a positioning table XY. The movement of the table is controlled numerically in directions X and Y. The nozzle is fixed and positioned by means of a vertical head, that allows the adjustment of the vertical distance between the nozzle and the cutting edge to be prepared. Additionally, with the vertical head it is possible to adjust the inclination of the nozzle axis with regard to the horizontal plane XY. The abrasive is stored in a container, which has in the inferior part, a valve that allows the transport of the abrasive by the pressurized air. The flux of air is activated by a valve to be able to generate the abrasive jet only when it is required during the process. Additionally to the showed system, there are a protection cover of the positioning table and of the cinematic system and a extraction system of used abrasive.

Figure 7-2, shows the relative positioning between the abrasive jet and the cutting edge to be prepared. The diagram illustrates a symmetric adjustment of the cutting edge in order to obtain a symmetric geometry of the edge contour, considering that the axis of the nozzle and the axis of symmetry of the wedge angle β are coincident. Additionally, the adjustment of the distance y between the nozzle and the target cutting edge is shown.

7.2 Materials and methods

In order to analyze the effect of the MAJM parameters on the cutting edge preparation characteristics, inserts of uncoated cemented carbide ISO K20-K40 were used as cutting tool material. The characteristics of the cutting tool material are presented in **Table 7-1**. The geometry of the considered precision cutting tool is described in **Figure 7-3**. Corundum and silicon carbide were considered as abrasives for the abrasive jet. The characteristics of the abrasives are shown in **Tables 7-2** and **7-3** respectively. Two geometries of the nozzles were considered: round (0.65 mm diameter) and rectangular (0.3mm x 3mm).

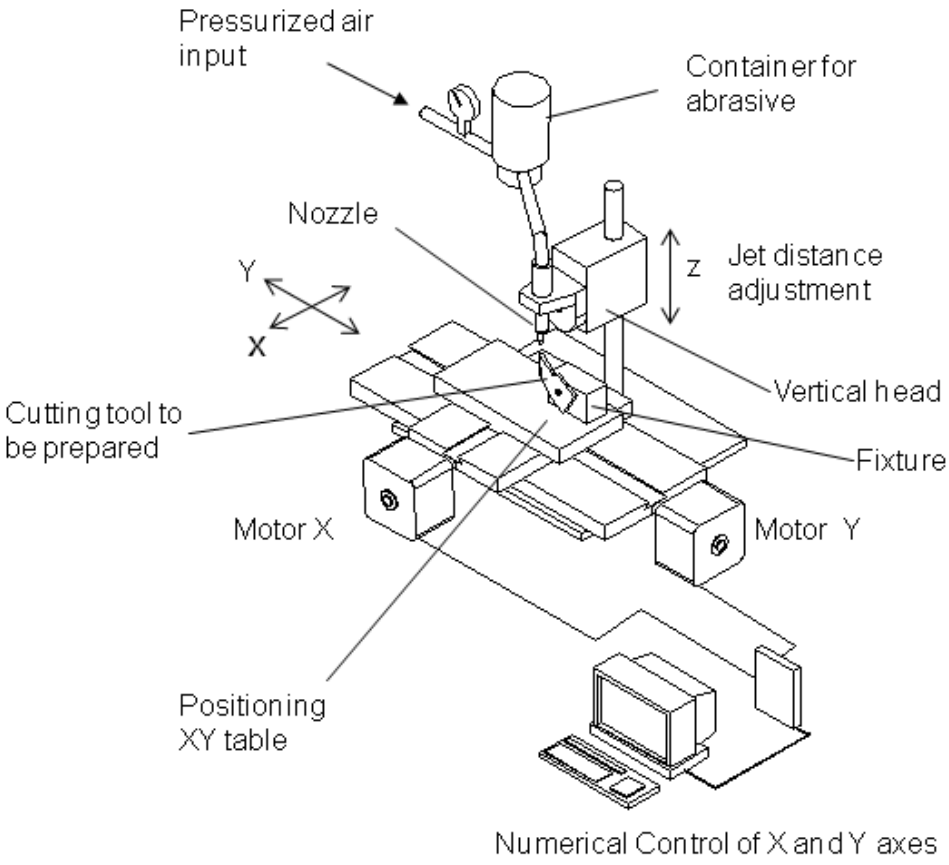

Figure 7-1: Experimental micro-abrasive jet machining equipment

Table 7-1: Data of the considered cutting material of the precision cutting tool

Cutting tool material: cemented carbide ISO K20-K40 (uncoated)		
Chemical composition (weight)	Co 10%, WC balance, other 0.7%	
Average grain	submicron	
Density	14.45	g/cm^3
Hardness	1680	HV
Transverse rupture strength	3700	MPa
Compressive strength	6600	MPa
Young modulus	580	GPa
Fracture toughness	9.4	$MPa.m^{1/2}$
Thermal conductivity	85	$W.m^{-1}K^{-1}$
Thermal expansion coefficient	5.5	$10^{-6}K^{-1}$

The cutting edge preparation was developed with a relative movement cycle between the abrasive jet and the cutting edge. This cycle with constant travel speed v_s is controlled

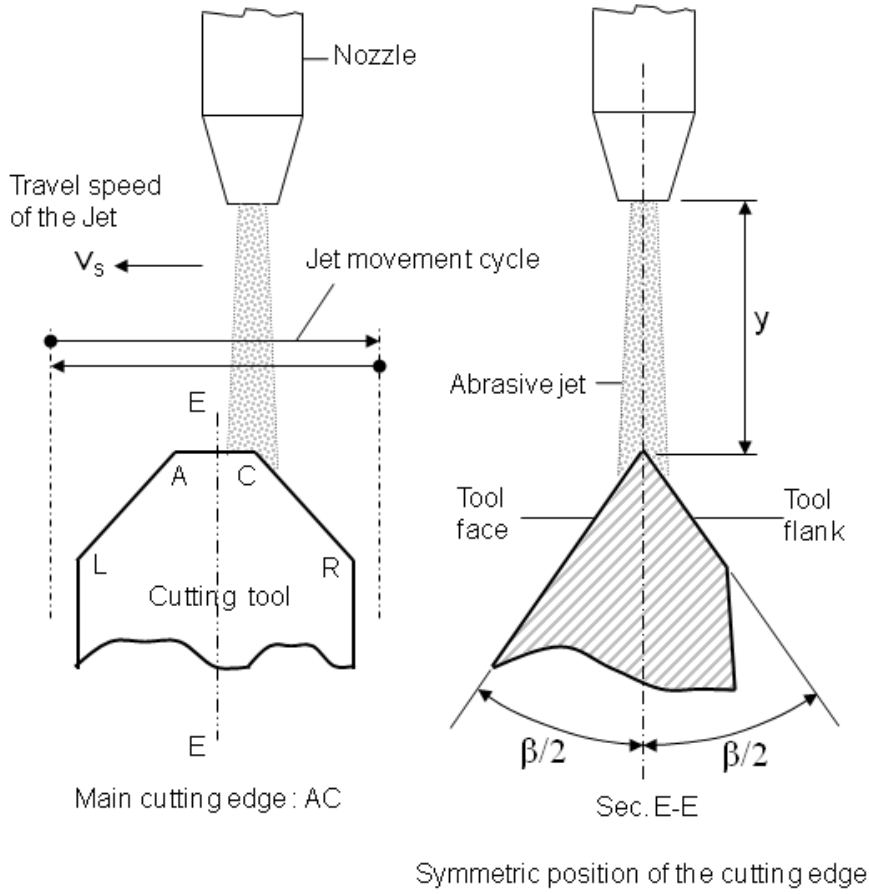

Figure 7-2: Relative positioning between abrasive jet and cutting tool

Table 7-2: Data of corundum used in micro-abrasive jet machining

Abrasive: white corundum	
Analysis typical	Al_2O_3: 99.7%, Na_2O: 0.2%, Fe_2O_3: 0.02%, SiO_2:0.02%
Hardness	2100 HV
Density	3.92 g/cm^3
Grit DIN 69101	F360
Average diameter of grain	22.8 μm
Thermal conductivity	6 $W.m^{-1}K^{-1}$

numerically. The jet movement cycle and the relative positioning between cutting edge and jet are shown in **Figure 7-2**.

For the measurement of the cutting edge radius, a white light chromatic sensor (see section 5.1), with horizontal resolution of 1 μm and vertical resolution of 60 nm was used. The measurement was obtained by scanning the cutting edge and obtaining and

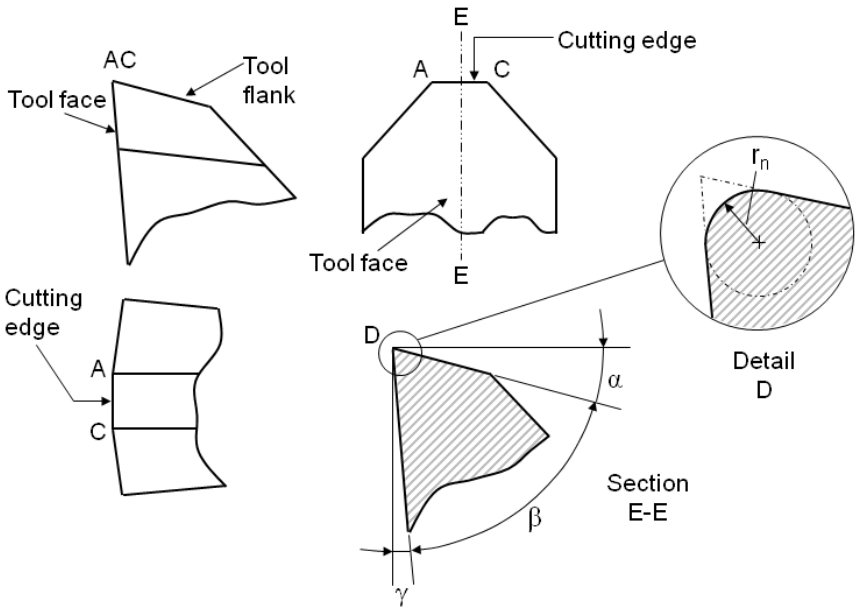

Figure 7-3: Macro and meso-geometry of the considered cutting tool: β= 65°, α= 15°, γ=10°, Length of main cutting edge AC = 0.8 mm, Initial cutting edge radius r_{1n}= 10 μm

Table 7-3: Data of silicon carbide used in micro-abrasive jet machining

Abrasive: silicon carbide	
Analysis typical	SiC: 76%, C free: 0.1%, SiO_2: 17.5%, Al_2O_3:5%
Hardness	2400 HV
Density	3.21 g/cm^3
Grit DIN 69101	F360
Average diameter of grain	22.8 μm
Thermal conductivity	55 W.m^{-1}K^{-1}

areal topographic image, as shown in **Figure 5-3**. Considering the length of the cutting edge AC= 0.8mm, a horizontal projection region of 0.6 mm x 0.4mm, for the topographic image was considered (with 0.6mm along the edge). With this topographic image, 24 sections (orthogonal to the edge) were considered to obtain the representative contours of the rounding of the cutting edge. With these contour the methodology described in section 5.3.1 was applied in order to obtain the nominal radius r_n.

The parameters for the roughness measurement of the tool face are presented in **Figure 7-4** and the measurement of the nominal notchedness of the cutting edge was carried out in accordance with the methodology presented in section 5.3.2.

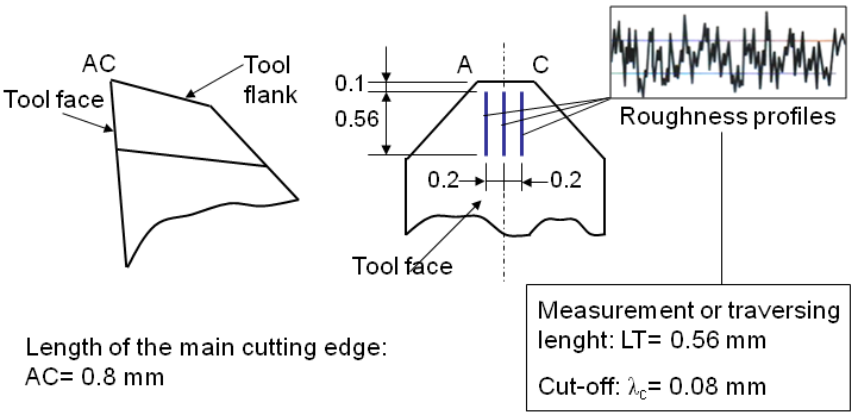

Figure 7-4: Roughness measurement parameters

7.3 Experimental design

In order to analyze the effects of the MAJM parameters on the characteristics of the cutting edge preparation and to obtain a regression model for describing the relationship between the process parameters and the removed material, methods of design of experiments (DoE) were applied [63, 70, 88, 89, 144].

To analyze the effects of the distance between nozzle and jet y, air jet pressure P_a, jet working time t_j, nozzle geometry N_g and type of abrasive A_b, on the removed area A_r, a fractional factorial design 2^{5-1} (resolution V) with 3 replicates was selected. In **Table 7-4** the constant conditions for experimenting are presented. Additionally, in **Table 7-5** the levels of the considered experimental factors are shown.

Table 7-4: Considered constants conditions for micro-abrasive jet machining

Experimental constant conditions	
Macrogeometry of the cutting tool	β= 65°, α= 15°, γ=10°
Length of main cutting edge	AC = 0.8 mm
Initial cutting edge radius	r_{1n}= 10 μm
Travel speed of the jet	v_s= 1.22 mm/s
Cutting tool material	Cemented carbide ISO K20-K40 (uncoated)
Abrasives	White Corundum (Al_2O_3) and Silicon Carbide (SiC)
Nozzle geometry	Round (0.65 mm diameter) and Rectangular(0.3mm x 3.5mm)

Table 7-5: Experimental factors considered for MAJM

	Factor				
	Distance (mm)	Pressure (bar)	Time (s)	Nozzle (Geometry)	Abrasive (Type)
Level	y	P_a	t_j	N_g	A_b
Low (-)	15	3	13	Round	SiC
High (+)	30	5	39	Rectangular	Corundum

Table 7-6 shows the final radius as measured response obtained from the application of MAJM as cutting edge preparation process. The average radius $\overline{r_{2n}}$ resultant from 3 replications (3 different cutting tools) for each parameter combination, the standard deviation of the radius $S_{r_{2n}}$ and the quantity six sigma $6 \cdot S_{r_{2n}}$ are shown. This information is used to observe the generated variability of the final radius r_{2n}, for each parameter combination. Likewise, in **Table 7-7**, the removed area A_r (obtained by using equations 6-1 and 6-2) for 3 replications, and the corresponding average $\overline{A_r}$ and standard deviation S_{A_r} are presented.

Table 7-6: Experimental factors and obtained final cutting edge radius for MAJM

	Experimental factors					Measured Response		
	Distance	Pressure	Time	Nozzle	Abrasive	Average Radius	Stand.Deviation	Six sigma
Nr.	y	P_a	t_j	N_g	A_b	$\overline{r_{2n}}$ (μm)	$S_{r_{2n}}$ (μm)	$6{\cdot}S_{r_{2n}}$ (μm)
1	-	-	-	-	+	19.17	0.35	2.10
2	+	-	-	-	-	11.90	0.34	2.04
3	-	+	-	-	-	26.10	0.36	2.16
4	+	+	-	-	+	19.33	2.52	15.10
5	-	-	+	-	-	27.00	1.01	6.06
6	+	-	+	-	+	23.73	1.55	9.32
7	-	+	+	-	+	28.10	0.95	5.72
8	+	+	+	-	-	25.70	0.46	2.75
9	-	-	-	+	-	33.33	4.16	24.98
10	+	-	-	+	+	12.00	1.00	6.00
11	-	+	-	+	+	27.67	2.10	12.60
12	+	+	-	+	-	29.77	3.06	18.33
13	-	-	+	+	+	28.33	2.09	12.54
14	+	-	+	+	-	29.00	4.58	27.50
15	-	+	+	+	-	51.00	2.65	15.87
16	+	+	+	+	+	29.67	2.08	12.49

Table 7-7: Experimental factors and response for MAJM

	Experimental factors					Response		
	Distance	Pressure	Time	Nozzle	Abrasive	Removed area	Average	Stand.Dev.
Nr.	y	P_a	t_j	N_g	A_b	A_r (μm^2)	$\overline{A_r}$ (μm^2)	S_{A_r} (μm^2)
1	-	-	-	-	+	152.08 143.48 158.66	151.41	7.61
2	+	-	-	-	-	18.26 24.91 27.65	23.61	4.83
3	-	+	-	-	-	320.22 326.09 340.95	329.09	10.68
4	+	+	-	-	+	147.76 107.00 217.39	157.38	55.82
5	-	-	+	-	-	326.09 387.23 356.09	356.47	30.97
6	+	-	+	-	+	297.21 217.39 274.93	263.18	41.19
7	-	+	+	-	+	419.50 393.59 359.15	390.75	30.28
8	+	+	+	-	-	302.90 329.04 320.22	317.39	13.30
9	-	-	-	+	-	452.90 523.10 760.87	579.96	161.40
10	+	-	-	+	+	11.89 39.06 24.91	25.29	13.59
11	-	+	-	+	+	326.09 453.90 356.09	378.36	66.27
12	+	+	-	+	-	559.89 356.09 419.50	445.16	104.29
13	-	-	+	+	+	297.21 269.47 193.05	253.24	53.94
14	+	-	+	+	-	387.23 297.21 597.82	427.42	154.28
15	-	+	+	+	-	1594.20 1302.65 1358.69	1418.51	154.71
16	+	+	+	+	+	387.23 523.10 419.50	443.28	70.99

For the significance analysis [112], a significance level $Alpha$= 0.05 was selected. **Figure 7-5** shows a Pareto′s chart that presents the absolute value of the effects for the main factors and interactions between two variables (two-way interactions). The vertical dashed-line defines the boundary of the main factors and two-way interactions that are significant considering the selected level $Alpha$. Factors that extend to the right beyond the boundary are significant. In this case, all the main factors and the two-way interactions result significant, except the interaction $y \cdot t_j$ (distance-time) . The distance y, between the nozzle and the cutting edge, results that of more significance, but in general, all the main factors result highly significant in comparison to the two-way interactions.

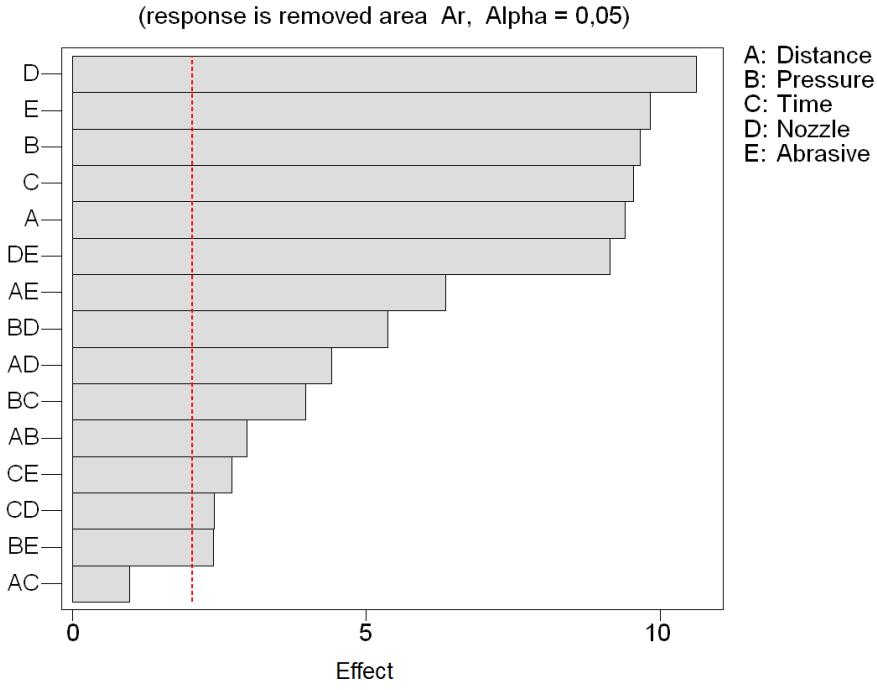

Figure 7-5: Pareto′s chart of effects on A_r

In **Figure 7-6** the effects and influence of the main factors distance y, pressure P_a, time t_j, nozzle geometry N_g and abrasive A_b, on removed area A_r are showed.

Figure 7-7 shows an interaction plot in order to observe the impact that changing the setting of one factor has on another factor. An interaction can magnify or diminish main effects, this aspect can be appreciated for the differing slopes for each two lines that represent the effects in each section of the interactions diagram. For example, considering the first row of the diagram, there is a high interaction between distance y and type of abrasive A_b, and low or almost null interaction between distance y and time t_j.

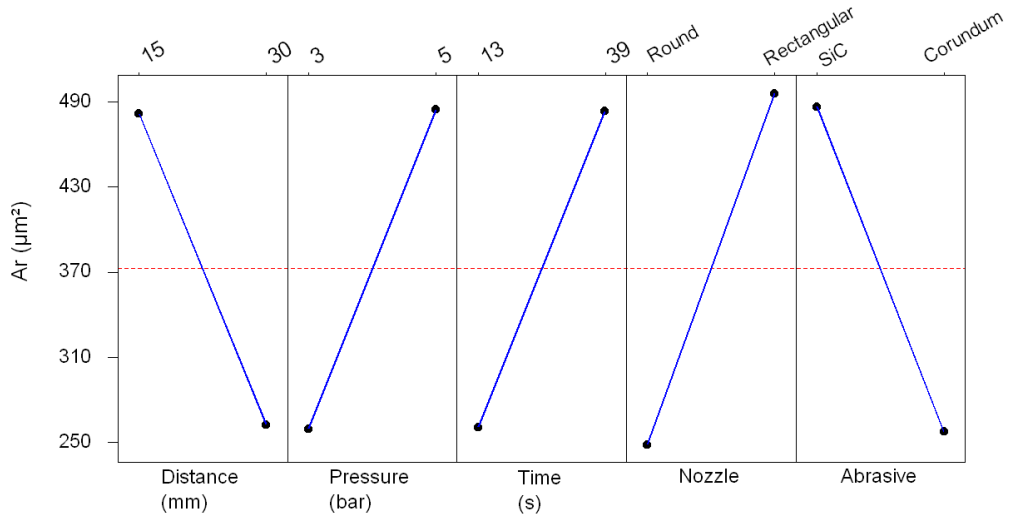

Figure 7-6: Main effects plot for removed area A_r

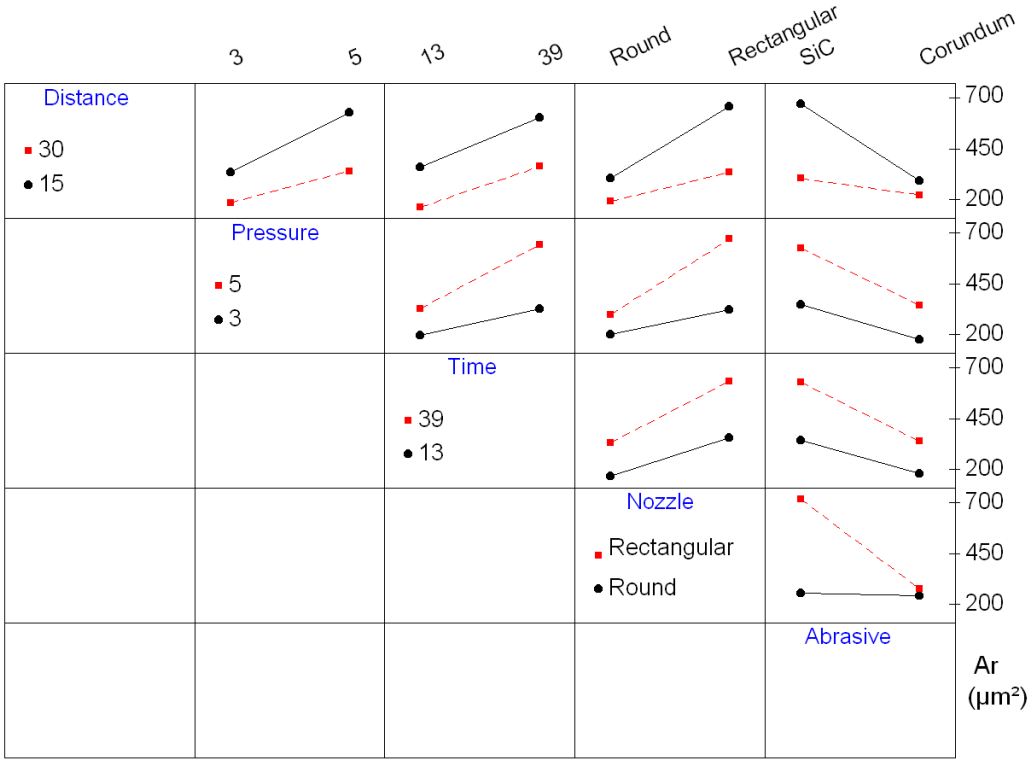

Figure 7-7: Interaction plot for removed area A_r

7.4 Variability of final cutting edge radius

Considering the data presented in **Table 7-6**, the values six sigma $6 \cdot S_{r_{2n}}$ can be used to estimate the variability of the final cutting edge radius generated by MAJM. It can be observed that for the same generated radius r_{2n}, there are different values of $6 \cdot S_{r_{2n}}$ depending on the combination of factors. For the combination of factors Nr.1 and Nr.4 the radii r_{2n} generated are 19μm in both cases, however the values of $6 \cdot S_{r_{2n}}$ are 2.1 and 15.1μm respectively. The same behavior is observed for the combinations Nr.2 and Nr.10 for r_{2n}=12μm with $6 \cdot S_{r_{2n}}$= 2.0 and 6.0 μm respectively and combinations Nr.12 and Nr.16 for r_{2n}=30μm with $6 \cdot S_{r_{2n}}$= 18.3 and 12.5μm respectively. Thus, the value $6 \cdot S_{r_{2n}}$, obtained for each combination of factors, is an important criteria to select the parameters to obtain a required radius r_{2n}.

7.5 Regression model for removed area

By using regression analysis [46] and considering the significant factors and two-way interactions observed in **Figure 7-5**, a regression model for the removed area A_r is proposed.

The obtained regression model for A_r can be written as:

$$\begin{aligned} A_r \; &= 67 + 0.79\, y + 89.2\, P_a - 5.37\, t_j + 157\, N_g - 111\, A_b - 427\, N_g \cdot A_b \\ &+19.7\, y \cdot A_b + 125\, P_a \cdot N_g - 13.7\, y \cdot N_g + 3.55\, P_a \cdot t_j - 4.61\, y \cdot P_a \\ &-4.86\, t_j \cdot A_b + 4.31\, t_j \cdot N_g - 55.9\, P_a \cdot A_b \end{aligned} \tag{7-1}$$

Where the geometry of the nozzle is N_g=0 for round and N_g=1 for rectangular, and the type of abrasive A_b=0 for SiC and A_b=1 for corundum.

By using the model presented in equation 7-1, plots to observe the behavior of the removed area A_r for different combinations of main factors can be generated. For each pair of factor combinations, the hold values considered for other factors are presented. **Figure 7-8** and **7-9** show a surface plot and a contour plot that illustrate the response A_r as function of time and pressure considering corundum as abrasive. To contrast, in **Figures 7-8** and **7-9** the response A_r is shown for other hold values with SiC as abrasive.

Additionally, in **Figure 7-12** and **7-13** the influence of the distance between the jet and the cutting edge and the air pressure on the removed area A_r is presented. Likewise **Figure 7-14** and **7-15** show the behavior of A_r related with distance and time.

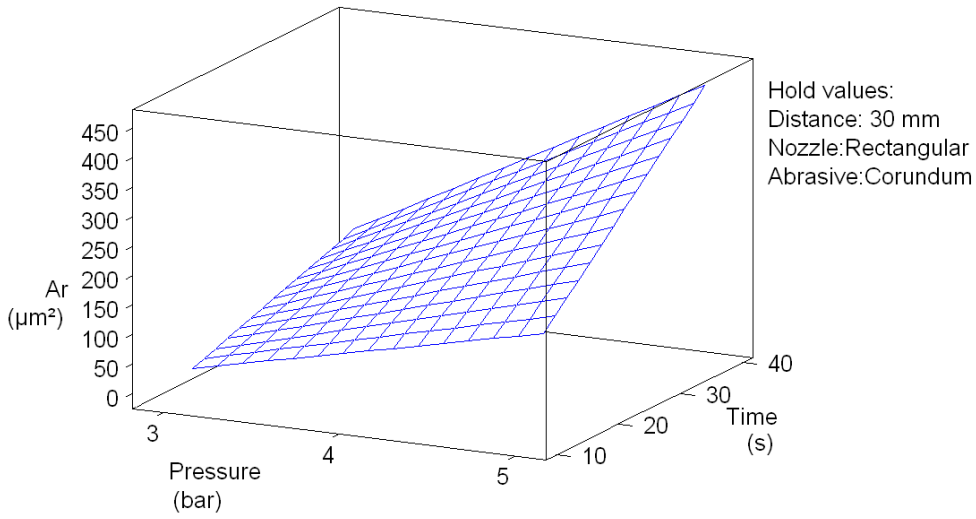

Figure 7-8: Surface plot for removed area A_r considering pressure and time

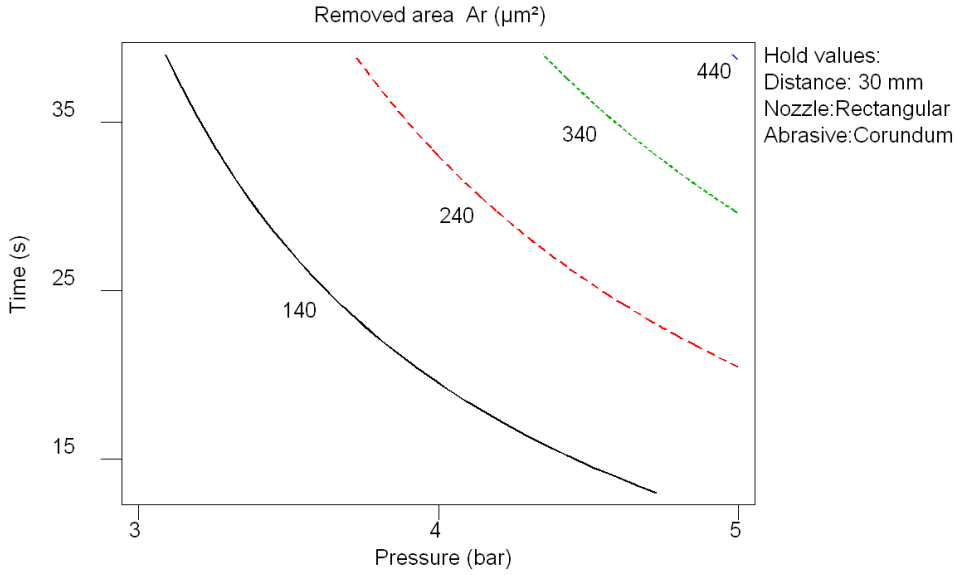

Figure 7-9: Contour plot for removed area A_r considering pressure and time

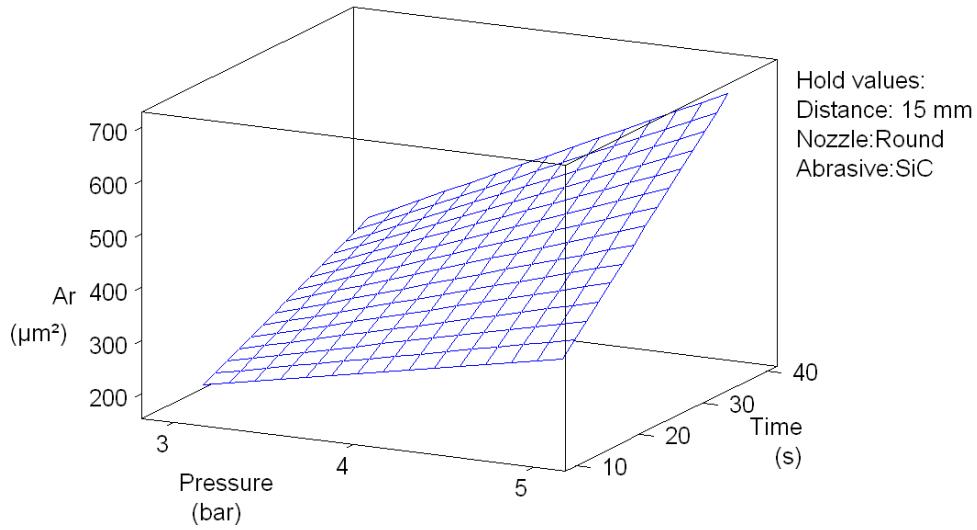

Figure 7-10: Surface plot for removed area A_r considering pressure and time with SiC as abrasive

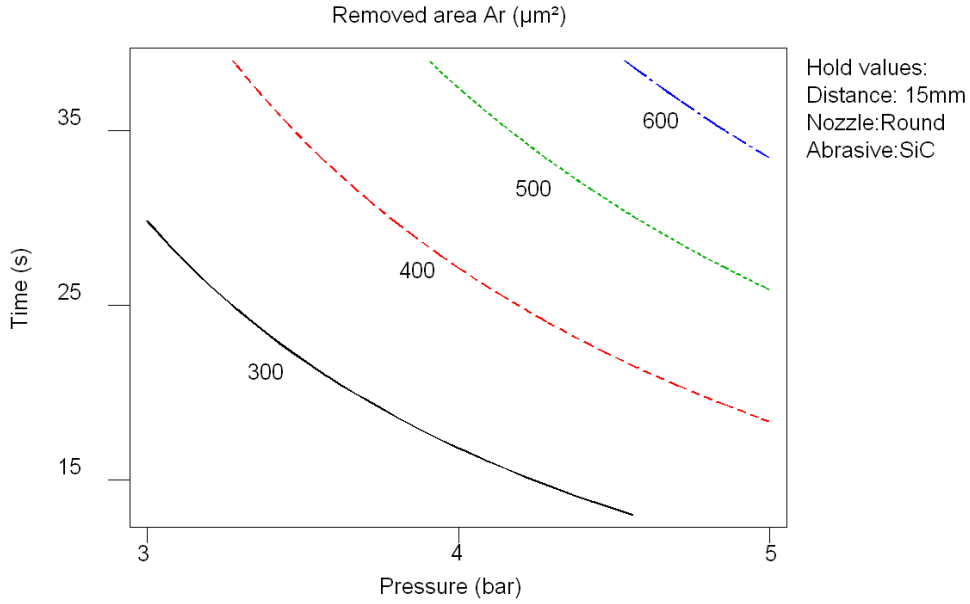

Figure 7-11: Contour plot for removed A_r considering pressure and time with SiC as abrasive

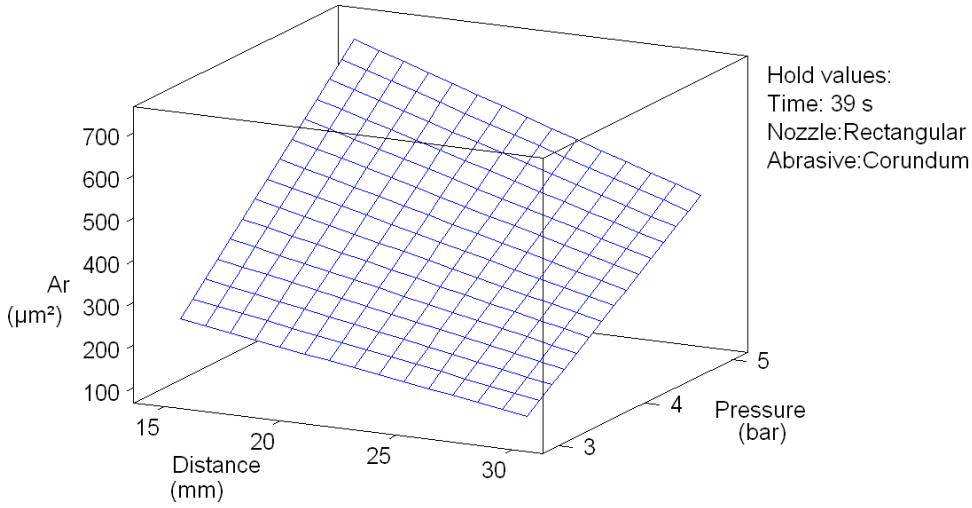

Figure 7-12: Surface plot for removed area A_r considering distance and pressure

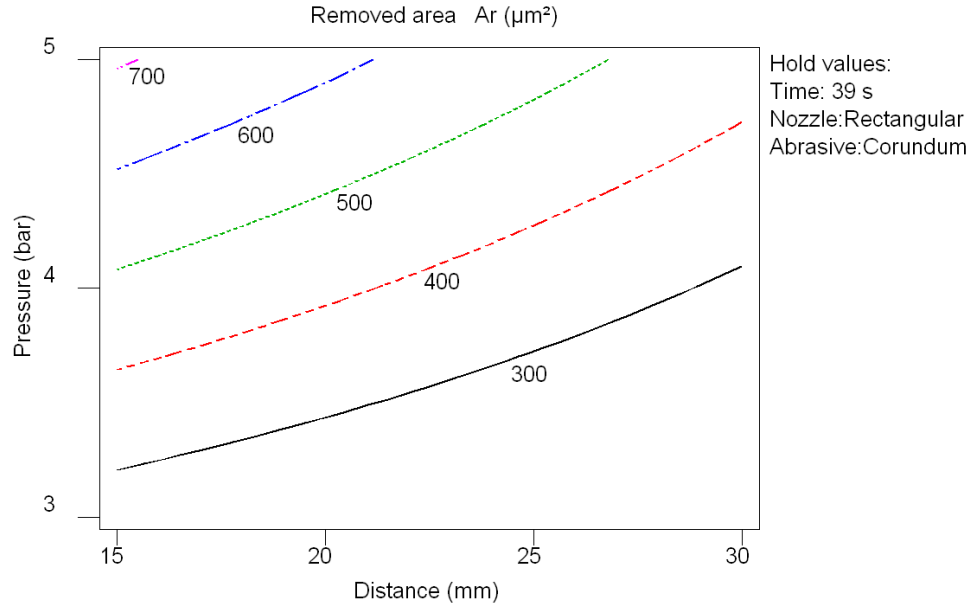

Figure 7-13: Contour plot for removed area A_r considering distance and pressure

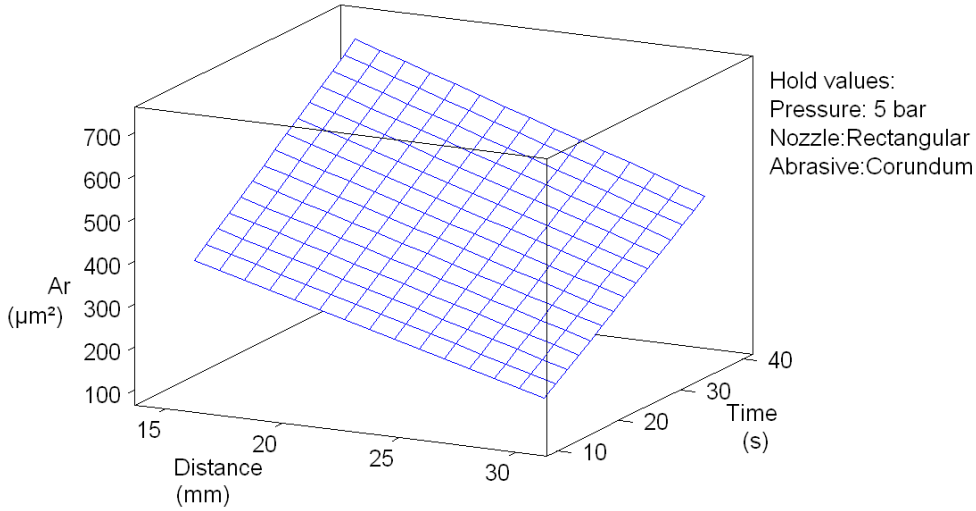

Figure 7-14: Surface plot for removed area A_r considering distance and time

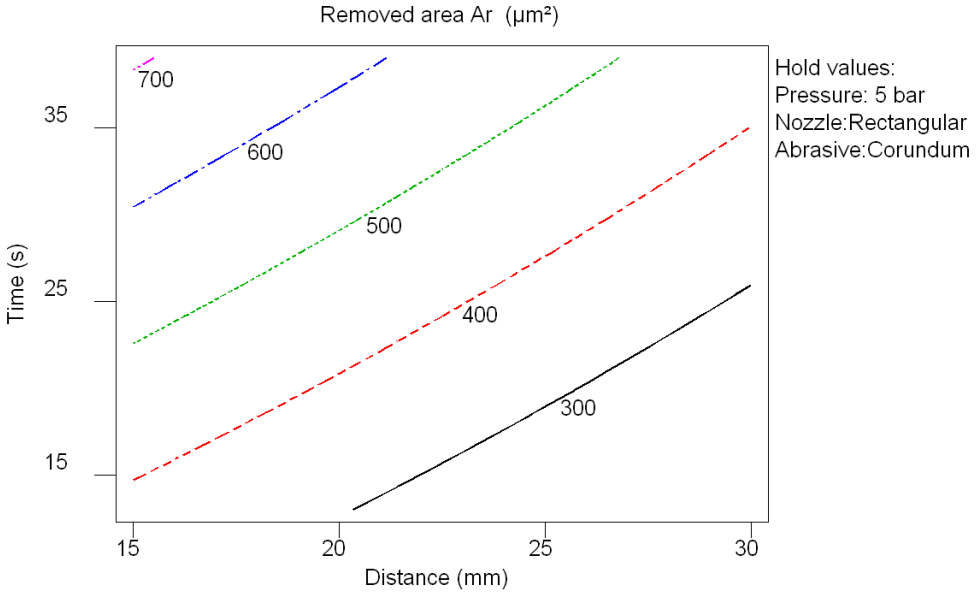

Figure 7-15: Contour plot for removed area A_r considering distance and time

7.6 Roughness

To analyze the influence of the experimental factors on the roughness R_z of the tool surfaces (measured as indicated in **Figure 7-4**), three treatments were considered : unprepared tool (as reference), and two extreme combinations of factors from **Table 7-7** (those that caused the lower and the higher remove area). Analysis of variance (ANOVA) [112] was applied to study if the roughness obtained by the application of the selected treatments has a significant difference.

The selected treatment were: J0 (unprepared), J1 (combination Nr.2) and J2 (combination Nr.15). **Table 7-8** shows the obtained data for R_z corresponding to treatments considered for ANOVA. To illustrate the results of the analysis, **Figure 7-16** shows a box-plot for R_z obtained by the considered treatments.

Table 7-8: Data of the treatments

Treatment	R_z (μm)			Mean	Std.Dev.
J0	1.08	1.17	1.14	1.13	0.045
J1	0.73	0.78	0.84	0.78	0.055
J2	0.80	0.94	0.74	0.82	0.102

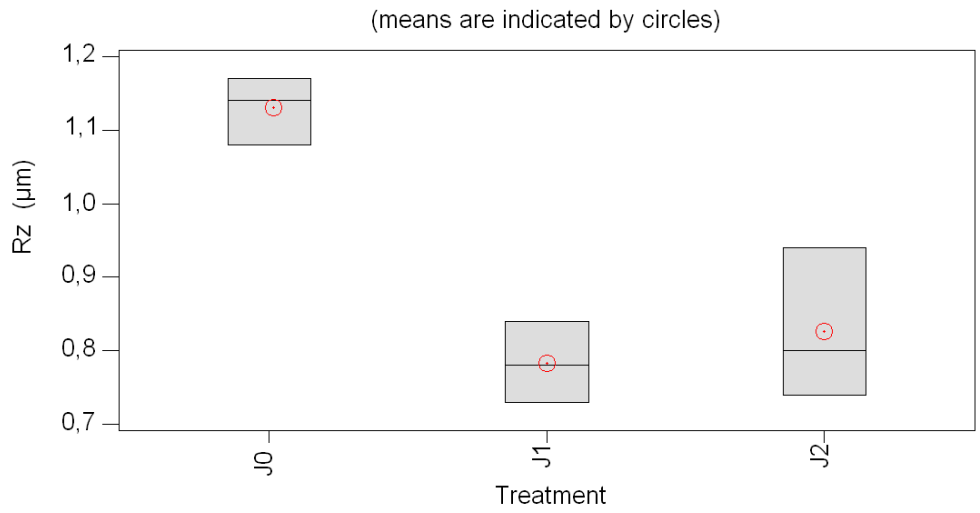

Figure 7-16: Box-plot for R_z by different treatments: J0 (unprepared), J1 and J2 are two different parameter combinations of MAJM

The results of the one-way ANOVA, considering a significance level of 5%, reveal that there is a significant difference among the means of the treatments. In addition, the Tukey's test [112] for pairwise comparisons was applied to observe which treatments are different among if. The result of the test evidences that there is no significant difference between treatments J1 and J2, but there is a significant difference between J0 and J1, and

between J0 and J2. Therefore, there is no significant difference between the roughness obtained by the two preparation treatments, but there is a significant difference between the roughness of the unprepared and prepared tools. In consequence, there is an improvement of roughness R_z of the tool face by applying MAJM for cutting edge preparation.

7.7 Microstructuring

The detailed description of the microstructuring of the tool surfaces was presented in section 5.3.2. In **Figure 5-30** the characterization of a typical microstructuring, by using areal parameters and autocorrelation function, for a tool face obtained by MAJM is shown. In **Figures 5-39** and **5-40**, the characterization of the microstructuring of the tool face by means of fractals is presented. As was described in section 5.3.2, the typical microstructuring of a tool surface obtained by MAJM is highly isotropic, as a result of the prints generated by random impacts of the abrasive of the jet on the tool surface.

7.8 Notchedness

To analyze the behavior of the notchedness for cutting edge preparation by MAJM, the parameters R_z and R_{pk} (see section 5.3.2) were observed as function of process time. In **Table 7-9**, the experimental conditions are presented. **Figure 7-17** shows the data of the measurements of R_z, R_{pk} and the ratio R_{pk}/R_z. As initial condition, cutting edges without preparation were considered.

Table 7-9: Conditions for analysis of notchedness by micro-abrasive jet machining

Experimental conditions MAJM	
Macrogeometry of the cutting tool	β= 65°, α= 15°, γ=10°
Length of main cutting edge	AC = 0.8 mm
Cutting tool material	Uncoated cemented carbide ISO K20-K40
Abrasive	White Corundum (Al_2O_3)
Diameter of abrasive grain	22μm
Nozzle geometry	Rectangular(0.3mm x 3.5mm)
Air pressure	3 bar
Distance nozzle-edge	30 mm
Position of the edge	Symmetric
Travel speed of the jet	1.22 mm/s

In **Figure 7-17**, a high decay of the roughness R_z in the first stage of the cutting edge preparation by MAJM can be observed. After a critical point of process time (approximately 12s), the decrease of roughness is not appreciable. A similar decay behavior can

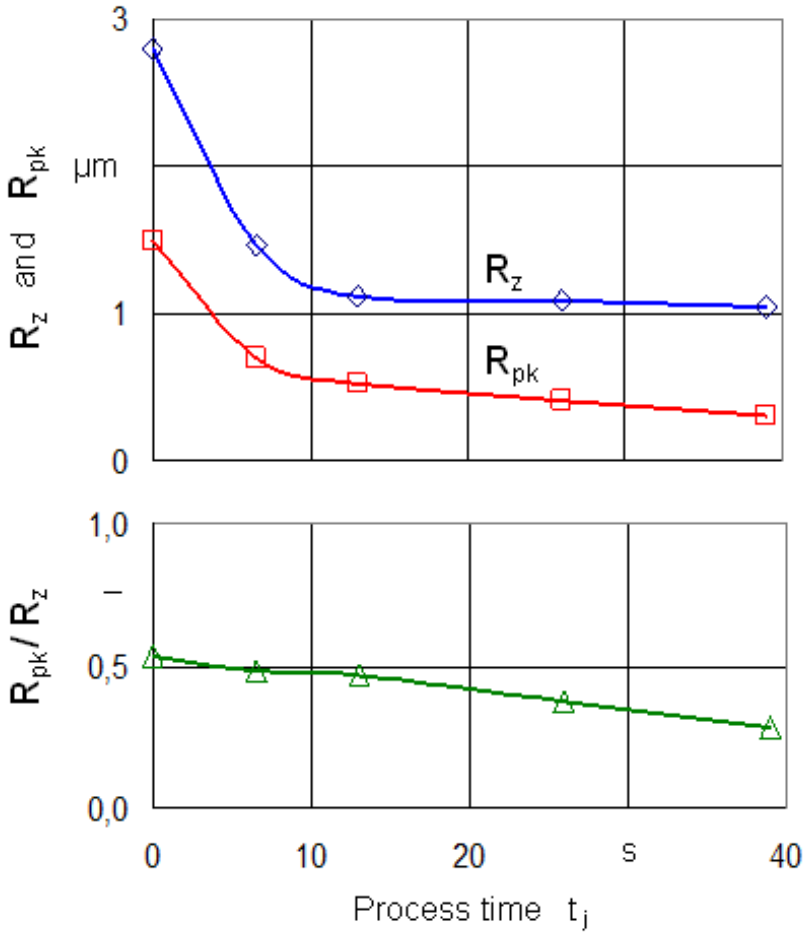

Figure 7-17: Analysis of notchedness for cutting edge preparation by MAJM.

be observed for R_{pk}. Additionally, a tendency to decrease the ratio R_{pk}/R_z is observed. In consequence of this, a tendency in the decrease of picks related with the nominal roughness R_z is presented, as the process time increases.

Finally, as considered in chapter 6, the behavior of the notchedness as function of process time t_j for MAJM, for the data presented in **Figure 7-17**, can be expressed as:

$$R_z(t_j) = 1.05 + e^{-0.23\,(t_j - 2.43)} \tag{7-2}$$

8 Brushing-polishing for cutting edge preparation

8.1 Description of the process and set-up

Brushing-polishing (BP) uses a soft brush with natural fibers as polishing pad and a polishing paste with diamond particles to remove material by abrasion (see section 4.4.2). **Figure 8-1** illustrates the experimental set-up for BP used for cutting edge preparation. The cutting tools to be prepared are mounted in a fixture on a table with alternative movement (5 stokes/min). A head mounted on a main column allows the vertical adjustment of the penetration depth between the natural fibers (filaments of 25 mm length) and the cutting edge to be prepared. Additionally, the system has a pneumatic device to get up and to approach the brush to the cutting edge and a vertical screw to the adjustment (with accuracy of 0.05 mm) of the penetration depth of the filaments. In the head are mounted the main motor and the polishing-brush (with 300 mm diameter) in horizontal position. The rotational movement of the polishing brush (between 150 and 600 1/min) can be adjusted in one direction or alternative.

Figure 8-2 shows the relative positioning between the polishing-brush and the cutting edge to be prepared. The diagram illustrates a symmetric adjustment of the cutting edge in order to obtain a symmetric geometry of the edge contour, considering alternating rotation of the polishing brush during the process cycle. Additionally, the adjustment of the penetration depth y_b of the filaments is shown.

8.2 Materials and methods

To analyze the effect of the BP parameters on the cutting edge preparation characteristics, the same uncoated cemented carbide ISO K20-K40 considered for MAJM were used as cutting tool material. The characteristics of the cutting tool material are presented in **Table 7-1**. The geometry of the considered precision cutting tool is described in **Figure 7-3**. Two brushes of different natural fibers were used. The elastic response of the fibers for the considered brushes and their dynamic behavior during the brushing-polishing process are substantially different. The brushes are formed for a metallic disk (300 mm diameter) in which natural fibers of two types (Rosshaar^{TM} and Vitex^{TM}) are mounted.

The cutting edge preparation was developed by means of a relative movement be-

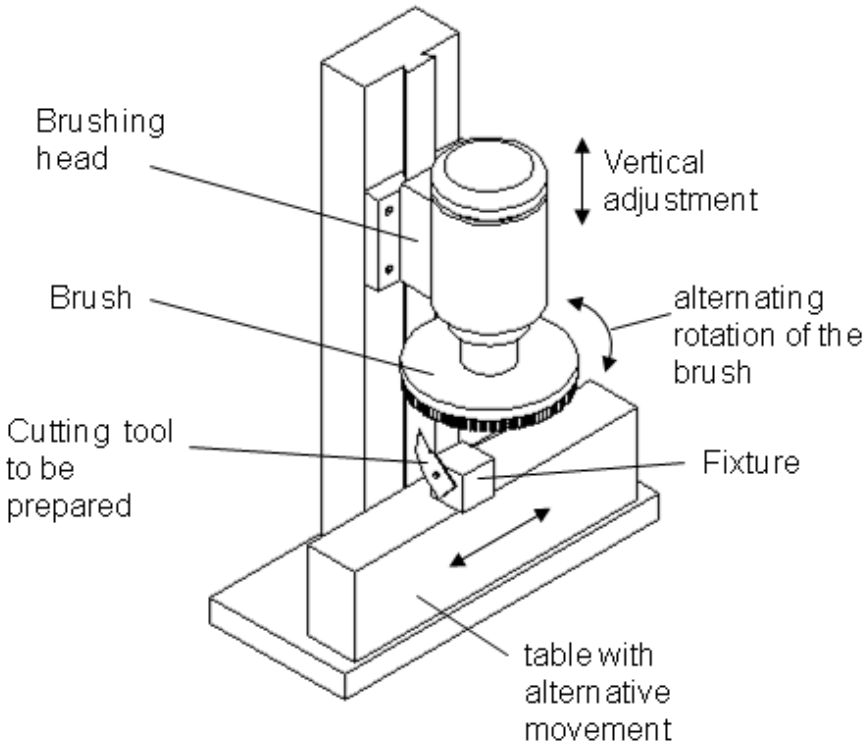

Figure 8-1: Experimental equipment for brushing-polishing

tween the brushing-polishing disk and the cutting edge. The relative movement is the combination of the alternating linear movement of the table and the alternating rotation of the brushing-polishing disk. The relative positioning between cutting edge and the brushing-polishing disk is shown in **Figure 8-2**.

The measurement of the generated radius was carried out by means of the methodology described in section 7.2. Likewise, the procedure used to measure the roughness of the tool face and the notchedness of the cutting edge is the same as the used for MAJM, and described in section 7.2.

8.3 Experimental design

To analyze the effects of the BP parameters on the characteristics of the cutting edge preparation and to obtain a regression model for describing the relationship between the considered process parameters and the removed material A_r, methods of design of experiments (DoE) were applied [63, 70, 88, 89, 144].

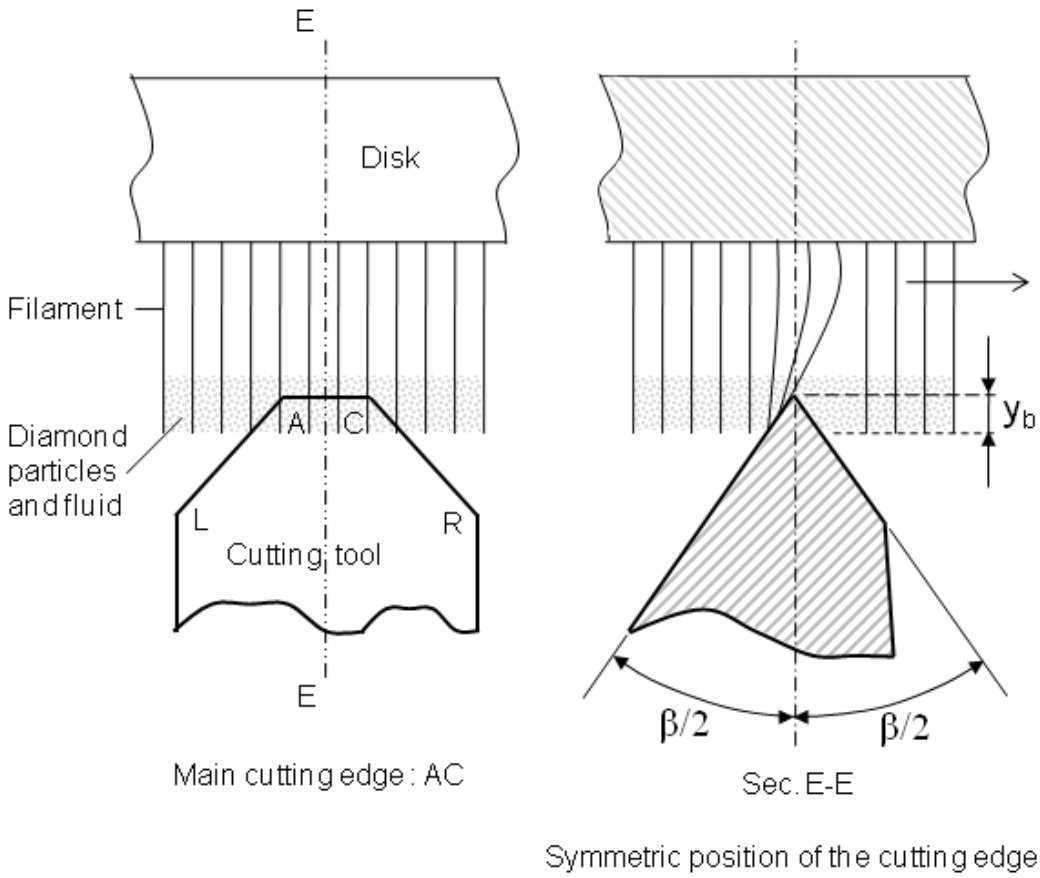

Figure 8-2: Relative positioning between polishing-brush and cutting tool

To analyze the effects of rotational speed N, working time t_b, penetration depth y_b, and brush type B_t, on the removed area A_r, a full factorial design 2^4 with 3 replicates was selected. In **Table 8-1** the constant conditions for experimenting are presented. Additionally, in **Table 8-2** the levels of the considered experimental factors are shown.

Table 8-1: Considered constants conditions for brushing-polishing

Experimental constant conditions	
Macrogeometry of the cutting tool	β= 65°, α= 15°, γ=10°
Initial cutting edge radius	r_{1n}= 10 μm
Cutting tool material	Cemented carbide ISO K20-K40 (uncoated)
Polishing Paste	Diastar 5-8 μm (1gr /cycle)
Interval for changing rotation direction	6 s

Table 8-2: Experimental factors considered for brushing-polishing

	Factor			
	Rotational speed (1/min)	Time (s)	Depth (mm)	Brush (Type)
Level	N	t_b	y_b	B_t
Low (-)	300	24	0,4	Rosshaar
High (+)	500	48	0,8	Vitex

Table 8-3 shows the final radius as measured response obtained from the application of BP as cutting edge preparation process. The average radius $\overline{r_{2n}}$ resultant from 3 replications (3 different cutting tools) for each parameter combination, the standard deviation of the radius $S_{r_{2n}}$ and the quantity six sigma $6 \cdot S_{r_{2n}}$ are shown. This information is used to observe the generated variability of the final radius r_{2n}, for each parameter combination. Likewise, in **Table 8-4**, the removed area A_r (obtained by using equations 6-1 and 6-2) for 3 replications, and the corresponding average $\overline{A_r}$ and standard deviation S_{A_r} are presented.

Table 8-3: Experimental factors and obtained final cutting edge radius for brushing-polishing

	Experimental factors				Measured response		
	Rot. speed	Time	Depth	Brush	Average Radius	Stand.Deviation	Six sigma
Nr.	N	t_b	y_b	B_t	$\overline{r_{2n}}$ (μm)	$S_{r_{2n}}$ (μm)	$6{\cdot}S_{r_{2n}}$ (μm)
1	-	-	-	-	17.07	0.32	1.93
2	+	-	-	-	17.43	0.46	2.76
3	-	+	-	-	17.57	1.16	6.95
4	+	+	-	-	20.07	1.19	7.16
5	-	-	+	-	18.17	0.50	3.02
6	+	-	+	-	21.83	1.06	6.36
7	-	+	+	-	19.70	1.54	9.24
8	+	+	+	-	25.13	1.29	7.74
9	-	-	-	+	20.23	0.57	3.41
10	+	-	-	+	20.86	0.84	5.02
11	-	+	-	+	23.33	0.45	2.71
12	+	+	-	+	24.23	0.61	3.67
13	-	-	+	+	23.62	0.96	5.77
14	+	-	+	+	24.13	0.47	5.84
15	-	+	+	+	27.82	0.42	2.53
16	+	+	+	+	31.74	1.22	7.29

Table 8-4: Experimental factors and response for brushing-polishing

Experimental factors					Response			
	Rot. speed	Time	Depth	Brush	Removed area A_r (μm^2)		Average $\overline{A_r}$ (μm^2)	Stand.Dev. S_{A_r} (μm^2)
Nr.	N	t_b	y_b	B_t				
1	-	-	-	-	112.96	111.01	101.40	108.46	6.19
2	+	-	-	-	113.36	116.91	116.52	115.60	1.95
3	-	+	-	-	114.93	143.66	97.64	118.75	23.25
4	+	+	-	-	190.92	141.53	183.86	172.11	26.71
5	-	-	+	-	141.53	129.02	120.90	130.49	10.39
6	+	-	+	-	237.98	217.67	186.20	213.95	26.09
7	-	+	+	-	193.29	126.97	172.32	164.20	33.90
8	+	+	+	-	332.42	311.91	261.71	302.01	36.38
9	-	-	-	+	161.07	186.20	179.21	175.50	12.97
10	+	-	-	+	212.70	183.86	174.38	190.32	19.96
11	-	+	-	+	264.40	240.57	251.05	252.01	11.94
12	+	+	-	+	294.76	261.71	272.54	276.34	16.85
13	-	-	+	+	284.67	233.35	261.44	259.82	25.70
14	+	-	+	+	278.03	259.02	283.56	273.54	12.87
15	-	+	+	+	397.30	371.99	377.31	382.20	13.34
16	+	+	+	+	564.73	481.05	498.65	514.81	44.12

For the significance analysis, a significance level $Alpha$= 0.05 was selected. A Pareto′s chart that presents the absolute value of the effects for the main factors and interactions between two variables (two-way interactions) is shown in **Figure 8-3**. The vertical dashed-line defines the boundary of the main factors and two-way interactions that are significant considering the selected level $Alpha$. Factors that extend to the right beyond the boundary are significant. The brush type B_t results that of more significance, follow by depth y_b, brushing time t_b and rotational speed N, respectively. The Main factors and the two-way interactions result significant, except the interaction $N \cdot y_b$ (speed-depth). The main factors result highly significant in comparison to the two-way interactions.

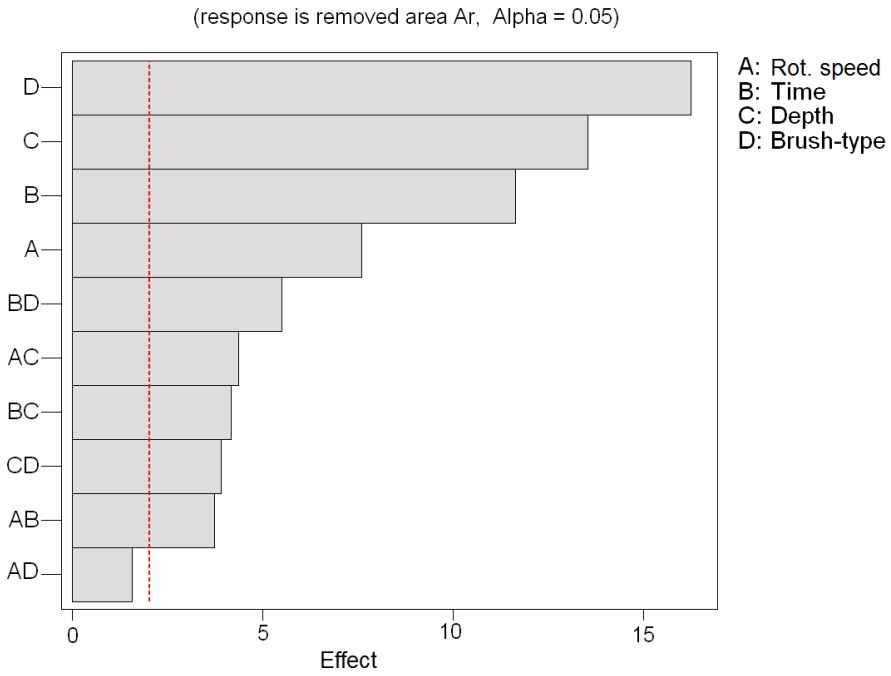

Figure 8-3: Pareto′s chart of effects on A_r in brushing-polishing

In **Figure 8-4** the effects and influence of the main factors; speed N, time t_b, depth y_b, and brush type B_t on removed area A_r are illustrated.

Figure 8-5 shows the interaction plot of the considered factors for brushing-polishing. that influence the removed area A_r. It can be observed that in general there is moderate two-way interaction for each pair of main factors. Being the more significant the interaction between time t_b and type of brush B_t.

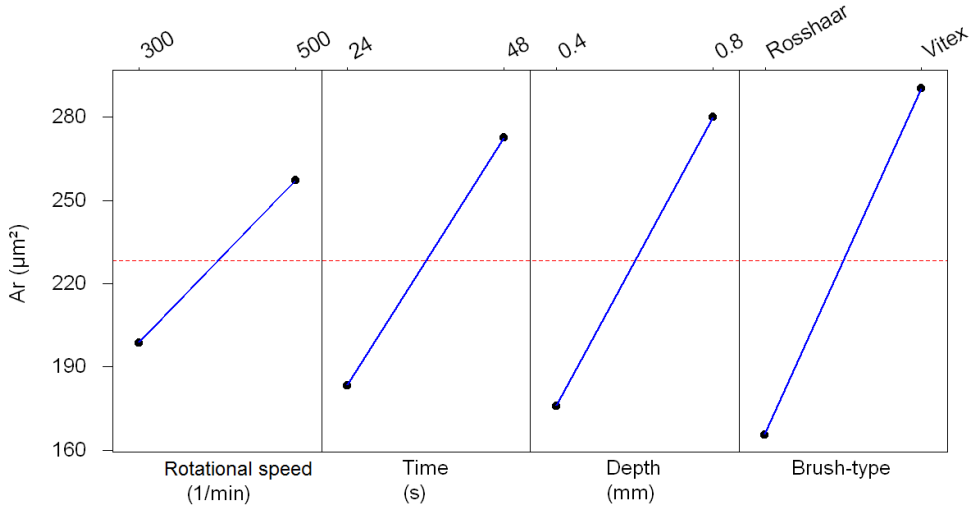

Figure 8-4: Main effects plot for removed area A_r in brushing-polishing

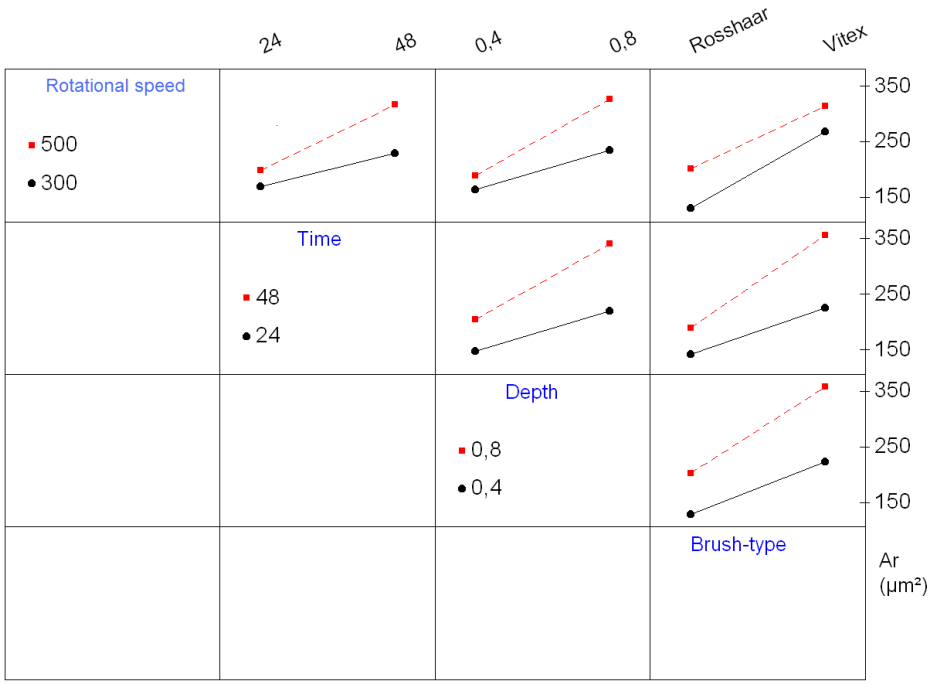

Figure 8-5: Interaction plot for removed area A_r in brushing-polishing

8.4 Variability of final cutting edge radius

Considering the data presented in **Table 8-3**, it can be observed that for the same generated radius r_{2n}, there are different values of $6 \cdot S_{r_{2n}}$ depending on the combination of factors. For the combination of factors Nr.4 and Nr.9 the generated radii r_{2n} are 20μm in both cases, however the values of $6 \cdot S_{r_{2n}}$ are 7.2 and 3.4μm respectively. The same behavior is observed for the combinations Nr.12 and Nr.14 for r_{2n}=24μm with $6 \cdot S_{r_{2n}}$= 3.6 and 5.8μm respectively and combinations Nr.1 and Nr.2 for r_{2n}=17μm with $6 \cdot S_{r_{2n}}$=1.9 and 2.8μm respectively. As was observed in chapter 7, the value $6 \cdot S_{r_{2n}}$, obtained for each combination of factors, is an important criteria to select the parameters to obtain a required radius r_{2n}.

8.5 Regression model for removed area

By using regression analysis [46] and considering the significant factors and two-way interactions observed in **Figure 8-3**, a regression model for the removed area A_r is proposed.

The obtained regression model can be written as:

$$\begin{aligned} A_r \; = 384 - 0.640\, N - 6.81\, t_b - 390\, y_b - 91.9\, B_t + 3.52\, t_b \cdot B_t + 0.837\, N \cdot y_b \\ +6.67\, t_b \cdot y_b + 150\, y_b \cdot B_t + 0.0119\, N \cdot t_b \end{aligned} \tag{8-1}$$

Where the type of brush is B_t=0 for Rosshaar and B_t=1 for Vitex.

By using the model presented in equation 8-1, plots to observe the behavior of the removed area A_r as function of the combinations of rotational speed N, brushing time t_b and depth y_b are presented. **Figures 8-6** and **8-7** show a surface plot and a contour plot of the response A_r as function of rotational speed N and depth y_b. To compare, in **Figures 8-8** and **Figure 8-9** the response A_r is shown for other hold values considering another brush type (Rosshaar).

Additionally, in **Figures 8-10** and **8-11** the influence of the distance between the jet and the cutting edge and the air pressure on the removed area A_r is presented. Likewise **Figure 8-12** and **8-13** show the behavior of A_r related with distance and time.

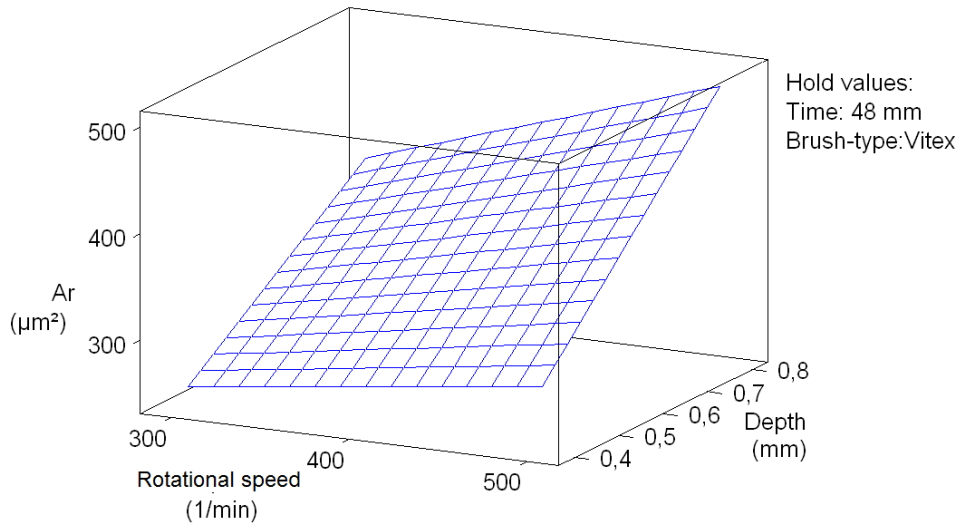

Figure 8-6: Surface plot for A_r considering speed and depth

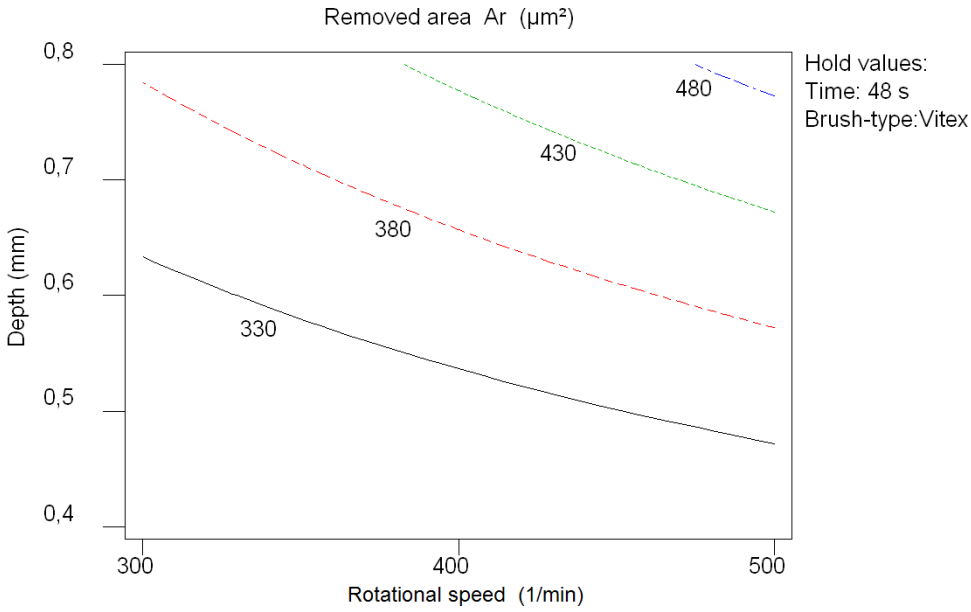

Figure 8-7: Contour plot for A_r considering speed and depth

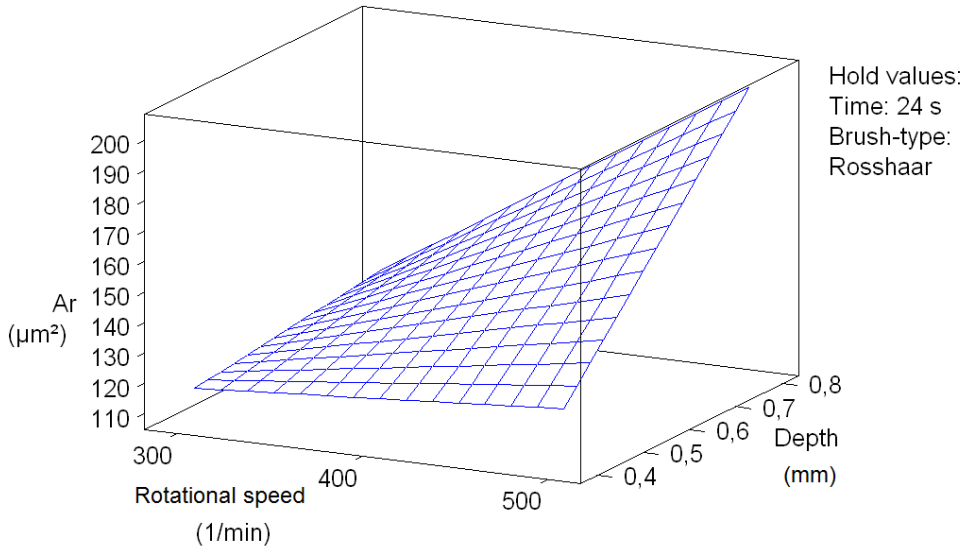

Figure 8-8: Surface plot for A_r considering speed and depth and Rosshaar brush

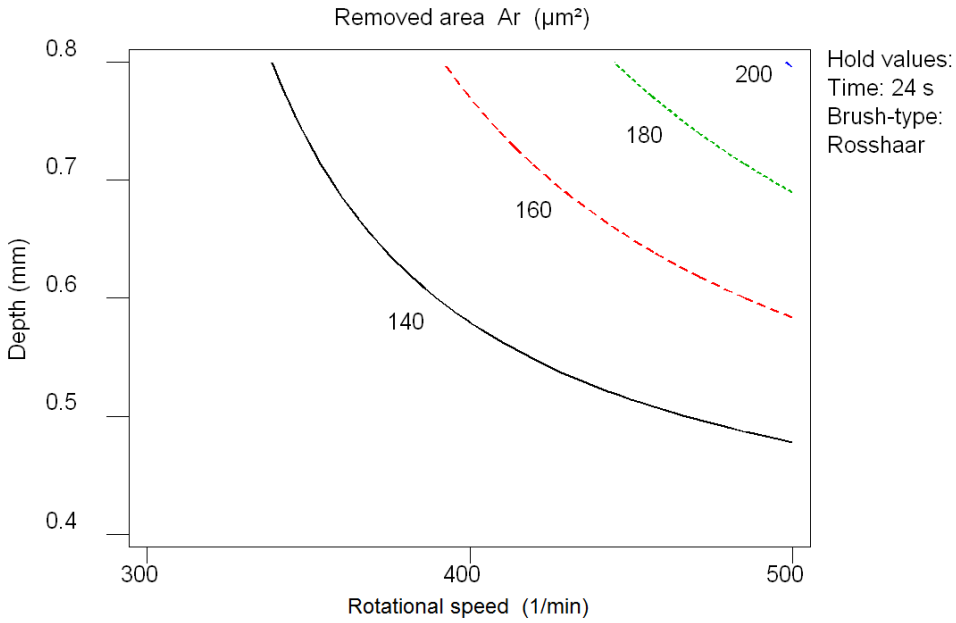

Figure 8-9: Contour plot for A_r considering speed and depth and Rosshaar brush

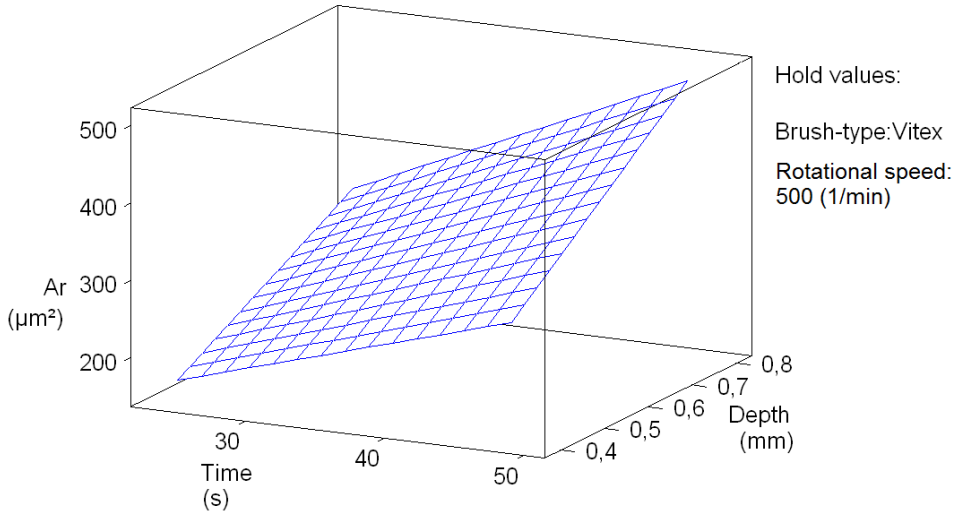

Figure 8-10: Surface plot for A_r considering time and depth

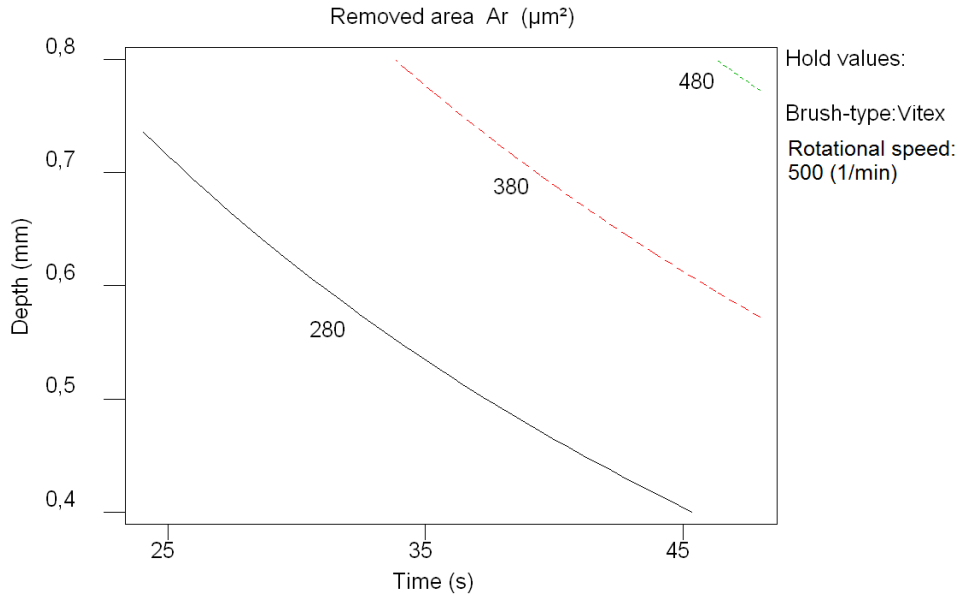

Figure 8-11: Contour plot for A_r considering time and depth

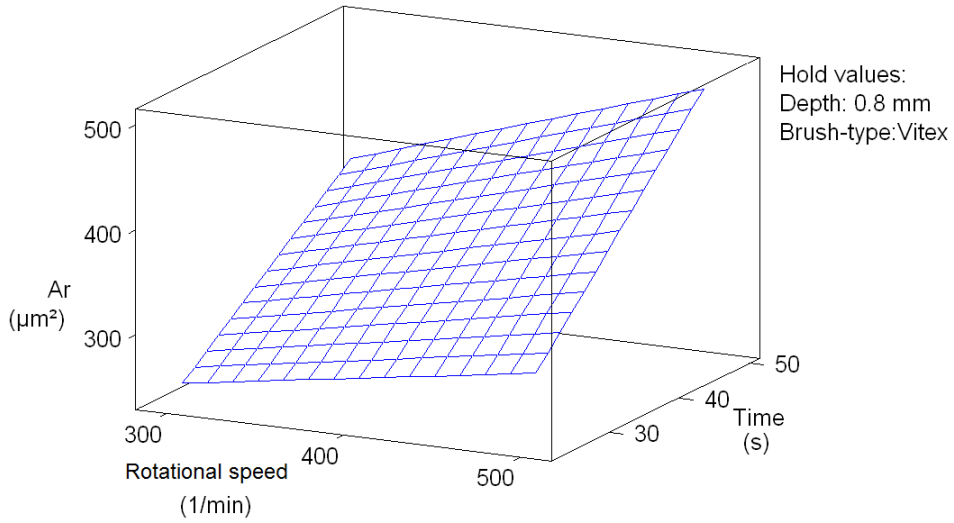

Figure 8-12: Surface plot for A_r considering speed and time

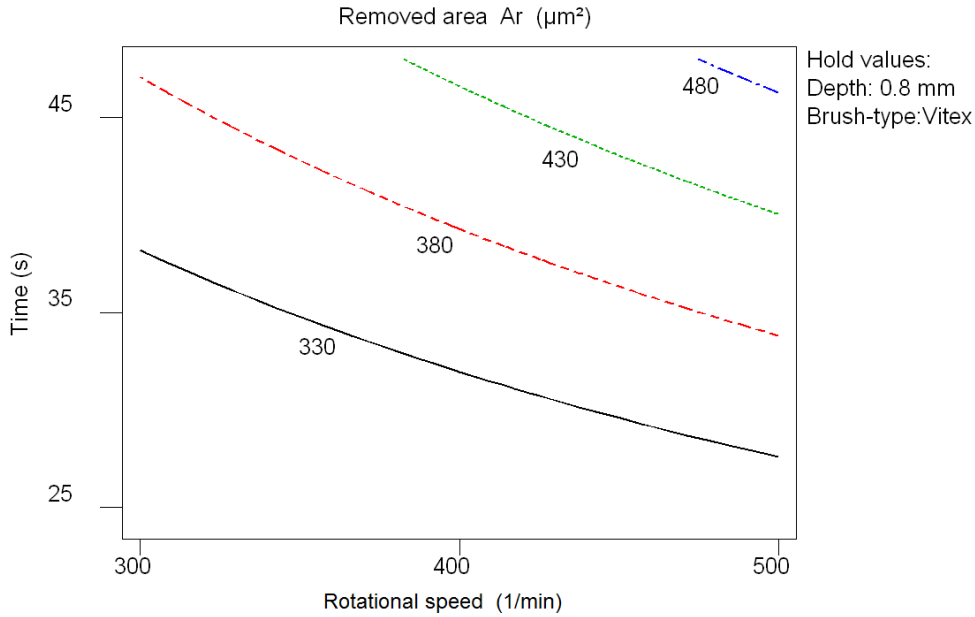

Figure 8-13: Contour plot for A_r considering speed and time

8.6 Roughness

To analyze the influence of the experimental factors on the roughness R_z of the tool surfaces (measured as indicated in **Figure 7-4**), three treatments were considered : unprepared tool (as reference), and two extreme combinations of factors from **Table 8-4** (those that caused the lower and the higher remove area, but considering only the treatments with y_b= 0.8 mm to guarantee that there is complete affectation on the selected area for measurement). Analysis of variance (ANOVA) [112] was applied to study if the roughness obtained by the application of the selected treatments has a significant difference.

The selected treatment were: B0 (unprepared), B1 (combination Nr.5) and B2 (combination Nr.16). **Table 8-5** shows the obtained data for R_z corresponding to treatments considered for ANOVA. To illustrate the results of the analysis, **Figure 8-14** shows a box-plot for R_z obtained by the considered treatments.

Table 8-5: Data of the treatments

Treatment	R_z (μm)			Mean	Std.Dev.
B0	1.03	0.98	0.83	0.94	0.104
B1	0.53	0.58	0.61	0.57	0.040
B2	0.37	0.44	0.50	0.43	0.065

Figure 8-14: Box-plot for R_z by different treatments: B0 (unprepared), B1 and B2 are two different parameter combinations of BP

The results of the one-way ANOVA, considering a significance level of 5%, reveal that there is a significant difference among the means of the treatments. In addition, the Tukey's test [112] for pairwise comparisons was applied to observe which treatments are different among if. The result of the test evidences that there is no significant difference

between treatments B1 and B2, but there is a significant difference between B0 and B1, and between B0 and B2. Therefore, there is no significant difference between the roughness obtained by the two preparation treatments, but there is a significant difference between the roughness of the unprepared and prepared tools. In consequence, there is an improvement of roughness R_z of the tool face by applying BP for cutting edge preparation.

8.7 Microstructuring

The detailed description of the microstructuring of the tool surfaces was presented in section 5.3.2. In **Figure 5-31** the characterization of a typical microstructuring, by using areal parameters and autocorrelation function, for a tool face obtained by BP is shown. In **Figures 5-41** and **5-42**, the characterization of the microstructuring of the tool face by means of fractals is presented. As was described in section 5.3.2, the typical microstructuring of a tool surface obtained by BP is slightly anisotropic, as result of a combination of the previous grinding microstructuring and the microstructuring generated by the kinematics of the brushing-polishing process.

8.8 Notchedness

In order to analyze the behavior of the notchedness for cutting edge preparation by BP, the parameters R_z and R_{pk} (see section 5.3.2) were observed as function of process time. In **Table 8-6**, the experimental conditions are presented. **Figure 8-15** shows the data of the measurements of R_z, R_{pk} and the ratio R_{pk}/R_z. As initial condition, cutting edges without preparation were considered.

Table 8-6: Conditions for analysis of notchedness by brushing-polishing

Experimental conditions BP	
Macrogeometry of the cutting tool	β= 65°, α= 15°, γ=10°
Length of main cutting edge	AC = 0.8 mm
Cutting tool material	Uncoated cemented carbide ISO K20-K40
Brush type	Vitex
Rotational speed	300 (1/min)
Depth	0.8 mm
Polishing paste	Diastar 5-8μm
Interval for changing rotation direction	6 s
Position of the edge	Symmetric

In **Figure 8-15**, a high decay of the roughness R_z in the first stage of the cutting edge preparation by BP can be observed. After a critical point of process time (approximately

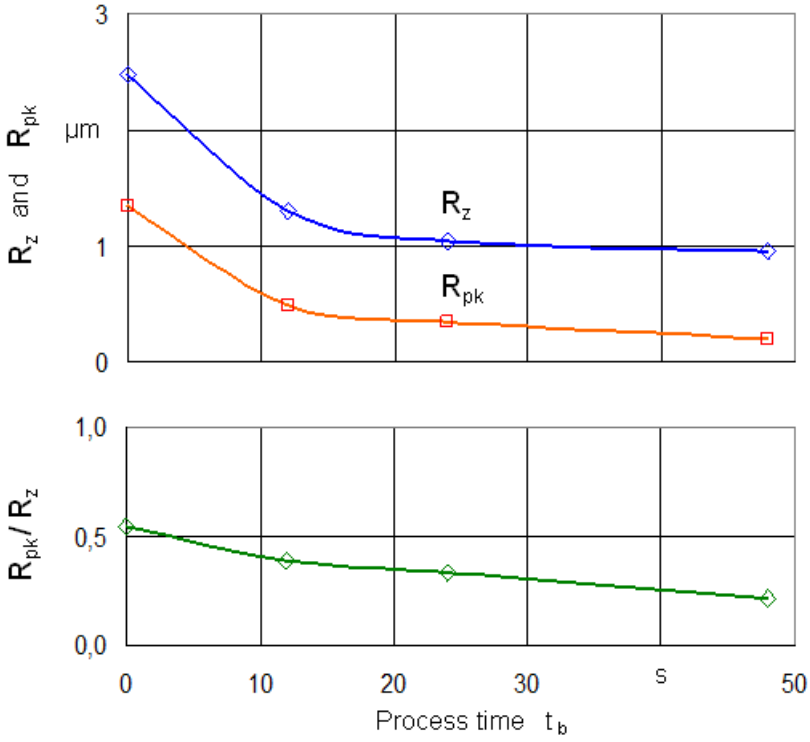

Figure 8-15: Analysis of notchedness for cutting edge preparation by BP

20s), the decrease of roughness is not appreciable. A similar decay behavior can be observed for R_{pk}. Additionally, a tendency to decrease the ratio R_{pk}/R_z is observed. In consequence, a tendency in the decrease of picks related with the nominal roughness R_z is presented, as the process time increases.

Additionally, the behavior of the notchedness as function of process time t_b for BP, for the data presented in **Figure 8-15**, can be expressed as:

$$R_z(t_b) = 0.97 + e^{-0.12\,(t_b - 3.32)} \tag{8-2}$$

9 Brushing with abrasive filaments for cutting edge preparation

9.1 Description of the process and set-up

Brushing with nylon abrasive filaments (BNAF) uses a brush with abrasive filaments formed by a nylon matrix and particles of hard abrasive (aluminium oxide, silicon carbide, cubic boron nitride and diamond) as filling material to remove material by abrasion (see section 4.4.3). The experimental set-up for cutting edge preparation by BNAF is illustrated in **Figure 9-1**. The cutting tool to be prepared is mounted in a fixture on a table that has movement in two orthogonal horizontal directions, one to adjust the penetration depth of the filaments and other to approximate the cutting tool to the brush before applying the alternating feed movement of the table. The brush is mounted with the axis in horizontal position coupled to a electric motor with controlled rotational speed and with the possibility of changing the rotational direction during the process cycle.

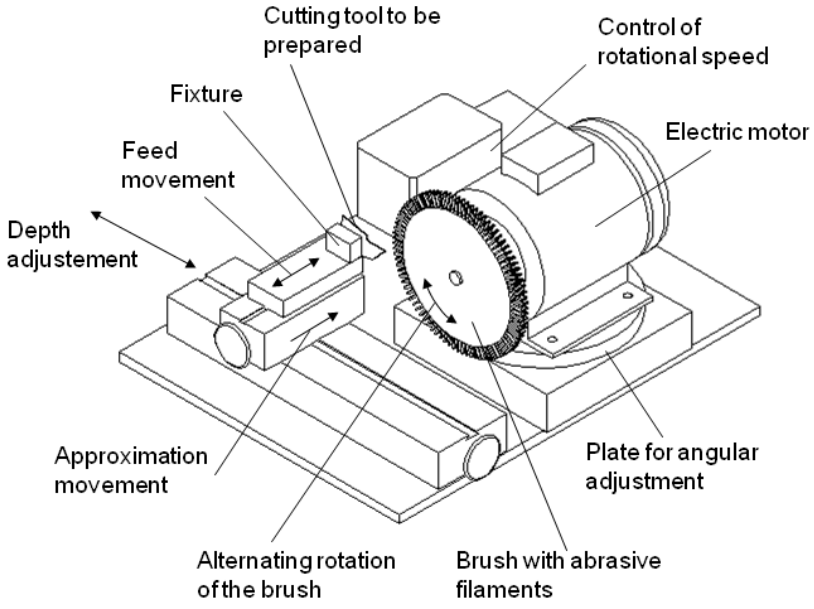

Figure 9-1: Diagram of the equipment for BNAF

Figure 9-2 shows the relative positioning between the brush and the cutting edge to

be prepared. The diagram illustrates a symmetric adjustment of the cutting edge in order to obtain a symmetric geometry of the edge contour, considering alternating rotation of the brush during the process cycle. Additionally, the adjustment of the penetration depth y_n of the filaments is shown.

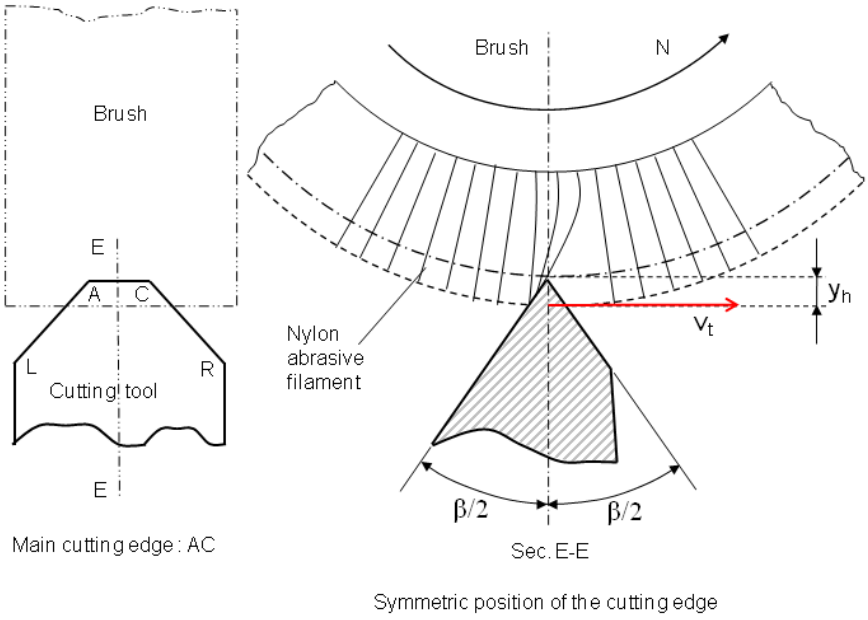

Figure 9-2: Relative positioning between abrasive brush and cutting tool

9.2 Materials and methods

In order to analyze the effect of the BNAF parameters on the cutting edge preparation characteristics, the same uncoated cemented carbide ISO K20-K40 considered for MAJM and BP were used as cutting tool material. The characteristics of the cutting tool material are presented in **Table 7-1**. The geometry of the considered precision cutting tool is described in **Figure 7-3**. Two types of brushes with nylon abrasive filaments were considered. The filaments use corundum and diamond as abrasive filling materials.

The cutting edge preparation was developed by means of a relative movement between brushing with nylon abrasive filaments and the cutting edge. The relative movement is generated by the alternating rotation of the brush and feed. The relative positioning between cutting edge and the brushing with abrasive filaments is shown in **Figure 9-2**.

The measurement of the generated radius was carried out by means of the methodology described in section 7.2. Likewise, the procedure used to measure the roughness of the tool face and the notchedness of the cutting edge is the same as the used for MAJM and BP, and described in section 7.2.

9.3 Experimental design

In order to analyze the effects of the BNAF parameters on the characteristics of the cutting edge preparation and to obtain a regression model for describing the relationship between the process parameters and the removed material, methods of design of experiments (DoE) were applied [63, 70, 88, 89, 144].

To analyze the effects of type of abrasive A_b, grit of abrasive G, depth y_h, speed v_t and time t_h on the removed area A_r, a fractional factorial design 2^{5-1} (resolution V) with 3 replicates was selected. In **Table 9-1** the constant conditions for experimenting are presented. Additionally, in **Table 9-2** the levels of the considered experimental factors are shown.

Table 9-1: Considered constants conditions for BNAF

Experimental constant conditions	
Macrogeometry of the cutting tool	β= 65°, α= 15°, γ=10°
Initial cutting edge radius	r_{1n}= 10 μm
Cutting tool material	Cemented carbide ISO K20-K40 (uncoated)
Interval for changing rotation direction	9 s

Table 9-2: Experimental factors considered for BNAF

	Factor				
	Abrasive (Type)	Grit (Mesh grade)	Depth (mm)	Speed (m/s)	Time (s)
Level	A_b	G	y_h	v_t	t_h
Low (-)	Corundum	240	1	10	18
High (+)	Diamond	800	2	20	36

Table 9-3 shows the final radius as measured response obtained from the application of BNAF as cutting edge preparation process. The average radius $\overline{r_{2n}}$ resultant from 3 replications (3 different cutting tools) for each parameter combination, the standard deviation of the radius $S_{r_{2n}}$ and the quantity six sigma $6 \cdot S_{r_{2n}}$ are shown. This information is used to observe the generated variability of the final radius r_{2n}, for each parameter combination. Likewise, in **Table 9-4**, the removed area A_r (obtained by using equations 6-1 and 6-2) for 3 replications, and the corresponding average $\overline{A_r}$ and standard deviation S_{A_r} are presented.

Table 9-3: Experimental factors and obtained final cutting edge radius for BNAF

	Experimental factors					Measured Response		
	Abrasive	Grit	Depth	Speed	Time	Average Radius	Stand.Deviation	Six sigma
Nr.	A_b	G	y_h	v_c	t_h	$\overline{r_{2n}}$ (μm)	$S_{r_{2n}}$ (μm)	$6{\cdot}S_{r_{2n}}$ (μm)
1	-	-	-	-	+	13.43	0.59	3.52
2	+	-	-	-	-	13.45	1.12	6.74
3	-	+	-	-	-	11.13	0.15	0.92
4	+	+	-	-	+	14.07	1.42	8.51
5	-	-	+	-	-	13.37	1.63	9.75
6	+	-	+	-	+	17.63	0.72	4.34
7	-	+	+	-	+	16.50	1.47	8.84
8	+	+	+	-	-	14.67	0.55	3.30
9	-	-	-	+	-	14.80	1.91	11.45
10	+	-	-	+	+	22.00	1.15	6.92
11	-	+	-	+	+	14.70	1.40	8.40
12	+	+	-	+	-	19.93	2.54	15.25
13	-	-	+	+	+	18.20	1.15	6.92
14	+	-	+	+	-	26.07	2.72	16.33
15	-	+	+	+	-	12.70	1.81	10.86
16	+	+	+	+	+	23.70	2.29	13.72

Table 9-4: Experimental factors and response for BNAF

	Experimental factors					Response		
	Abrasive	Grit	Depth	Speed	Time	Removed area	Average	Stand.Dev.
Nr.	A_b	G	y_h	v_c	t_h	A_r (μm^2)	$\overline{A_r}$ (μm^2)	S_{A_r} (μm^2)
1	-	-	-	-	+	42.03 39.06 55.94	45.68	9.01
2	+	-	-	-	-	60.78 49.64 27.65	46.02	16.86
3	-	+	-	-	-	15.68 11.89 13.14	13.57	1.93
4	+	+	-	-	+	81.16 51.20 36.14	56.17	22.92
5	-	-	+	-	-	36.14 26.27 74.18	45.53	25.30
6	+	-	+	-	+	128.85 103.17 126.81	119.61	14.28
7	-	+	+	-	+	74.18 91.96 128.85	98.33	27.89
8	+	+	+	-	-	75.91 59.15 60.78	65.28	9.24
9	-	-	-	+	-	33.27 88.31 84.71	68.76	30.80
10	+	-	-	+	+	245.48 219.89 188.31	217.89	28.63
11	-	+	-	+	+	40.54 82.93 75.91	66.46	22.72
12	+	+	-	+	-	235.10 156.45 120.75	170.77	58.51
13	-	-	+	+	+	132.98 107.00 154.26	131.41	23.67
14	+	-	+	+	-	426.09 288.77 277.68	330.85	82.67
15	-	+	+	+	-	69.07 18.26 20.88	36.07	28.61
16	+	+	+	+	+	285.98 195.43 308.63	263.35	59.90

For the significance analysis, a significance level $Alpha$= 0.05 was selected [112]. **Figure 9-3** shows a Pareto′s chart that presents the absolute value of the effects for the main factors and interactions between two variables (two-way interactions). The vertical dashed-line defines the boundary of the main factors and two-way interactions that are significant considering the selected level $Alpha$. Factors that extend to the right beyond the boundary are significant. The speed v_t and abrasive type A_t result that of more significance, follow by two-way interaction abrasive-speed $A_t \cdot v_t$ and depth y_h. Grit G and time t_h are the main factors that have the lower significance.

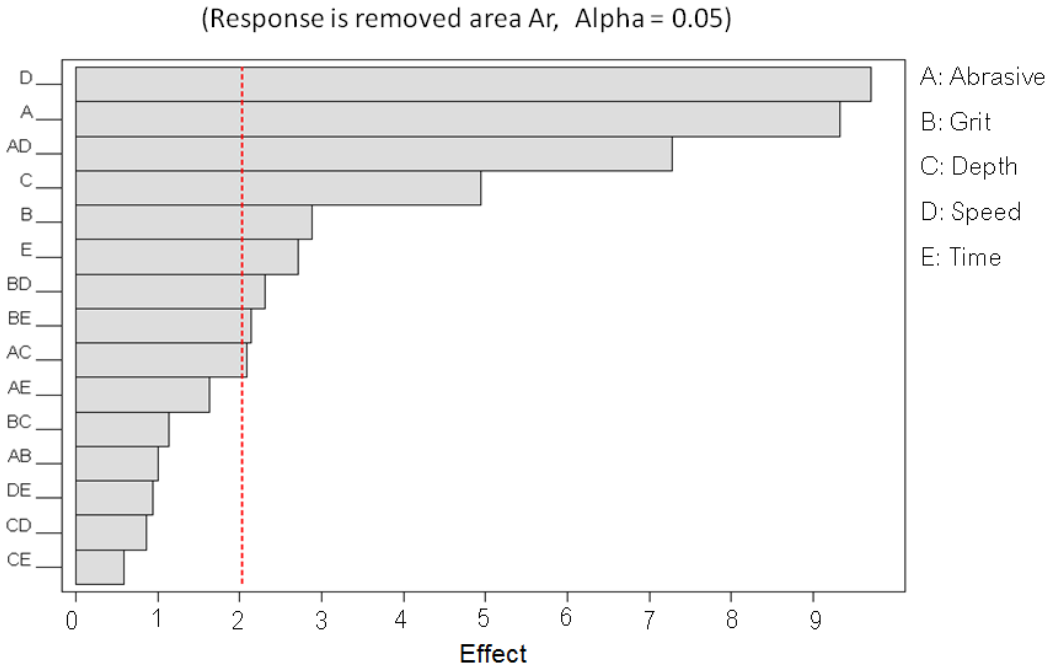

Figure 9-3: Pareto′s chart of effects on A_r in BNAF

In **Figure 9-4** the effects and influence of the main factors; abrasive type A_b, grit G, depth y_h, speed v_t and time of brushing t_h on removed area A_r area shown.

Figure 9-5 shows the interaction plot of the considered factors for brushing with nylon abrasive filaments, that influence the removed area A_r. It can be observed that in general there is two-way interaction for each pair of main factors. Being the more significant the interaction between abrasive type A_b and speed v_t. There are low or almost null interaction between distance speed v_t and depth y_h and speed v_t and time t_h.

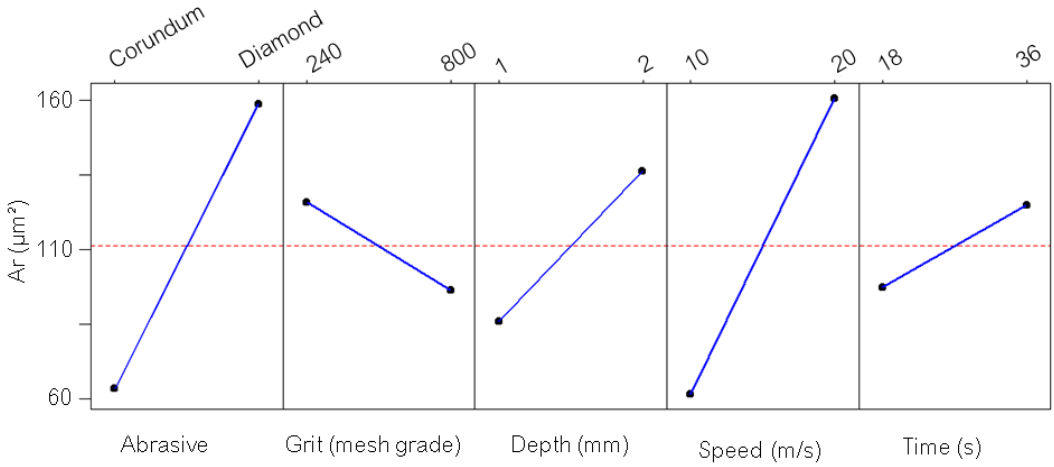

Figure 9-4: Main effects plot for removed area A_r in BNAF

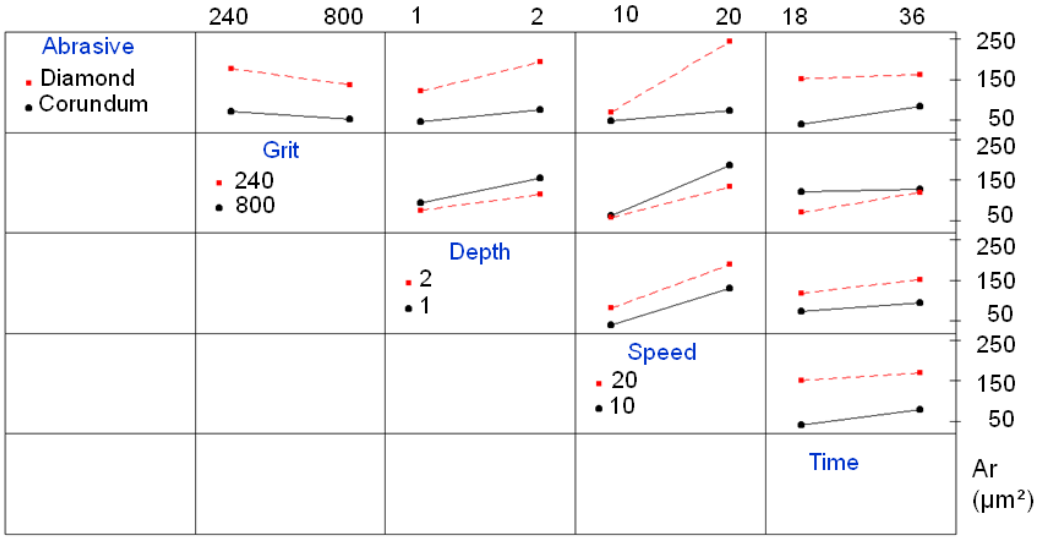

Figure 9-5: Interaction plot for removed area A_r in BNAF

9.4 Variability of final cutting edge radius

Considering the data presented in **Table 9-3**, it can be observed that for the same generated radius r_{2n}, there are different values of $6 \cdot S_{r_{2n}}$ depending on the combination of factors. For the combination of factors Nr.1, Nr.2 and Nr.5 the generated radii r_{2n} are 13μm in the three cases, however the values of $6 \cdot S_{r_{2n}}$ are 3.52, 6.74 and 9.75μm respectively. The same behavior is observed for the combinations Nr.8, Nr.9 and Nr.11 for r_{2n}=15μm with $6 \cdot S_{r_{2n}}$= 3.3, 11.5 and 8.4μm respectively. As was observed in chapter 7, the value $6 \cdot S_{r_{2n}}$, obtained for each combination of factors, is an important criteria to select the parameters to obtain a required radius r_{2n}.

9.5 Regression model for removed area

By using regression analysis [46] and considering the significant factors and two-way interactions observed in **Figure 9-3**, a regression model for the removed area A_r is proposed.

The obtained regression model can be written as:

$$\begin{aligned} A_r \; = -37,0 - 192\, A_b - 0,0435\, G + 29,2\, y_h + 6,87\, v_t - 0,72\, t_h + 14,9\, A_b \cdot v_t \\ -0,00843\, G \cdot v_t + 0,00434\, G \cdot t_h + 42,8\, A_b \cdot y_h \end{aligned} \tag{9-1}$$

Where the type of abrasive is A_b=0 for corundum and A_b=1 for diamond.

By using the model presented in equation 9-1, plots to observe the behavior of the removed area A_r as function of the combinations of abrasive A_b, grit G, depth y_h, speed v_t and brushing time t_h are presented. **Figures 9-6** and **9-7** show a surface plot and a contour plot of the response A_r as function of depth y_h and speed v_t. To compare, in **Figures 9-8** and **9-9** the response A_r is shown for other hold values considering another abrasive (Corundum).

Additionally, in **Figures 9-10** and **9-11** the influence of the time t_h and depth y_h on the removed area A_r is presented. Likewise **Figures 9-12** and **9-13** show the behavior of A_r related with time t_h and speed v_t.

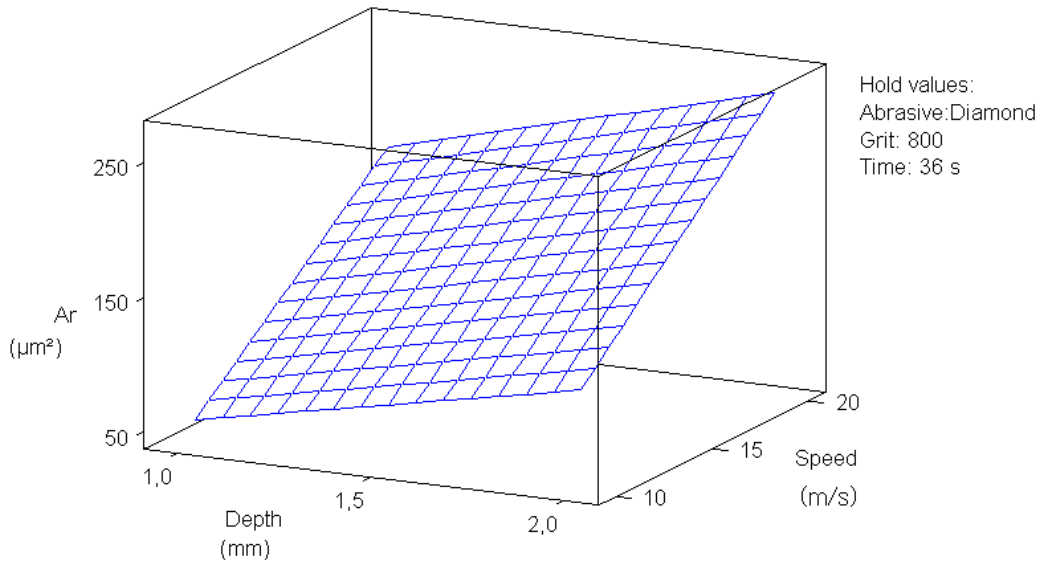

Figure 9-6: Surface plot for A_r considering depth and speed

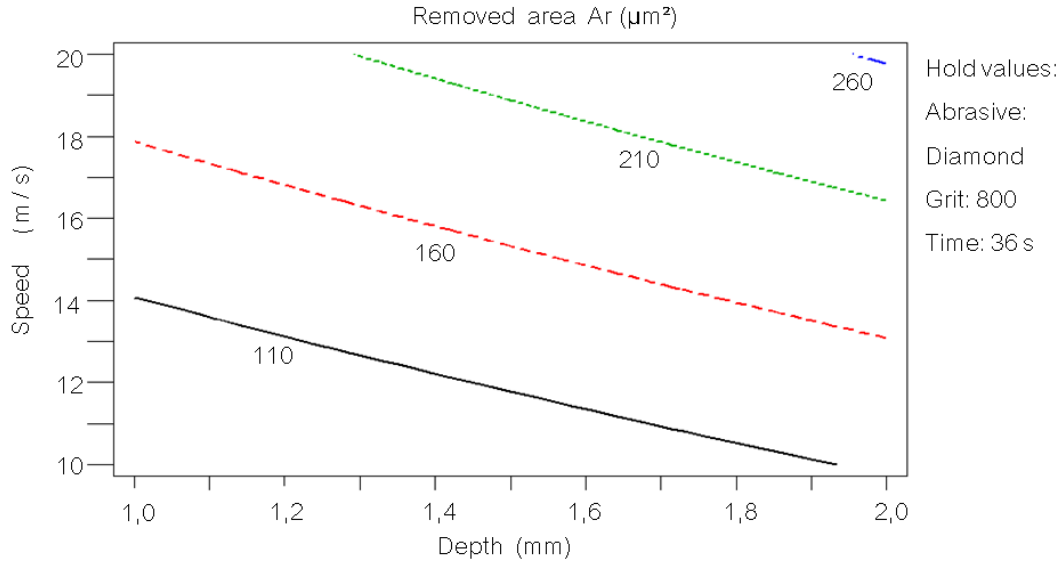

Figure 9-7: Contour plot for A_r considering depth and speed

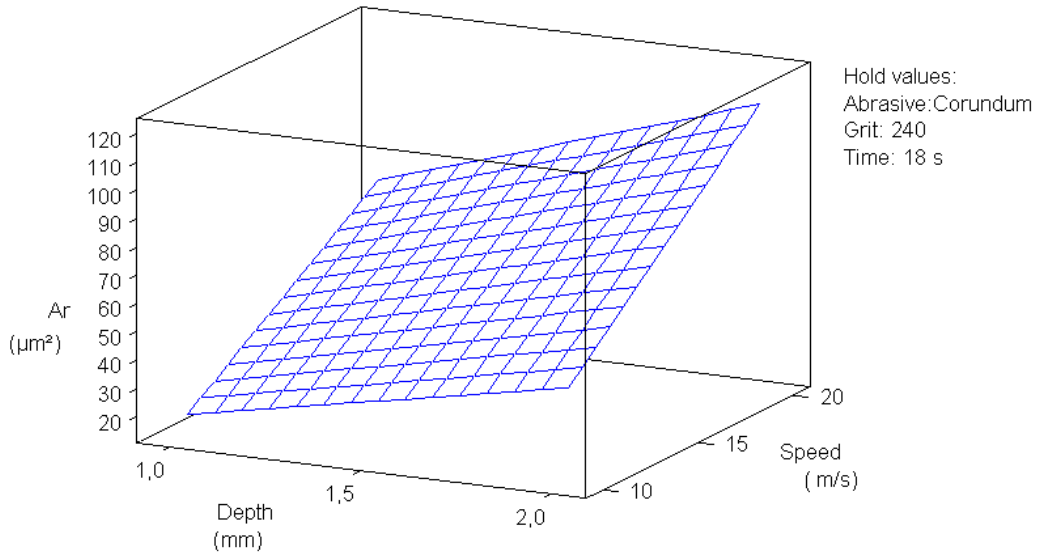

Figure 9-8: Surface plot for A_r considering depth and speed with corundum as abrasive

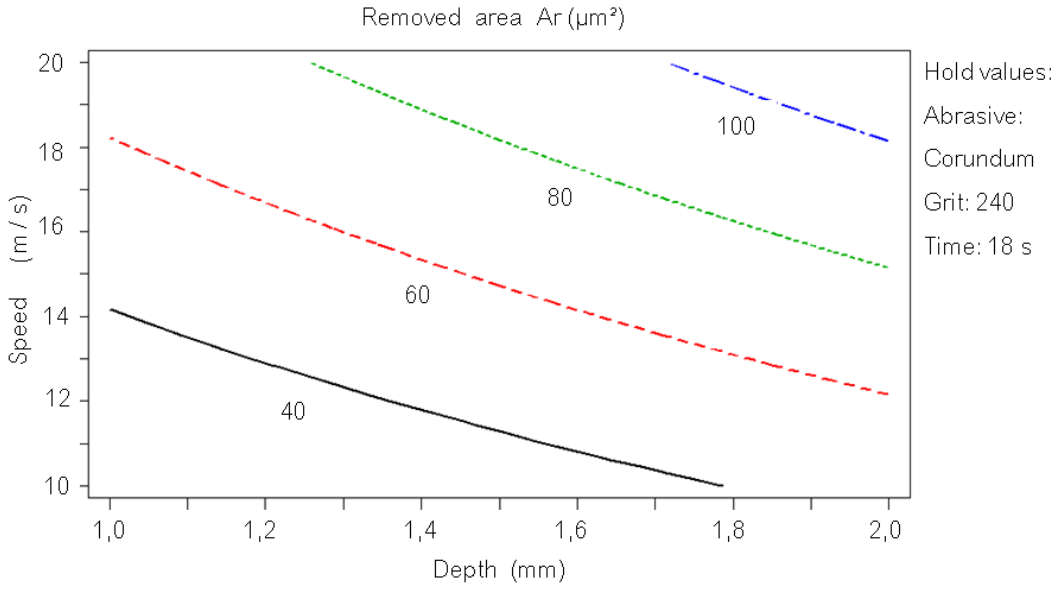

Figure 9-9: Contour plot for A_r considering depth and speed with corundum as abrasive

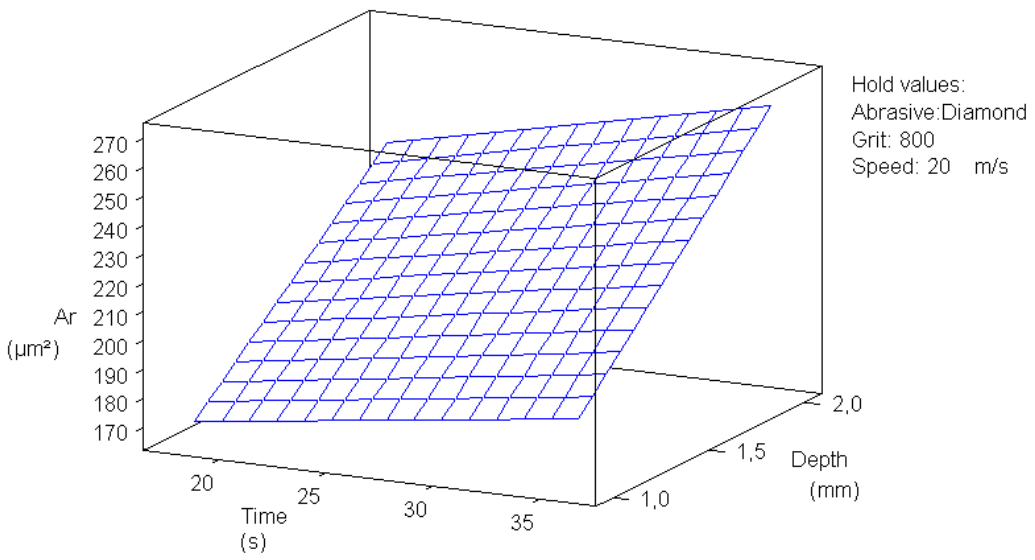

Figure 9-10: Surface plot for A_r considering time and depth

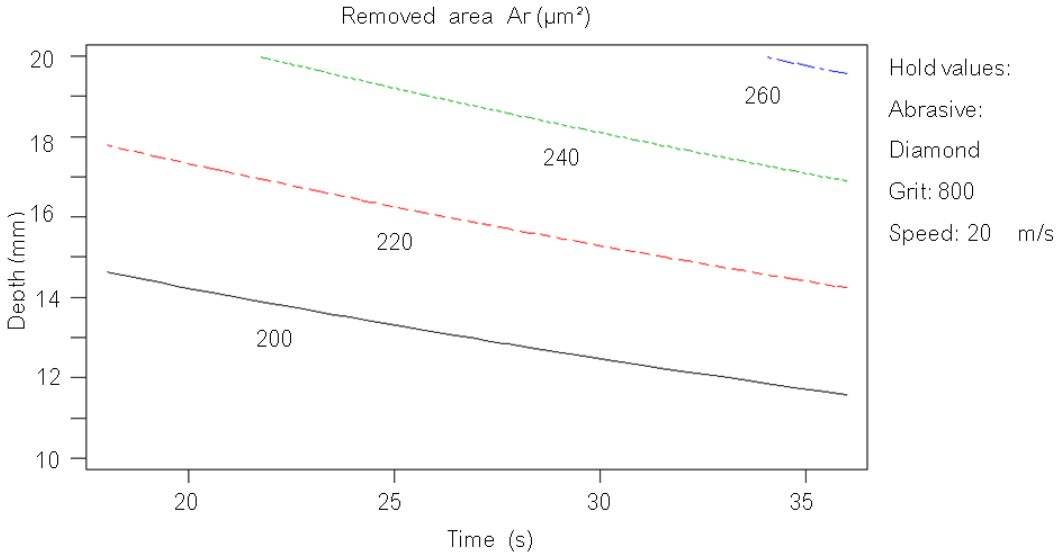

Figure 9-11: Contour plot for A_r considering time and depth

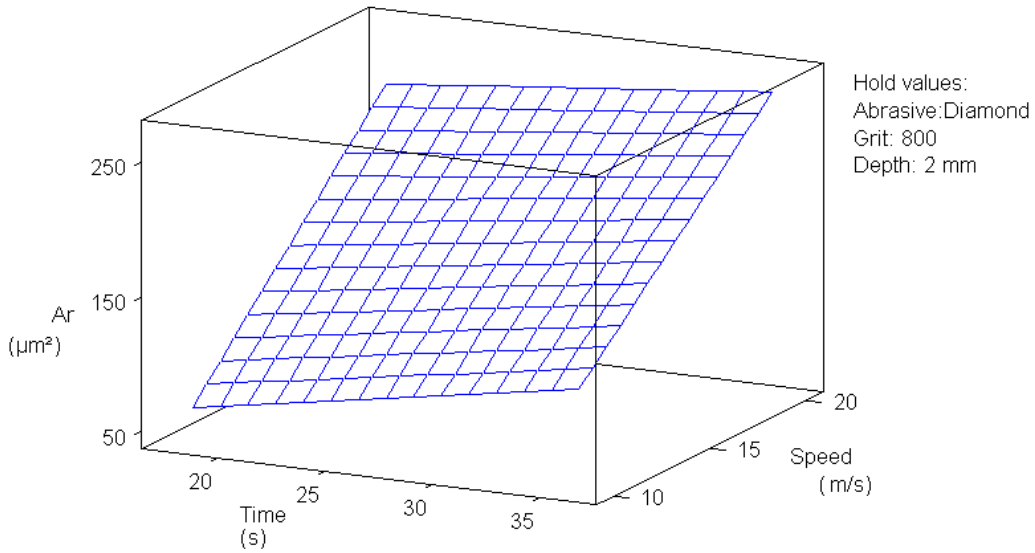

Figure 9-12: Surface plot for A_r considering time and speed

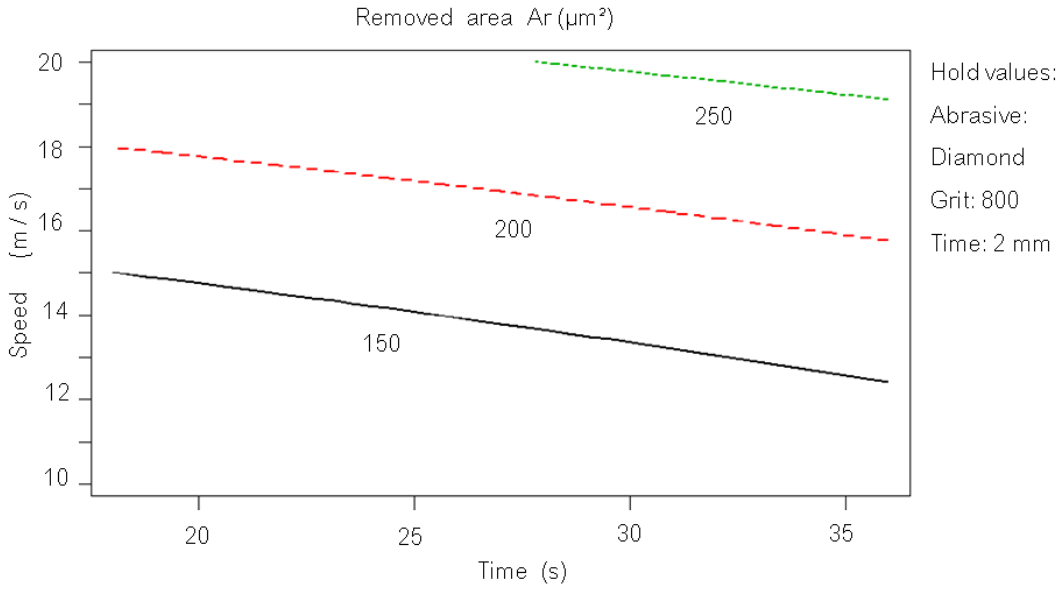

Figure 9-13: Contour plot for A_r considering time and speed

9.6 Roughness

To analyze the influence of the experimental factors on the roughness R_z of the tool surfaces (measured as indicated in **Figure 7-4**), three treatments were considered : unprepared tool (as reference), and two extreme combinations of factors from **Table 9-4** (those that caused the lower and the higher remove area). Analysis of variance (ANOVA) [112] was applied to study if the roughness obtained by the application of the selected treatments has a significant difference.

The selected treatment were: F0 (unprepared), F1 (combination Nr.3) and F2 (combination Nr.14). **Table 9-5** shows the obtained data for R_z corresponding to treatments considered for ANOVA. To illustrate the results of the analysis, **Figure 9-14** shows a box-plot for R_z obtained by the considered treatments.

Table 9-5: Data of the treatments

Treatment	R_z (μm)			Mean	Std.Dev.
F0	0.93	1.03	0.99	0.98	0.050
F1	0.93	0.98	0.87	0.92	0.055
F2	0.88	0.93	1.02	0.94	0.070

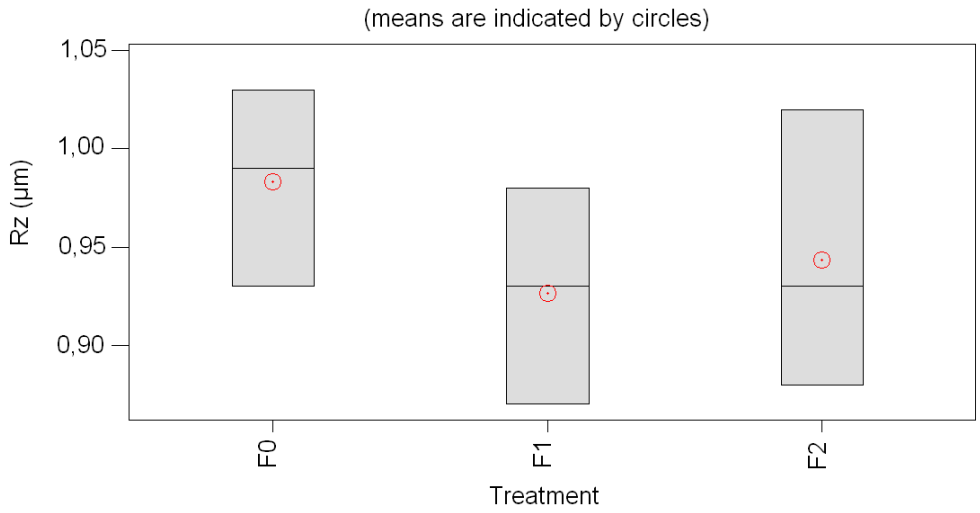

Figure 9-14: Box-plot for R_z by different treatments: F0 (unprepared), F1 and F2 are two different parameter combinations of BNAF

The results of the one-way ANOVA, considering a significance level of 5%, reveal that there is no significant difference among the means of the treatments. In addition, the Tukey′ test [112] for pairwise comparisons was applied to observe which treatments are different among if. The result of the test evidences that there is no significant difference between treatments F1 and F2, between F0 and F1, and between F0 and F2. Therefore,

there is no significant difference between the roughness obtained by the two preparation treatments and there is no significant difference between the roughness of the unprepared and prepared tools. In consequence, there is no significant change of roughness R_z of the tool face by applying BNAF for cutting edge preparation. The behavior previously described can be due to the relative position of the cutting edge and the filaments, considering additionally the wedge angle β. The angle between the filaments and the surfaces of the tool added to the high elasticity of the filaments could cause an effect of deburring in which the removal is focused more on the contour of the cutting edge than on the surfaces of the tool (flank and face).

9.7 Notchedness

To analyze the behavior of the notchedness for cutting edge preparation by BNAF, the parameters R_z and R_{pk} (see section 5.3.2) were observed as function of process time. In **Table 9-6**, the experimental conditions are presented. **Figure 9-15** shows the data of the measurements of R_z, R_{pk} and the ratio R_{pk}/R_z. As initial condition, cutting edges without preparation were considered.

Table 9-6: Conditions for analysis of notchedness by BNAF

Experimental conditions BNAF	
Macrogeometry of the cutting tool	β= 65°, α= 15°, γ=10°
Length of main cutting edge	AC = 0.8 mm
Cutting tool material	Uncoated cemented carbide ISO K20-K40
Abrasive of filaments	Diamond
Grit	Mesh grade 240
Depth	2 mm
Speed	20 m/s
Interval for changing rotation direction	9 s
Position of the edge	Symmetric

In **Figure 9-15**, a high decay of the roughness R_z in the first stage of the cutting edge preparation by BNAF can be observed. After a critical point of process time (approximately 18s), the decrease of roughness is not appreciable. A similar decay behavior can be observed for R_{pk}. Additionally, a tendency to decrease the ratio R_{pk}/R_z is observed. In consequence, a tendency in the decrease of picks related with the nominal roughness R_z is presented, as the process time increases.

Finally, as considered in chapter 6, the behavior of the notchedness as function of process time t_h for BNAF, for the data presented in **Figure 9-15**, can be expressed as:

$$R_z(t_h) = 1.44 + e^{-0.22\,(t_h+0.11)} \tag{9-2}$$

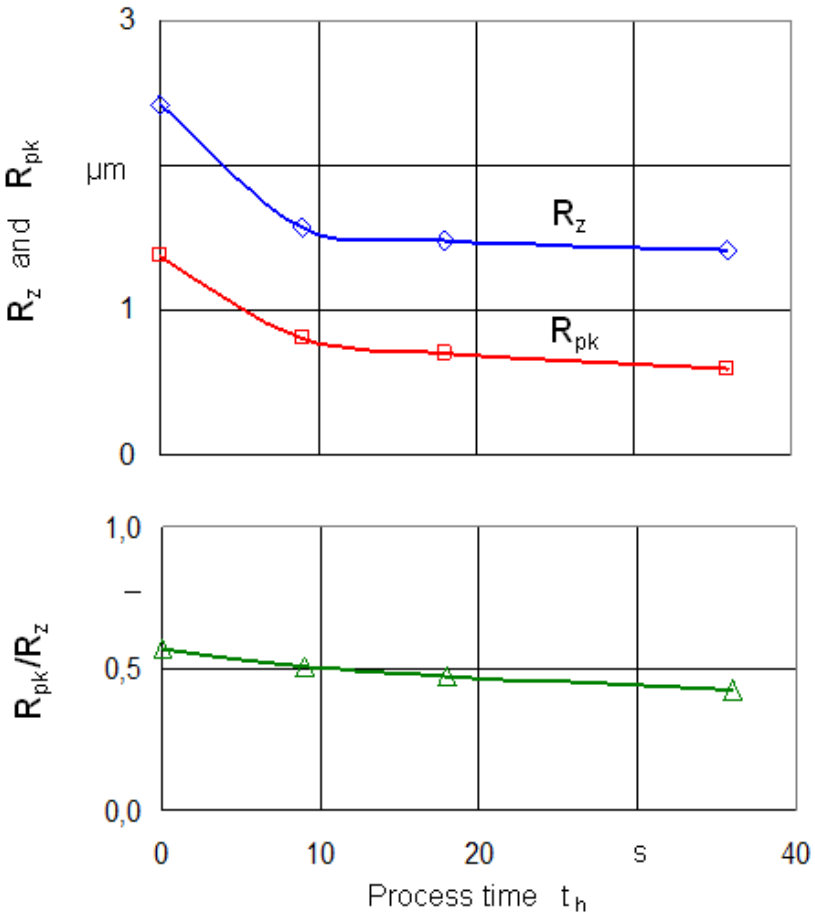

Figure 9-15: Analysis of notchedness for cutting edge preparation by BNAF

10 Evaluation of cutting edge preparation processes

The objective of the machining tests is to compare the behavior of prepared cutting tools in terms of cutting forces and tool wear (VB flank land), considering the preparation of the cutting edges by means of micro-abrasive jet machining (MAJM), brushing-polishing (BP) and brushing with nylon abrasive filaments (BNAF) with different cutting edge radii.

10.1 Materials and methods

In order to observe the forces and tool wear, orthogonal turning tests were carried out. For the machining tests, a precision cutting tool with macro- and meso-geometry as specified in **Figure 10-1** and **Figure 7-3** was used. As cutting tool material, inserts of uncoated cemented carbide ISO K20-K40 (see **Table 7-1**) was considered. As workpiece material, steel CK45 (1.1191) was selected. A cylinder (diameter 300 mm and length 600 mm) with four longitudinal grooves and a helical groove of 1 mm wide and 4 mm of pitch was used as workpiece.

The machining tests were carried out in a CNC-lathe type Voest-Alpine-Steinel® WCN 700S with control Siemens Sinumerik® 880T, with 60 KW power, rotational speed 10-3150 min^{-1} and feed speed 0-5000 mm/min. For measurement of cutting forces, a piezo-electric measurement platform Kistler® 9255B was used. **Figure 10-1** shows the reference force system for the measurement of the cutting forces and the precision cutting tool considered. The measurement of average wear flank land VB (**Figure 10-1**) was carried out by photographing the tool flank in an stereo-microscope Olympus® SHZ 10 and later the corresponding picture analysis with software Image-C®.

10.2 Cutting forces

For each considered cutting edge radii, r_n of 12, 18 and 26 μm, and for each cutting edge preparation process (MAJM, BP, and BNAF) three tools were tested. Additionally, as reference, unprepared tools with r_n= 7 μm were considered. The cutting forces were monitored with relationship to the cutting time up to 34 minutes. For the analysis, the average of the cutting forces was obtained considering the data of the three tools

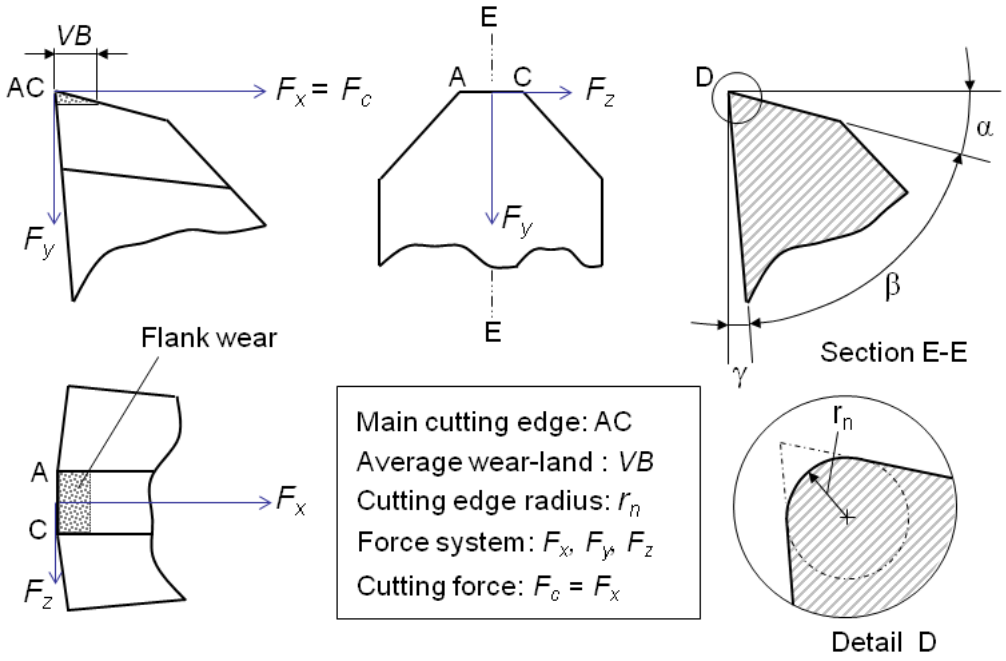

Figure 10-1: Force system considered and tool geometry: β= 65°, α= 15°, γ=10°, Length of main cutting edge AC = 0.8 mm, Cutting edge radii r_n= 7, 12, 18, and 26 μm

Table 10-1: Experimental conditions for machining tests

Experimental conditions	
Macrogeometry of the cutting tool	β= 65°, α= 15°, γ=10°
Length of main cutting edge	AC = 0.8 mm
Cutting edge radius	r_n= 7, 12, 18 and 26 μm
Cutting edge preparation process	Without, MAJM, BP, BNAF
Cutting tool material	Cemented carbide ISO K20-K40 (uncoated)
Workmaterial	CK45 (1.1191)
Cutting parameters	v_c= 105 m/min, a_p= 0.018 mm Cutting fluid: emulsion 10%

tested by each radius and preparation process. Parameters were selected to have different ratios r_n/h of cutting edge radius r_n and undeformed chip thickness h (r_n/h <1, =1, and >1). Selecting h=18 μm, the ratios r_n/h = 0.39, 0.67, 1.00, and 1.44, were considered, corresponding to r_n of 7, 12, 18 and 26 μm respectively. In all the considered cases, h is bigger to h_{min} required to material removal (h_{min}= 0.36 r_n according to [208], see **Figure 3-9** in section 3.4.1). h_{min}= 2.5, 4.4, 6.5 and 9.4 μm for r_n= 7, 12, 18 and 26 μm

respectively. **Table 10-2** synthesizes the geometric conditions considered for machining tests. The effective rake γ_e was determined according to equation 3.2. Additionally **Table 10-3** shows the conditions of the cutting edge preparation for the machining test.

Table 10-2: Geometric conditions for machining tests

r_n (μm)	r_n/h	γ_e	h_{min} (μm)
7	0.39	10°	2.5
12	0.67	10°	4.4
18	1.00	0°	6.5
26	1.44	-18°	9.4
Constants: h=18μm, γ= 10°			

Table 10-3: Mean cutting edge preparation conditions for machining tests

Process	Roughness (tool face)[1]	Nom. notchedness[2]		Microstructuring
	R_z (μm)	R_z (μm)	R_{pk} (μm)	(tool face)
Without	1.2	2.8	1.20	Anisotropic[3]
MAJM	0.8	1.1	0.45	Isotropic[4]
BP	0.5	1.0	0.38	Slightly anisotropic[5]
BNAF	1.1	1.4	0.56	Anisotropic[6]

[1] See Figure 7-4 for measurement parameters

[2] Measurement method presented in Figures 5-23 and 5-24

[3] See details in Figures 5-29, 5-37 and 5-38

[4] See details in Figures 5-30, 5-39 and 5-40

[5] See details in Figures 5-31, 5-41 and 5-42

[6] Similar to microstructuring without preparation (grinding)

In this section, the results of the tests for measuring cutting forces F_c and F_y as function of cutting time t_c are presented. **Figures 10-2**, **10-3** and **10-4** synthesizes the results for the forces F_c, F_y and the ratio F_y/F_c, for tools prepared by MAJM, BP and BNAF respectively. The forces obtained for prepared tools are compared in each case with the forces obtained for unprepared tools.

Next, certain trends that have been observed in the behavior of the forces F_c, F_x and the ratio F_y/F_c, for unprepared and prepared tools, are presented.

As can be seen from **Figures 10-2**, **10-3** and **10-4**, in general, in the first stage of machining the cutting force F_c is lower for the sharp edge (unprepared), but after a critical point the force begins to be lower for the edge with r_n=12μm, and later appears another critical point where the force for the edge with r_n=18μm begins to be lower than for the unprepared edge, finally appears a critical point where the force for the edge

with r_n=26μm is lower than for the unprepared edge. Considering the three preparation processes, these critical points appear between 7 and 16 minutes approximately from the beginning of the cutting process.

Likewise, from **Figures 10-2**, **10-3** and **10-4**, for the considered preparation processes, the force F_y is lower for the cutting edge without preparation than the forces for the rounded cutting edges in the first stage of the cutting process, before 7 to 9 minutes of cutting time approximately, after that a gradual increase of the force F_y begins for the unprepared cutting edge, until being able to overcome the values of the forces obtained for the three radii considered in the preparation. Before the first 7 to 9 minutes of cutting time, a marked influence of the plowing force is noticed due to the rounding of the cutting edge. The behavior of the cutting forces, considering the three radii (r_n= 12, 18 and 26μm) obtained by the considered preparation processes, shows as general tendency that the force F_y is higher as the radius is greater.

In **Figures 10-2**, **10-3** and **10-4** the behavior of the force ratio F_y/F_z is reported for MAJM, BP and BNAF respectively. In general, as cutting proceeds, wear increases causing an increase in the values of force ratio F_y/F_z. The increase of the force ratio F_y/F_z, depends on the severity of the conditions on the cutting edge. For the cutting edge without preparation, in the first stage of the cutting process (before 10 min of cutting time), the rate of increase of the force ratio F_y/F_z is higher compared with the prepared tools for the three preparation process. As can be observed from the behavior of F_y/F_z for the prepared edges, there is no severe changes in the rate of increase of the ratio F_y/F_z. On the contrary, for the unprepared tools, there is a higher rate of increase of the ratio F_y/F_z in the first stage of the cutting process (before 10 min), and later on a decrease in the rate of increase of the ratio F_y/F_z is observed.

The increases of the ratio F_y/F_z as cutting time increases, indicates that F_y is more sensitive to tool wear than F_c, as reported in [121] for tests to relate forces ratio with tool wear. In the case of the unprepared tool, the high increase of the ratio F_y/F_z in the first stage of the cutting process, can indicate an accelerate failure of the cutting edge that is presented by the unfavorable initials conditions of the contact between cutting edge and workpiece.

The differences between the observed forces for prepared tools with cutting edge radii r_n= 12, 18 and 26μm, are due principally to the plowing effect. The cutting forces increase as the cutting edge radius increases. This trend can be related with the data presented in **Table 10-2** observing the values of r_n/h and γ_e. Additionally, differences between the forces for the same radius but considering different preparation processes can be due to different conditions of the prepared cutting edge. Differences in roughness of the tool face, notchedness and microstructuring, as shown in **Table 10-3** change the contact and friction conditions and the general tribological behavior in the tool-workpiece and tool-chip interfaces. In general, for the same radius r_n the forces F_c and F_y as well as the ratio F_y/F_z are lower for the edges prepared by BP, and higher for the edges prepared by BNAF. The edges prepared by MAJM have a behavior near to those prepared by BP.

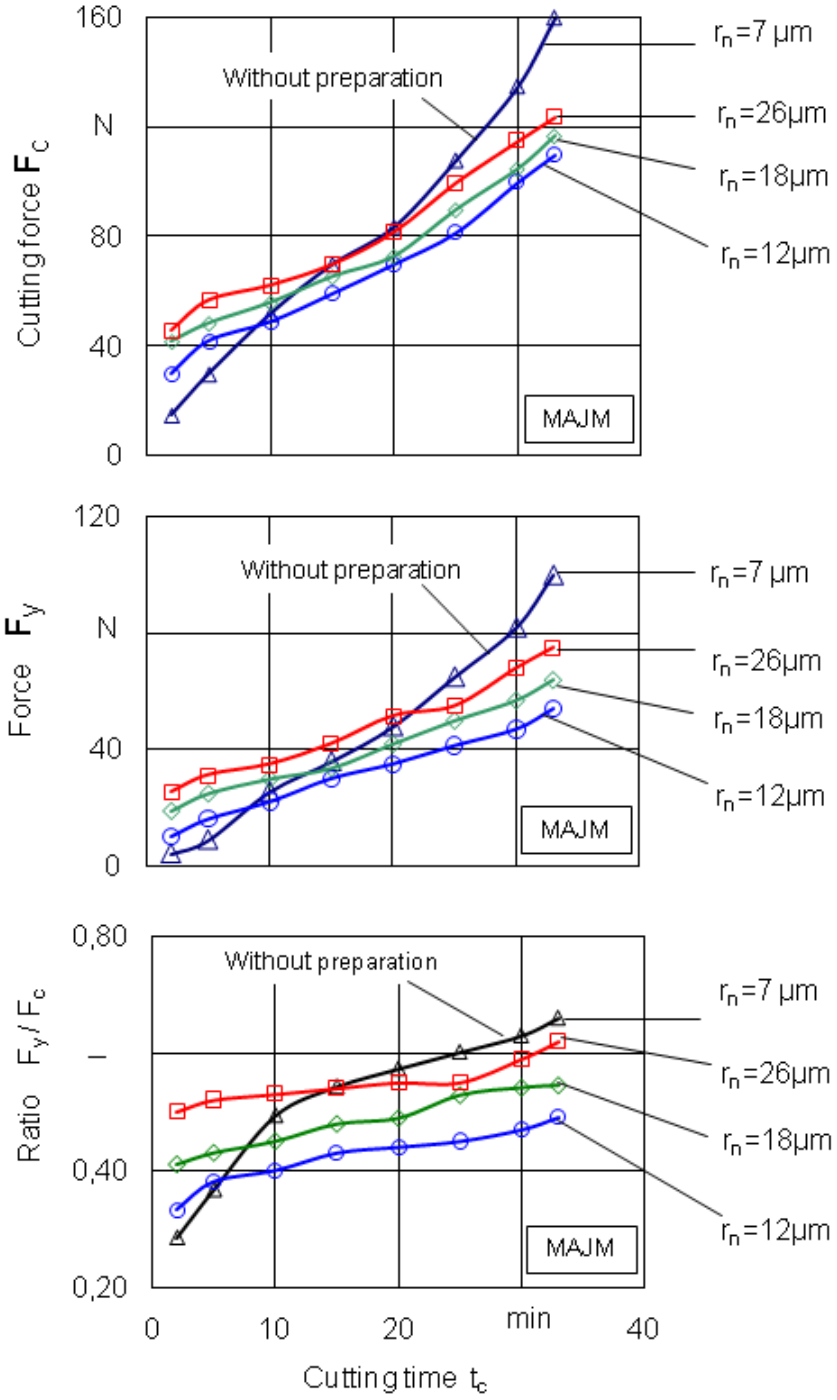

Cutting edge preparation process: MAJM: Micro-abrasive jet machining
Cutting tool material : ISO K20-K40 (uncoated) Workpiece material : CK45
Tool macrogeometry : α=15°, β=65°, γ=10°, Cutting edge radius : r_n= 7, 12,18, 26 µm
Cutting speed : v_c= 105 m/min Depth: a_p = 0.018 mm Cutting fluid: Emulsion 10%

Figure 10-2: Forces for cutting edges prepared by micro-abrasive jet machining

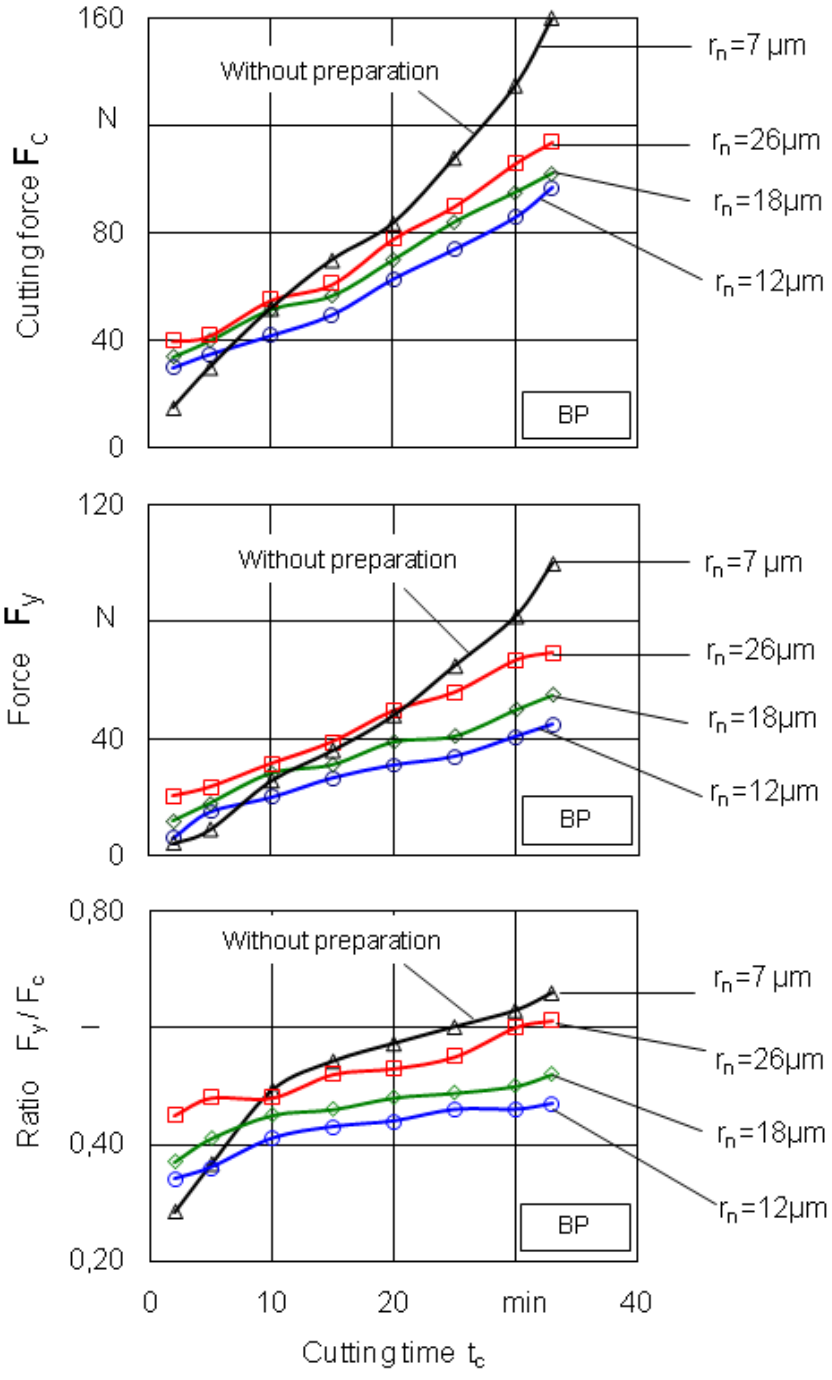

Cutting edge preparation process: BP: Brushing-polishing	
Cutting tool material : ISO K20-K40 (uncoated)	Workpiece material : CK45
Tool macrogeometry : α=15°, β=65°, γ=10°, Cutting edge radius : r_n= 7, 12,18, 26 µm	
Cutting speed : v_c= 105 m/min	Depth: a_p = 0.018 mm Cutting fluid: Emulsion 10%

Figure 10-3: Forces for cutting edges prepared by brushing-polishing

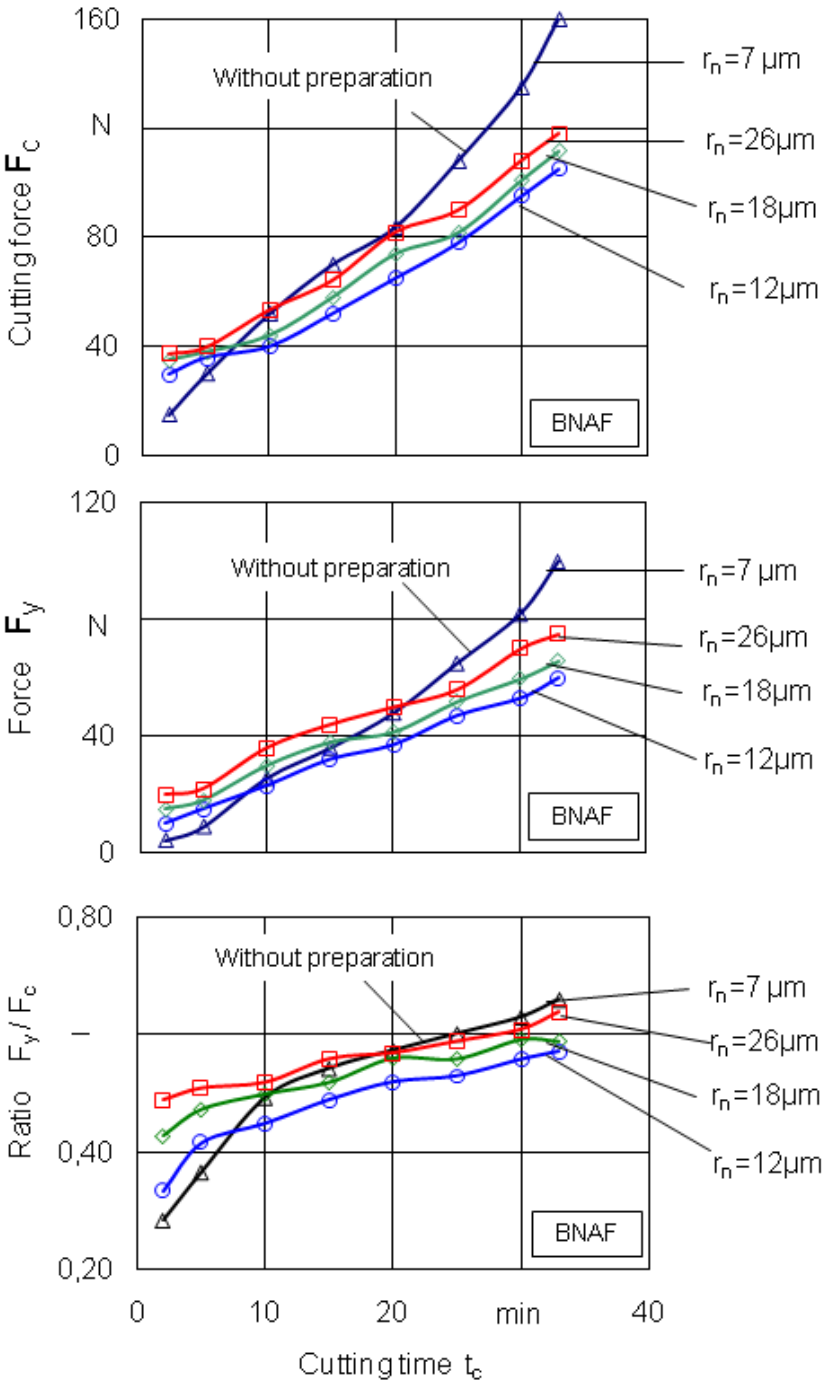

Cutting edge preparation process: BNAF: Brushing with nylon abrasive filaments
Cutting tool material : ISO K20-K40 (uncoated) , Workpiece material : CK45
Tool macrogeometry : α=15°, β=65°, γ =10°, Cutting edge radius : r_n= 7, 12,18, 26 m
Cutting speed : v_c= 105 m/min Depth : a_p = 0.018 mm Cutting fluid: Emulsion 10%

Figure 10-4: Forces for cutting edges prepared by brushing with nylon abrasive filaments

10.3 Tool wear

The same three tools tested to observe the cutting forces, for each radii r_n and each preparation process, were considered to observe the development of the average wear flank land VB. VB was monitored with relationship to the cutting time up to 34 minutes. For the analysis, the average of VB was obtained considering the data of the three tools tested by each case.

As example of a typical observation, **Figure 10-5** illustrates the behavior of the wear flank land VB considering a cutting edge with r_n= 12 μm and prepared by brushing-polishing. Likewise, **Figure 10-6** shows the pictures of the initial and final states of the cutting edge after 34 minutes of cutting time t_c for different cutting edge radii r_n.

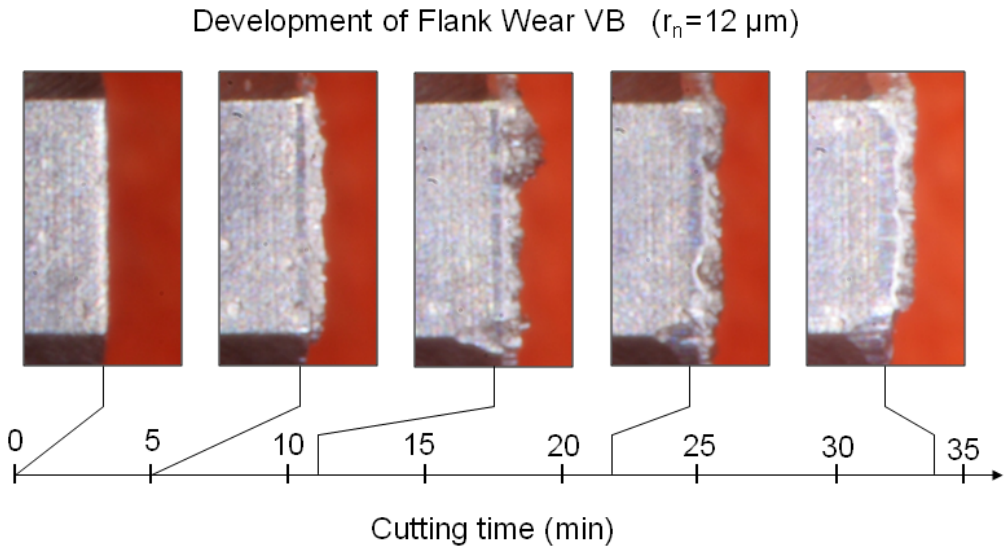

Figure 10-5: Development of the average width of wear flank land VB depending on cutting time

Figures 10-7, **10-8** and **10-9** show the behavior of the flank wear VB as function of cutting time for cutting edges prepared by MAJM, BP and BNAF respectively. To compare the behavior of VB for the three considered preparation processes, in **Figure 10-10** the wear VB for cutting edges with r_n= 12μm, prepared by MAJM, BP and BNAF are shown.

As can be seen from **Figures 10-7**, **10-8** and **10-9**, for the considered cutting time, the final value of the flank wear VB is lower for the tools with rounded cutting edges.

In **Figures 10-7**, **10-8** and **10-9** can be appreciated that in the first stage of the cutting process (before 7 min approximately) the wear VB is lower for the cutting in edge without preparation than for the prepared edges. Later on critical points appear where the wear for the cutting edge without preparation begins to be higher than the wear of the rounded edges. First appears the critical point where the wear for the cutting edge

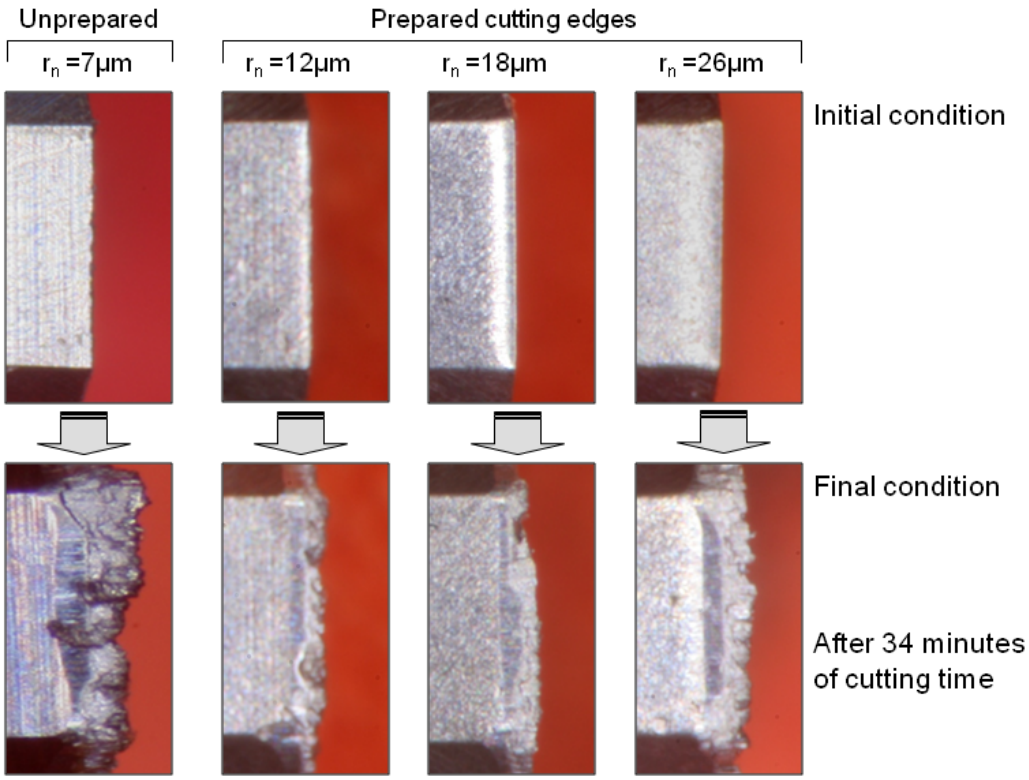

Figure 10-6: Development of average width of wear flank land VB depending on radii r_n

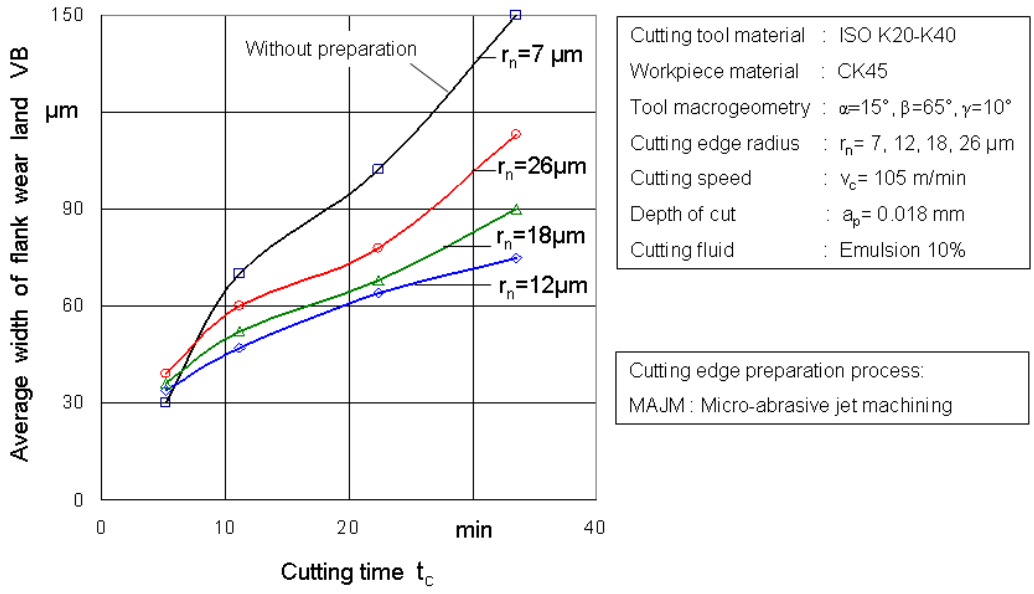

Figure 10-7: Wear for cutting edges prepared by micro-abrasive jet machining

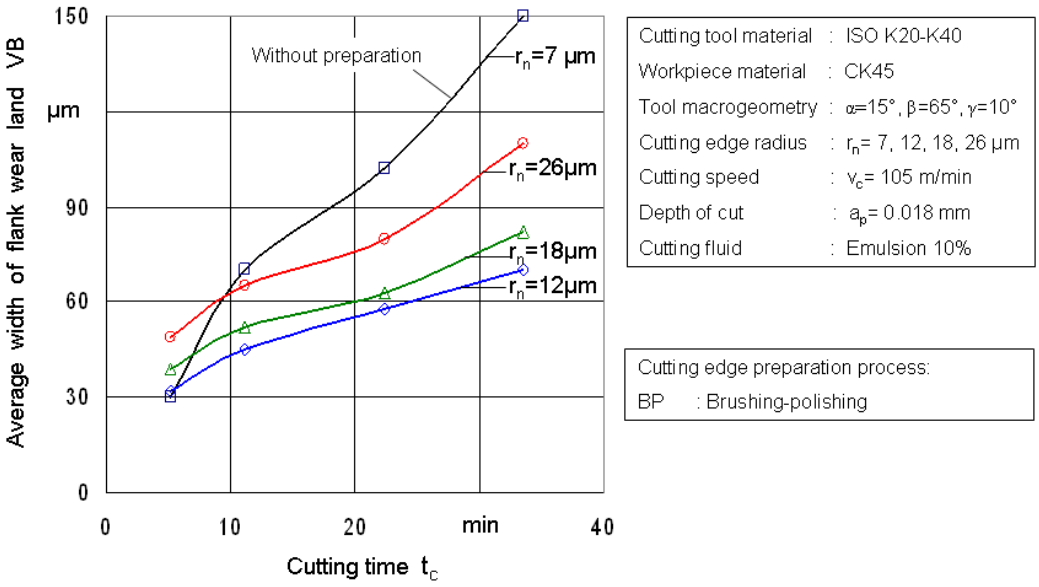

Figure 10-8: Wear for cutting edges prepared by brushing-polishing

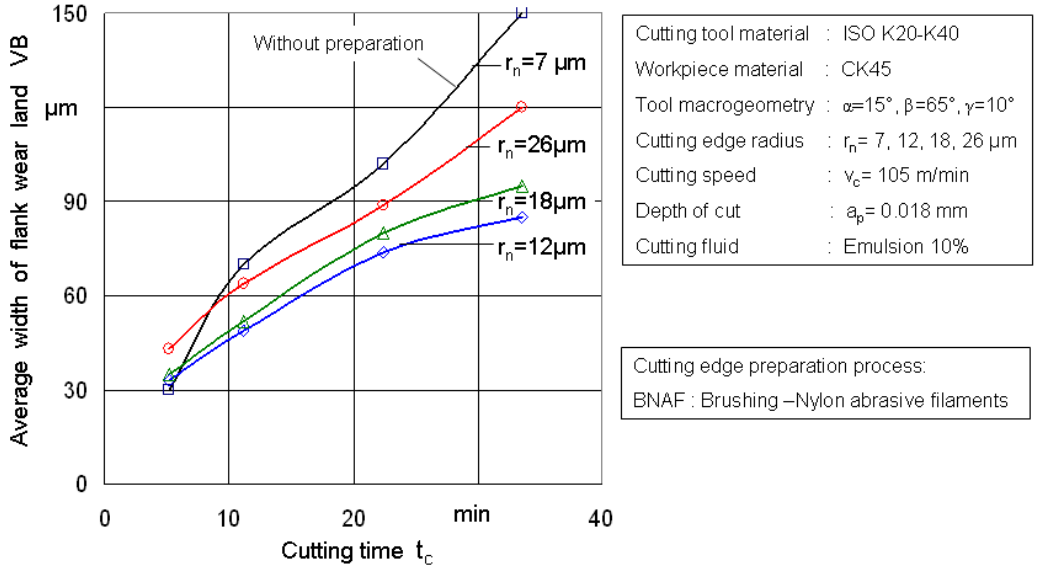

Figure 10-9: Wear for cutting edges prepared by brushing with nylon abrasive filaments

without preparation overcomes to the wear of the edge with radius r_n= 12μm, followed by an equivalent point for r_n= 18μm, and finally appears the corresponding critical point point for r_n= 26μm. After overcoming these critical points, for the maximum considered cutting time, the wear for the cutting edge without preparation is higher than the wear for the rounded edges. Additionally, after the critical points appear, the wear VB increases as the radii r_n of the prepared edges increase.

Considering the results of flank wear land VB for cutting tools prepared by the three considered preparation process (MAJM, BP, and BNAF) and taking as reference the obtained VB (150 μm as 100%) for the unprepared edge (r_n= 7μm) after 34 minutes of cutting time, the value of VB for the edges with r_n= 26μm, is between 73% and 80%. For the edges with r_n= 18μm, is between 53% and 60%, and for the edges with r_n= 12μm, is between 46% and 50%, of the reference value.

In general, comparing the three processes considered, the wear VB, after 34 minutes of cutting time, is lower for the cutting edges prepared by BP, followed by the the edges prepared by MAJM. The higher value of VB corresponds to the edges prepared by BNAF. As an example of these tendency, **Figure 10-10** shows the comparison of processes for r_n= 12 μm. The mentioned tendency can be related to the conditions of the cutting edges reported in **Table 10-3**. Differences in roughness of tool surfaces, notchedness of cutting edge and microstructuring of tool surfaces, affect the tribological conditions in the tool-workpiece and tool-chip interfaces.

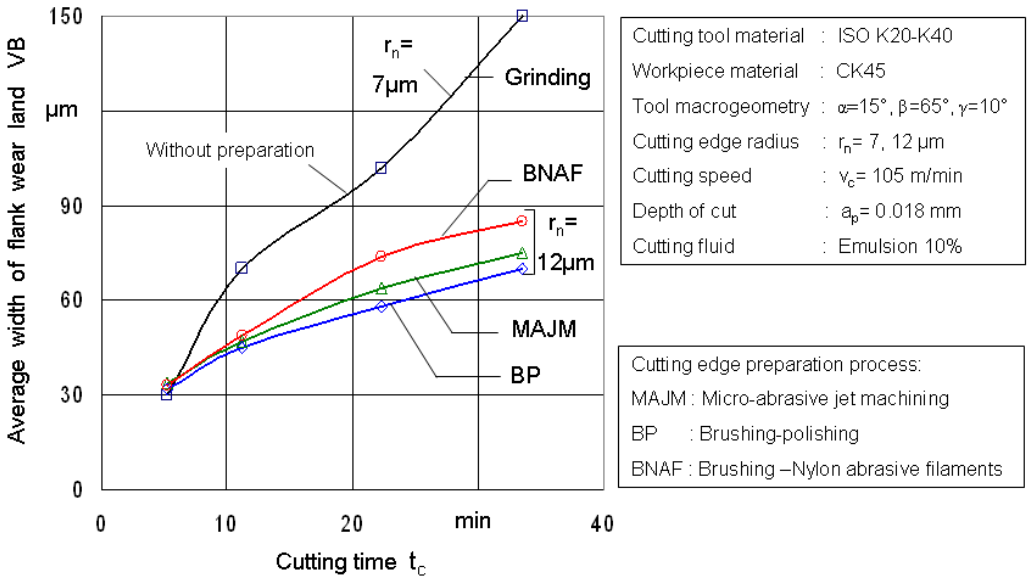

Figure 10-10: Comparison of wear for different cutting edge preparation processes

In **Figure 10-11**, the wear VB as function of the cutting edge radius r_n, for the three considered preparation processes is shown. The data of the point with r_n= 7 μm corresponds to the cutting edge without preparation. The shape of the curves allow to outline the existence of an optimum value of the radius that has been revealed experimentally as reported in [136] and [135].

As general observation, a radius in the cutting edge prevents fast and unpredictable wear, as mentioned in [136]. Likewise the modifications of the edge radius r_n and the modifications of notchedness of the cutting edge and the surface microstructuring are important criteria influencing the wear resistance of the cutting edge.

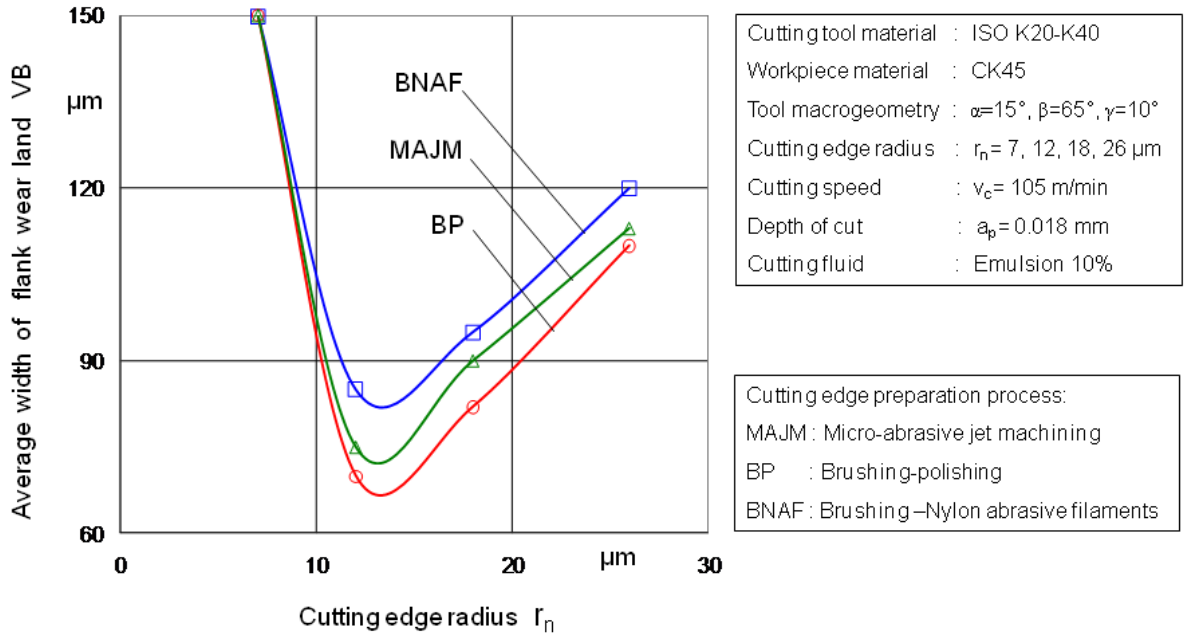

Figure 10-11: Average width of wear flank land VB depending on radii r_n for different preparation processes

11 Conclusions

The results of the research showed the positive effect of the cutting edge preparation on the performance of the precision cutting tool. The geometry of the cutting edge, in terms of nominal radius, as well as the notchedness and the microstructuring of the tool face and tool flank has relevant influence on the performance of the precision cutting tool. This aspect can be used to improve ostensibly the quality of the precision cutting tool. Thus, a relative low investment in the preparation process, compared with other processes in the production chain of of precision cutting tools, can result in a high increase in reliability and tool life.

In this work, diverse strategies that allow the appropriate characterization of the cutting edge preparation and planning of the cutting edge preparation processes, were proposed. Moreover, an analysis oriented to observe the influence of the parameters of the considered preparation processes on the variability of the generated cutting edge radius, the removed material, roughness and notchedness, was carried out. In addition, machining tests to observe the behavior of prepared edges, in terms of cutting forces and tool wear, allowed to evidence the advantages of the cutting edge preparation.

Although, the analysis was centered in three preparation processes (micro-abrasive jet machining, brushing-polishing and brushing with nylon abrasive filaments) and uncoated cemented carbide as tool material, the methodology and strategies of analysis can be extended to other processes or tool materials, for later research on process characterization, planing, modeling and analysis.

An important aspect of the work is the definition of the measurement methodology, based principally on optic technology by using a chromatic sensor. With this method, it is possible to have a 3D representation of the surface of the cutting edge and the tool face and tool flank surfaces in the proximity of the edge. From this information, a detailed description of the geometry of the cutting edge is proposed, in terms of mesogeometry and microgeometry. The mesogeometry is represented by convex contours obtained from the 3D representation of the surface. A complete description of the contours is proposed by means of differential geometry. The curvature function, the radius function, turning angle, effective contour, effective rake, nose radius, position of the nose tip, asymmetry and nominal radius are new concepts proposed for a complete description of the convex contour that represents the rounding of the cutting edge. This mathematical description is useful for modeling, characterization and quality control of the cutting edge preparation.

Likewise, for the description of the microgeometry, the definition of notchedness is proposed in terms of nominal notchedness and notchedness of the effective contour by

using amplitude roughness parameters principally R_z and material ratio with the parameter R_{pk} and the ratio R_{pk}/R_z that represents the proportion of picks of the profile related with the nominal roughness R_z, and indicates the susceptibility to initial failure and chipping because of its capacity to support loads in the first contact at the beginning of the cutting process. In addition, the description of the microstructuring of the tool flank and the tool face, principally to determine the texture and anisotropy is carried out by using the 3D roughness parameters and the autocorrelation function. To quantify the anisotropy of the surfaces, fractal geometry is used to characterize the roughness and texture defining the fractal dimension in different directions by using the Fourier power spectrum of the profiles obtained from the 3D representation of the surfaces. This information is useful for the characterization of the tribological aspects of the interaction between the tool flank and workpiece and chip and tool face. Moreover, the characterization of the microstructuring allows to describe the state of the surfaces before the coating process and study the influence of the surface topography and coating quality.

Planning the cutting edge preparation process is an strategic aspect to obtain the required characteristics of the meso and microgeometry of the cutting tools. The concept of nominal removed area A_r is proposed to establish a relationship among the process parameters, initial radius, wedge angle β and required final radius. Likewise, a description of the removed area as function of process time is proposed to be used for planning and controlling the preparation process. Additionally, an analysis of the process variability is considered to determine the origin of the variability in the required final radius. All of these aspects are useful for productivity and quality considerations.

Analysis of the considered preparation processes (micro abrasive jet machining MAJM, brushing-polishing BP and brushing with nylon abrasive filaments BNAF) was carried out by applying design of experiments (DoE). The effects of the the process parameters on the removed area, surface roughness of the tool surfaces and notchedness were studied. Likewise, the variability of the generated radius, expressed by six-sigma, was studied for the combinations of parameters defined by factorial experiments. Regression models of the removed area, considering the significant parameters that affects the response of the process were proposed. The regression models are useful to plan the preparation processes and to compare the processes in terms of productivity.

The cutting edge preparation plays an important role, specially in the first stage of machining, at the beginning of the tool-life. The characteristics of the first contact between cutting edge and workpiece defines the later performance of the cutting tool. In general, it was observed that the cutting edge without preparation fails in the first stage of the machining, generating an accelerated wear of the tool flank. The tests showed that in general, the cutting forces and the force ratio are lower for the unprepared sharp cutting edges (with small radius) in the first stage of the machining, later appear critical points where the forces and force ratio for the prepared edges begin to be lower than for the unprepared edge. These points appears later on, as the radius is greater.

The machining tests show that the cutting edge preparation has a positive effect

on flank wear development and tool-life. Considering the results of flank wear land VB, after 34 minutes of cutting time, for cutting tools prepared by the three considered process (MAJM, BP, and BNAF) and taking as reference the obtained VB (150μm as 100%) for the unprepared edge (r_n= 7μm), the value of VB for the edges with r_n= 26μm, is between 73% and 80% of the reference. For the edges with r_n= 18μm, is between 53% and 60%, and for the edges with r_n= 12μm, is between 46% and 50%, of the reference value. Although in the first stage of the cutting process, VB is lower for the unprepared edge, later appear critical points where VB for the prepared edges begin to be lower than for the unprepared edge. These points appear later on, as the radius is greater.

The aspects related with the problem definition concerning with characterization of cutting edge preparation, analysis of the preparation processes and evaluation of prepared cutting tools were considered by means of the strategies presented previously.

Finally, the meaning of cutting edge preparation can be outlined. Cutting edge preparation adds value and quality to precision cutting tools by means of modifications to the meso and microgeometry of the edge, with relative low investment compared with other processes of the production chain.

From the observations and proposed strategies, future works can be developed in different aspects of cutting edge preparation. Regarding the measurement and characterization of the cutting edge preparation, a description of the notchedness based on 3D data from optic sensors, for example by means of fractal geometry, principally to characterize the complexity of the topography of the surface on the cutting edge. The results are important to study the tribological aspects of the cutting process fair on the cutting edge and to observe the relationship between notchedness and the quality of the tool coating.

Likewise, the methodology of analysis applied for the considered preparation process can be applied, among others, to magnetic-finish, drag-finishing, abrasive flow machining and ultra-short pulse laser.

The observation of the influence of the generated notchedness and microstructuring on the quality of the tool coating is another important aspect to study considering different preparation processes and types of coatings for different tool materials. In addition, another research topic to consider is the study by means of modeling and experimentation, of the optimal cutting edge radius for different machining processes, cutting tools and combination of workpiece-tool materials. These study can be carried out by using design of experiments and surface response methodology.

Additionally, an study of the influence of cutting edge radius, notchedness and microstructuring on tool life and quality of the uncoated and coated tools can give criteria to define design strategies for optimization of the performance of precision cutting tools. Equally, the analysis of new geometries of the edge contour is another aspect to consider, taking account that the proposed measurement technology allows to quantify the characteristics of the edge to be used in experimentation and simulation.

Bibliography

[1] Achtsnick, M. ; Hoogstrate, A.M. ; Karpuschewski, B.: Advances in high performance micro abrasive blasting. In: *CIRP Annals* 54 issue 1 (2005), S. 281–284

[2] Achtsnick, M. ; Hoogstrate, M ; Karpuschewski.B.: Einfluss der Düsengeometrie auf das Arbeitsergebnis beim Mikro-Abrasiven-Druckluftstrahlen. In: *Jahrbuch Schleifen,Honen,Läppen und Polieren: 62 Ausgabe*, Vulkan-Verlag, 2005, S. 466–483

[3] Andersson, C.: Bandsawing. Part III: stress analysis of saw tooth microgeometry. In: *International Journal of Machine Tools and Manufacture* 41 (2001), S. 255–263

[4] Astakhov, V.: *Metal cutting mechanics*. 1st ed. Boca Raton, London : CRC Press, 1999

[5] Balasubramanian, R. ; Krishnan, J. ; Ramakrishnan, N.: Investigation of AJM for deburring. In: *Journal of materials processing technology* 79 (1998), S. 52–58

[6] Balasubramanian, R. ; Krishnan, J. ; Ramakrishnan, N.: An empirical study on the generation of an edge radius in abrasive jet external deburring. In: *Journal of materials processing technology* 99 (2000), S. 49–53

[7] Balasubramanian, R. ; Krishnan, J. ; Ramakrishnan, N.: A study on the shape of the surface generated by abrasive jet machining. In: *Journal of materials processing technology* 121 (2002), S. 102–106

[8] Benedict, G.: Nontraditional machining processes. In: *ASM Handbook Vol 16: machining*, ASM International, 1989, S. 509–510

[9] Berens, A. ; Westhoff, B.: Fundamental aspects of investigation the HSC-chip formation process by FEM. In: *Scientific fundamentals of HSC*, Carl Hanser Verlag, 2001, S. 53–65

[10] Beste, U. ; Hammerström, L. ; Engqvist, H. ; S., Rimlinger ; Jacobson, S.: Particle erosion of cemented carbides with low Co content. In: *Wear* 250 (2001), S. 809–817

[11] Bhattacharyya, B. ; Munda, J. ; Malapati, M.: Advancement in electrochemical micro-machining. In: *International journal of machine tools and manufacture* 44 (2004), S. 1577–1589

[12] Biermman, D. ; Weinert, K. ; Felderhoff, F. ; Mohn, T. ; Terwey, I.: Die Werzeugherstellung als Schlüssel zu optimalen Zerspanprozessen. In: *VDI-Z Integrierte Produktion* August (2008), S. 20–22

[13] Bodschwinna, H. ; Hillmann, W.: *DIN Beuth-Kommentare: Oberflächenmesstechnik mit Tastschnittgeräten in der industriellen Praxis.* 1. Auflage. Berlin : Beuth Verlag, 1992

[14] Boothroyd, G. ; Knight, W.: *Fundamentals of machining and machine tools.* 3rd ed. Boca Raton : Taylor and Francis Group, 2006

[15] Bouzakis, K.-D. ; Michailidis, N. ; Skordaris, G. ; Efstathiou, K. ; Erkens, G.: Optimization of the cutting edge roundness and its manufacturing procedures of cemented carbide inserts, to improve their milling performance after a PVD coating deposition. In: *Surface and coatings technology* 163-164 (2003), S. 625–630

[16] Bouzakis, K.-D. ; Michailidis, N. ; Vidakis, N. ; Efstathiou, K. ; Skordaris, G. ; Leyendecker, T. ; Erkens, G. ; Wenke, R ; Fuss, H.-G.: Optimization of the cutting edge radius of PVD coated inserts in milling considering film fatigue failure mechanisms. In: *Surface and coatings technology* 133-134 (2000), S. 501–507

[17] Bouzakis, K.-D. ; Skordakis, G. ; Mirisidis, I. ; Mesomeris, G. ; Pavlidou, E. ; Erkens, G.: Micro-blasting of PVD Films, an Effective Way to Increase the Cutting Performance of Coated Cemented Carbide Tools. In: *CIRP Annals* 54 issue 1 (2005), S. 95–98

[18] Bouzakis, K.-D. ; Skordaris, G. ; Michailidis, N.: Effect on PVD coated cemented carbide inserts cutting performance of micro-blasting and lapping of their substrates. In: *Surface and coatings technology* 200 (2005), S. 128–132

[19] Bouzakis, K.-D. ; Skordaris, G. ; Mirisidis, I. ; Michailidis, N. ; Mesomeris, G. ; Pavlidou ; Erkens, G.: Cutting performance improvement through micro-blasting on well-adherent PVD films on cemented carbide inserts. In: *Surface and coatings technology* 200 (2005), S. 1879–1884

[20] Byrne, G. ; Dornfeld, D. ; Denkena, B.: Advanced cutting technology. In: *CIRP Annals* 52 issue 2 (2003), S. 483–507

[21] Cai, M. ; Li, X. ; M., Rahman ; Tay, A.: Crack initiation in relation to the tool edge radius and cutting conditions in nanoscale cutting of silicon. In: *International Journal of Machine Tools and Manufacture* 47 (2007), S. 562–569

[22] Cheung, F.Y. ; Zhou, Z.F. ; Geddam, A. ; Li, K.Y.: Cutting edge preparation using magnetic polishing and its influence on the performance of high-speed steel drills. In: *Journal of material processing technology* 208 (2008), S. 196–204

[23] Choudhury, I.A. ; See, N.L. ; Zukhairi, M.: Machining with chamfered tools. In: *Journal of materials processing technology* 170 (2005), S. 115–120

[24] Chung, Y.: Characterization of topography of engineering surfaces. In: *Surfaces diagnosis in tribology*, World Publishing, 1993, S. 33–46

[25] Clausen, M. ; Tracht, K. ; Jivishov, V.: Cutting force modelling and simulation. In: *Proceedings of the 36th CIRP International Seminar on Manufacturing Systems*, Universität des Saarlandes, 2003, S. 425–432

[26] Coehlo, R.T. ; Silva, L.R ; Braghini, A. ; Bezerra, A.A.: Some effects of cutting edge preparation and geometric modifications when turning INCONEL 718 at high cutting speeds. In: *Journal of materials processing technology* 148 (2004), S. 147–153

[27] Czichos, H. ; Habig, K.-H.: *Tribologie-Handbuch.* Wiesbaden : Vieweg, 2003

[28] Degner, H.-C.: *Handbuch Feinbearbeitung.* 1. Auflage. Berlin : VEB Verlag Technik, 1979

[29] Degner, W. ; Lutze, H. ; Smejkal, E.: *Spanende Formung.* München,Wien : Hanser, 2002

[30] Denkena, B. *Lasertechnologie für die Generierung und Messung der Mikrogeometrie an Zerspanwerkzeugen: Ergebnisbericht des BMBF Verbundprojektes GEOSPAN.* 2005

[31] Denkena, B. ; Boehke, D. ; Köhler, J.: Leistungsoptimierung an der Schneidkante: Teil 2. In: *VDI-Z Special Werkzeuge-/Formenbau* November (2007), S. 39–42

[32] Denkena, B. ; Friemuth, T. ; Fedorenko, S. ; Groppe, M.: An der Schneide wird das Geld verdient. In: *Werkzeuge* Dezember (2002), S. 24–26

[33] Denkena, B. ; Friemuth, T. ; Spengler, C. ; Weinert, K. ; Schulte, M. ; Kötter, D.: Kantenpräparation an Hartmetall-Werkzeugen. In: *VDI-Z Special Werkzeuge* März (2003), S. 51–54

[34] Denkena, B. ; Kramer, N. ; Siegel, F. ; Kästner, J.: Leistungsoptimierung an der Schneidkante. In: *VDI-Z Special Werkzeuge* August (2007), S. 24–26

[35] Derrico, G.E. ; Bugliosi, S. ; Cuppini, D.: Erosion of ceramics and cermets. In: *International materials processing technology* 118 (2001), S. 448–453

[36] DIN. *DIN 6582: ergänzende Begriffe am Werkzeug, am Schneidkeil und an der Schneide.* 1988

[37] DIN. *DIN EN ISO 13565-2: Oberflächenbeschaffenheit: Tastschnittverfahren.* 1998

[38] DIN. *DIN EN ISO 4287: Oberflächenbeschaffenheit: Tastschnittverfahren.* 1998

[39] DIN. *DIN EN ISO 4288: Oberflächenbeschaffenheit: Tastschnittverfahren ; Regeln und Verfahren für die Beurteilung der Oberflächenbeschaffenheit.* 1998

[40] Dornfeld, D. ; Min, S. ; Takeuchi, Y.: Recent advances in mechanical micromachining. In: *CIRP Annals* 55 (2006), S. 745–768

[41] Dutschke, W. ; C., Keferstein: *Fertigungsmesstechnik.* 6. Auflage. Wiesbaden : Teubner Verlag, 2007

[42] Elsharkawy, M.: Einfluss des Ecken- und Schneidkantenradius auf die Oberflächengute beim Feindrehen. In: *Fertigungstechnik und Betrieb* 25 (1975), S. 230–233

[43] Engqvist, H. ; Axen, N.: Abrasion of cemented carbides by small grits. In: *Tribology international* 32 (1999), S. 527–534

[44] Engqvist, H. ; Jacobson, S. ; Axen, N.: A model for the hardness of cemented carbides. In: *Wear* 252 (2002), S. 384–393

[45] Evans, C.J. ; Paul, E. ; Dornfeld, D. ; Lucca, D.A. ; Byrne, G. ; Tricard, M. ; Klocke, F. ; Dambon, O. ; Mullany, B.A.: Material removal mechanisms in lapping and polishing. In: *CIRP Annals* 52 issue 2 (2003), S. 611–633

[46] Fahrmeir, L. ; Kneib, T. ; Lang, S.: *Regression, Modelle, Methoden und Anwendungen.* 1. Auflage. Berlin, Heidelberg : Springer-Verlag, 2007

[47] Fang, F. Z. ; Wu, H. ; Liu, X. D. ; Liu, Y. C.: Tool geometry study in micromachining. In: *Journal of Micromechanics and Microengineering* 13 (2003), S. 726–731

[48] Fang, F.Z. ; Wu, H. ; Liu, Y.C.: Modelling and experimental investigation on nanometric cutting of monocrystalline silicon. In: *International Journal of Machine Tools and Manufacture* 45 (2005), S. 1681–1686

[49] Fang, N.: Slip-line modeling of machining with a rounded edge tool-Part 1: new model and theory. In: *Journal of the mechanics and physics of solids* 51 (2003), S. 715–742

[50] Fang, N.: Slip-line modeling of machining with a rounded edge tool-Part 2: analysis of the size effect and the shear strain rate. In: *Journal of the mechanics and physics of solids* 51 (2003), S. 743–762

[51] Fang, N. ; Fang, G.: Theorical and experimental investigations of finish machining with a rounded edge tool. In: *Journal of materials processing technology* 191 (2007), S. 331–334

[52] Fang, N. ; Wu, Q.: The effects of chamfered and honed tool edge geometry in machining of three aluminium alloys. In: *International Journal of Machine Tools and Manufacture* 45 (2005), S. 1178–1187

[53] Finnie, I.: Some reflexions on the past and future of erosion. In: *Wear* 186-187 (1995), S. 1–10

[54] Flöter, A.: Sharf, spiegelglatt und extrem verschleissfest. In: *Konstruktion* 11-12 (2004), S. 3–4

[55] Friemuth, T.: *Herstellung spanender Werkzeuge*. 1. Auflage. Düsseldorf : VDI Verlag, 2002

[56] Fries, T.: Oberflächenmesstechnik: Brückenschlag vom Nanometer zun Meter. In: *VDI-Berichte 1669: Metrologie in der Mikro- und Nanotechnik*, VDI Verlag, 2003, S. 73–81

[57] Fries, T.: Oberflächenmesstechnik für Labor und Produktion. In: *VDI-Berichte 1806*, VDI Verlag, 2003, S. 217–225

[58] Fries, T.: Multi Sensor Oberflächenmesstechnik für die Nano und Mikrotechnik. In: *VDI-Berichte 1950: Messtechnik für Mikro- and Nano-Engineering*, VDI Verlag, 2006, S. 163–172

[59] Gao, W. ; Motoki, T. ; Kiyono, S.: Nanometer edge profile mesurement of diamond cutting tools by atomic force microscope with optical alignment sensor. In: *Precision engineering* 30 (2006), S. 396–405

[60] Gatzen, H.H. ; Maetzig, C.: Nanogrinding. In: *Precision engineering* 21 (1997), S. 134–139

[61] GFM, GmbH: Schneidkantenmessung: Bestimmung von K-Faktor, Delta r und Kantenradius. In: *MAV* März (2006)

[62] GFM, GmbH: Schnelle 3D-Schneidkanten-Messung. In: *Quality Engineering* 4 (2006)

[63] Gies, C.: *Evaluation der Prozesseinflussgröss en beim Fliesslochformen mittels DoE.* Kassel, Universität Kassel, Dissertation, 2006

[64] Gray, A.: *Modern differential geometry of curves and surfaces with Mathematica.* 2nd ed. Boca Raton, Boston : CRC Press, 1998

[65] Guo, Y.B. ; Chou, Y.K.: The determination of ploughing force and its influence on material properties in metal cutting. In: *Journal of materials processing technology* 148 (2004), S. 368–375

[66] Gustavsson, M.: Fluid dynamic mechanisms of particle flow causing ductile and brittle erosion. In: *Wear* 252 (2002), S. 845–858

[67] H.-M., Beier: *Handbuch Entgrattechnik.* München, Wien : Carl Hanser Verlag, 1999

[68] Han, J.H. ; Ping, S. ; Shengsun, H.: Fractal characterization and simulation of surface profiles of copper electrodes and aluminium sheets. In: *Materials science and engineering* 403 (2005), S. 174–181

[69] Hasegawa, M. ; Liu, J. ; Okuda, K. ; Nunobiki, M.: Calculation of the fractal dimensions of machined surface profiles. In: *Wear* 192 (1996), S. 40–45

[70] Holsten, S.: *FEM unterstützte Parameterstudie des Innengewinde Fertigungsverfahrens Gewindefurchen.* Kassel, Universität Kassel, Dissertation, 2005

[71] Horowitz, I.: *Oberflächenbehandlung mittels Strahlmitteln.* Essen : Vulkan-Verlag, 1982

[72] Horsch, C. ; Schulze, V. ; Löhe, D.: Konfokale Schneidkantenvermessung. In: *Werkstattstechnik Online* 11-12 (2002)

[73] Horst, C. ; Habig, K-H.: *Tribologie Handbuch.* Wiesbaden : Vieweg, 2003

[74] Hua, J. ; Shivpuri, R. ; Chen, X. ; Bedekar, V. ; Matsumoto, Y.: Effect of feed rate, workpiece hardness and cutting edge on subsurface residual stresses in the hard turning of bearing steel using chamfer+hone cutting edge geometry. In: *Materials science and engineering* 394 (2005), S. 238–248

[75] ISO. *Draft international standard ISO/DIS 25178-2: Geometrical product specifications (GPS)-surface texture: Areal- Part 2: terms, definitions and surface texture parameters.* 2007

[76] ISO. *Draft international standard ISO/DIS 25178-6: Geometrical product specifications (GPS)-surface texture: Areal- Part 6: classification of methods for measuring surface texture.* 2007

[77] ISO. *Draft international standard ISO/DIS 25178-602: Geometrical product specifications (GPS)-surface texture: Areal- Part 602: Nominal characteristics of non-contact (confocal chromatic probe) instruments.* 2007

[78] Jain, N.K. ; Jain, V.K.: Modeling of material removal in mechanical type advanced machining processes: a state of the art review. In: *International journal of machine tools and manufacture* 41 (2001), S. 1573–1635

[79] Jandeleit, J. ; Horn, A. ; Weichenhain, R. ; Kreutz, E.W. ; Propawe, R.: Fundamental investigations of micromachining by nano- and picosecond laser radiation. In: *Applied surface science* 127-129 (1998), S. 885–891

[80] Jiang, Z. ; Wang, H. ; Fei, B.: Research into the application of fractal geometry in characterising machined surfaces. In: *International journal of machine tools and manufacture* 41 (2001), S. 2179–2185

[81] Kahnis, P.: Potenziale der Fräsbearbeitung zur Herstellung von Mikrostrukturen aus Stahl. In: *Spanende Fertigung*, Vulkan Verlag, 2005, S. 148–155

[82] Kendall, L.A.: Tool wear and tool life. In: *Metals Handbook Vol 16: machining*, ASM International, 1989, S. 37–48

[83] Khairy, A.: Aspects of surface and edge finishing by magnetoabrasive particles. In: *International materials processing technology* 116 (2001), S. 77–83

[84] Kim, J. ; Kim, D.: Theorical analysis of micro-cutting characteristics in ultra-precision machining. In: *Journal of materials processing technology* 49 (1995), S. 387–398

[85] Kim, J.-H.: The influence of cutting edge radius on the machined surface of brittle materials in simulated orthogonal machining. In: *International Journal of Machine Tools and Manufacture* 36 (1996), S. 971–983

[86] Kim, K. ; Lee, W. ; Sin, H.: A finite-element analysis of machining with the tool edge considered. In: *Journal of materials processing technology* 86 (1999), S. 45–55

[87] Klamecki, B.: Comparison of material removal rate models and experimental results for the double-sided polishing process. In: *International materials processing technology* 109 (2001), S. 248–253

[88] Klein, B.: *Versuchsplanung DoE.* 2. Auflage. München, Wien : Oldenbourg Verlag, 2007

[89] Kleppmann, W.: *Taschenbuch Versuchsplanung.* 3. Auflage. München : Hanser, 2006

[90] Klocke, F. ; Fritsch, R. ; Grams, J.: CVD-Diamant auf Hartmetall-Eingenschaften und Einsatzverhalten beim Schaftfräsen. In: *Spanende Fertigung*, Vulkan Verlag, 2005, S. 114–122

[91] Klocke, F. ; König, W.: *Fertigungsverfahren 2: Schleifen, Honen, Lappen.* 4. Auflage. Berlin, Heidelberg : Springer-Verlag, 2005

[92] Klocke, F. ; König, W.: *Fertigungsverfahren 3: Abtragen, Generieren und Lasermaterialbearbeitung.* 4. Auflage. Berlin, Heidelberg : Springer-Verlag, 2007

[93] Koehler, W.: Einfluss der Schneidenform auf die Belastungen des Hochleistungsbohrprozesses. In: *Spanende Fertigung*, Vulkan Verlag, 2005, S. 254–262

[94] Komanduri, R. ; Chandrasekaran, N. ; Raff, L.M.: Effect of tool geometry in nanometric cutting: a molecular dynamics simulation approach. In: *Wear* 219 (1998), S. 84–97

[95] König, W. ; Klocke, F.: *Fertigungsverfahren 1: Drehen, Fräsen, Bohren.* 8. Auflage. Berlin, Heidelberg : Springer-Verlag, 2008

[96] Kosel, T.: Solid particle erosion. In: *ASM Handbook Vol 5: surface engineering*, ASM International, 1994, S. 199–213

[97] Kötter, D.: *Herstellung von Schneidkantenverrundungen und deren Einfluss auf das Einsatzverhalten von Zerspanwerzeugen.* Dormund, Universität Dortmund, Dissertation, 2006

[98] Krüger-Sehm, W.: Praktische Umsetzung der Anforderungen von Normen und Regeln in der optischen Oberflächenmesstechnik. In: *VDI-Berichte 1996: Optische Messung technicher Oberflächen in der Praxis*, VDI Verlag, 2007, S. 153–165

[99] Lai, X. ; Li, H. ; Li, C. ; Lin, Z. ; Ni, J.: Modelling and analysis of micro scale milling considering size effect, micro cutter edge radius and minimum chip thickness. In: *International Journal of Machine Tools and Manufacture* 48 (2008), S. 1–14

[100] Landenberger, D.: Feinbearbeitung von metallischen Konstruktionswerkstoffen durch Bürstspanen. In: *Jahrbuch Schleifen, Honen, Läppen und Polieren*, Vulkan Verlag, 2007, S. 437–450

[101] Lehmann, P.: Geometrie Erfassung an Mikrobauteilen mittels Weisslichtinterferometrie und konfokaler Mikrosensoren. In: *VDI-Berichte 1950: Messtechnik für Mikro- and Nano-Engineering*, VDI Verlag, 2006, S. 119–128

[102] Lettenbauer, H. ; Imkamp, D.: Einsatz der 3D-Computertomographie in der dimensionellen Messtechnik. In: *VDI-Berichte 1914: Koordinatenmesstechnik*, VDI Verlag, 2005, S. 201–208

[103] Lewis, D.B. ; Bradbury, S.D. ; Sarwar, M.: The effect of substrate surface preparation on the wear and failure modes of TiN coated high speed steel circular saw blades. In: *Wear* 197 (1996), S. 82–88

[104] Li, C. ; Dong, S. ; Zhang, G.: Evaluation of the root-mean-square slope of 3D surface topography. In: *International journal of machine tools and manufacture* 40 (2000), S. 445–454

[105] Liu, K. ; Melkote, S.: Finite element analysis of the influence of tool edge radius in orthogonal micro-cutting process. In: *International Journal of mechanical sciences* 49 (2007), S. 650–660

[106] Lo Casto, S. ; Passannanti, G.: On the influence of the radius between face and rake on the tool life of sintered carbides. In: *CIRP Annals* 34 (1985), S. 83–85

[107] Lung, D. ; Abouridouane, M ; Sangermann, H.: Skalierungseffekte bei der Mikrozerspanung. In: *VDI-Z Integrierte Produktion* August (2008), S. 42–43

[108] Luo, X. ; Cheng, K. ; Holt, R. ; X., Liu.: Modeling flank wear of carbide tool insert in metal cutting. In: *Wear* 259 (2005), S. 1235–1240

[109] Mainsah, E ; Greenwood, J ; Chetwynd, D.: *Metrology and properties of engineering surfaces*. 1st ed. Boston, London : Kluwer academic publisher, 2001

[110] Miyamoto, I. ; Ezawa, T ; Nishimura, K.: Ion beam machining of single-point diamond tools for nano-precision turning. In: *Nanotechnology* 1 (1990), S. 44–49

[111] Moneim, A.: Tool edge roundness in finish machining at high cutting speeds. In: *Wear* 58 (1980), S. 173–192

[112] Montgomery, D.: *Design and analysis of experiments*. 6. Auflage. New Jersey : John Wiley and sons, 2005

[113] Mori, T. ; Hirota, K. ; Kawashima, Y.: Clarification of magnetic abrasive finishing mechanism. In: *International materials processing technology* 143-144 (2003), S. 682–686

[114] M'Saoubi, R. ; Chandrasekaran, H.: Investigation of the effects of tool micro-geometry and coating on tool temperature during orthogonal turning of quenched and tempered steel. In: *International Journal of Machine Tools and Manufacture* 44 (2004), S. 213–224

[115] Nasr, N.A. ; Elbestawi, M.A.: Modelling the effects of tool-edge radius on residual stresses when orthogonal cutting AISI 316L. In: *International Journal of Machine Tools and Manufacture* 47 (2007), S. 401–411

[116] Natsu, W. ; Ikeda, T. ; Kunieda, M.: Generating complicated surface with electrolyte jet machining. In: *Precision engineering* 31 (2007), S. 33–39

[117] Neuschaefer-Rube, U.: Sensoren und Geräteprinzipien für kleine Merkmale. In: *VDI-Berichte: Koordinatenmesstechnik VDI-Berichte*, VDI Verlag, 2005, S. 225–238

[118] Ng, C.K. ; Melkote, S.N. ; Rahman, M. ; Kumar, A.S.: Experimental study of micro- and nano-scale cutting of aluminium 7075-T6. In: *International Journal of Machine Tools and Manufacture* 46 (2006), S. 929–936

[119] Ofen, R.: 3-D-Erfassung von Radien und Kanten an Werkzeugen und Bauteilen. In: *VDI-Berichte 1996: Optische Messung technicher Oberflächen in der Praxis*, VDI Verlag, 2007, S. 53–68

[120] Ong, N.S. ; Venkatesh, V.C.: Semi-ductile grinding and polishing of Pyrex glass. In: *International materials processing technology* 83 (1998), S. 261–266

[121] Oraby, S.E. ; Hayhurst, D.R.: Tool life determination based on the measurement of wear and tool force ratio variation. In: *International journal of machine tools and manufacture* 44 (2004), S. 1261–1269

[122] Otec Präzisionsfinish, GmbH: Dem Werzeug dir Kante geben. In: *Maschine + Werkzeug* 10 (2005), S. 36–37

[123] Ovenholser, R.W. ; Stango, R.J. ; Fournelle, R.A.: Morpholoy of metal surface generated by nylon/abrasive filament brush. In: *International journal of machine tools and manufacture* 43 (2003), S. 193–202

[124] Oxley, P.L.B.: *Mechanics of machining.* 1st ed. New York, Chichester, Brisban, Toronto : Ellis Horwood Limited, 1989

[125] Özel, T.: Modeling of hard part machining: effect of insert edge preparation in CBN cutting tools. In: *Journal of materials processing technology* 141 (2003), S. 284–293

[126] Özel, T. ; Hsu, T.-K. ; Zeren, E.: Effects of cutting edge geometry, workpiece hardness, feed rate and cutting speed on surface roughness and forces in finish turning of hardened AISI H13 steel. In: *International Journal of Advanced Manufacturing Technology* 25 (2005), S. 262–269

[127] Papula, L.: *Mathematik für Ingenieure und Naturwissenschaftler-Band 3.* 2. Auflage. Braunschweig, Wiesbaden : Vieweg, 1997

[128] Patent DE 697 06 558, T2. *Verfahren zur Erziehlung genau definierter Kantenradien mittels Elektropolieren.* 2001

[129] Paucksch, E. ; Holsten, S. ; Linss, M. ; Tikal, F.: *Zerspantechnik*. 12. Auflage. Braunschweig : Vieweg, 2008

[130] Pawade, R.S. ; Joshi, S.S. ; Brahmankar, P.K.: Effect of machining paramaters and cutting edge geometry on surface integrity of high-speed turned Inconel 718. In: *International Journal of Machine Tools and Manufacture* 48 (2008), S. 15–28

[131] Pirso, J. ; Letunovits, S. ; Viljus, M.: Friction and wear behaviour of cemented carbides. In: *Wear* 257 (2004), S. 257–265

[132] Poprawe, R.: *Lasertechnik für die Fertigung*. 1. Auflage. Berlin, Heidelberg : Springer-Verlag, 2005

[133] Prengel, H.G. ; Santhanam, A.T.: State of the art in hard coatings for carbide cutting tools. In: *Surface and coatings technology* 102 (1998), S. 183–190

[134] Rech, J.: Cutting edge preparation and surface issues. In: *International Conference Smart solutions for metal cutting*, HSS Forum Aachen, 2005, S. 1–12

[135] Rech, J.: Influence of cutting edge preparation on the wear resistance in high speed dry gear hobbing. In: *Wear* 261 (2006), S. 505–512

[136] Rech, J. ; Yen, Y.-C. ; Schaff, M. ; Hamdi, H. ; Altan, T. ; Bouzakis, K.D.: Influence of cutting edge radius on the wear resistance of PM-HSS milling inserts. In: *Wear* 259 (2005), S. 1168–1176

[137] Risse, K.: *Einflüsse von Werkzeugdurchmesser und Schneidkantenverrundung beim Bohren mit Wendelbohrern in Stahl*. Aachen, RWTH Aachen, Dissertation, 2006

[138] Russ, J.: *Fractal surfaces*. 1st ed. New York and London : Plenum press, 1994

[139] Russ, J.: Fractal dimension measurement of engineering surfaces. In: *International journal of machine tools and manufacture* 38 (1998), S. 567–571

[140] Saito, H. ; Iwabuchi, A. ; Shimizu, T.: Effects of Co content and WC grain size on wear of WC cemented carbide. In: *Wear* 261 (2006), S. 126–132

[141] Santhanam, A. T. ; Tierney, P.: Cemented carbides. In: *ASM Handbook Vol 16: machining*, ASM International, 1989, S. 71–89

[142] Santhanan, A.T. ; Quinto, D.T.: Surface engineering of carbide, cermet, and ceramic cutting tools. In: *ASM Handbook Vol 5: surface engineering*, ASM International, 1994, S. 900–908

[143] Schäfer, F.: *Engraten: Theorie, Verfahren, Anlagen*. Mainz : Krausskopf-Verlag, 1975

[144] Scheffler, E.: *Statistische Versuchsplanung und -auswertung.* Stuttgart : Deutscher Verlag für Grundstoffindustrie, 1997

[145] Schmidt-Sandte, T.: *Laserstrahlbasierte Engratverfahren für feinwerktechnische Anwendungen.* Braunschweig, TU Braunschweig, Dissertation, 2002

[146] Schulz, H.: *Hochgeschwindigkeitsfräsen metallischer und nichtmetallischer Werkstoffe.* 1. Auflage. München, Wien : Carl Hanser Verlag, 1989

[147] Scussel, H.: Friction and wear of cemented carbides. In: *ASM Handbook Vol 18: friction, lubrication and wear technology*, ASM International, 1992, S. 795–800

[148] Seegiw, J.: Rauheitskenngrössen für die 3D-Oberflächenmesstechnik im Bereich der Mikro- und Nanotechnik. In: *VDI-Berichte 1669: Metrologie in der Mikro- und Nanotechnik*, VDI Verlag, 2003, S. 31–42

[149] Shatla, M. ; Kerk, C. ; Altan, T.: Process modeling in machining. Part II :validation and applications of the determined flow stress data. In: *International Journal of Machine Tools and Manufacture* 41 (2001), S. 1659–1680

[150] Shedler, W.: *Hartmetall für den Praktiker.* Düsseldorf : VDI-Verlag, 1988

[151] Shia, C.-Y. ; Stango, R.J. ; S.M., Heinrich: Analysis of contact mechanics for a circular filamentary brush/workpart system. In: *Journal of manufacturing science and engineering. Transactions of the ASME* 120 (1998), S. 715–721

[152] Siegmann, S. ; Brown, C.A.: Einfluss der Haftgrundvorbereitung auf die entstehende Topographie und Schichthaftung; Ein dreidimensionales Fraktalanalyse-Verfahren. In: *Tagungsband zum 2. GTV Kolloquium*, GTV, 2002, S. 1–11

[153] Singh, D. ; Jain, V.K. ; Raghuram, V.: Parametric study of magnetic abrasive finishing process. In: *International materials processing technology* 149 (2004), S. 22–29

[154] Singh, S. ; Shan, H.S.: Development of magneto abrasive flow machining process. In: *International journal of machine tools and manufacture* 42 (2002), S. 953–959

[155] SME: Nontraditional machining. In: *Tool and manufacturing engineers handbook: Volume 1 Machining*, Society of manufacturing engineers, 1983, S. 14–1 to 14–93

[156] Sockman, J.: Deburring with Nylon Filament Brushes. In: *Manufacturing Engineering* 126 N6 (2000)

[157] Son, S. ; Lim, H. ; Ahn, J.: Effects of the friction coefficient on the minimum cutting thickness in microcutting. In: *International Journal of Machine Tools and Manufacture* 45 (2005), S. 529–535

[158] Sreejith, P.S.: Material removal mechanisms in precision machining of new materials. In: *International journal of machine tools and manufacture* 41 (2001), S. 1831–1843

[159] Stango, R.J. ; Chen, L. ; Cariapa, V.: Automated deburring with a filamentary brush: prescribed burr geometry. In: *Journal of manufacturing science and engineering. Transactions of the ASME* 121 (1999), S. 385–392

[160] Stango, R.J. ; Fournelle, R.A. ; chada, S.: Morphology of surfaces generated by circular wire brushes. In: *Journal of engineering for industry. Transactions of the ASME* 117 (1995), S. 9–15

[161] Stango, R.J. ; Shia, C.-Y.: Analysis of filament deformation for a freely rotating cup brush. In: *Journal of manufacturing science and engineering. Transactions of the ASME* 119 (1997), S. 298–306

[162] Stango, R.J. ; Shia, C.-Y. ; Henderson, J.A.: Development of a rational basis for design of advanced brushing tools. In: *Journal of engineering for industry. Transactions of the ASME* 116 (1994), S. 308–315

[163] Storck, G.E. ; White, S.S.: Abrasive jet machining. In: *ASM Handbook Vol 16: machining*, ASM International, 1989, S. 511–513

[164] Subbiah, S. ; Melkote, S.: Effect of finite edge radius on ductile fracture ahead of the cutting tool edge in micro-cutting of Al2024-T3. In: *Materials science and engineering* 474 (2008), S. 283–300

[165] Subramanian, K.: Classification and selection of finishing processes. In: *ASM Handbook Vol 5: surface engineering*, ASM International, 1994, S. 81–83

[166] Tang, W.: *Optische Messung der Kantenschärfe von Schneidwerkzeugen.* Kaiserslautern, Universität Kaiserslautern, Dissertation, 1990

[167] Thiele, J.F. ; Melkote, S.: Effect of cutting edge geometry and workpiece hardness on surface generation in the finish hard turning of AISI 52100 steel. In: *Journal of materials processing technology* 94 (1999), S. 216–226

[168] Thilow, A.: *Entgrat-Technik.* 1. Auflage. Ehningen : Expert Verlag, 1992

[169] Thomas, T.R. ; Rosen, B.-G. ; Amini, N.: Fractal characterisation of the anisotropy of rough surfaces. In: *Wear* 232 (1999), S. 41–50

[170] Tikal, F. ; Heiler, R. ; Müller, P.: *Bohrer und Gewindewerkzeuge.* 1. Auflage. Landsberg : Verlag moderne Industrie, 2003

[171] Tong, S. ; Gracewski, S.M. ; Funkenbusch, P.D.: Measurement of the Preston coefficient of resin and bronze bond tools for deterministic microgrinding of glass. In: *Precision engineering* 30 (2006), S. 115–122

[172] Tönshoff, H. ; Denkena, B.: *Spanen*. 2. Auflage. Berlin : Springer-Verlag, 2004

[173] Tönshoff, H.K. ; Blawit, C.: Influence of surface integrity on performance of coated cutting tools. In: *Thin solid films* 308-309 (1997), S. 345–350

[174] Tönshoff, H.K. ; Hessel, D. ; Spengler, C.: Schleifen von Werkzeugen. In: *Jahrbuch Schleifen, Honen, Läppen und Polieren*, Vulkan Verlag, 2002, S. 152–160

[175] Tönshoff, H.K. ; Mohlfeld, A. ; Gey, C. ; Winkler, J.: Surface modification of cemented carbide cutting tools for improved adhesion of diamond coatings. In: *Surface and coatings technology* 108-109 (1998), S. 543–550

[176] Tönshoff, H.K. ; Seegers, H.: Influence of residual stress gradients on the adhesion strength of sputtered hard coatings. In: *Thin solid films* 377-378 (2000), S. 340–345

[177] Trent, E. ; Wright, P.: *Metal Cutting*. 4th ed. Boston, Oxford : Butterworth-Heinemann, 2000

[178] Tushinsky, L. ; Kovensky, I. ; Plokhov, A. ; Sindeyev, V. ; Reshedko, P.: *Coated metal: structure and properties of metal-coating compositions*. 1st ed. Berlin, Heidelberg : Springer-Verlag, 2002

[179] Uchiyama, T. ; Fukase, A.: Three-dimensional vortex simulation of particle-laden air jet. In: *Chemical Engineering Science* 61 (2006), S. 1767–1778

[180] Uetz, H. ; Gross, K-J.: Strahlverschleiss. In: *Abrasion und Erosion*, Carl Hanser Verlag, 1986, S. 236–237

[181] Upadhyaya, G.: *Cemented tungsten carbides: production, properties and Testing*. 1st ed. Westwood, New Jersey : Noyes publications, 1998

[182] Utcke, S.: Error-bounds on Curvature Estimation. In: *Scale-Space 2003*, Springer-Verlag, 2003, S. 657–666

[183] Valentin, J. ; Weber, M. ; Brodmann, R. ; Grigat, m.: Optische 3D-Charakterisierung technischer Oberflächen mittels konfokaler Mikroskopie. In: *Spanende Fertigung*, Vulkan Verlag, 2005, S. 33–42

[184] Vallance, R. ; Morgan, C. ; Shreve, S. ; Marsh, E.: Micro-tool characterization using scanning white light interferometry. In: *Journal of micromechanics and microengineering* 14 (2004), S. 1234–1243

[185] Wakuda, M. ; Yamauchi, Y. ; Kanzaki, S.: Effect of workpiece properties on machinability in abrasive jet machining of ceramic materials. In: *Precision engineering* 26 (2002), S. 193–198

[186] Wakuda, M. ; Yamauchi, Y. ; Kanzaki, S.: Material response to particle impact during abrasive jet machining of alumina ceramics. In: *Journal of materials processing technology* 132 (2003), S. 177–183

[187] Wang, C.-C. ; Lin, S.-C. ; Hochen, H.: A material removal model for polishing glass-ceramic and aluminium magnesium storage disks. In: *International journal of machine tools and manufacture* 42 (2002), S. 979–984

[188] Warnecke, W.: *Fertigungsmesstechnik: Handbuch für industrie und wissenschaft.* 1 Auflage. Berlin : Springer-Verlag, 1984

[189] Weber, M.A.: Konfokale 3D Mikroskopie zuir Oberflächenanalyse mikrostrukturierter Materialien. In: *VDI-Berichte 1669: Metrologie in der Mikro- und Nanotechnik*, VDI Verlag, 2003, S. 95–102

[190] Weinert, K. ; Koehler, D. ; Kötter, D.: Kantenpräparation durch Strahlen am Beispiel eines Wendelbohrers. In: *Jahrbuch Schleifen,Honen,Läppen und Polieren: 62 Ausgabe*, Vulkan-Verlag, 2005, S. 484–491

[191] Westkämper, E. ; Osten, W. ; Regin, J. ; Wiesendager, T.: Multiskalige Mess- und Prüfstrategien in der Mikro- und Nanomesstechnik. In: *VDI-Berichte 1950: Messtechnik für Mikro- and Nano-Engineering*, VDI Verlag, 2006, S. 141–150

[192] Whitehouse, D.: *Handbook of Surface Metrology.* 1st ed. London : Rank Taylor Hobson, 1994

[193] Whitehouse, D.: *Surfaces and their measurement.* 1st ed. London : Kogan Page Science, 2002

[194] Wieland, M. ; P., Hänggi ; Hotz, W. ; Textor, M. ; Keller, B.A. ; Spencer, N.D.: Wavelength-dependent measurement and evaluation of surface topographies: application of a new concept of window roughness and surface transfer function. 237 (2000), S. 231–252

[195] Wienert, K. ; Koehler, F.-W. B. ; Schäperkötter, M.: Analyse der Wirkzusammenhänge beim Bohren mit hohen Geschwindigkeiten. In: *Hochgeschwindigkeitsspanen*, Wiley-VCH Verlag, 2005, S. 229–254

[196] Winkelbach, S. ; Wahl, F.M.: Shape from single stripe pattern illumination. In: *Pattern Recognition, Lecture Notes in Computer science*, Springer Verlag, 2002, S. 240–247

[197] Woon, K. ; Rahman, M. ; Fang, Z. ; Neo, K. ; Liu, K.: Investigations of tool edge radius effect in micromachining: A FEM simulation approach. In: *Journal of material processing technology* 195 (2008), S. 204–211

[198] Wu, H.B. ; Chen, Y. ; Guan, C.R. ; Yu, X.: 3D measurement technology by structured light using stripe-edge-based gray code. In: *International symposium on instrumentation science and technology*, Institute of physics publishing, 2006, S. 537–541

[199] Wu, J.-J.: Structure function and spectral density of fractal profiles. In: *Chaos, solitons and fractals* 12 (2001), S. 2481–2492

[200] Wu, J.-J.: Analysis and simulation of anisotropic fractal surfaces. In: *Chaos, solitons and fractals* 13 (2002), S. 1791–1806

[201] Xie, Y. ; Bhushan, B.: Effects of particle size, polishing pad and contact pressure in free abrasive polishing. In: *Wear* 200 (1996), S. 281–295

[202] Yen, Y.-C. ; Anurag, J. ; Altan, T.: A finite element analysis of orthogonal machining using different tool edge geometries. In: *Journal of materials processing technology* 146 (2004), S. 72–81

[203] Yen, Y.C. ; Jain, A. ; Altan, T.: A finite element analysis of orthogonal machining using different tool edge geometries. In: *Journal of materials processing technology* 146 (2004), S. 72–81

[204] Yen, Y.C. ; Söhner, J. ; Lilly, B. ; Altan, T.: Estimation of tool wear in orthogonal cutting using the finite element analysis. In: *Journal of materials processing technology* 146 (2004), S. 82–91

[205] Yeo, S.H. ; Bryan, B. ; Ngoi, A. ; Chua, Y.: Ultrasonic deburring. In: *International journal of advanced manufacturing technology* 13 (1997), S. 333–341

[206] Yin, S. ; Shinmura, T.: Vertical vibration-assisted magnetic abrasive finishing and deburring for magnesium alloy. In: *International journal of machine tools and manufacture* 44 (2004), S. 1297–1303

[207] Yuan, C.Q. ; Li, J. ; Yan, X.P. ; Peng, Z.: The use of the fractal description to characterise engineering surfaces and wear particles. In: *Wear* 255 (2003), S. 315–326

[208] Yuan, Z.J. ; Zhou, M. ; Dong, S.: Effect of diamond tool sharpness on minimun cutting thickness and cutting surface integrity in ultraprecision machining. In: *Journal of materials processing technology* 62 (1996), S. 327–330

[209] Zepke, S.: Scharte ausgewetzt. In: *MM Maschinen Markt* Mai (2006)

[210] Zhang, B. ; Zhou, L.: Effect of sandblasting on adhesion of diamond coatings. In: *Thin solid films* 307 (1997), S. 21–28

[211] Zhang, C. ; Rentsch, R. ; Brinksmeier, E.: Advances in micro ultrasonic assisted lapping of microstructures in hard-brittle materials: a brief review and outlook. In: *International journal of machine tools and manufacture* 45 (2005), S. 881–890

[212] Zhang, J.: Calculation of fractal dimension of fractal surfaces using fft. In: *http://www.mathworks.com/matlabcentral/fileexchange/6167*, Mathworks, 2005

[213] Zhang, Y. ; Luo, Y. ; Wang, J. ; Li, Z.: Research on the fractal of surface topography of grinding. In: *International journal of machine tools and manufacture* 41 (2001), S. 2045–2049

[214] Zhou, G.: *Statistical, random and fractal characterizations of surface topography with engineering applications.* New Jersey, New Jersey Institute of Technology, Dissertation, 1993

[215] Zong, W.J. ; Sun, T. ; Li, D. ; Cheng, K. ; Liang, Y.C.: FEM optimization of tool geometry based on the machined near surface's residual stresses generated in diamond turning. In: *Journal of material processing technology* 180 (2006), S. 271–278